A Progressive Endeavor to Develop Efficient Organic Chromogenic and Fluorogenic Sensing Probes for Ionic and Neutral Guests

A Dissertation

Submitted in partial fulfillment for the degree of

Doctor of Philosophy

Soham Samanta

(Roll No. 126122031)

Thesis Supervisor: Prof. Gopal Das

Department of Chemistry

Indian Institute of Technology Guwahati

Assam-781039, India

Dedicated to

my parents

INDIAN INSTITUTE OF TECHNOLOGY GUWAHATI

Department of Chemistry

STATEMENT

I do hereby declare that the matter embodied in this thesis is the result of investigations carried out by me in the Department of Chemistry, Indian Institute of Technology Guwahati, India, under the guidance of Prof. Gopal Das, Department of Chemistry, Indian Institute of Technology Guwahati, India.

In keeping with the general practice of reporting scientific observations, due acknowledgements have been made wherever this work is based on the findings of other investigators.

16th November, 2016 **Soham Samanta**

IIT Guwahati

INDIAN INSTITUTE OF TECHNOLOGY GUWAHATI

Department of Chemistry

CERTIFICATE

This is to certify that Mr. Soham Samanta has been working under my supervision since August, 2012 as a regular registered Ph. D. student. His thesis entitled **"A Progressive Endeavor to Develop Efficient Organic Chromogenic and Fluorogenic Sensing Probes for Ionic and Neutral Guests"** is authentic record of the results obtained from the research work carried out under my supervision in the Department of Chemistry, Indian Institute of Technology Guwahati, Assam, India. I am forwarding his thesis to submit for the award of degree of Doctor of Philosophy, from this institute. I hereby certify that he has fulfilled all the requirements, according to the rules of this institute regarding the investigations embodied in his thesis and this work has not been submitted elsewhere for a degree.

Prof. Gopal Das
(Thesis Supervisor)
Professor
Department of Chemistry
IIT Guwahati
Assam - 781039, India

Acknowledgement

At this final stage of truly memorable journey towards my intellectual destination, it is really hard to list all the people who sincerely helped me and I would like to thank all of them who have made this thesis possible. I would like to express my deepest gratitude to my father Susanta Samanta and mother Krishna Samanta, two people with irrational and unbreakable belief on me. Their unconditional love and support made me reach this stage of my life. I am grateful to my younger sister Sudeshna Samanta, my grandmother (from mother's side) Satadal Parua, my late uncle Prasun parua (from mother's side) and my late grandfather (from mother's side) Jagadish Parua along with all my relatives and family members; who selflessly always supported me, helped me, encouraged me by every possible means throughout my academic life. I am highly indebted to my thesis supervisor Prof. Gopal Das for his kind support, insightful advice and encouragement. I earnestly thank him for his nice guidance, freedom to work, encouragement and inspiration which helped me to enrich myself.

Besides my supervisor, I would also like to express my sincere gratitude to my doctoral committee members, Dr. Chandan Mukherjee, Dr. A.S. Achal Kumar and Dr. Kingsuk Mahata for their advices and valuable suggestions. I shall always be obliged to Prof. Aiyagari Ramesh for his admirable support throughout my research work. I am also very grateful to my M.Sc. project supervisor Prof. Jubaraj Bikash Baruah who was the first person to introduce me to the world of scientific research. I also wish to thank staff members of the department of chemistry for their cooperation. My sincere thanks to the staffs of central instrument facility, for their help to use several analytical instruments required during my research work.

Alongside I am very lucky to have wonderful seniors like Sandeep da, Arghya da, Chirantan da, Jiban da, Najbul da, Romen da, Abhijit da, Barun da and extraordinary associates like Nilotpal, Rupinder, Utsab, Biswajit, Madhurima, Santanu and Senjuti. It was great to work and spend times with these lovely human beings and I will always cherish the memories of their jokes, laughter and humors throughout my life. I never felt bored, frustrated or disappointed in these few years just because of you people, you guys always stood by me in my need; you are real friends and fellow warrior. I shall always be obliged to Chirantan da and Barun da, they were my mentors who taught me the basics of lab techniques, without their support I would have given this up a long time ago.

I also owe my obligations to my other seniors, batch mates and juniors of PhD fraternity of chemistry department for their help and support. I have also got opportunity to mingle with friends of Biosciences & Bioengineering, IIT Guwahati. I owe my gratitude to Sudeep, Thiyagaranjan, Sandipan and Poulomi for their unconditional support and all the help they extended from time to time whenever required.

I would also take this opportunity to thank my friends Mitali, Papri, Manab-da (Manas Mondal), Narayan, Sanjoy, Kuldeep, Surajit, Lakhsmikanta, Snehasis, Abhishek and all others for being a source of my encouragement and love throughout this period. Also, I would recall the love and support I got from my brothers (juniors) - Turjaya, Nilu, Utasab, Rajat, Bapan, Ayan, Mostakim, Gourab and Rana.

Truly guys, you all are not less than my blood-brothers; you all have made my IITG journey memorable, I would rejoice this for my entire life.

No words would be sufficient to express my gratitude to my teachers, Tapas babu, Kamal babu, Debashis babu, Seuli ma'am, Taniya ma'am, Kunal sir, Biplab (Mondal) sir, Sandip (Pal) sir and Candan (Mukherjee) sir from my school, college and university; whose teachings, advices and blessings guided me to shape my academic career. I have the rare opportunity to come in touch with some extraordinary personalities like Pintu da, Asim Da, Gobinda da, Anup da, Laltu da, Susovan da and Bivas da during my graduation days. They are so humble, so kind, so helpful, and so inspirational that no word is sufficient to acknowledge that.

Finally, I would like to thank the Microsoft Corporation for presenting the MS word, from grammar check to synonyms, from equation to symbols without this software, the thesis would have taken another five years.

Still many names are missing whose contribution and help is worth mentioning.

Soham

Synopsis

Title of this thesis is - "**A Progressive Endeavor to Develop Efficient Organic Chromogenic and Fluorogenic Sensing Probes for Ionic and Neutral Guests".** This thesis has been divided into six chapters which indigenously covered the results of experimental work performed during the research period.

Chapter 1: Introduction

There are sayings that 'Eyes don't lie' and 'Seeing is believing'. Indeed eyes are the best among five main senses that a normal human being uses to perceive the world. Hence, the idea of optical detection or recognition constitutes to be the most effective means of chemo-sensing so far. Developing sensor systems for the effective and rapid detection of analytes continues to be a hot topic in supramolecular and biological chemistry as the detection of chemical species comprised of cations, anions and neutral molecules related to environment, agriculture sciences, biology, medicine and health sciences; has become an indispensable task to endure. By broad definitions, chemo-sensors are basically chemical systems that can convert chemical stimuli into some form of easily detectable response. Essentially, in the presence of appropriate specific target analyte, a chemosensor generates signal through electrochemical, mass, optical and a variety of other changes. Numerous reports can be cited to endorse that chemosensors can offer the simple and sensitive detection of several analytes, especially in extreme and complicated environmental or biological systems where traditional methods have failed to be utilized. However, among these various types of sensing methods, optical (colorimetric & fluorescent) chemo-sensors have grabbed the limelight popularly due to their simplicity, easy handling, ability to work in a more relaxed condition, fast response time and simple reliable signal interpretation ability with high sensitivity. Especially, the fluorescence-based sensing probes are advantageous over other sensing systems for the detection of biological species as they can render rapid, non-invasive, temporal and sensitive detection of target analytes. Fluorescent probes not only provide valuable insights in understanding physiological alterations in pathological settings but also serve as useful tools for the development of personalized medicine and targeted therapies. Hence, in recent years, numerous **colorimetric** and **fluorescent** chemo-sensors are developed extensively for their potential applications in environmental detection, molecular catalysis, and biological fluorescence imaging, etc.

Hence, in this thesis, we have extensively worked on designing various fluorogenic and chromogenic sensing systems that can sense cation(s), anion(s), cation plus anion together and neutral species.

Chapter 2: Experimental Section

This chapter explains comprehensive information about the various materials used in the synthesis of the receptors/probes. Also in this chapter, the synthetic techniques, crystallization details, binding studies; specifications of instruments used for the characterization of the synthesized compounds were discussed in detail.

Chapter 3: An Aggregation-Induced Emission (AIE) Active Probe Renders Al(III) Sensing and Tracking of Subsequent Interaction with DNA

This chapter describes the detailed sensing properties of an bis-imine Schiff base probe (**L_1**). The rationally designed probe (**L_1**) displayed interesing aggregation-induced emission (AIE) properties in methanol-water mixed solvent. Essentially, the aggregation-induced emission (AIE) active probe **L_1** rendered highly selective TURN-ON fluorescence response toward Al^{3+} among vaious tested metal ions in CH_3OH/aqueous HEPES buffer (5 mM, pH 7.3; 9:1, v/v) and in live HeLa cells. Addition of 10 equivalents of Al^{3+} to the solution of weakly emissive (λ_{em}=506 nm) **L_1** resulted in the dramatic enhancement in the fulorescence intensity accompanied by 31 nm red shift in the emission maxima to establish a new emission maximum at 537 nm and showed a highly intense bright yellowish green fluorescence, when excited at 400 nm. Plausibly excess Al^{3+} helped to form aggregates of **L_1**-Al^{3+} complex in the solution, which in turn triggered the AIE activity of **L_1** to enable the TURN-ON fluorescence. Detailed HRMS, DLS, AFM and FESEM studies were carried out to validate the sensing mechanism. The highly emissive **L_1**-Al^{3+} ensemble was subsequently utilized to track the interaction with ct-DNA in solution by dose dependent fluorescence quenching.

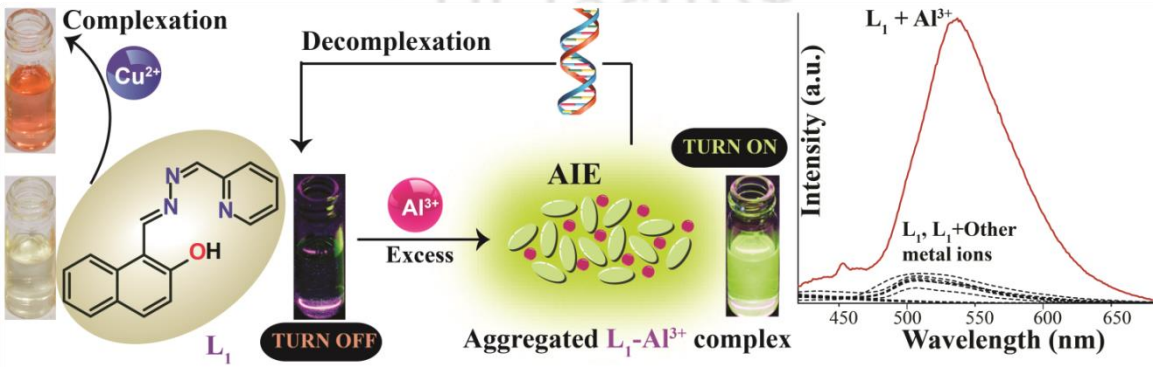

Scheme 1: A comprehensive representation of the research work described in **chapter 3**

Interestingly **L_1** can also detect Cu^{2+} at nano-molar level in similar condition through a selective visual colorimetric response due to 1:1 complexation wherein interaction of Cu^{2+} with almost colorless solution of **L_1** could turn the solution into intense red color.

Chapter 4: A Solo Fluorogenic Probe for Real-time Sensing of $SO_3^{2-}$and SO_4^{2-}/ HSO_4^- in Aqueous Medium and Live Cells by Distinct Turn-On Emission Signals

In this chapter, we described a new fluorogenic probe **L_2**, which is basically an α,β–unsaturated compound. The design of the probe was based on the fundamental notion of a nucleophilic addition reaction (Scheme 2), which can subsequently be tracked by a rapid change in fluorescence as SO_2 derivatives (SO_3^{2-} and HSO_3^-) can readily react withα,β–unsaturated compounds. This versatile fluorescent probe **L_2** demonstrated highly sensitive dual yet discerning sensing of SO_3^{2-} and SO_4^{2-}/HSO_4^- over various competing analytes with beneficial attributes such as sensing in completely aqueous medium and an extremely fast response time. Addition of SO_3^{2-} to **L_2** resulted in a high Turn-On fluorescence and a dramatic enhancement (~12 fold) in the florescence intensity at 442 nm was observed upon excitation at 380 nm. On the other hand, addition of SO_4^{2-}/HSO_4^- to **L_2** under similar conditions resulted in the emergence of a new red shifted emission maximum at 511 nm accompanied by ~10 fold enhancement in the fluorescence intensity of **L_2**. These highly selective and distinct Turn-On fluorescence responses of **L_2** towards SO_3^{2-} and SO_4^{2-}/HSO_4^- were also noticeable by naked eye as the non-fluorescent solution of **L_2** emitted strong bluish-green fluorescence upon interaction with SO_3^{2-} and greenish-yellow fluorescence upon interaction with SO_4^{2-}/HSO_4^-. The ratiometric fluorescence-based sensing of SO_3^{2-} was explained by restriction in intramolecular charge transfer (ICT), while SO_4^{2-} sensing was attributed to an aggregation induced emission phenomenon. Importantly, the designed probe was biocompatible and capable of demonstrating differential intracellular sensing of SO_3^{2-} and SO_4^{2-} inside live HeLa cells.

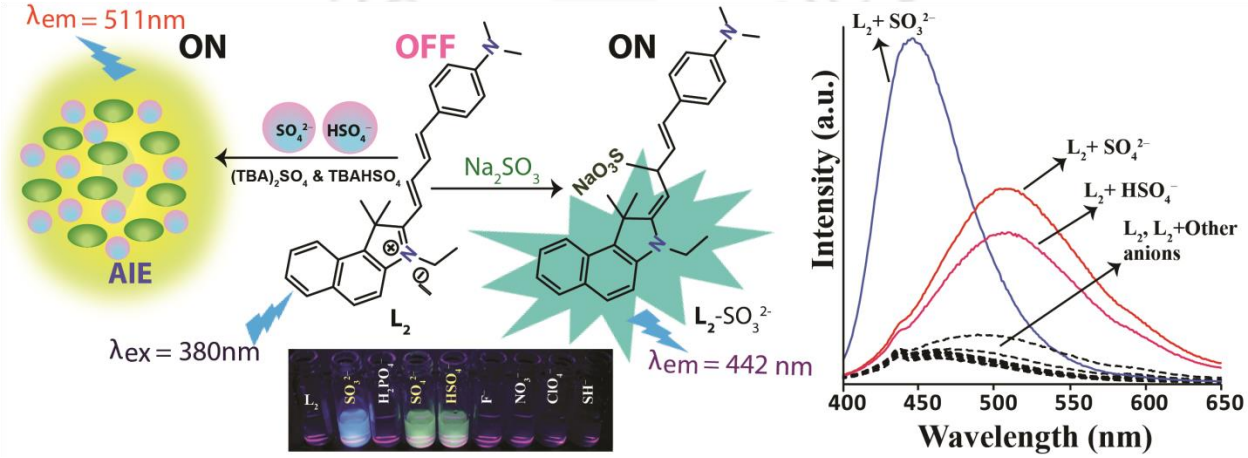

Scheme 2: A comprehensive representation of the research work included in **chapter 4**

Chapter 5: An Aggregation-Induced Emission (AIE) active probe for multiple targets: Fluorescent sensor for Zn^{2+} and Al^{3+} & colorimetric sensor for Cu^{2+} and F^-

This chapter provides detailed information about a thiosemicarbazone based probe (**L_3**) which can detect multiple targets at a time through different fluorescent and colorimetric outputs. Rationally designed probe **L_3**, consist of both cation and anion binding sites is capable of displaying interesting aggregation induced emission (AIE) property. **L_3** not only can sense Al^{3+} and Zn^{2+} through selective turn-on fluorescence responses in 9:1 methanol-HEPES buffer (5mM, pH 7.3; 9:1, v/v) medium due to metal ion triggered AIE activity, but also can distinguish them through individual emission signals. Moreover, naked eye detection of these selective individual TURN-ON responses of **L_3** toward Al^{3+} and Zn^{2+} was also feasible under UV light, which rendered a bright yellowish green fluorescence for Al^{3+} and a bluish-green fluorescence for Zn^{2+}. **L_3** can also detect Cu^{2+} in mixed buffer medium and F^-in acetonitrile through sharp colorimetric responses. These colorimetric responses are also conspicuous through naked eye. Theoretical study strongly backed the proposed sensing mechanisms.

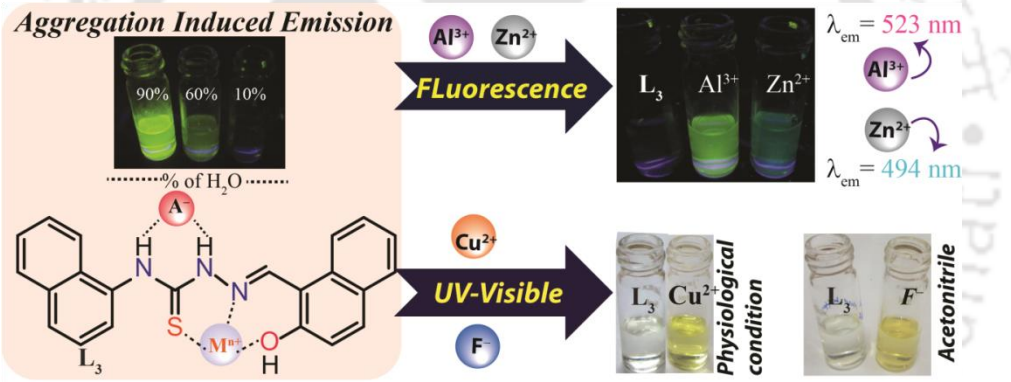

Scheme 3: A comprehensive representation of the research work discussed in **chapter 5**

Chapter 6: Colorimetric and Fluorometric Discrimination of Geometrical Isomers (Maleic Acid vs Fumaric Acid) With Real-Time Detection of Maleic Acid in Solution and Food Additives

The final chapter describes a new hetero-bis imine Schiff base probe **L_4**, which can discriminate geometrical isomers (Maleic acid *vs.* Fumaric acid) through sharp colorimetric as well as fluorogenic responses, even conspicuous with naked eye. On excitation at 450 nm, **L_4** renders a sharp emission maximum around 590 nm in a 9:1 ethanol-HEPES buffer (5mM, pH~7.4) solvent and emits a strong orange-yellow fluorescence. Addition of maleic acid (200 equivalents) induced a slight decrease in the fluorescent intensity of **L_4** with about ~15 nm red shift in the emission maximum to render a new emission maximum at 606 nm while interaction of fumaric acid with **L_4** remain quiet to the spectral change. Moreover, **L_4** can also sense the

maleic acid among various mono, di and tri-carboxylic acids in mixed aqueous ethanol-buffer solution. UV-Visible spectra of **L_4** in mixed solvent revealed a sharp absorbance maximum at 430 nm due to π-π* transition. However, addition of excess of Maleic acid to **L_4** in mixed solvent resulted in the generation of a new red shifted absorbance maximum at 552 nm with the subsequent decrease in the absorbance of its prior original maxima at 430 nm. This unique UV-Visible spectral outcome was accompanied by a distinct visual change in the color of the experimental solution from pale yellow (only **L_4**) to dark red (**L_4**+Maleic acid). On the other hand, **L_4** showed a very weak fluorescence when excited at 550 nm. Interestingly, among various tested carboxylic acids, only maleic acid revealed a certain enhancement in the fluorescence intensity of **L_4** with a well-defined emission maximum at 606 nm upon interaction with **L_4** in similar condition. The sensing process was also replicated in starch rich food to detect added Maleic acid.

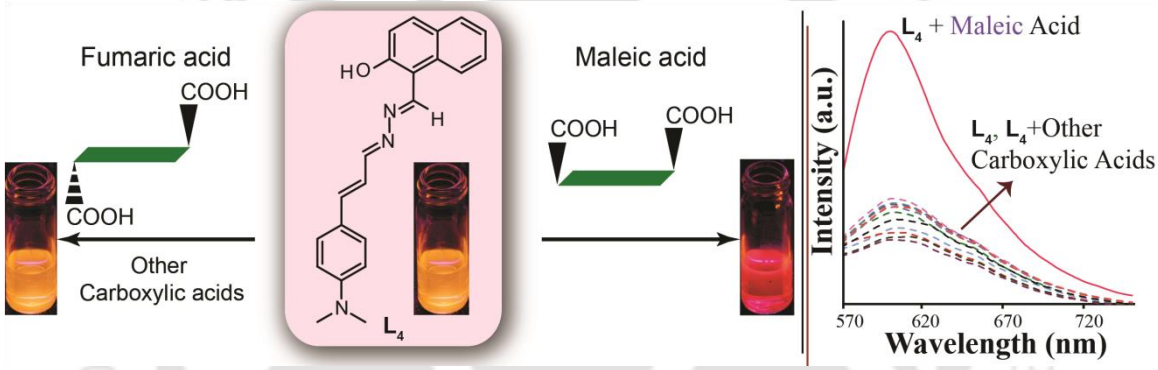

Scheme 4: Schematic illustration of the research work presented in **chapter 6**

Conclusion and future perspective

In conclusion, the overall thesis not only elucidates some important results in the field of developing advanced chemosensors for some biologically and environmentally relevant analytes but also addresses some critical issues related to discrimination of geometrical isomers in solution and/or in biological medium. AIE active probe **L_1** can selectively sense Al^{3+} through selective turn-on fluorescence response in solution and live cells. **L_1** can also selectively detect Cu^{2+} through sharp colorimetric response. Moreover, the highly emissive **L_1**-Al^{3+} ensemble can track the ct-DNA by dose dependent quenching of the fluorescence. Fluorescent probe **L_2** not only can specifically sense SO_2 derivative (SO_3^{2-}) and SO_4^{2-}/HSO_4^- in 100% aqueous medium and live HeLa cells but also can distinguish them by individual Turn-On emission signals. Another AIE active probe **L_3** can sense multiple targets at a time. It can sense cations Al^{3+} and Zn^{2+} through individual Turn-On fluorescence responses and Cu^{2+} through colorimetric changes. Interestingly, **L_3** can also selectively sense anion fluoride by specific colorimetric response. Lastly, sensing probe **L_4** can discriminate geometrical Isomers (Maleic Acid vs Fumaric Acid)

by colorimetric as well as fluorescent changes. Alongside **L_4** can also detect Maleic acid over various other carboxylic acids in solution and food additives.

Hence, we have designed, synthesized and investigated some unique sensing platforms (**L_1-L_4**) which encompassed both simple and complex structures of the sensing probes. As mentioned in the introduction, our primary aim was to introduce sensing systems that can rapidly sense target analytes by some form of optical responses which is conspicuous by naked eye; so that even an uneducated person could identify the sensing outcomes. Hence, all of the reported probes in this thesis were purposely designed to have the inherent feature of naked eye sensing ability. It should also be highlighted that to maintain a chronology we moved from developing all cation sensor (**chapter 3**) to all anion sensor (**chapter 4**) to cation and anion sensing together (**chapter 5**) to neutral molecule sensor at last (**chapter 6**). Essentially we believe that this chronological progress in designing optical probes would be instrumental in understanding comprehensive advancement in the particular field to the analytical chemists community.

Contents

Chapter 3

An Aggregation-Induced Emission (AIE) Active Probe Renders Al(III) Sensing and Tracking of Subsequent Interaction with DNA

Chapter 4

A Solo Fluorogenic Probe for Real-time Sensing of SO_3^{2-} and SO_4^{2-}/ HSO_4^- in Aqueous Medium and Live Cells by Distinct Turn-On Emission Signals

Chapter 5

An Aggregation-Induced Emission (AIE) active probe for multiple targets: Fluorescent sensor for Zn^{2+} and Al^{3+} & colorimetric sensor for Cu^{2+} and F^-

Chapter 6

Colorimetric and Fluorometric Discrimination of Geometrical Isomers (Maleic Acid vs Fumaric Acid) With Real-Time Detection of Maleic Acid in Solution and Food Additives

Chapter 1

Introduction

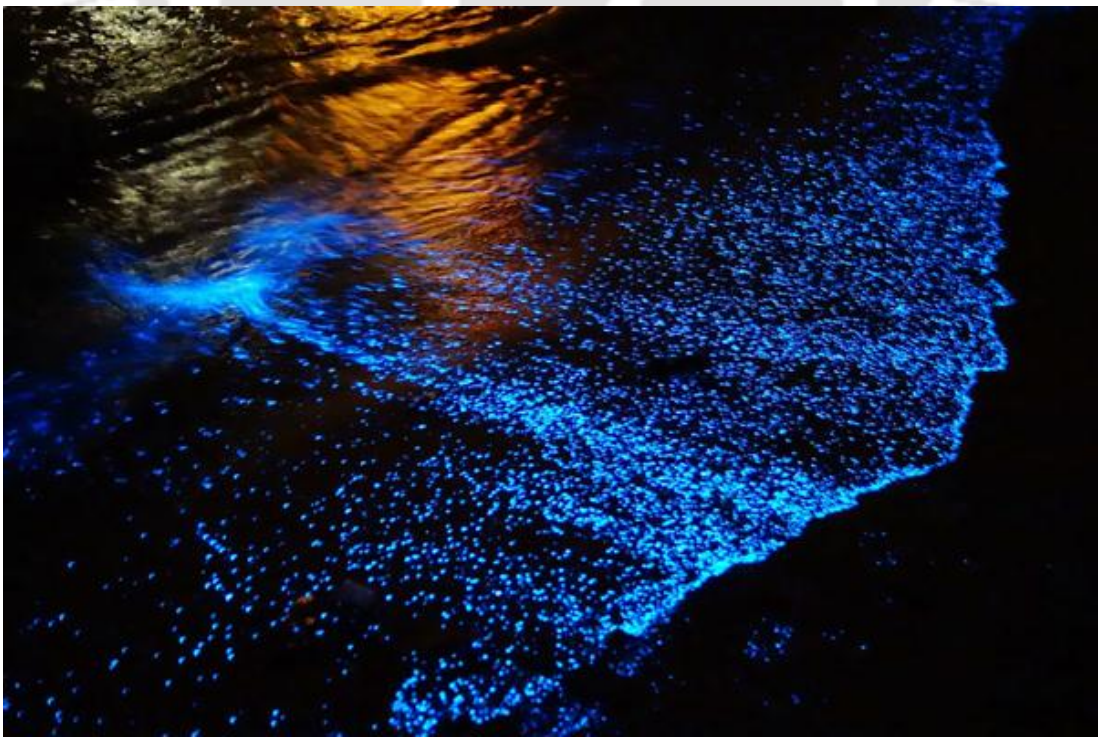

Chapter 1

1.1. Optical Sensors: A Brief Introduction

There are sayings that 'Eyes don't lie' and 'Seeing is believing'. Indeed eyes are the best among five main senses that a normal human being uses to perceive the world. Hence, the idea of optical detection or recognition constitutes to be the most effective means of chemo-sensing so far. The detection of chemical species comprised of cations, anions and neutral molecules related to environment, agriculture sciences, biology, medicine and health sciences; has become an indispensable task to endure.[1.1] By broad definitions, chemo-sensors are basically chemical systems that can convert chemical stimuli into some form of easily detectable response. Essentially, in the presence of appropriate specific target analyte, a chemosensor generates signal through electrochemical, mass, optical and a variety of other changes. Numerous reports can be cited to endorse that chemosensors can offer the simple and sensitive detection of several analytes, especially in extreme and complicated environmental or biological systems where traditional methods have failed to be utilized. However, among these various types of sensing methods, optical sensors are mostly preferred due to their simplicity, easy handling, low cost, fast response time and simple reliable signal interpretation ability.[1.2–1.8]

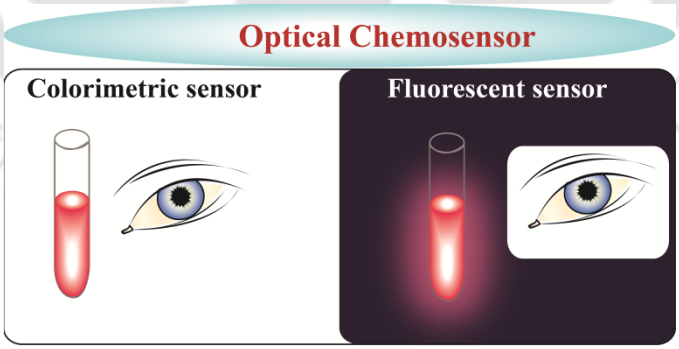

Scheme 1.1: A representative figure of optical chemosensor

Moreover, optical (colorimetric & fluorescent) sensors often bring out sharp visual changes which are conspicuous by naked eye (**Scheme 1.1**). Hence it could offer the opportunity of instant naked eye detection of the target analytes. Therefore, the chemo-sensors that utilize color and/or fluorescence intensity as responses have been developed as the useful tools for sensing various analytes.[1.9–1.11] Generally, in a typical optical chemo-sensor, a receptor (the recognition

site) is linked to a chromophore and/or fluorophore (the signaling moiety), which could translate the recognition event into the detectable colorimetric and/or fluorescence signal.[1.12]

So, optical sensors are mainly comprised of two types of sensing systems- (i) colorimetric or chromogenic sensors (ii) Luminescent sensors. In simple term, Luminescence is basically the emission of light from electronically excited states of a substance. Depending on the nature of the excited state luminescence can be divided into two main categories —fluorescence (emission from singlet excited states) and phosphorescence (emission from triplet excited states).[1.13] However, fluorescence has occupied the majority of the area related to chemo-sensing over the years with remarkable growth in the use of fluorescence in the broad area of biological and chemical sciences as a primary tool. Hence it would be rational to briefly have a close look on the background and progress in using fluorescence technology as a sensing tool.

1.2. Evolution of Fluorogenic Probes: A Comprehensive Overview

1.2.1. Prologue:

The first observation of fluorescence was reported by Sir John Frederick William Herschel in 1845 and it was from a quinine solution in sunlight. In the middle of the 19th century G. Stokes reported that the fluorescence typically occurs at lower energies or longer wavelengths than that of absorption or excitation.[1.14] This photo-physical phenomenon is known as ‘‘Stokes shift’’ which introduced the conceptual basis of fluorometric analysis. In 1923, Harvey was first to report the use of luminescence as an analytical tool wherein he reported the minimum concentration of a light-emitting biological dye (found in some organisms) luciferin[1] required to detect visible light.[1.15] Later, Sousa and Larson developed some functionalized naphthalene crown-ether ligands as the effective fluorescent chemo-sensors for alkaline metal ion.[1.16] In early 1980s, Tsien *et al.* reported the synthesis of the first fluorescent chemosenor for calcium and demonstrated that molecular recognition event could generate detectable fluorescence signal.[1.17-1.18]Since then an enormous effort has been made to design new fluorescent sensors. However, in 1994, Czarnik first articulated the classical design of fluorescence chemosensors or probes wherein he defined the fluorescent chemosensor as an abiotic molecular device comprised of a binding site, a fluorophore and a mechanism that correlates both.[1.19] Basically, the design, synthesis and application of fluorescent and/or colorimetric probes capable of detecting specific target analytes (metal ions or anions or neutral species), especially in a extreme and complicated environment, is related to a vast and strong research area involving organic, inorganic, analytical and physical chemistry, all of them converging into the multidisciplinary field of supramolecular chemistry. Hence, in the last decades, the chemistry of sensor materials has entered a phase

wherein the creation is going further than pure research in chemistry.[1.20] Moreover, use of chemosensor devices offered the opportunity to avoid classical costly and difficult analytical methodologies for the *in situ*, real time detections as well as quantification of analytes to reduce the analytical cost largely. In this rapidly developing world economy it is crucial to develop new chemosensors; especially which can be directly applied in process control, food control, food analysis and environmental monitoring, medical diagnosis and treatment, and many other interrelated disciplines chemistry, biology, medicine, military security, new materials, nano-devices and environmental science.[1.21–1.26] However, there is an urgent need to improve the efficiency of specific sensing systems and make them more sophisticated and user friendly so that it could be used extensively in a more complex matrix for more specialized detection purpose. Several important analytes wide-ranging from metal ions to anions to neutral molecles have occupied the centre stage of chemo-sensing in their own rights which may directly impact environment, human life and development.

1.2.2. Advantages of fluorescence based probes over other sensing systems:

Especially, the fluorescence-based sensing probes are advantageous over other sensing systems for the detection of biological species as they can render rapid, non-invasive, temporal and sensitive detection of target analytes.[1.27–1.35] Fluorescent probes not only provide valuable insights in understanding physiological alterations in pathological settings but also serve as useful tools for the development of personalized medicine and targeted therapies. Moreover, the fine instrument manipulability, commercial availability, lower detection limit, and in situ and in vivo detection ability added far more glamour to the technique to be used in biological and environmental sciences.[1.36–1.40] Hence, in recent years, numerous fluorescent chemo-sensors are developed extensively for their potential applications in environmental detection, molecular catalysis, and biological fluorescence imaging, etc. Fluorescent sensing and imaging of biologically and environmentally significant chemical species has been emerged as a most important and fast developing field in recent time with the improvement of confocal microscopy and optical imaging techniques.

1.2.3. Challenges to overcome for an ideal chemo-sensor:

An ideal chemosensor must satisfy a demanding set of criteria depending on its purpose of utilization. For example a chemosensor functioning *in vitro* or *in vivo* should fulfill certain criteria depicted in **Scheme 1.2**, which may be different from the criteria require to effectively sense the same target analyte in an environmental sample.

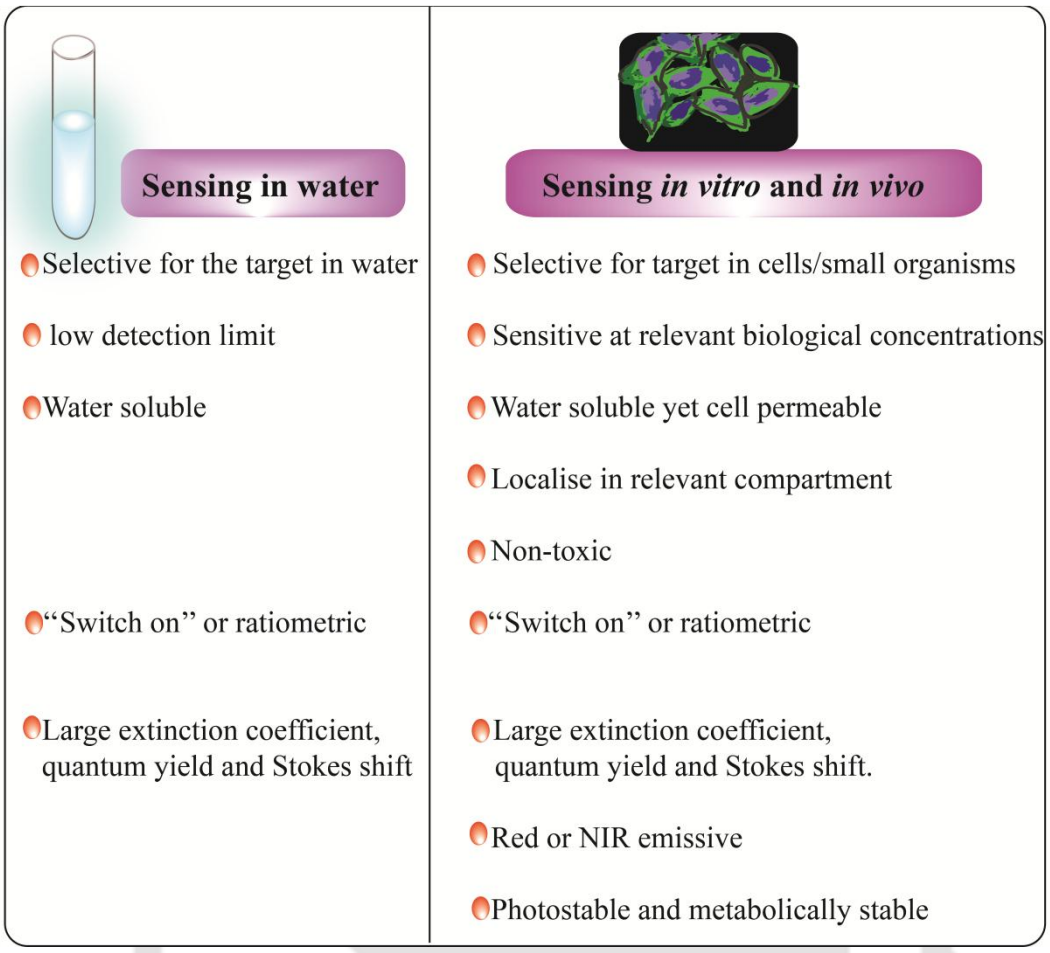

Scheme 1.2: Design criteria for sensors *versus* sensing probes *in vitro* and *in vivo*

A close look at **Scheme 1.2** clearly suggests that an imaging agent must have some additional qualities than a sensor. Key challenges including (i) suitable choice of fluorophore, (ii) introducing an effective switching mechanism and (iii) effectiveness of the probe in biological environment, are needed to overcome for designing an efficient fluorescent probe.

1.2.4. Strategies to design and develop fluorescent chemo-sensors:

As chemosensors are mostly applied in food analysis, process control, environmental monitoring, medical diagnosis, and many other disciplines, a thorough understanding of the sensing mechanism at the molecular level can be helpful to elucidate and improve the design of fluorescent chemosensors to develop more sophisticated sensing systems.[1.41–1.43] Now a days, chemists have adopted a rational approach to design more advanced chemical sensors by utilizing the principles of supramolecular chemistry.[1.43–1.44] The integration of chemosensors into a real macroscopic sensory device without any loss of important properties such as sensitivity and selectivity further upgraded the applicability. With the continuous progress, newer application strategies based on sol–gel materials, polymers, micelle aggregates, silica

nanoparticles, glass and gold surfaces, quantum dots or magnetic nanoparticles have emerged.[1.45–1.47] It might be highlighted that fluorescence spectroscopy itself made the fluorescent chemosensors unique, rightly so, because it does not require any reference and it consume no analytes; and thus becomes one of the most significant sensing tools. Hence basically, by modifying three basic constituents- the receptor unit, the signalling unit and the spacer units, different sensing strategies can be outlined. Based on the sensing approaches fluorescent sensor could be broadly divided into four categories – (a) Turn Off; (b) Turn On; (c) ratio-metric and (d) chemodosimeter (**Scheme 1.3**).

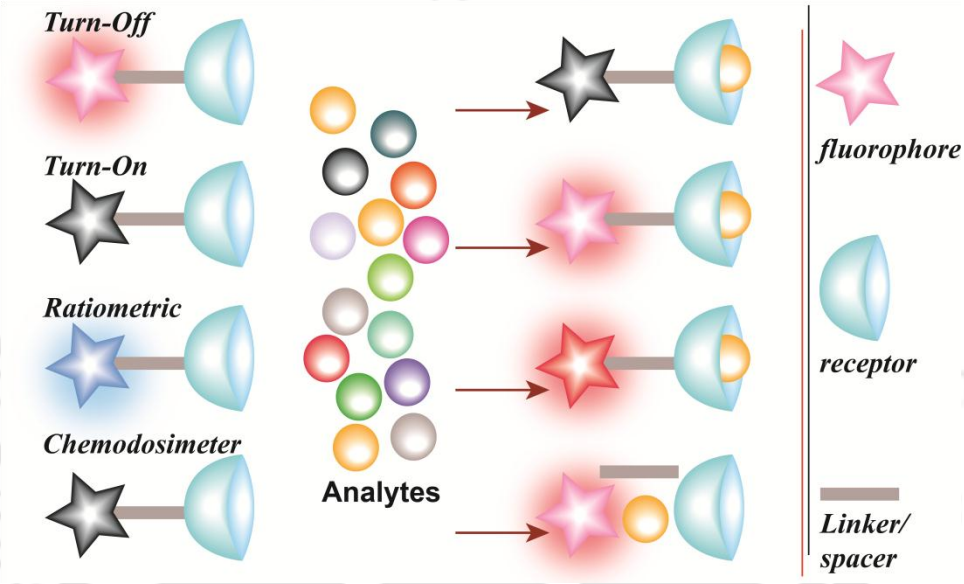

Scheme 1.3: Different types of fluorescent chemosensors.

However, light-up probes are always much more attractive due to their reduced false-positive responses as compared to their turn-off counterparts. Hence much more focus has been shifted towards developing turn-on fluorescent probes rather than designing turn-off sensors. On the other hand, ratiometric sensors[1.48–1.49] can provide exact quantification of the target analyte by measuring the emission response from the active signaling moiety against that of the 'constant' fluorophore part. Similarly, chemodosimeters have grabbed the attention of many analytical chemists as it can offer extremely high selectivity and sensitivity compared to coordination-based sensors. In this thesis we have exclusively designed several fluorogenic probes which have covered all the mentioned strategies (Turn On; ratio-metric and chemodosimeter) having beneficial sensing attributes.

However, the sensing strategies always need to be correlated with some particular photoluminescence mechanism to ensure expected fluorescence signal. In this context, to

achieve effective fluorescence sensing, a number of strategies, including photoinduced electron transfer (PET), intramolecular charge transfer (ICT), metal– ligand charge transfer (MLCT), twisted intramolecular charge transfer (TICT), electronic energy transfer (EET), and fluorescence resonance energy transfer (FRET), and excimer/exciplex formation have long been utilized extensively.[1.50–1.60] Although a wide array of fluorescent bio-probes have been developed via aforementioned strategies, they usually suffer from the notorious aggregation-caused quenching effect, which prohibits them from being used at high concentrations that leads to reduced fluorescence and compromised sensitivity. However, as mentioned earlier amongst the many fluorescent probes, turn-off probes have disadvantage in terms of generating false-positive responses whereas the light-up probes always produce more reliable responses. Also, only those chemo-sensors, capable of working in aqueous medium or in physiological condition, can readily be applied for biological studies. Hence, in recent time a lot more effort has been invested on designing advanced optical probes that can tackle these important issues. Therefore, with the rapid development of supramolecular chemistry, very recently a novel class of fluorogenic molecules with aggregation-induced emission (AIE) characteristics based on conformational restriction has sparked intense research interest in the design and synthesis of AIE probes for biosensing and imaging applications.[1.61–1.65] Unlike the conventional fluorophores, AIE fluorogens (AIEgens) are nearly non-emissive in the molecular state but emit strongly in the aggregated state, which conveniently helped in overcoming the aggregation-caused quenching effect. Hence, designing AIE active probes, to study their applications in sensing of target analytes, has got huge attention of the analytical chemists.

Besides considering the photo-physical mechanism in designing the fluorogenic probe it is equally important to monitor the reaction mechanisms or chemical events to achieve the desired sensing outcome. Literature review suggests that the detection of analyte by the chemo-sensors is generally achieved by one of the following reaction mechanisms: (1) protonation & deprotonation; (2) complexation; (3) cleavage and formation of covalent bonds; and (4) redox reactions. However, in recent times many examples have been come forth wherein these chemical events can simultaneously operate in a chemosensor to govern the sensing outcome. Especially after the exploration of AIE active probes it has been often observed that these chemical events could couple with aggregation phenomenon to lead the optical fate of the probe. The work involved in this thesis discusses design, synthesis and application of sensor molecules which encompassed most of the above mentioned reaction mechanisms.

1.3. Recent Developments in the Field of Optical Sensing: A Thorough Literature Review

The enormous demand of low cost sensor devices with high reliability and efficiency prompts the researchers to invest more and more effort in this field which is ultimately resulting in some of the novel sensing strategies. Moreover, exploring the newer sensing mechanisms introduced some new principles which enriched the wisdom of chemical science as a whole. Hence, it is necessary to have a close look on the current advancement in the field of optical chemo-sensing, before confronting the challenges ahead and articulating the probable improvements that can be made in developing newer fluorogenic and/or chromogenic sensing probes. A brief discussion of the recent advancements in the field including most of the aforementioned reaction mechanisms or chemical events (protonation & deprotonation; complexation; and cleavage and formation of covalent bonds) has been presented below.

1.3.1. Protonation & deprotonation based chromogenic and fluorogenic probes:

Monitoring pH changes is essential for studying various important physiological and pathological processes. Protonation & deprotonation based chromogenic and fluorogenic probes mainly contribute in developing the pH sensors. Fan *et. al* recently developed two novel vis-NIR pH probes[1.66] **I_1** and **I_2,** based on styrylcyanine which can response to acidic pH (**Figure 1.1**). The probes displayed high fluorescence in acidic media but remained non-fluorescent in neutral as well as in basic environments. The highly sensitive pH responsive probes **I_1** and **I_2** could display large Stokes shift to avoid native fluorescence from cellular species. Moreover, high selectivity, photostability, fine reversibility and low cytotoxicity of **I_1** and **I_2** facilitated the intracellular pH imaging. However, lower solubility **I_1** and **I_2** in aqueous solution in comparison with the traditional pH sensitive molecules raises concern about their potential applications *in vivo*.

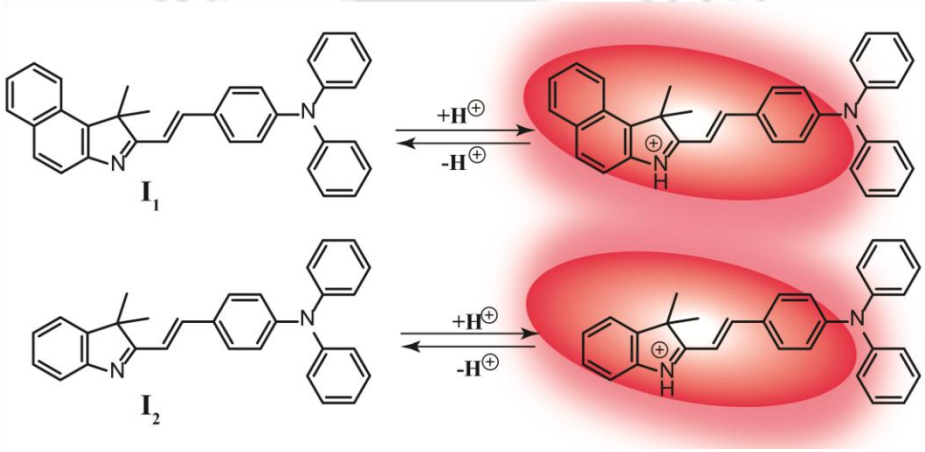

Figure 1.1: Sensing mechanism of the pH responsive probes **I_1** and **I_2**.

Tang and co-workers also have recently designed and synthesized a heteroatom-containing organic fluorophore (**I_3**), from carbazole, pyridine and diphenylethene building blocks, which can exhibit both intramolecular charge transfer (ICT) as well as aggregation-induced emission (AIE) characteristics (**Figure 1.2**).[1.67] Its emission can be reversibly switched between blue and dark states by repeated protonation and deprotonation which allows it to work as an efficient pH sensor in both solution and the solid state. Incidentally **I_3** can also act as a chemosensor for detecting acidic and basic organic vapors.

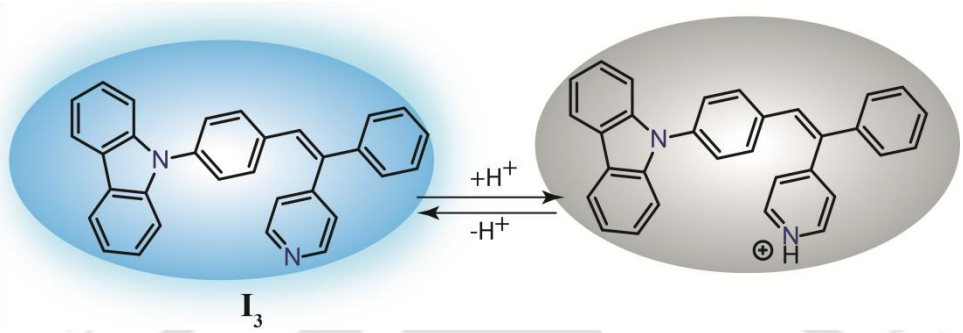

Figure 1.2: Reversible transformation of **I_3** by repeated protonation and deprotonation.

A protonation & deprotonation based chromogenic and/or fluorogenic probe could be utilized sometimes as an indirect sensor for other analytes. For example, Tang and colleagues have recently reported a pyridinyl-functionalized tetraphenylethylene fluorogen (**I_4**) for specific sensing of trivalent cations. The AIE-active probe **I_4**, demonstrated colorimetric as well as ratiometric fluorescence responses to trivalent metal cations (M^{3+}, M = Cr, Fe, Al) over a variety of mono and divalent metal cations in ethanol-water mixed solvent (**Figure 1.3**).[1.68]

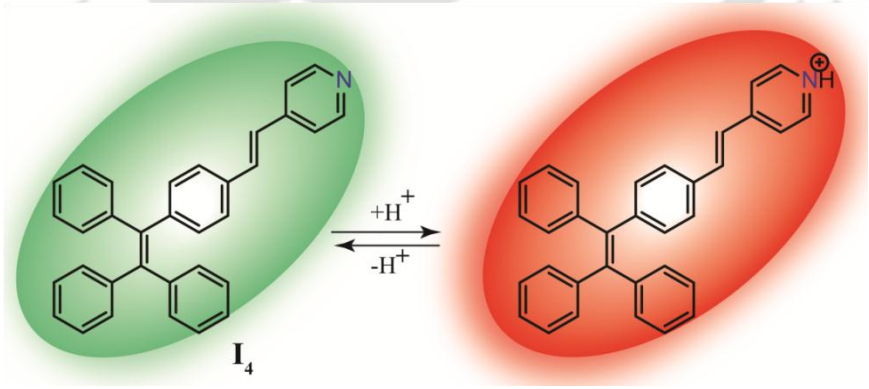

Figure 1.3: Sensing of trivalent metal ions by **I_4** through protonation.

The authors elucidated the sensing mechanism as a consequence of the protonation of the fluorogenic probe **I_4** in presence of M^{3+}. They proposed that higher charged M^{3+} has intensively

hydrolyzed in water to generate H^+ in the mixed aqueous solvent, which in turn facilitated the protonation of **I_4** in presence of M^{3+}. Lower, K_{sp} values for $M(OH)_3$ compared to other hydroxides $M(OH)_n$ (M=1 and 2) has been credited for the generation of H^+ according to the master equation-

$$M^{3+} + xH_2O \rightleftharpoons M(OH)_x^{3-x} + xH^+$$

The colorimetric (blue to red) and ratiometric characteristics of the fluorescent probe might offer advantages of using this sensor in terms of naked eye detection and biological application respectively.

1.3.2. Complexation based chromogenic and fluorogenic probes:

Generally there are two different types of complexation-based chromogenic and fluorogenic probes: one involves direct complexation approach, and the other follows competitive displacement complexation strategy (**Scheme 1.4**). In direct complexation approach, receptor unit of the probe is covalently linked with the signalling unit and it forms strong complex with target analyte through coordination or electrostatic interaction, or hydrogen bonding (**Scheme 1.4**). This strategy usually offers the advantages like rapid spectroscopic response and good reversibility, which are important to monitor the dynamic change in the analyte concentration. On the contrary, in case of competitive displacement complexation, the receptor is not covalently linked with the signalling unit (reporter); instead, it forms a complex (molecular ensemble), which serves as an active probe. Basically, in this case target analyte interacts with the receptor-reporter ensemble due to the stronger affinity of the analyte towards the receptor, resulting in the release of the reporter to enable the spectroscopic signal (**Scheme 1.4**). Complexation-based probes are frequently influenced by the change in pH of the sensing medium due to the presence of electronegative atoms in the ligands with different protonation states. Thus a pH buffer is often required as the sensing medium in regulating detection system. However, the key issue for designing complexation-based chromogenic and fluorogenic probes remains to be constructing a sensing system that is highly selective and specific to the target analyte. Moreover, an efficient complexation based probe must be able to overcome the interference of other analytes having similar chemical properties (e.g., Mg^{2+} vs Ca^{2+}, Ag^+ vs Hg^{2+}, and Cd^{2+} vs Zn^{2+}). Hence, both direct complexation approach, and competitive displacement complexation strategy requires several important issues to deal with before acting as a chemo-sensor.

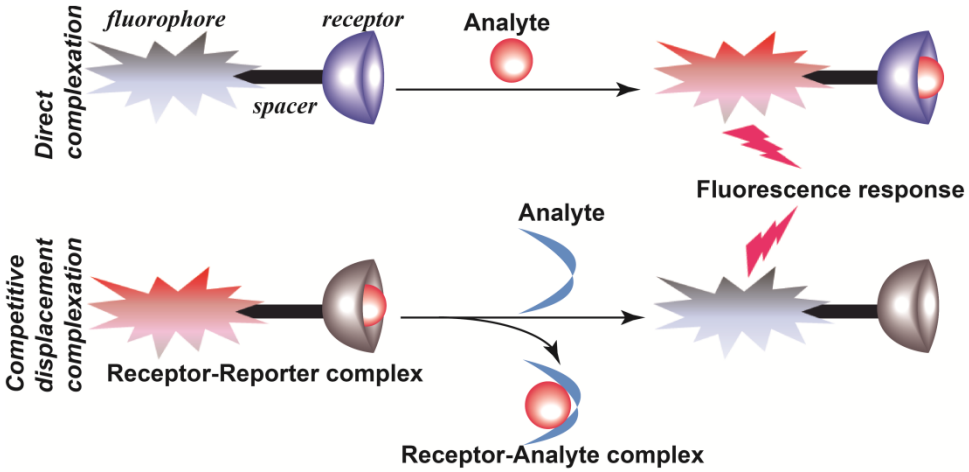

Scheme 1.4: Different types of complexation- based chemosensors.

However, recent advancement in designing chromogenic and fluorogenic probes, especially after the extensive study of AIE phenomenon, reveals that sometimes complexation-based sensors undergo aggregation in solution as well as in solid state and the complexation along with aggregation simultaneously become operational to dictate the sensing outcomes. All these aspects with recent examples have been discussed in detail below.

Direct complexation approach:

In general, chromogenic and fluorogenic probes for metal ions (Ca^{2+}, Zn^{2+}, Cu^{2+}, Hg^{2+}, etc.) are developed using direct complexation approach. Selectivity of a chemosensor designed by a direct complexation approach mainly depends on : (1) suitable match of ring/cavity size for a given ion (e.g. crown ethers with different ring sizes for alkali and alkaline earth metal ions); (2) formation of stable five- and six-membered ring complexes with metal ions (e.g. the probes with EGTA (ethylene glycol tetraacetic acid) moiety for Ca^{2+}); and (3) soft-hard acid-base principle, such as the soft sulfur-containing receptors with high affinity for soft metal ions (e.g., Ag^{+} and Hg^{2+}). However, it is necessary to combine a photophysical process like photoinduced electron transfer (PET), internal charge transfer (ICT), or fluorescence resonance energy transfer (FRET) with the complexation process to translate analyte binding into a spectroscopic signal. Recently, Das and co-workers developed a rhodamine-diformyl p-cresol conjugate (**I_5**) which can act as a selective fluorometric and colorimetric sensor for Al^{3+} based on the FRET mechanism.[1.69] A strong 2:1 complex formation between **I_5** and Al^{3+} was attributed to the high selectivity of the probe. Interestingly, the interaction of **I_5** with Al^{3+} was elucidated through time-dependent PET−CHEF−FRET processes (**Figure 1.4**). Additionally, the probe displayed tunable absorbance and emission with varying pH.

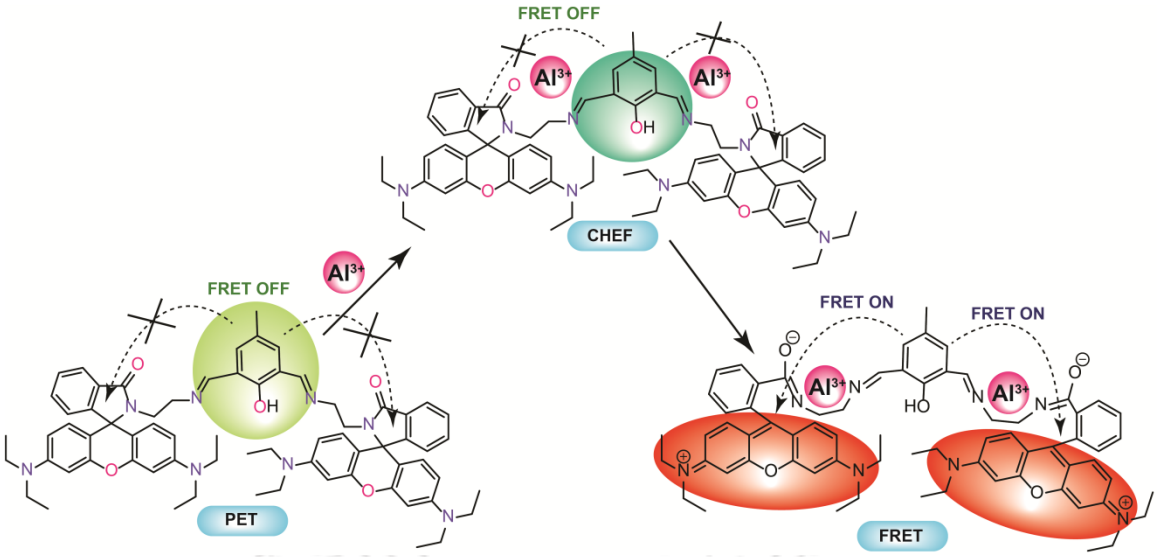

Figure 1.4: Sensing mechanism of the Al^{3+} sensor $\mathbf{I_5}$.

Cao *et. al.* also developed a 6-hydroxyindole BODIPY based Schiff-base probe ($\mathbf{I_6}$) in recent past. $\mathbf{I_6}$ rendered highly selective colorimetric as well as NIR turn-on fluorescence responses towards Zn^{2+} in solution (**Figure 1.5**).[1.70] The highly selective turn-on fluorescence response of the probe $\mathbf{I_6}$ in the NIR region (680 nm) towards Zn^{2+} was attributed to the coordination of $\mathbf{I_6}$ with Zn^{2+}. Strong Zn^{2+} binding with the Schiff-base ligand on the basis of the CHEF effect resulted in the deprotonation of the phenol group which in turn made the C=N bond rigid and enabled the high turn-on fluorescence (**Figure 1.5**). Very little interference from Cd^{2+} further underlined the specific detection ability of the probe. Moreover, the attractive NIR emission of the cell-permeable probe $\mathbf{I_6}$ offered several advantages such as deep light penetration and weak auto fluorescence of biological tissues; which helped in exploring the probe for bio-imaging of Zn^{2+}.

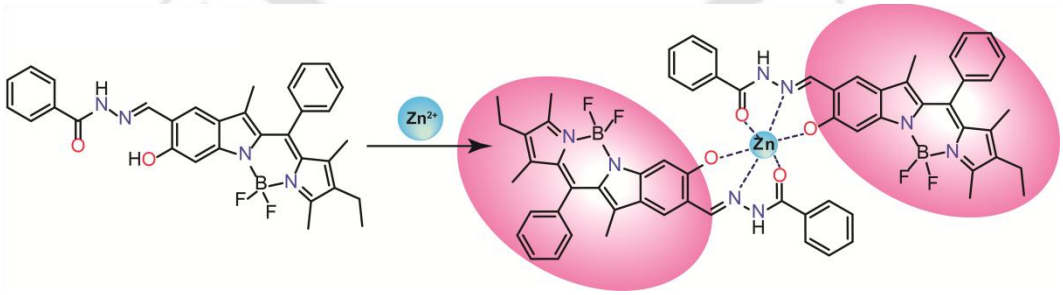

Figure 1.5: Sensing mechanism of the Zn^{2+} sensor $\mathbf{I_6}$.

Competitive displacement complexation approach:

As mentioned earlier, in case of competitive displacement complexation, a receptor-reporter ensemble/complex is used as an active probe. The receptor selectively binds with the target

analyte more strongly than the reporter which leads to the subsequent release of the reporter and as a result, produces the spectroscopic signal. Several sensing systems have been developed in recent past based on competitive displacement complexation strategy for detecting specific analytes. More often it has been observed that a particular ligand can sense a specific metal ion by direct complexation approach and then the in-situ generated metal-ligand complex can be used subsequently for detecting a specific analyte (mostly anion) through competitive displacement complexation strategy. For example, Kar *et. al.* designed a rhodamine B-indole based Schiff base ligand (**I_7**) that can selectively bind with Cu^{2+} and hence can sense Cu^{2+} through direct complexation approach (**Figure 1.6A**).[1.71] Subsequently the Cu^{2+} complex of the ligand has been used as an active probe to sense sulfide (S^{2-}) ion wherein the stronger binding affinity of S^{2-} towards Cu^{2+} resulted in the formation of CuS and released the free ligand (reporter) to enable the spectroscopic response (**Figure 1.6A**).

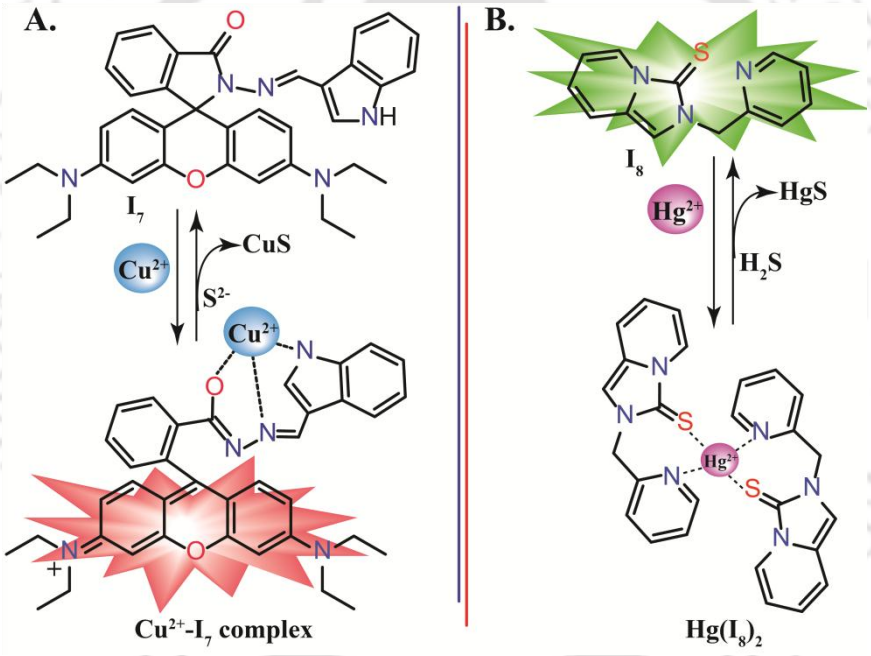

Figure 1.6: Mechanism of sulfide sensing using (A) Cu^{2+} complex of **I_7** and (B) Hg^{2+} complex of **I_8**.

Similarly, Ma *et. al.* has also reported an imidazolethione based turn-on fluorescent probe for the detection of hydrogen sulfide using competitive displacement complexation strategy (**Figure 1.6B**).[1.72] As Hg^{2+} could rapidly react with sulfide to form a more stable product compared to other organic ligands, a Hg^{2+} complex of an imidazolethione compound, 2-(pyridin-2-ylmethyl)imidazo[1,5-a] pyridine-3(2H)-thione (**I_8**) was designed and synthesized by the researchers for the sensing purpose. Interestingly, **I_8** was found to be highly fluorescent in nature, though it becomes non-fluorescent after forming a 1:2 metal-ligand complex with Hg^{2+}. Hence, they used Hg complex of the ligand; $Hg(I_8)_2$ as the active probe to sense H_2S (**Figure**

1.6B). H_2S reacted with the metal center, Hg^{2+} rapidly to form stable HgS and released the fluorophore $\mathbf{I_8}$ to display intense turn-on fluorescence response (**Figure 1.6B**).[1.72]

However, sometimes this approach follows a slightly modified strategy which does not fully comply with the typical criteria of the competitive displacement complexation. In those cases instead of displacement of the receptor-analyte complex; a reporter-receptor-analyte complex formation takes place, which actually leads to the spectral outcome.

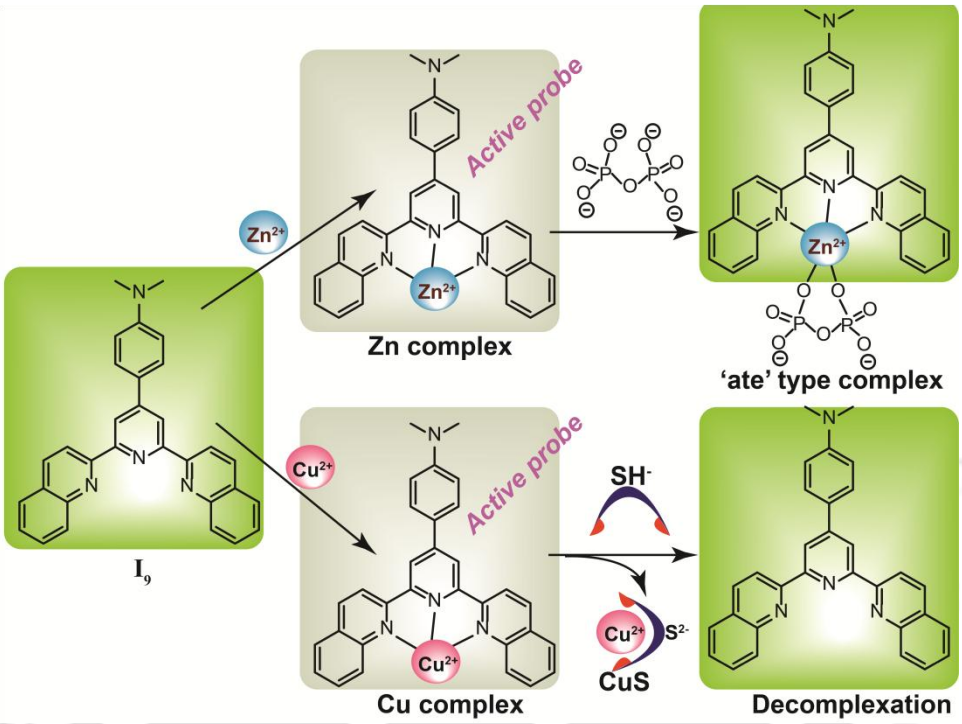

Figure 1.7: Sensing of sulfide and pyrophosphate using Cu-complex and Zn-complex of $\mathbf{I_9}$ respectively.

For example, Liang and co-workers recently reported a pyridine−biquinoline−Cu^{2+} complex and a pyridine−biquinoline−Zn^{2+} complex for the sensing hydrogen sulfide and pyrophosphate respectively in aqueous buffer and in live cells (**Figure 1.7**).[1.73] The designed ligand, pyridine−biquinoline derivative ($\mathbf{I_9}$) was itself highly fluorescent in nature, which formed non-fluorescent, stable 1:1 complexes with Zn^{2+} and Cu^{2+} respectively. Thereafter, $\mathbf{I_9}$-Cu^{2+} complex acted as an active turn-on fluorescent probe for the specific detection of H_2S following a typical competitive displacement complexation strategy wherein the formation of more stable CuS led to the release of the free ligand to render high turn-on fluorescence response (**Figure 1.7**). However, even though the $\mathbf{I_9}$-Zn^{2+} complex acted as an active turn-on fluorescent probe for the specific detection of PPi; it did not follow a typical competitive displacement complexation approach. Instead of displacement of a Zn-PPi complex, $\mathbf{I_9}$-Zn^{2+} formed an 'ate' type complex with PPi, which was actually responsible for the sensing outcome (**Figure 1.7**).[1.73]

Chelation coupled AIE based probes:

Most of the conventional fluorescent probes have high background signals. Moreover, conventional organic fluorescent probes often suffer from aggregation-caused quenching effect, which restricts their use at high concentrations. As a result these probes generally encounter with several drawbacks like reduced fluorescence and compromised sensitivity. However, the discovery of aggregation-induced emission (AIE) active fluorogenic molecules has sparked immense research interest in designing newer probes for bio-sensing and imaging applications as they can overcome the aforementioned problems. In contrast with the conventional fluorogenic probes, AIE active compounds are nearly non-emissive in the molecular state but become highly emissive upon aggregation.

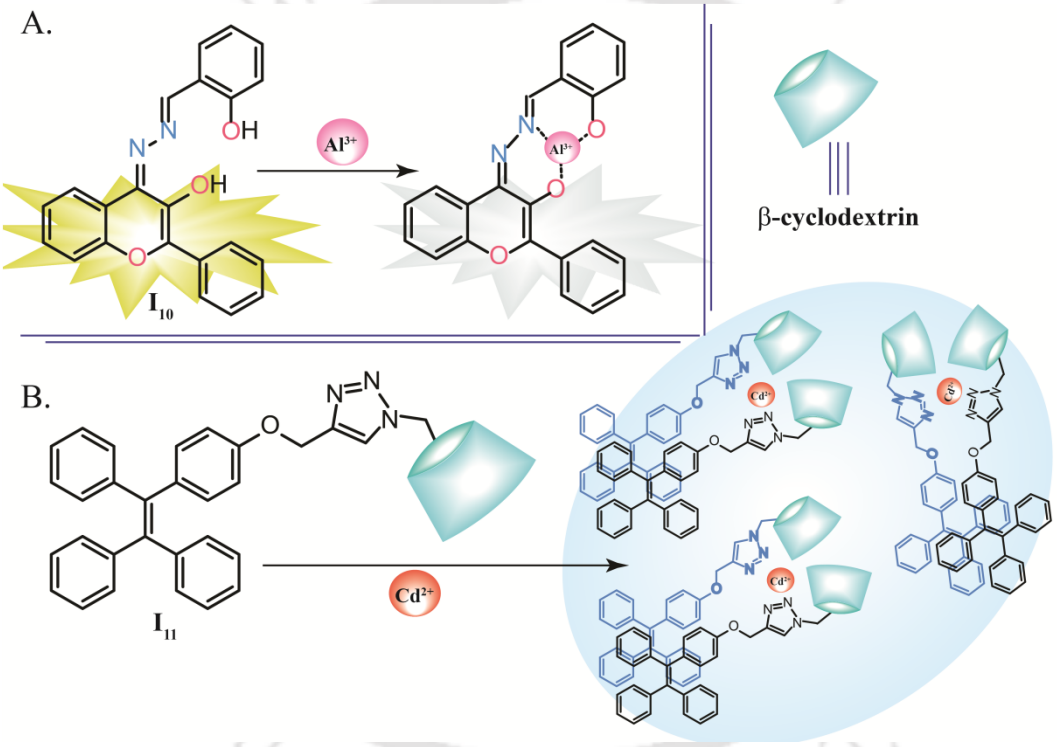

Figure 1.8: (A) Sensing mechanism of the Al^{3+} sensor $\mathbf{I_{10}}$ and (B) sensing mechanism of the Cd^{2+} sensor $\mathbf{I_{11}}$

Recently, Tong and coworkers developed a new ratiometric fluorescent chemosensor ($\mathbf{I_{10}}$) which can detect of Al^{3+} in aqueous solution (**Figure 1.8A)** based on aggregation-induced emission (AIE).[1.74] The chemosensor ($\mathbf{I_{10}}$) showed the fluorescence in its aggregated state in the absence of Al^{3+}. However, it became soluble in presence of Al^{3+} due to formation of a 1:1 chelate complex with Al^{3+} and resulted in a ratiometric fluorescence response in neutral aqueous solution. The detection limit was as low as 0.29 $\mu mol.L^{-1}$. Advantage of the AIE characteristics of the chemosensor was successfully deployed to apply the probe on test papers for simple and rapid detection of Al^{3+}. Also the Al^{3+} induced ratiometric fluorescence changes in

living cells was also achieved by the authors. More recently, Wang and coworkers synthesized a novel aggregation induced emission (AIE) active fluorogenic probe (**I_{11}**) by combining tetraphenylethene (TPE) and cyclodextrin (CD) via click chemistry (**Figure 1.8B)**.[1.75] The chemosensor exhibited excellent selective turn-on fluorescence response to Cd^{2+} in DMSO/H_2O (1/1, v/v) mixed solvent with a detection limit as low as 0.01 μM. According to the authors, the triazole bridges and CD hydroxyl groups provided interaction sites for specific coordination of the probe with Cd^{2+}. Authors proposed that complexation of the obe with Cd^{2+} led to aggregation to enable AIE behavior of the probe to show the turn-on fluorescence.

1.3.3. Chromogenic and fluorogenic probes based on cleavage and formation of covalent bonds:

Chromogenic and fluorogenic probes based on cleavage and formation of covalent bonds are commonly known as chemodosimeters. Compared with coordination-based optical sensors, chemodosimeters could offer several advantages in terms of selectivity and sensitivity. Unlike the traditional probes, chemodosimeters can be extensively used to measure cumulative amounts of dynamic analytes based on reversible/irreversible chemical processes. Within the human body, various types of chemical reactions are constantly going on under ‘‘mild’’ conditions. Hence, ‘‘mild’’ reactions based chemosensors are appropriate to highly selective as well as sensitive detection of various target analytes *in-vitro* and *in-vivo* .[1.76–1.78] As a result, recent development of some fascinating chemodosimeters or more commonly, chromogenic and fluorogenic probes based on cleavage and formation of covalent bonds with improved sensitivity and selectivity have become very important in real-world environmental and biological applications.

Recently, an oxime based fluorescent probe (**I_{12}**) was designed and synthesized by Kumar and co-authors, which could detect free as well as enzymatically generated hypochlorite with a low detection limit and high sensitivity among the various tested reactive oxygen species (**Figure 1.9A**).[1.79] The selective fluorescence response of the probe toward OCl^- was attributed to the conversion of the oxime into the nitrile oxide. The probe was also successfully utilized to monitor the endogenously produced hypochlorite in LPS stimulated cell lines, C6 glioma and BV2 microglia.

Sun *et.al.* has presented a new fluorescent probe (**I_{13}**) for specific detection H_2S by two-photon absorption and turn-on NIR emission. Interestingly the probe exhibited a selective turn-on fluorescence response for H_2S over other reactive oxygen species and biologically relevant reactive sulfide species (**Figure 1.9B**).[1.80] The sensing mechanism was involved with a typical

chemical reaction wherein the azide group of the probe reacted with H_2S to form corresponding amine which resulted in the spectral outcome. The sensor was successfully utilized to realize H_2S imaging in bovine serum, living cells and tissues as well as in living mice.

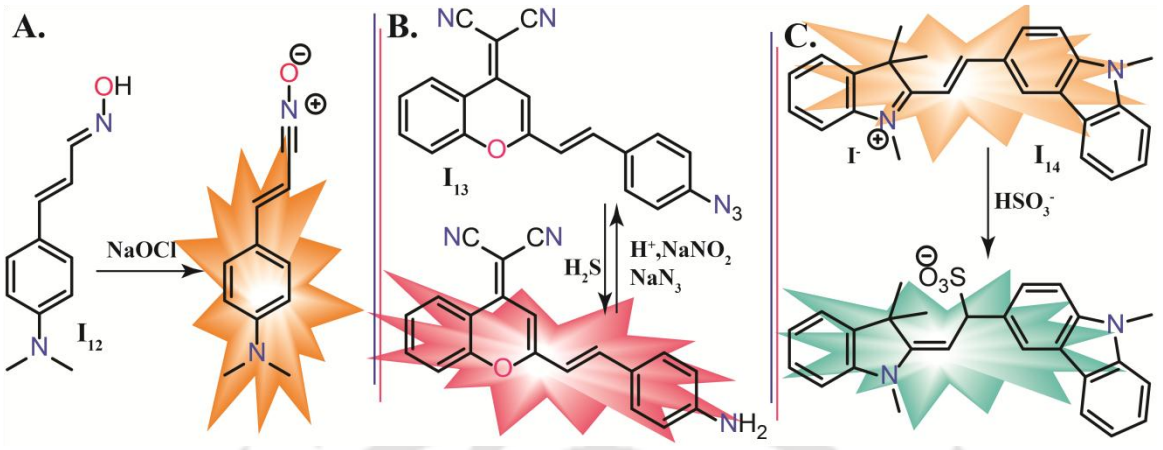

Figure 1.9: (A) Sensing mechanism of the OCl^- sensor $\mathbf{I_{12}}$ (B) sensing mechanism of the H_2S sensor $\mathbf{I_{13}}$ and (B) sensing mechanism of the HSO_3^- sensor $\mathbf{I_{14}}$.

More recently, a ratiometric fluorescent probe ($\mathbf{I_{14}}$) was developed by Liu. et al. based on the conjugate of carbazole and indolium for the effective sensing of SO_2 derivatives.[1.81] It could selectively respond to HSO_3^- over other thiol compounds (**Figure 1.9C**). More importantly it exhibited novel mitochondria-targeted ratiometric fluoresce response and hence could be used to image exogenous SO_2 derivatives.

1.4. Concluding Remarks and Objective of Thesis

The huge popularity and importance of the chemosensors, especially the optical (fluorogenic and chromogenic) chemosensors have attracted the attention of analytical chemists at large all over the world. However, the high demand of developing newer sensing probes are laid in their wide spread advantages and applications. All the above examples of the optical chemosensors and the related discussions clearly indicate that the field of chemosensing has entered an advanced phase in recent years. It is not enough anymore to just develop a system that is only selective to a specific target. Several other factors like stability of the probe, water solubility, switch-on or ratiometric response, large stokes shift and extinction coefficient, non-cytotoxicity, cell permeability etc. have become equally important to be looked into. However, as discussed earlier turn-on or ratiometric probes are always advantageous over its turn-off counter part because turn-off probes often generates false-positive responses whereas the light-up probes always produce more reliable responses. Fluorescence turn-on probes could offer the advantage of easy rapid qualitative detection of the analyte at very low-concentration whereas ratiometric

probes are more efficient as they could easily eliminate the influence of several variants (e.g., probe concentration, instrumental efficiency, and environmental conditions) by built-in correction of two emission bands, which is rather suited for accurate quantitative analysis. Hence, in this thesis most of the probes have been designed rationally to achieve either turn-on or ratiometric fluorescence responses.

A number of mechanisms, including photoinduced electron transfer (PET), intramolecular charge transfer (ICT), metal– ligand charge transfer (MLCT), twisted intramolecular charge transfer (TICT), electronic energy transfer (EET), and fluorescence resonance energy transfer (FRET), and excimer/exciplex formation have been used extensively to design fluorescent sensors. However fluorescent probes designed by these strategies often encounter drawbacks like aggregation-caused quenching effect, which bars them from being used at high concentrations and hence result in reduced fluorescence and compromised sensitivity. Recent development of a novel class of fluorogenic molecules with aggregation-induced emission (AIE) characteristics based on conformational restriction has come to the limelight and the design and synthesis of AIE probes for biosensing and imaging applications has become a hot research subject. As, unlike the conventional fluorophores, AIE fluorogens (AIEgens) emit strongly in the aggregated state, it conveniently offers the solution to overcome the aggregation-caused quenching effect. However, even though these AIE active compounds are very interesting in nature, their exact function, chemistry, physical properties, and structural variations are still not very clear. Very few AIE-gens have been reported till date which underlines the need of developing newer AIE active systems. Also to further study the nature, characteristics and properties of these AIE active probes, it is important to have extensive new research. Hence exploring the simple new fluorogenic systems capable of demonstrating AIE properties is a huge challenge. Besides developing AIE active probes, introducing some beneficial attributes such as water solubility, cell permibility etc in it are far more challenging and requires a scope of exploring novel ideas. So, a significant part of the thesis has been dealt with designing AIE active probes and their applications in sensing of target analytes.

Metal ions and common biologically as well as environmentally important anions remain to be the central targets of the mostly developed optical probes even in recent times. However, with the rapid advances in the chemical science, biology, health science and environmental science several new species (ionic as well as neutral) come to the forefront which needs to be detected using newer sensing probes. Thus, much focus has been shifted in designing optical probes such as H_2S, SO_2 derivatives, HOCl, reactive oxygen species etc. Hence, besides developing several

common metal ion and anion sensors this thesis also discusses design and synthesis of some sensing systems for detecting relatively newer target such as SO_2 derivatives. .

As mentioned in the introduction, our primary aim was to introduce sensing systems that can rapidly sense target analytes by some form of optical responses which is conspicuous by naked eye; so that even an uneducated person could identify the sensing outcomes. Hence, all of the reported probes in this thesis are purposely designed to have the inherent feature of naked eye sensing ability.

On the other hand, in general designing an effective sensing system that can selectively sense a neutral species is itself a difficult task due to the relatively weaker binding affinity as well as reactivity of the neutral guests. Moreover, if a neutral molecule comprises of two geometrical isomers then it is even more difficult to distinguish them. Hence, in this thesis, we have also worked on designing sensing system that not only can sense a neutral species but also can distinguish it from its geometrical isomer.

So in short, the focus of the thesis-work is (i) to design and synthesize new water soluble (or soluble in mixed aqueous solvent) fluorogenic and/or chromogenic probes for the optical detection of target analytes, (ii) exploring the scope of introducing new sensing mechanisms involving AIE phenomenon (iii) application of the developed sensing probes in environmental or biological samples (iv) designing fluorescent pobes to generate turn-on or ratio-metric fluorescence responses (v) designing sensing system to distinguish geometrical isomers and (vi) overall, to get sharp conspicuous optical responses, even detectable by naked eye.

References

1.1. D. Sareen, P. Kaur and K. Singh, *Coord. Chem. Rev*., 2014, **265**, 125–154

1.2. A. T. Wright and E. V. Anslyn, *Chem. Soc. Rev.*, 2006, **35**, 14.

1.3. X. Chen, T. Pradhan, F. Wang, J. S. Kim and J. Yoon, *Chem. Rev.*,2012, **112**, 1910.

1.4. J. S. Kim and D. T. Quang, *Chem. Rev.*, 2007, **107**, 3780.

1.5. R. Martinez-Manez and F. Sancenon, *Chem. Rev.*, 2003, **103**, 4419.

1.6. D. T. Quang and J. S. Kim, *Chem. Rev*., 2010, **110**, 6280.

1.7. E. M. Nolan and S. J. Lippard, *Chem. Rev.*, 2008, **108**, 3443.

1.8. M. Vendrell, D. Zhai, J. C. Er and Y. T. Chang, *Chem. Rev.*,2012, **112**, 4391.

1.9. T. Gunnlaugsson, M. Glynn, G. M. Tocci, P. E. Kruger and F. M. Pfeffer, *Coord. Chem. Rev.*, 2006, **250**, 3094.

1.10. X. Chen, Y. Zhou, X. Peng and J. Yoon, *Chem. Soc. Rev.*, 2010, **39**, 2120.

1.11. Z. Xu, S. K. Kim and J. Yoon, *Chem. Soc. Rev.*, 2010, **39**, 1457.

1.12. A. P. de Silva, H. Q. N. Gunaratne, T. A. Gunnlaugsson, T. M. Huxley, C. P. McCoy, J. T. Rademacher and T. E. Rice, *Chem. Rev*., 1997, **97**, 1515.

1.13. J. R. Lakowicz, *Principles of Fluorescence Spectroscopy*, 3rd Edition, *Springer*, 2006.

1.14. G. G. Stokes, *Philos. Trans. R. Soc. London*, 1852, **142**, 463.

1.15. E. N. Harvey, *Science*, 1923, **57**, 501.

1.16. L. R. Sousa and J. M. Larson, *J. Am. Chem. Soc.*, 1977, **99**, 307.

1.17. R. Y. Tsien, *Biochemistry*, 1980, **19**, 2396-2404.

1.18. G. Grynkiewicz, M. Poenie and R. Y. Tsien, *J. Biol. Chem*., 1985, **260**, 3440.

1.19. A. W. Czarnik, *Acc. Chem. Res*., 1994, **27**, 302.

1.20. C. Lodeiro, J. L. Capelo, J. C. Mejuto, E. Oliveira, H. M. Santos, B. Pedras and C. Nunez, *Chem. Soc. Rev.*, 2010, **39**, 2733.

1.21. M. E. Germain and M. J. Knapp, *Chem. Soc. Rev*., 2009, **38**, 2543.

1.22. C. Bazzicalupi, A. Bencini, S. Biagini, A. Bianchi, E. Faggi, C. Giorgi, M. Marchetta, F. Totti and B. Valtancoli, *Chem.–Eur. J.*, 2009, **15**, 8049.

1.23. L. Prodi, F. Bolleta, M. Montalti and N. Zaccheroni, *Coord. Chem. Rev*., 2000, **205**, 59.

1.24. F. Pina, M. A. Bernardo and E. Garcia-Espana, *Eur. J. Inorg. Chem*., 2000, 2143.

1.25. V. Amendola, L. Fabbrizzi, F. Foti, M. Liccheli, C. Mangano, P. Pallavicini, A. Poggi, D. Sacchi and A. Taglietti, *Coord. Chem. Rev*., 2006, **250**, 273.

1.26. G. Astray, C. Gonzalez-Barreiro, J. C. Mejuto, R. Rial-Otero and J. Simal-Ga´ ndara, *Food Hydrocolloids*, 2009, **23**, 1631.

1.27. B. C. Dickinson, D. Srikun and C. J. Chang, *Curr. Opin. Chem. Biol*., 2010, **14**, 50.

1.28. H. Kobayashi, M. Ogawa, R. Alford, P. L. Choyke and Y. Urano, *Chem. Rev*., 2010, **110**, 2620.

1.29. R. W. Sinkeldam, N. J. Greco and Y. Tor, *Chem. Rev*., 2010, **110**,2579.

1.30. Y. Zhou and J. Yoon, *Chem. Soc. Rev*., 2012, **41**, 52.

1.31. Y. Zhou, Z. Xu, and J.Yoon, *Chem. Soc. Rev.*, 2011, **40**, 2222.

1.32. Y. Zhou, J. F. Zhang and J. Yoon, *Chem. Rev.*, 2014, **114**, 5511.

1.33. H. S. Jung, X. Chen, J. S. Kim and J. Yoon, *Chem. Soc. Rev*., 2013, **42**, 6019.

1.34. J. F. Zhang, Y. Zhou, J. Yoon and J. S. Kim, *Chem. Soc. Rev.*, 2011, **40**, 3416.

1.35. Y. Zhou and J. Yoon, *Chem. Soc. Rev*., 2012, **41**, 52.

1.36. *Fluorescent Chemoprobes for Ion and Molecule Recognition*, ed. A. W. Czarnik, American Chemical Society, Washington, D.C., 1993.

1.37. B. Valeur, *Molecular Fluorescence: Principles and Applications*,Wiley-VCH, Weinheim, 2001.

1.38. H. Kobayashi, M. Ogawa, R. Alford, P. L. Choyke and Y. Urano, *Chem. Rev*., 2010, **110**, 2620.

1.39. R. Y. Tsien, *Annu. Rev. Biochem.*, 1998, **67**, 509.

1.40. T. Terai and T. Nagano, *Curr. Opin. Chem. Biol*., 2008, **12**, 515.

1.41. T. D. Ashton, K. A. Jolliffe, and F. M. Pfeffer, *Chem. Soc. Rev.***,** 2015., **44**, 4547.

1.42. P. J. Jiang and Z. J. Guo, *Coord. Chem. Rev*., 2004, **248**, 205.

1.43. T. W. Bell and N. M. Hext, *Chem. Soc. Rev.*, 2004, **33**, 589.

1.44. L. Basabe-Desmonts, D. N. Reinhoudt and M. Crego-Calama, *Chem. Soc. Rev*., 2007, **36**, 993.

1.45. *Chem. Rev*., 2000; **100**, special issue on Chemosensors.

1.46. *Comprehensive Supramolecular Chemistry*, ed. J. M. Lehn, J. L. Atwood, J. E. D. Davies D. D. MacNicol, F. Vogtle and D. N. Reinhoudt, Pergamon, Oxford, UK, 1996, vol. 10.

1.47. E. F. Mancin Rampazzo, P. Tecilla and U. Tonellato, *Chem.–Eur. J.*, 2006, **12**, 1844.

1.48. A. Demchenko, *J. Fluoresc*., 2010, **20**, 1099.

1.49. J. Fan, M. Hu, P. Zhan and X. Peng, Chem. Soc. Rev., 2013, 42, 29.

1.50. T. Gunnlaugsson, H. D. P. Ali, M. Glynn, P. E. Kruger,G. M. Hussey, F. M. Pfeffer, C. M. D. Santos and J. Tierney, *J. Fluoresc*., 2005, **15**, 287.

1.51. J. F. Callan, A. P. de Silva and D. C. Magri, *Tetrahedron*, 2005, **61**, 8551.

1.52. B. Valeur and I. Leray, *Coord. Chem. Rev*., 2000, **205**, 3.

1.53. Z. C. Xu, J. Yoon and D. R. Spring, *Chem. Soc. Rev*., 2010, **39**, 1996.

1.54. B. Daly, J. Ling and A. P. de Silva, *Chem. Soc. Rev*., 2015,**44**, 4203.

1.55. Z. Liu, W. He and Z. Guo, *Chem. Soc. Rev.*, 2013, **42**, 1568.

1.56. Q. Zhao, F. Y. Li and C. H. Huang, *Chem. Soc. Rev*., 2010, **39**, 3007.

1.57. M. Ren, B. Deng, X. Kong, K. Zhou, K. Liu, G. Xu and W. Lin, *Chem. Commun*., 2016,**52**, 6415.

1.58. K. E. Sapsford, L. Berti and I. L. Medintz, *Angew. Chem., Int. Ed*., 2006, **45**, 4562.

1.59. H. J. Carlson and R. E. Campbell, *Curr. Opin. Biotechnol*., 2009, **20**, 19.

1.60. C. Lodeiro and F. Pina, *Coord. Chem. Rev*., 2009, **253**, 1353.

1.61. J. Luo, Z. Xie, J. W. Y. Lam, L. Cheng, H. Chen, C. Qiu, H. S. Kwok, X. Zhan, Y. Liu, D. Zhuc and B. Z. Tang, *Chem. Commun*., 2001, 1740.

1.62. Y. Hong, J. W. Y. Lam and B. Z. Tang, *Chem. Soc. Rev*., 2011, **40**, 5361-5388 and references therein.

1.63. J. E. Kwon and S. Y. Park, *Adv. Mater*., 2011, **23**, 3615.

1.64. J. Zhao, S. Ji, Y. Chen, H. Guo and P. Yang, *Phys. Chem. Chem. Phys*., 2012, **14**, 8803-8817.

1.65. J. Mei, N. L. C. Leung, R. T. K. Kwok, J. W. Y. Lam and B. Z. Tang, *Chem. Rev*., 2015, **115**, 11718.

1.66. L. Fan, Y.-J. Fu, Q.-L. Liu, D.-T. Lu, C. Dong and S.-M. Shuang, *Chem. Commun*., 2012, **48**, 11202.

1.67. Z. Yang, W. Qin, J. W. Y. Lam, S. Chen, H. H. Y. Sung, I. D. Williams and B. Z. Tang, *Chem. Sci*., 2013,**4**, 3725.

1.68. X. Chen, X. Y. Shen, E. Guan, Y. Liu, A. Qin, J. Z. Sun and B. Z. Tang, *Chem. Commun.*, 2013, **49**, 1503.

1.69. A. Sahana, A. Banerjee, S. Lohar, B. Sarkar, S. K. Mukhopadhyay and D. Das, *Inorg. Chem.*, 2013, **52**, 3627.

1.70. J. Cao, C. Zhao, X. Wang, Y. Zhang and W. Zhu, *Chem. Commun.*, 2012, **48**, 9897.

1.71. C. Kar, M. D. Adhikari, A. Ramesh and G. Das, *Inorg. Chem.*, 2013, **52**, 743.

1.72. F. Ma, M. Sun, K. Zhang, H. Yu, Z. Wang and S. Wang, *Anal. Chim. Acta*, 2015, **879**, 104.

1.73. Z. Hai, Y. Bao, Q. Miao, X. Yi, and G. Liang, *Anal. Chem.*, 2015, **87**, 2678.

1.74. L. Peng, Z. Zhou, X. Wang, R. Wei, K. Li, Y. Xiang and A. Tong, *Anal. Chim. Acta*, 2014, **829**, 54.

1.75. L. Zhang, W. Hua, L. Yu and Y. Wang, *Chem. Commun.*, 2015,**51**, 4298.

1.76. E. L. Que, D. W. Domaille and C. J. Chang, *Chem. Rev*., 2008, **108**, 1517.

1.77. K. Kikuchi, *Chem. Soc. Rev*., 2010, **39**, 2048.

1.78. X. Qian, Y. Xiao, Y. Xu, X. Guo, J. Qian and W. Zhu, *Chem.Commun*., 2010, **46**, 6418.

1.79. S. I. Reja, V. Bhalla, A. Sharma, G. Kaur and M. Kumar, *Chem.Commun*., 2014, **50**, 11911.

1.80. W. Sun, J. Fan, C. Hu, J. Cao, H. Zhang, X. Xiong, J. Wang, S. Cui, S. Sun and X. Peng, *Chem. Commun.*, 2013, **49**, 3890.

1.81. Y. Liu, K. Li, M.-Yu. Wu, Y.-H. Liu, Y.-M. Xie and X.-Q. Yu, *Chem. Commun.*, 2015, **51**, 10236.

Chapter 2

Experimental Section

2.1.1. General Information and Materials

All the materials for synthesis were purchased from commercial suppliers and used without further purification. The absorption spectra were recorded on a Perkin-Elmer Lamda-25 UV-visible spectrophotometer using 10 mm path length quartz cuvettes, while the fluorescence measurements were carried on a Horiba Fluoromax-4 spectrofluorometer using 10 mm path length quartz cuvettes with a slit width of 3 nm at 298 K. The mass spectra were obtained using Waters Q-ToF Premier mass spectrometer. NMR spectra were recorded on a Varian FT-400 MHz instrument and a Bruker Advance 600 MHz instrument. The chemical shifts were recorded in parts per million (ppm) on the scale. The following abbreviations are used to describe spin multiplicities in ^{1}H NMR spectra: s = singlet; d = doublet; t = triplet; q = quartet; m= multiplet

2.1.2. UV−Vis and fluorescence spectroscopic studies of L_1

Stock solutions of various ions (1×10^{-3} mol.L^{-1}) were prepared in deionized water. A stock solution of **L_1** (5×10^{-3} mol.L^{-1}) was prepared in DMSO. The solution of **L_1** was then diluted to 10×10^{-6} mol.L^{-1} with CH_3OH/aqueous HEPES buffer (5mM, pH 7.3; 9:1, v/v). In titration experiments, a quartz optical cell of 1 cm path length was filled with a 2.0 mL solution of **L_1** to which the ion stock solutions were gradually added using a micropipette. In selectivity experiments, the test samples were prepared by placing appropriate amounts of the cations stock into 2.0 mL of **L_1** solution (10×10^{-6} mol.L^{-1}). For fluorescence measurements, excitation was provided at 400 nm, and emission was acquired from 420 nm to 700 nm.

2.1.3. Detection limit for Al^{3+} and Cu^{2+} (using probe L_1)

The detection limits were calculated on the basis of the fluorescence titration (for Al^{3+}) and UV-Vis titration (for Cu^{2+}). The fluorescence emission spectrum or UV-Vis spectrum of **L_1** was measured 10 times, and the standard deviation of blank measurement was achieved. To gain the slope, the fluorescence emission at 537 nm was plotted as a concentration of Al^{3+} and absorbance at 502 nm was plotted as a concentration of Cu^{2+}. The detection limits were calculated using the following equation:

Detection limit = 3σ/k

where σ is the standard deviation of blank measurement, and k is the slope between the fluorescence emission intensity versus [Al^{3+}] or absorbance versus [Cu^{2+}].

2.1.4. Dynamic light scattering (DLS) studies (for the probe L_1)

The particle size of the $\mathbf{L_1}$-Al^{3+} aggregates was measured by dynamic light scattering (DLS) experiments on a Malvern Zetasizer Nano ZS instrument equipped with a 4.0 mW He–Ne laser operating at a wavelength of 633 nm. The samples and the background were measured at room temperature (25°C) at a scattering angle of 173°. DLS experiments were carried out with an optically clear solution of $\mathbf{L_1}$ (10 μM) in MeOH in the presence of 1 equivalent and 10 equivalents of Al^{3+} ion. The solution was equilibrated for 30 minutes before taking the measurements.

2.1.5. Atomic Force Microscope (AFM) Studies (for the probe L_1)

The overall morphology of the $\mathbf{L_1}$ was investigated from NT-MDT micro-40 AFM instrument using a semicontact mode at a scan rate of 1 Hz. To a solution of $\mathbf{L_1}$ (10 μM) in mixed aqueous-organic (H_2O/MeOH, 1:9, v/v) medium 10 equivalents of Al^{3+} was added and mixed well then it was drop-casted on a cover slip and left open to atmosphere for 12 h, followed by dessication prior to acquiring AFM images.

2.1.6. Field Emission Scanning Electron Microscope (FESEM) Studies (for the probe L_1)

The morphology of $\mathbf{L_1}$-Al^{3+} complex was ascertained in a Jeol JEM 6700 field emission scanning electron microscope (FESEM). To a solution of $\mathbf{L_1}$ (10 μM) in mixed aqueous-organic (H_2O/MeOH, 1:9, v/v) medium 10 equivalents of Al^{3+} was added and mixed well then it was drop-casted on cover slip and left open to atmosphere for 12 h, followed by dessication prior to acquiring FESEM images.

2.1.7. Cytotoxic effect on HeLa cells by L_1

The cytotoxic effect of the ligand and ligand-aluminium complex on cultured HeLa cells was determined by an MTT assay as per the manufacturer instruction (Sigma-Aldrich, MO, USA). HeLa cells were initially grown in a 25 cm^2 tissue culture flask in DMEM medium supplemented with 10% (v/v) FBS, penicillin (100 μg/mL) and streptomycin (100 μg/mL) under a humidified atmosphere of 5% CO_2 in an incubator until the cells were approximately 90%

confluent. Prior to MTT assay, cells were trypsinized and seeded into 96-well tissue culture plates at a cell-density of 10^4 cells per well and incubated with varying concentrations (12, 24, 36, 48, 60, 72, 84 and 96 μM) of the ligand, ligand-aluminium complex and the metal salt solution made in methanol solvent (0.1% v/v) and incubated for a period of 24 h under 5% CO_2. Solvent control samples (cells incubated in 0.1% methanol) were also included in parallel sets. Following incubation, the growth media was carefully aspirated, and fresh DMEM containing MTT solution was added to the wells. The plate was incubated for 4 h at 37°C. Following incubation, the supernatant was collected and the insoluble colored formazan product was solubilized in DMSO and its absorbance was measured in a microtiter plate reader (Infinite M200, TECAN, Switzerland) at 550 nm. The assay was performed in six sets for each concentration of the test samples. Data analysis and determination of standard deviation was performed with Microsoft Excel 2010 (Microsoft Corporation). In the MTT assay, the absorbance for the solvent control cells was considered as 100% cell viability and the absorbance for the treated cells was compared to determine % cell viability with respect to the solvent control.

2.1.8. Cell imaging studies by L_1

HeLa cells were initially cultured in a 25 cm^2 tissue culture flask as mentioned before. Cells were then seeded into a 6 well plate and grown till 80% confluency in a CO_2 incubator at 37°C. The cells were washed thrice with sterile phosphate buffered saline (PBS) and incubated with 5.0 μM **L_1** in DMEM at 37°C for 1 h in a CO_2 incubator. The cells were again washed thrice with sterile PBS to remove the free ligand and bright field and dark field images were acquired using an epifluorescence microscope (Nikon eclipse Ti) having a filter that allowed blue light excitation at 445-495 nm. Subsequently, the cells were incubated in sterile PBS with 50 μM of aluminium chloride salt for 1 h and washed thoroughly with sterile PBS. Bright field and dark field images of the cells were again acquired in an epifluorescence microscope as mentioned before.

2.1.9. Interaction of L_1-Al^{3+} Ensemble with Calf Thymus DNA

In this experiment formation of **L_1**-Al^{3+} ensemble was initially accomplished by mixing 1.0 equivalent of the ligand with 10 equivalent of Al^{3+} solution as mentioned before. Subsequently the emission spectra were recorded by varying the concentrations of calf thymus DNA (30 μM-330 μM) which was added in appropriate amount using micropipette to the **L_1**-Al^{3+} ensemble. The fluorescence emission spectra of the samples were recorded in a spectrofluorometer in a scanning mode from 420 nm to 700 nm by setting the excitation wavelength at 400 nm.

2.1.10. Crystallizaton of L_1

A small quantity of yellow powder of **L_1** (0.027 mM) was taken in a test tube containing DCM and stirred for few minutes to obtain a clear solution. Then solution was allowed to evaporate slowly and after one week X-ray mountable needle shaped yellow colored crystals appeared at the bottom of test tube.

2.1.11. Crystallographic Refinement Details of L_1

The crystallographic data and details of data collection of **L_1** are given in **Table A2.1 (Appendix)**. In each case, a crystal of suitable size was selected from the mother liquor and immersed into silicone oil, then mounted on the tip of a glass fiber and cemented using epoxy resin. Intensity data for the all crystals were collected Mo-Kα radiation (λ = 0.71073Å) at 298(2) K, with increasing ω (width of 0.3° per frame) at a scan speed of 6 s/ frame on a Bruker SMART APEX diffractometer equipped with CCD area detector. The data integration and reduction were processed with SAINT[2.1] software. An empirical absorption correction was applied to the collected reflections with SADABS.[2.2] The structures were solved by direct methods using SHELXTL[2.3] and were refined on F^2 by the full-matrix least-squares technique using the SHELXL-97 program package.[2.4] Graphics are generated using MERCURY 3.0.[2.5] In all cases, non-hydrogen atoms are treated anisotropically. The hydrogen atoms are located on a difference Fourier map and refined. In other cases, the hydrogen atoms are geometrically fixed.

2.2.1. UV−Vis and fluorescence spectroscopic studies with L_2

Stock solutions of various analytes (1×10^{-1} mol.L^{-1}) were prepared in methanol or Millipore water depending upon the preferred solubility of the analytes chosen. Na or $(NH)_4$ or tetrabutyl ammonium (TBA) salts of various anions were chosen for the selectivity experiments which encompassed TBAF, TBACl, TBABr, TBAI, $NaNO_2$, $TBANO_3$, TBA(OAc), $TBAH_2PO_4$, NaPPi, $TBAHCO_3$, $(TBA)_2SO_4$, $TBAHSO_4$, $TBAPF_6$, $TBAClO_4$, NH_4SCN, $Na_2S_2O_3$, $Na_2S_2O_8$, $NaC_6H_7O_6$ (Na-ascorbate), Na_2SO_3 and NaSH. A stock solution of **L_2** (5×10^{-3} mol.L^{-1}) was prepared in DMSO. The solution of **L_2** was then diluted to 10×10^{-6} mol.L^{-1} with Millipore water for spectral studies by taking only 4 µL stock solution of **L_2** and making the final volume 2mL adding Millipore water. In fluorescence selectivity experiment, the test samples were prepared by placing appropriate amounts of the stock solutions of the respective anions/analytes into 2.0 mL of probe solution (10×10^{-6} mol.L^{-1}). For UV-Visible and fluorescence titration experiments another sets of anions (SO_3^{2-} and SO_4^{2-}) standard solutions having 5mM concentrations were prepared by diluting the earlier prepared stock solutions (1×10^{-1} mol.L^{-1}) in Millipore water. Quartz optical cells of 1 cm path length were filled with 1.0 mL and 2.0 mL

solutions of **L_2** for UV-Visible and fluorescence titration experiments respectively, to which the 5mM anions (SO_3^{2-} and SO_4^{2-}) stock solutions were gradually added using a micropipette. For fluorescence measurements, excitation was provided at 380 nm, and emission was acquired from 400 nm to 650 nm for usual selectivity and titration experiments. However to ascertain the ratio-metric fluorescence change in case of titration experiment with SO_3^{2-}, another excitation was provided at 580 nm, and emission was acquired from 630 nm to 800 nm. Spectral data were recorded within 1 minute after addition of the analytes.

2.2.2. Detection limit for SO_3^{2-} and SO_4^{2-} (using probe L_2)

The detection limits were calculated on the basis of the fluorescence titration. The fluorescence emission spectrum of **L_2** was measured 10 times, and the standard deviation of blank measurement was achieved. To gain the slope, the fluorescence emission at 442 nm was plotted as a concentration of SO_3^{2-} and the fluorescence emission at 511 nm was plotted as a concentration of SO_4^{2-}. The detection limits were calculated using the following equation:

Detection limit = $3\sigma/k$

where σ is the standard deviation of blank measurement, and k is the slope between the fluorescence emission intensity versus [SO_3^{2-}] or, emission intensity versus [SO_4^{2-}].

2.2.3. Dynamic light scattering (DLS) studies (for the probe L_2)

The particle size of **L_2**, **L_2**- SO_4^{2-}aggregate were measured by dynamic light scattering (DLS) experiments on a Malvern Zetasizer Nano ZS instrument equipped with a 4.0 mW He–Ne laser operating at a wavelength of 633 nm. The samples and the background were measured at room temperature (25^{o}C). DLS experiments were carried out with optically clear solutions of **L_2** (10 μM) in aqueous medium, both in the absence and presence of 20 equivalents of SO_4^{2-} to determine the change in particle size on interaction of **L_2** with SO_4^{2-}. The solution was equilibrated for 30 minutes before taking the measurements.

2.2.4. Atomic Force Microscope (AFM) Studies (for the probe L_2)

The overall morphology of the **L_2**- SO_4^{2-} aggregate was investigated from NT-MDT micro-40 AFM instrument using a semicontact mode at a scan rate of 1 Hz. To a solution of **L_2** (10 μM) in aqueous medium 20 equivalents of SO_4^{2-} was added and mixed well then it was drop-casted on a cover slip and left open to atmosphere for 12 h, followed by desiccation prior to acquiring AFM images.

2.2.5. Cytotoxicity assay (for the probe L_2)

HeLa cells (human cervical carcinoma cells) were initially cultured in a 25 cm^2 tissue culture flask in DMEM medium supplemented with 10% (v/v) FBS, penicillin (100 µg/mL) and streptomycin (100 µg/mL) under a humidified atmosphere of 5% CO_2 until the cells were approximately 80% confluent. Prior to MTT assay, cells were trypsinized and seeded into 96 well tissue culture plates at 10^4 cells per well and incubated with varying concentrations (0.5 µM-50 µM) of the probe **L_2** made in DMEM and incubated for a period of 24 h under 5% CO_2. Solvent control samples (cells incubated in 0.1% methanol) were also included in separate sets. Following incubation, the growth media was carefully removed, and fresh DMEM containing MTT solution was added to the wells. The plate was subsequently incubated for 4 h at 37°C. Following incubation, the supernatant was carefully collected and the insoluble colored formazan product was solubilized in DMSO and its absorbance was measured in a microtiter plate reader (Infinite M200, TECAN, Switzerland) at 550 nm. For each concentration of the test samples, MTT assay was performed in six independent sets. Data analysis and determination of standard deviation was performed with Microsoft Excel 2010 (Microsoft Corporation). In the MTT assay, the absorbance for the solvent control cells was considered as 100% cell viability and the absorbance for the treated cells was compared to ascertain % cell viability with respect to the solvent control. MTT assay was also conducted in separate set of experiments to determine the cytotoxic potential of **L_2**-SO_3^{2-} and **L_2**-SO_4^{2-} ensemble in cells. To this end, HeLa cells seeded into 96 well tissue culture plates at 10^4 cells per well and incubated with varying concentrations 0.5 µM -5.0 µM of the probe **L_2** made in DMEM for 30 min under 5% CO_2. Subsequetly, sodium sulphite and sodium sulfate salts were added in separate sets to HeLa cells pre-incubated with **L_2** so as to achieve an **L_2**-sulfite and **L_2**-sulfate ensemble ratio of 1:5 and 1:10. The cells were then incubated for a period of 24 h under 5% CO_2 following which MTT assay was performed for the samples as mentioned before.

2.2.6. Cell imaging studies (by the probe L_2)

HeLa cells were initially cultured in a 25 cm^2 tissue culture flask containing DMEM medium supplemented with 10% FBS, penicillin (100 µg/ mL) and streptomycin (100 µg/mL) in a CO_2 incubator at 37°C. Prior to performing cell imaging studies, HeLa cells were seeded into a 6 well plate and grown in DMEM medium at 37°C till 80% confluency in a CO_2 incubator. Subsequently, the cells were washed thrice with sterile phosphate buffered saline (PBS) and DAPI stain (6.0 µM in sterile PBS) was added to the cells and incubated for 5 min. The cells were again washed thrice with sterile PBS in order to eliminate excess DAPI stain. Subsequently, the cells were incubated with 5.0 µM **L_2** in DMEM at 37°C for 1 h in a CO_2

incubator. Following incubation, the cells were washed with sterile PBS to remove excess **L_2** and their images were acquired using a fluorescence microscope (Eclipse Ti-U, Nikon, USA) with filters that allowed blue emission (λ_{ex} = 340-380 nm and λ_{em} = 435-485 nm for DAPI stain) and green emission (λ_{ex} = 465-495 nm and λ_{em} = 515-555 nm for **L_2**). The cells were further incubated for 1 h in separate sets with 25 μM each of sodium sulfite and tetrabutylammonium sulfate (to achieve the final ratio of 1:5 **L_2**-analyte ratio) prepared in sterile PBS. The images of the cells were again acquired with a fluorescence microscope. The colocalization of the images was performed using ImageJ software and the JACoP plugin.[2.6]

2.3.1. UV−Vis and fluorescence spectroscopic studies of L_3 for metal ion (Zn^{2+}, Al^{3+} and Cu^{2+}) sensing

Stock solutions of various ions (1×10^{-1} mol.L^{-1}) were prepared in deionized water. A stock solution of **L_3** (5×10^{-3} mol.L^{-1}) was prepared in DMSO. The solution of **L_3** was then diluted to 10×10^{-6} mol·L^{-1} and 20×10^{-6} mol.L^{-1} with CH_3OH/aqueous HEPES buffer (5mM, pH 7.3; 9:1, v/v) for the fluorescence experiments and UV-Visible experiments respectively. In UV-Visible selectivity experiment, the test samples were prepared by placing appropriate amounts of the stock solutions of the respective cations into a quartz optical cell of 1 cm path length filled with 1.0 mL of probe solution (20×10^{-6} mol.L^{-1}). In fluorescence selectivity experiment, the test samples were prepared by placing appropriate amounts of the stock solutions of the respective cations into 2.0 mL of probe solution (10×10^{-6} mol.L^{-1}). For UV-Visible and fluorescence titration experiments two different sets of metal ions (Zn^{2+}, Al^{3+} and Cu^{2+}) standard solutions having 1mM and 5mM concentrations were prepared by diluting the earlier prepared stock solutions (1×10^{-1} mol.L^{-1}) in 9:1 methanol-water medium. Quartz optical cells of 1 cm path length were filled with 1.0 mL and 2.0 mL solutions of **L_3** for UV-Visible and fluorescence titration experiments respectively, to which the (1mM and 5mM) ion stock solutions were gradually added using a micropipette. For fluorescence measurements, excitation was provided at 390 nm, and emission was acquired from 410 nm to 700 nm. Spectral data were recorded within 2 minutes after addition of the ions.

2.3.2. UV−Vis spectroscopic studies of L_3 for anion (F^-) sensing

Stock solutions of various anions (1×10^{-1} mol.L^{-1}) were prepared in methanol. A stock solution of **L_3** (5×10^{-3} mol.L^{-1}) was prepared in DMSO. The solution of **L_3** was then diluted to 20×10^{-6} mol.L^{-1} with CH_3CN for the UV-Visible experiments. In the selectivity experiment, the test samples were prepared by placing appropriate amounts of the stock solutions of different anions into a quartz optical cell of 1 cm path length filled with 1.0 mL of probe solution (20 ×

10^{-6} mol.L^{-1}). In the titration experiment, a quartz optical cell of 1 cm path length was filled with a 1.0 mL solution of **L_3** to which another sets of fluoride ion stock solutions (5mM, prepared in methanol by diluting the previous stock solution) was gradually added using a micropipette.

2.3.3. Calculation of detection limit for different ions (using probe L_3)

The detection limits were calculated on the basis of the fluorescence titrations. The fluorescence emission spectrum of **L_3** was measured 10 times, and the standard deviation of blank measurement was achieved. To gain the slope, the fluorescence emission at 523 nm was plotted as a concentration of Al^{3+} and the fluorescence emission at 494 nm was plotted as a concentration of Zn^{2+}. The detection limits were calculated using the following equation-

Detection limit = $3\sigma/k$ (1)

Where σ is the standard deviation of blank measurement, and k is the slope between the fluorescence emission intensity versus [Zn^{2+}] or, emission intensity versus [Al^{3+}].

2.3.4. Job's plot experiment with UV−Vis method

Ten sets of 2 mL CH_3OH/aqueous HEPES buffer (5mM, pH 7.3; 9:1, v/v) solution were prepared with label 1 to 10. Now appropriate amount of ligand stock solutions were (5×10^{-3} mol.L^{-1}) added to each set of solution so that the concentration of **L_3** in the solutions varies from 100μM to 10μM respectively in the ten vials. Then appropriate amount of Cu^{2+} solution (5×10^{-3} mol.L^{-1}) added to each set of solution so that the concentration of Cu^{2+} in the solutions varies from 0μM to 100μM respectively in the ten vials. In each set the total concentration (metal + ligand) was kept constant at 100μM. Now, UV-Vis spectra of all these 10 sets of solutions were recorded and from that absorbance at 456 nm were plotted against the mole fraction of Cu^{2+} to get Job's plot.

2.3.5. Dynamic light scattering (DLS) studies (for the probe L_3)

The particle size of **L_3**, **L_3**-Al^{3+} and **L_3**-Zn^{2+} aggregates were measured by dynamic light scattering (DLS) experiments on a Malvern Zetasizer Nano ZS instrument equipped with a 4.0 mW He–Ne laser operating at a wavelength of 633 nm. The samples and the background were measured at room temperature (25°C) at a scattering angle of 173°. DLS experiments were carried out with optically clear solutions of **L_3** (10 μM) in 9:1 MeOH-H_2O and 1:9 MeOH-H_2O to observe the change in particle size upon increasing water fraction. DLS studies were also carried out with an optically clear solution of **L_3** (10 μM) in 9:1 MeOH-H_2O, in the presence of 20 equivalents of Al^{3+} and Zn^{2+} ion separately to determine the changes in particle size on

interaction of **L_3** with these metal ions. The solution was equilibrated for 30 minutes before taking the measurements.

2.4.1. UV−Vis and fluorescence spectroscopic studies of L_4

Stock solutions of various carboxylic acids (1×10^{-1} mol.L^{-1}) were prepared in methanol. A stock solution of **L_4** (5×10^{-3} mol.L^{-1}) was prepared in DMSO. The solution of **L_4** was then diluted to 20×10^{-6} mol.L^{-1} with EtOH/aqueous HEPES buffer (5mM, pH 7.4; 9:1, v/v) for spectral studies by taking only 8 μL stock solution and making the final volume 2mL adding EtOH/aqueous HEPES buffer. In fluorescence titration experiments, a quartz optical cell of 1 cm path length was filled with a 2.0 mL solution of **L_4** **(**20×10^{-6} mol.L^{-1}) to which the carboxylic acid stock solutions were gradually added using a micropipette. In UV-Visible titration experiments, a quartz optical cell of 1 cm path length was filled with a 1.0 mL solution of **L_4** to which the carboxylic acid stock solutions were gradually added using a micropipette. In selectivity experiments, the test samples were prepared by placing appropriate amounts of the carboxylic acids stock into 2.0 mL of **L_4** solution (20×10^{-6} mol.L^{-1}). For fluorescence measurements, excitation was provided at 450 nm, and emission was acquired from 470 nm to 750 nm for the discrimination of maleic and fumaric acid and then excitation was provided at 550 nm, and emission was acquired from 570 nm to 800 nm for the sensing of Maleic acid.

2.4.2. Detection Limit for maleic acid (using probe L_4)

The detection limit was calculated on the basis of the fluorescence titration. The fluorescence emission spectrum of **L_4** was measured 10 times, and the standard deviation of blank measurement was achieved. To gain the slope, the fluorescence emission at 606 nm was plotted as a concentration of maleic acid. The detection limits were calculated using the following equation:

Detection limit = $3\sigma/k$

where σ is the standard deviation of blank measurement, and k is the slope between the fluorescence emission intensity versus [maleic acid].

2.4.3. Detection of maleic acid in food additives (using probe L_4)

Sample for the detection of maleic acid in starch rich food was prepared by the following procedure. First 10g of starch rich food was taken in a 500 ml beaker and to it 200 ml of methanol was added and the mixture was stirred vigorously for 24 hrs. The extract was filtered and the filtrate was collected. From this, 27 ml of the filtrate was taken and and 3 ml HEPES buffer (7.4 pH) solution was added to it and then mixed well to get a homogeneous solution.

Then this 30 ml solution was divided into three parts each containing 10 ml of solution. Among these three, in two parts maleic acid and fumaric acid were added (4mM) respectively from outside. Now the three 10 ml solutions containing none, maleic acid and fumaric acid were subjected to the spectral study.

2.5. Synthesis and characterization of the compounds

2.5.1. Synthesis of L_1

In a 100ml round bottomed flask 10mmol (1.72g) of 2-hydroxy-1-naphthaldehyde was taken and it was dissolved in 50 mL of methanol by constant stirring. To this solution, excess of hydrazine hydrate (5.0 mL, ~100 mmol) was added. The mixture was allowed to stir for 24 h to obtain pale yellow colour solid product which was filtered and washed thoroughly with methanol. This product constituted the Schiff base having mono-imine bond and a free amine group of hydrazine (**See scheme 3.1, chapter 3**).

In the next step 1.0 mmol of this product, obtained in step1 was dissolved in methanol and 1.1 mmol of 2-pyridinecarboxaldehyde was added and the mixture was stirred for 18 h to obtain a deep yellow colored solid product (**See scheme 3.1, chapter 3**) which was washed several times with methanol and then dried in a desiccator.

Calculated yield: 81%. ^{1}H NMR [600 MHz, $CDCl_3$, TMS, J (Hz), δ (ppm)]: 13.28 (1H, s), 9.80 (1H, s), 8.75 (1H, s), 8.17 (1H, d, J=8.4), 8.09 (1H, d, J=7.8), 7.90-7.79 (3H, m), 7.58 (1H, t, J=7.8), 7.43-7.37 (2H, m), 7.27-7.23 (2H, m), 7.26(1H, s, $CDCl_3$). ^{13}C NMR [150 MHz, $CDCl_3$, TMS, δ (ppm)]: 163.42, 161.87, 161.64, 150.45, 136.87, 135.36, 133.10, 129.44, 128.39, 128.26, 125.37, 124.00, 122.99, 120.23, 119.48, 119.37, 108.35. ESI-MS (positive mode, m/z) Calculated for $C_{17}H_{13}N_3O$: 276.11. Found: 276.1315 [$(M+H^+)$].

2.5.2. Synthesis of L_2

10mmol (2.09g) of 1,1,2-Trimethylbenz[e]indole was dissolved in 50 mL of acetonitrile and 12 mmol of iodoethane (1.87g) was added to this solution. The mixture was refluxed for 10 h and the resultant solution was then kept for slow evaporation to get crystalline solid product of 3–ethyl–1,1,2–trimethyl–1*H*–benzo[*e*]indol–3–ium (first step of the **scheme 4.1, chapter 4**); which was then filtered and washed with cold methanol.

In the next step, 1.0 mmol of this 3–ethyl–1,1,2–trimethyl–1*H*–benzo[*e*]indol–3–ium was dissolved in dry EtOH and 1.1 mmol of 4-(Dimethyl-amino)cinnamaldehyde was added to it. Resultant mixture was then refluxed for 12 h to yield the dark blue colour product.

Calculated yield: 64%. ^{1}H NMR [600 MHz, CD_3OD, J (Hz), δ (ppm)]: 8.41-8.26 (3H, m), 8.17 (1H, d, J=7.8), 8.12(1H, t, J= 7.8), 7.85 (1H, d, J=9.0), 7.75 (1H, d, J=7.2), 7.66 (2H, d, J=8.4),

7.33 (1H, t, J=10.2), 7.00-6.93 (2H, m), 6.83 (1H, t, J=7.8), 4.89 (s, H_2O in CD_3OD), 4.58 (1H, d, J=6.6), 3.62 (2H, q, J=6.6), 3.31 (6H, s), 3.15 (m, CD_3OD), 2.03 (6H, s), 1.19 (3H, t, J=7.2). ^{13}C NMR [150 MHz, $CDCl_3$, TMS, δ (ppm)]:179.34, 156.14, 153.33, 138.32, 137.09, 133.19, 132.82, 131.55,130.41, 128.48, 127.90, 126.75, 124.89, 123.99, 122.67, 112.40, 111.92, 111.62, 110.72, 52.82, 42.60, 40.37, 27.43, 14.11. ESI-MS (positive mode, m/z) Calculated for $C_{28}H_{31}N_2^+$: 395.2487. Found: 395.2507.

2.5.3. Synthesis of L_3

5 mmol of 1-Naphthyl isothiocyanate was dissolved in 30 ml THF solution and then to it excess of hydrazine hydrate (50 mmol) was added at once. Then the mixture solution was stirred for 12 hours to get a faint yellow-white precipitate (**Scheme 5.1, step 1, chapter 5**). Then 1 mmol of the product obtained in step1 was dissolved in pure ethanol and to it 1 mmol of 2-hydroxy-1-naphthaldehyde was added. The mixture was then stirred for 16 hours to get a pale yellow precipitate which was collected by filtration and washed thoroughly by methanol and the product was dried in desiccator. The calculated yield of **L_3** was found to be 82%.

^1H NMR [600 MHz, DMSO-d_6, TMS, J (Hz), δ (ppm)]: 12.86 (1H, s), 11.15 (1H, s), 9.89 (1H, s), 9.07 (1H, s), 8.61 (1H, d, J=8.4), 8.03 (1H, d, J=9.0), 7.91 (1H, d, J=8.4), 7.72-7.70 (2H, m), 7.61 (1H, t, J=7.2), 7.44-7.40 (3H, m), 7.26 (1H, d, J=8.4), 7.01-6.97 (3H, m). ^{13}C NMR [150 MHz, DMSO-d_6, TMS, δ (ppm)]: 162.74, 162.40, 161.79, 160.13, 158.61, 134.81, 133.17, 132.26, 131.06, 128.89, 128.02, 127.82, 123.81, 121.70, 119.58, 118.72, 118.17, 116.59, 108.36. ESI-MS (positive mode, m/z) Calculated for $C_{22}H_{11}N_3OS$: 372.1092 Found: 372.1067 [$(M+H^+)$].

2.5.4. Synthesis of L_4

10mmol (1.72g) of 2-hydroxy-1-naphthaldehyde was dissolved in 50 mL of methanol and excess of hydrazine hydrate (5.0 mL, ~100 mmol) was added to this solution. The mixture was allowed to stir for 24 h to obtain pale yellow colour solid product which was filtered and washed thoroughly with cold methanol. This product constituted the Schiff base having mono-imine bond and a free amine group of hydrazine (**Scheme 6.1, step 1, chapter 6**).

In the next step, 1.0 mmol of this mono-imine product was dissolved in MeOH and 1.1 mmol of 4-(Dimethyl-amino)cinnamaldehyde was added. Resultant mixture was refluxed for 18 h to yield an orange solid. The product was washed with methanol and then dried in a desiccator.

Calculated yield: 74%. ^1H NMR [400 MHz, $CDCl_3$, TMS, J (Hz), δ (ppm)]: 13.40 (1H, s), 13.00 (1H', s), 9.64 (1H, s), 9.55 (1H', s), 8.41 (1H, d, J=9.6), 8.10 (1H, d, J=8.4), 7.80 (1H, d,

J=9.2),7.75 (1H, d, J=8.0), 7.52 (1H, t, J=7.2), 7.42-7.31 (2H, m), 7.22(1H, s, $CDCl_3$),, 7.19 (1H, d, J=8.8), 7.06 (2H, d, J=15.6), 6.91-6.85(2H, m), 6.681(2H, d, J=9.2), 3.00 (6H, s). ^{13}C NMR [100 MHz, $CDCl_3$, TMS, δ (ppm)]:164.19, 160.85, 160.13, 159.43, 145.01, 134.03, 133.01, 129.19, 129.08, 128.13, 127.73, 123.68, 123.52, 120.06, 119.79, 119.16, 111.98, 108.55, 40.158. ESI-MS (positive mode, m/z) Calculated for $C_{22}H_{21}N_3O$: 344.1685. Found: 344.1755 [$(M+H^+)$].

References

2.1. SAINT and *XPREP*, 5.1 ed.; Siemens Industrial Automation Inc.: Madison, WI, 1995. G. M. Sheldrick.

2.2. *SADABS, empirical absorption Correction Program*; University of Göttingen: Göttingen, Germany, 1997.

2.3. G. M. Sheldrick, *SHELXTL Reference Manual: Version 5.1*; Bruker AXS: Madison, WI, 1997.

2.4. G. M. Sheldrick, *SHELXL-97: Program for Crystal Structure Refinement;* University of Göttingen: Göttingen, Germany, 1997.

2.5. Mercury 2.3 Supplied with Cambridge Structural Database; CCDC: Cambridge, U.K., 2011 -2012.

2.6. S. Bolte and F.P. Cordelieres, *Journal of Microscopy*, 2006, **224**, 213.

Appendix

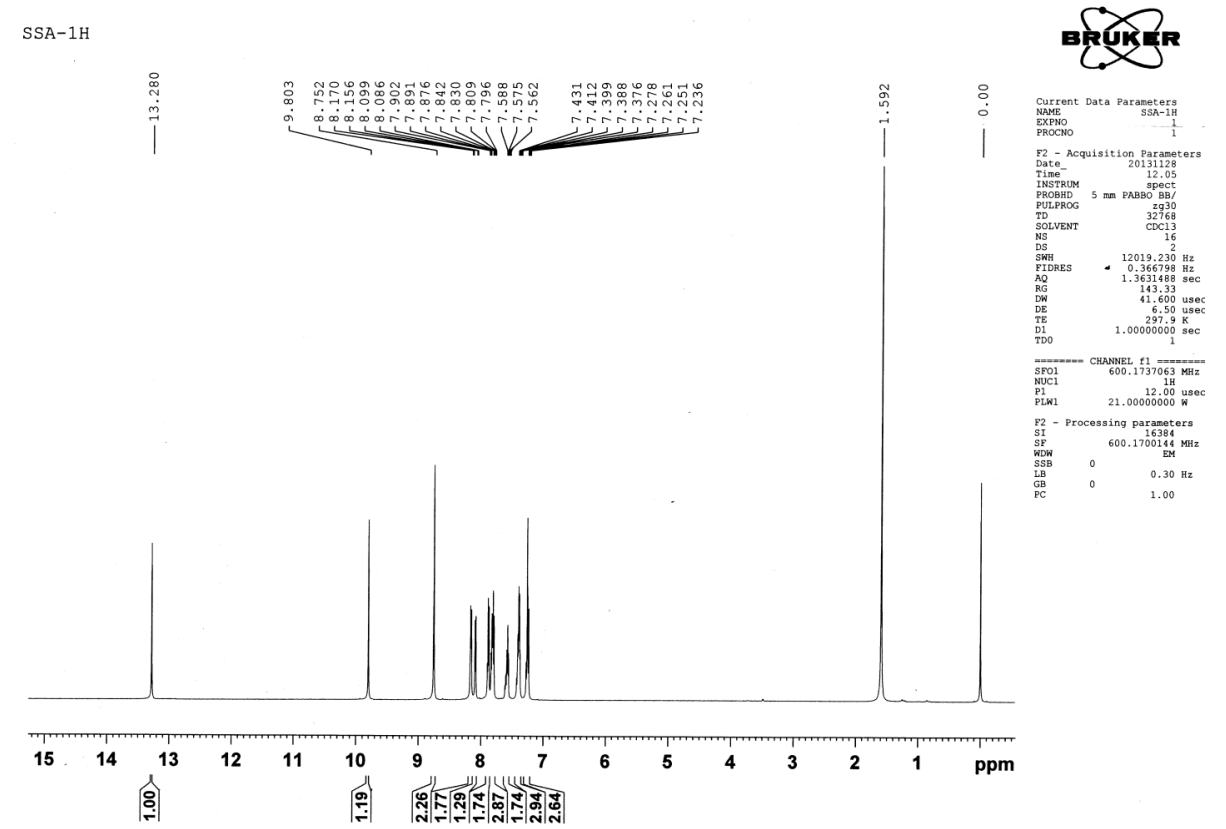

Figure A2.1. ^{1}H NMR spectrum of $\mathbf{L_1}$ in $CDCl_3$

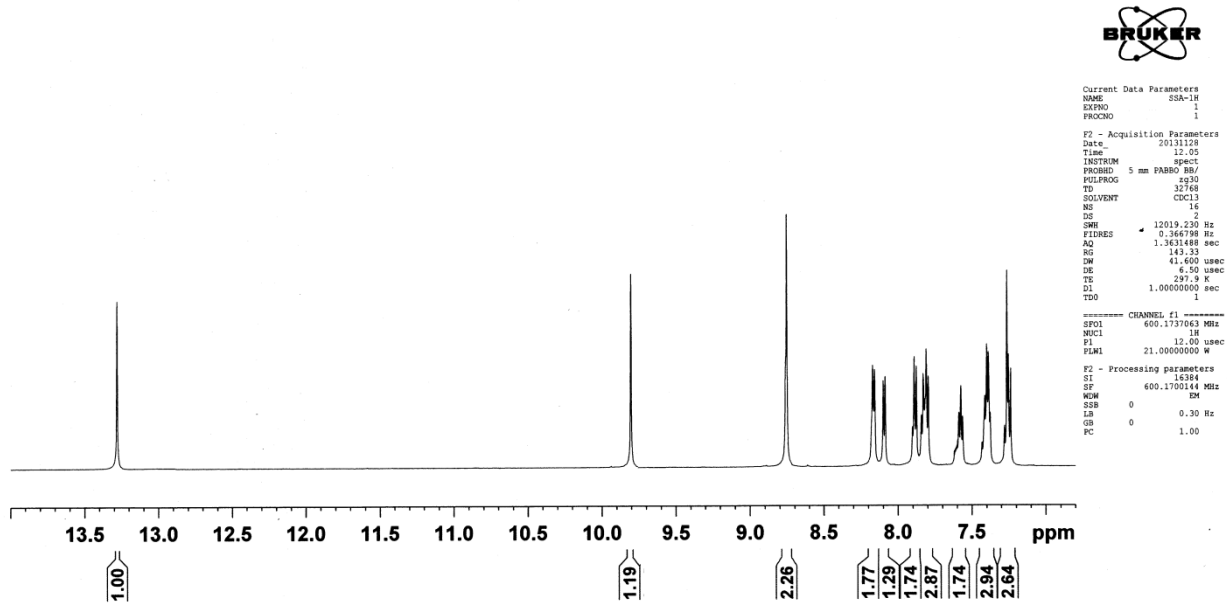

Figure A2.2. Expanded ^{1}H-NMR spectra of $\mathbf{L_1}$ in $CDCl_3$

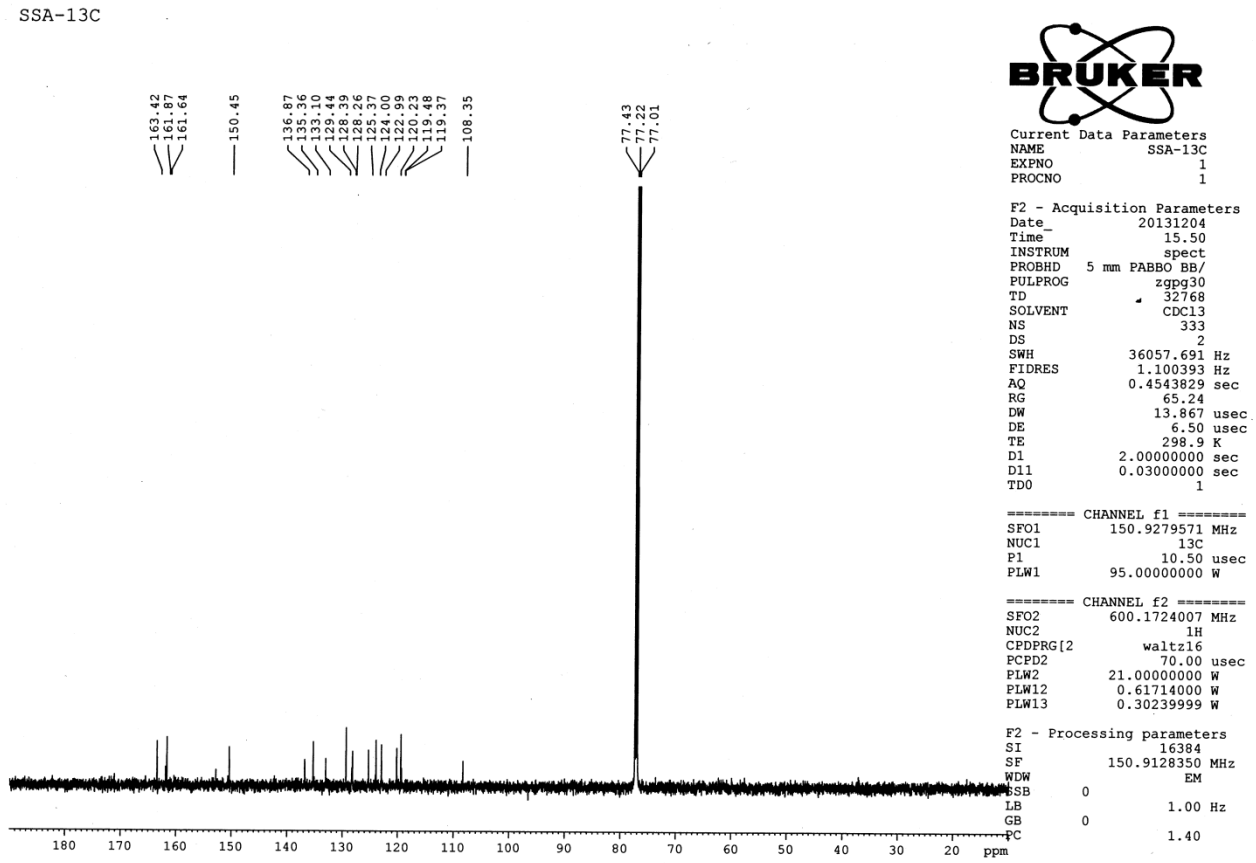

Figure A2.3. ^{13}C-NMR spectra of $\mathbf{L_1}$ in $CDCl_3$

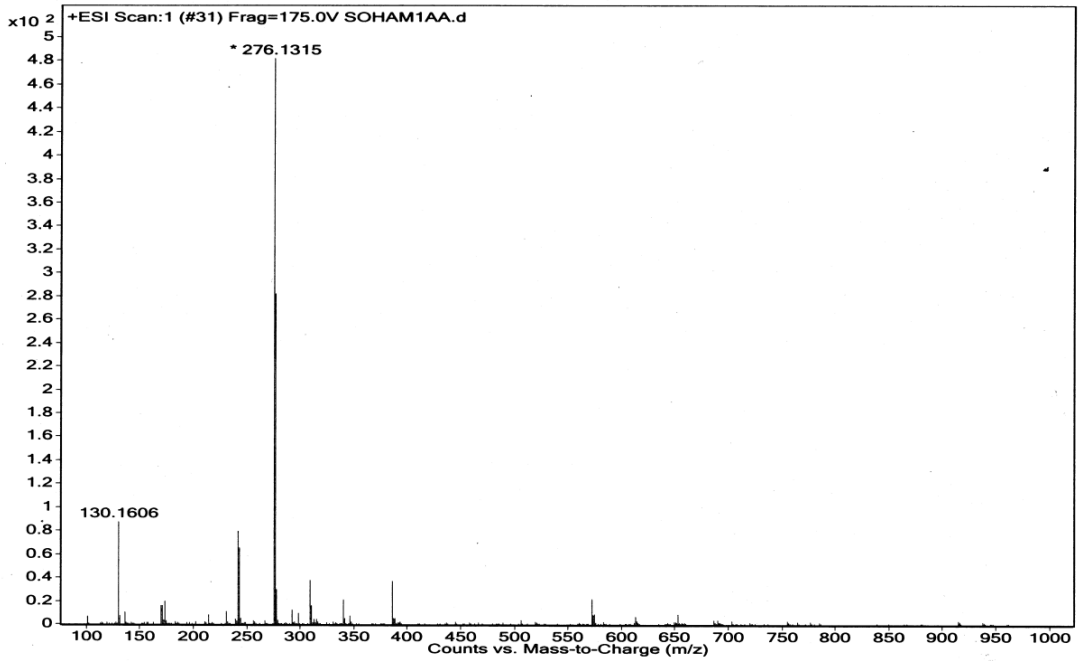

Figure A2.4. Mass spectrum of $\mathbf{L_1}$

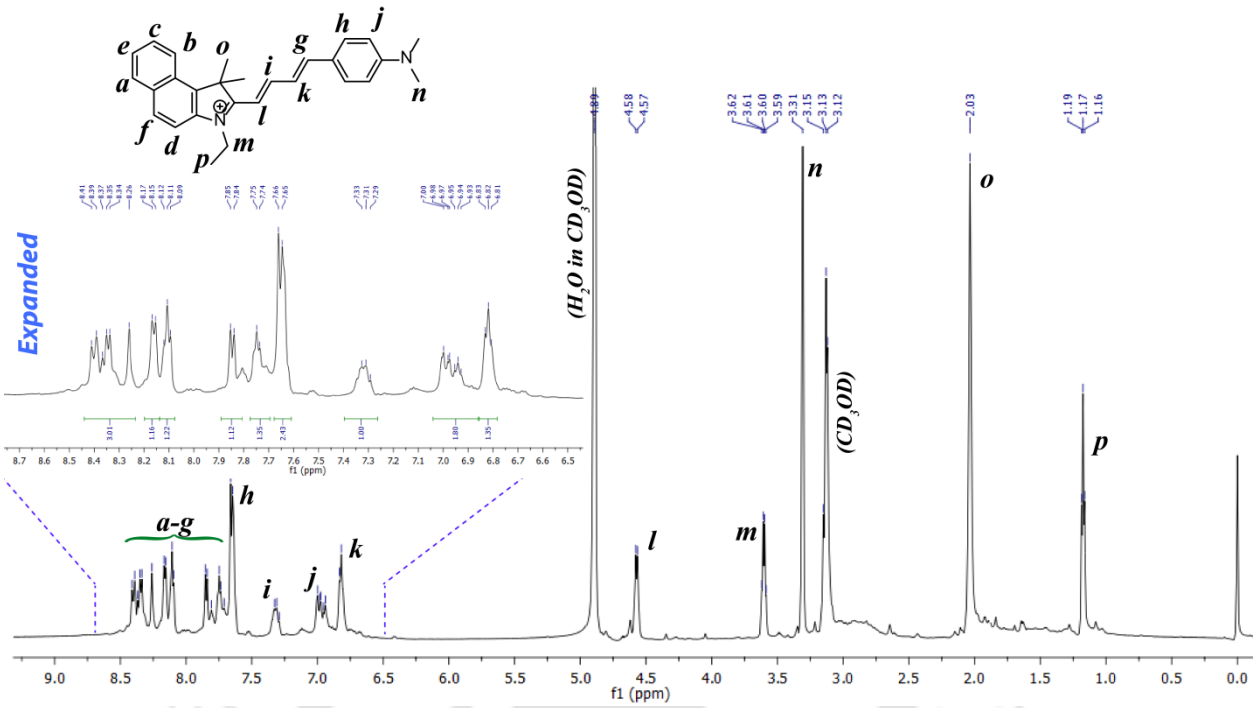

Figure A2.5. ^{1}H-NMR spectra of $\mathbf{L_2}$ in CD_3OD

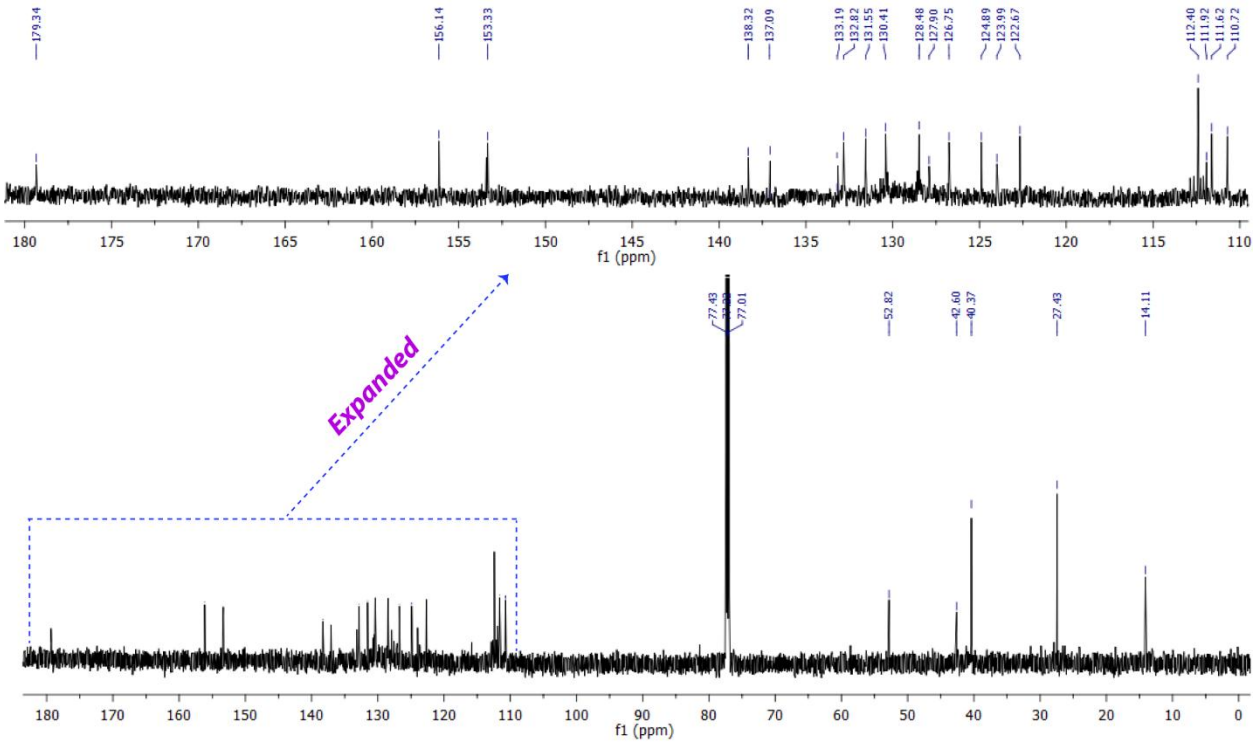

Figure A2.6. ^{13}C-NMR spectra of $\mathbf{L_2}$ in $CDCl_3$

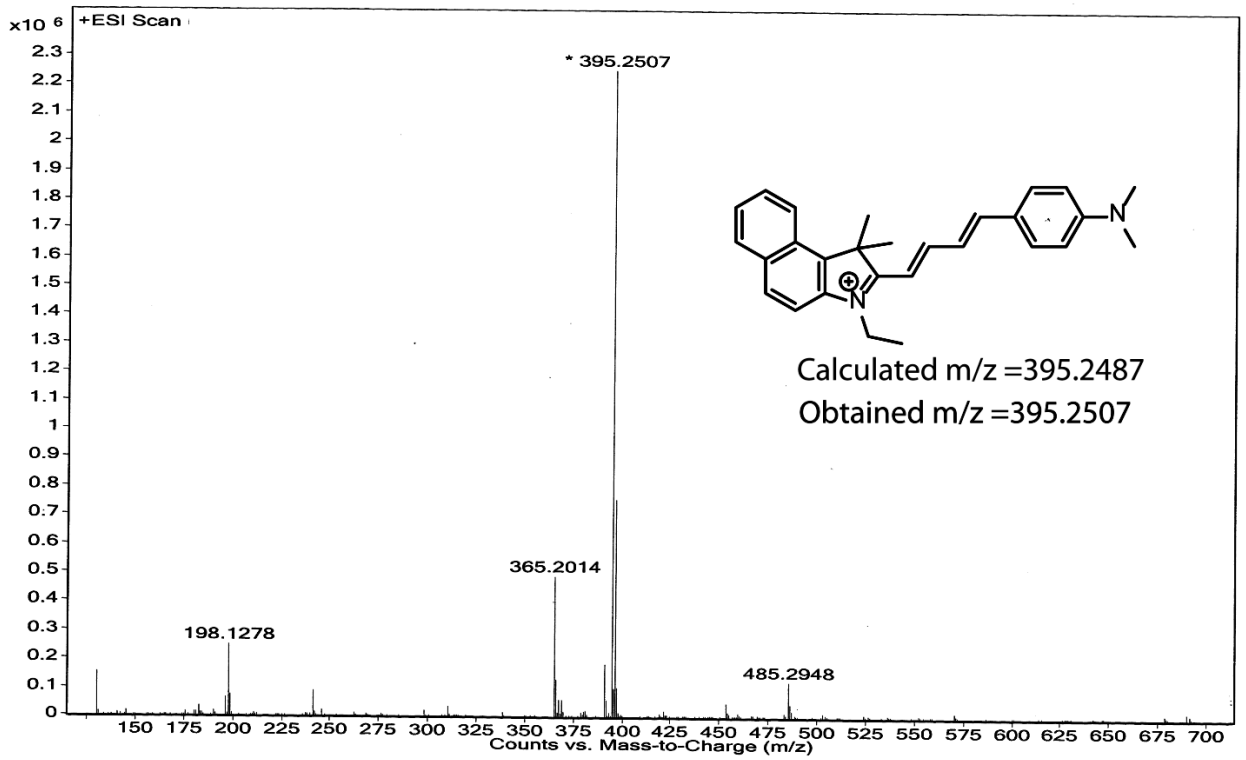

Figure A2.7. Mass spectrum of $\mathbf{L_2}$

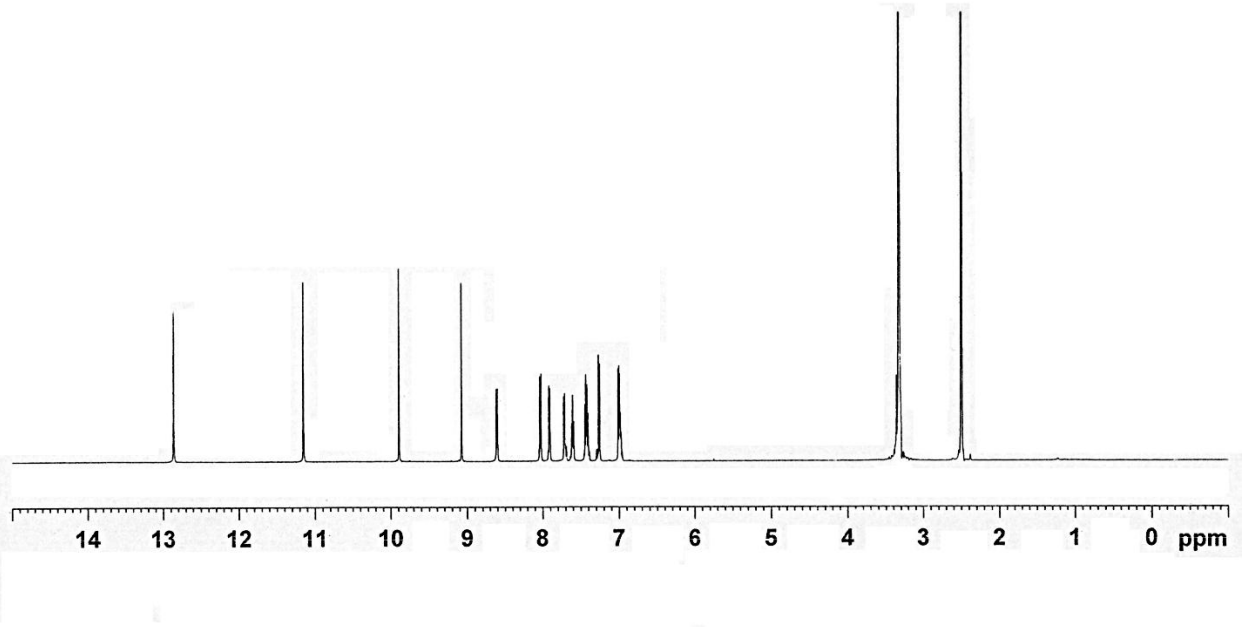

Figure A2.8. ^{1}H-NMR spectra of $\mathbf{L_3}$ in DMSO-d_6

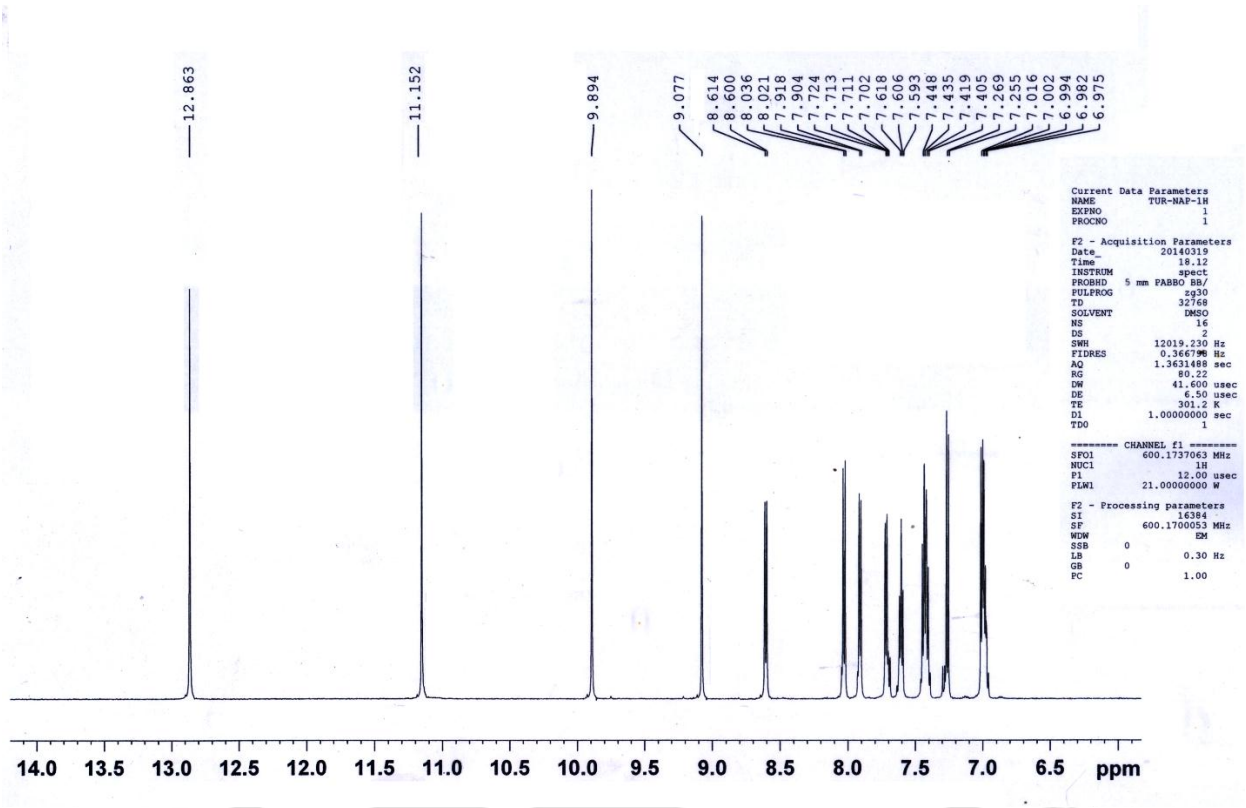

Figure A2.9. Expanded ^{1}H-NMR spectra of $\mathbf{L_3}$ in DMSO-d_6

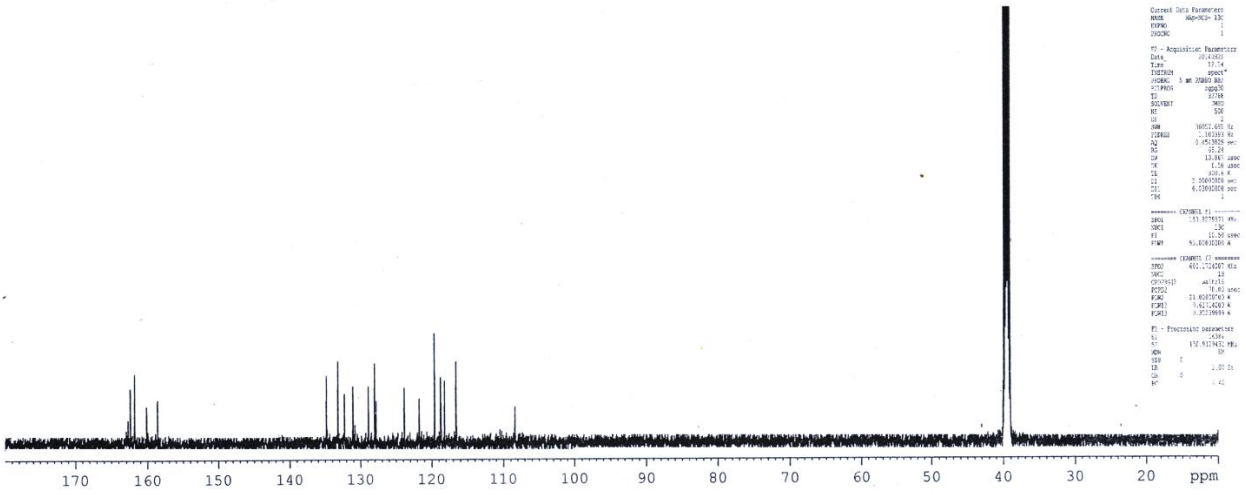

Figure A2.10. ^{13}C-NMR spectra of $\mathbf{L_3}$ in DMSO-d_6

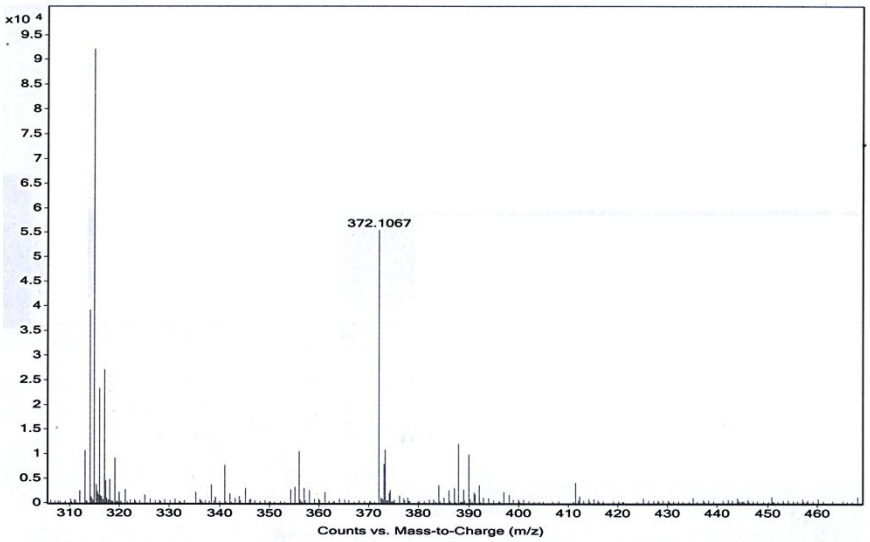

Figure A2.11. Mass spectrum of $\mathbf{L_3}$

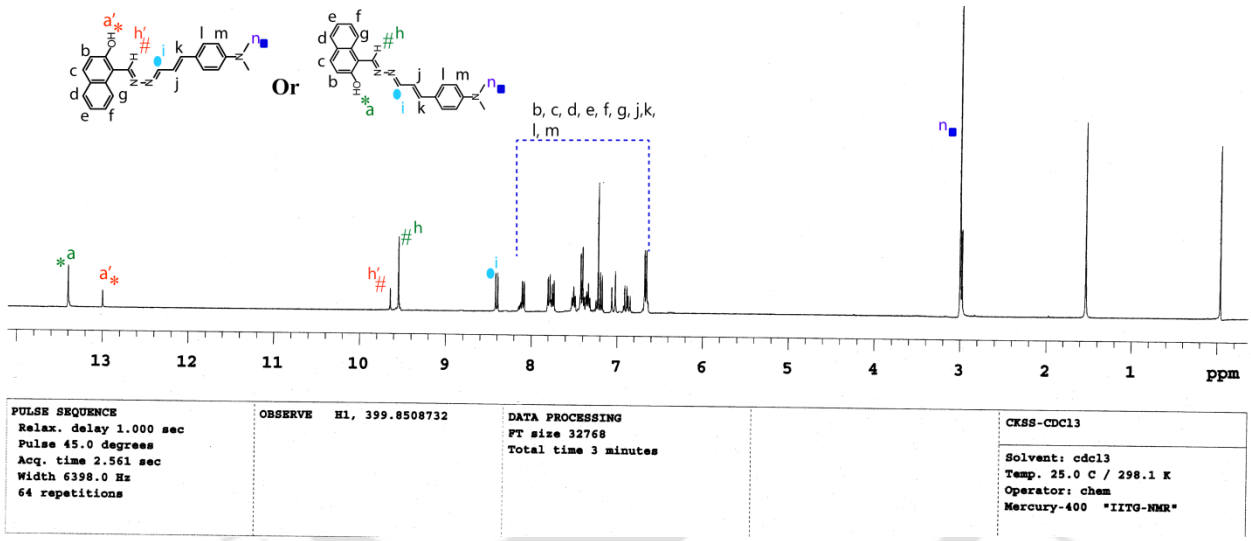

Figure A2.12. ^{1}H-NMR spectra of $\mathbf{L_4}$ in $CDCl_3$

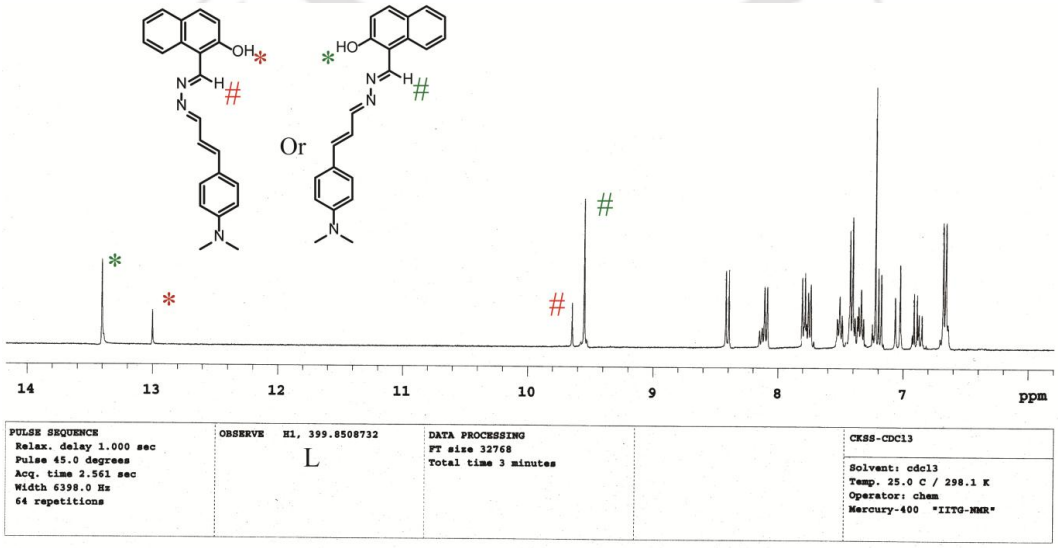

Figure A2.13. Expanded ^{1}H-NMR spectra of $\mathbf{L_4}$ in $CDCl_3$

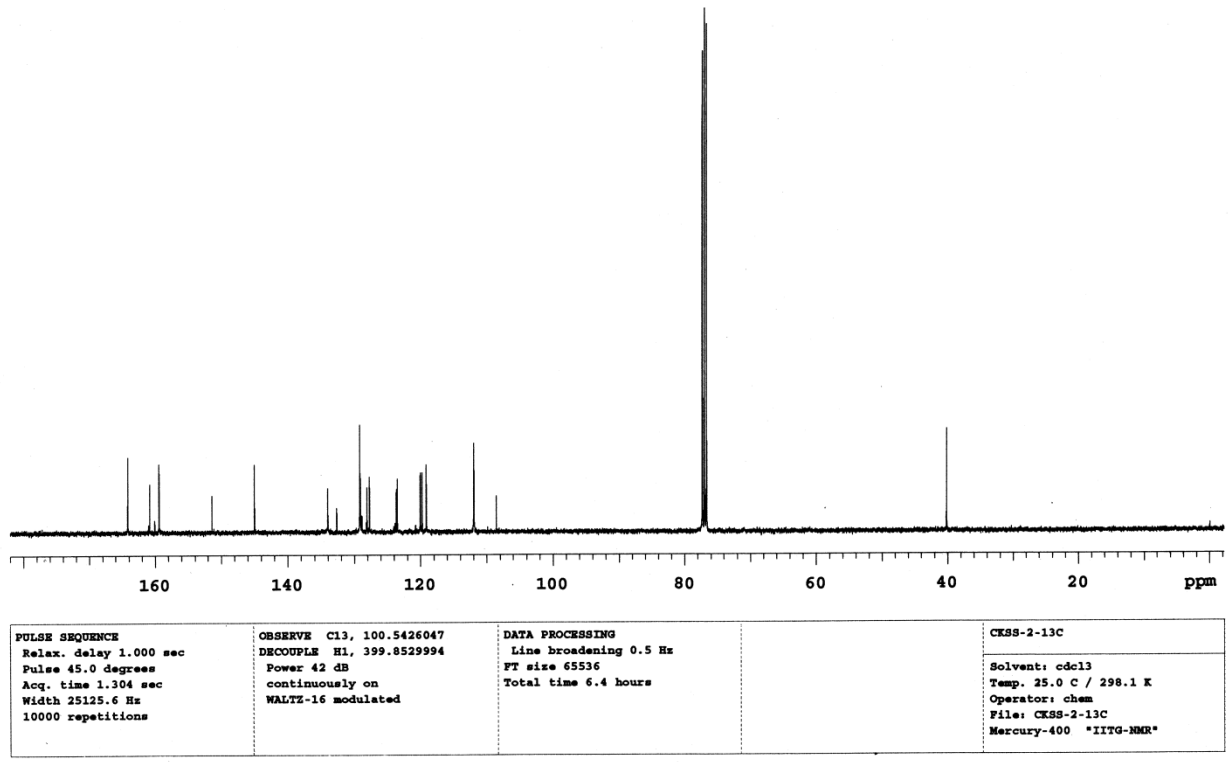

Figure A2.14. ^{13}C-NMR spectra of $\mathbf{L_4}$ in $CDCl_3$

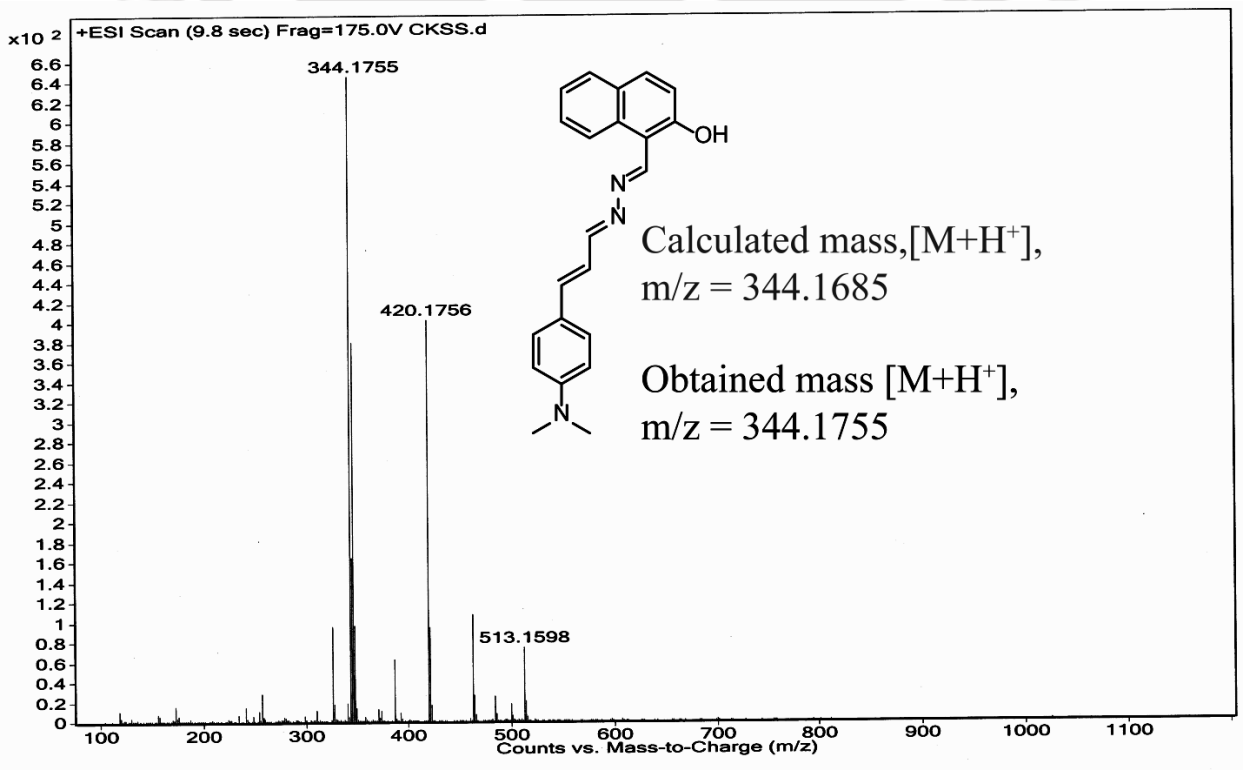

Figure A2.15. Mass spectrum of $\mathbf{L_4}$

Table A2.1. Crystal parameters and refinement data

Code name	**L_1**
Empirical formula	$C_{17}H_{13}N_3O$
Formula weight	275.30
Cryst syst	Monoclinic
a (Å)	17.916(5)
b (Å)	4.6430(12)
c (Å)	20.248(12)
α (degree)	90.00
β (degree)	124.13(3)
γ (degree)	90.00
V ($Å^3$)	1394.2(10)
Space group	$P2_1/c$
Z value	4
ρ(cal)(g/cm^3)	1.312
μ(Mo Kα) (mm^{-1})	0.085
T(K)	298(2)
R1; wR2 (I> 2 σ(I))	0.0969; 0.1463
R1; wR2(all)	0.1839 ; 0.1715
Residual electron density (e $Å^{-3}$)	0.284/-0.238
Good-of-fit	1.362
Reflection measured	3664
Unique reflections	2136
Reflection parameters	123
CCDC No.	1000232

Chapter 3

An Aggregation-Induced Emission (AIE) Active Probe Renders Al(III) Sensing and Tracking of Subsequent Interaction with DNA

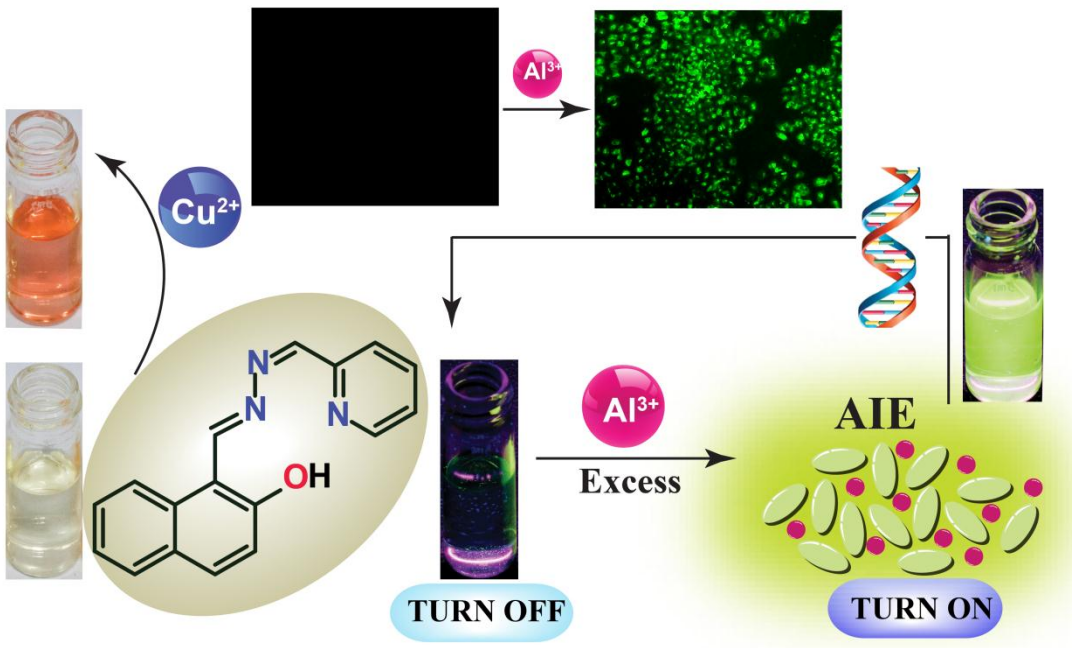

Chapter 3

3.1. Background and focus of the chapter

Aluminium is the third most abundant metal in the earth's crust and is widely acknowledged as a neurotoxic agent. In spite of being a nonessential element, Aluminum is a competitive inhibitor in different biological processes involving several essential elements viz. Mg^{2+}, Ca^{2+}, and Fe^{3+} due to its similarities in atomic size and charge. The leaching of aluminum from soil by acid rain increases the free Al^{3+} in the environment and surface water, which is deadly to growing plants.[3.1-3.2] The widespread use of aluminum in water treatment, as a food additive, and in many industrial activities including the manufacturing of cars and computers often exposes people to this metal.[3.3-3.4] The superfluous ingestion of aluminum influences the absorption of calcium in the bowel to cause softening of the bone, atrophy, and even aberrance. Overdose of Aluminium also affects the absorption of iron in blood which may eventually lead to anemia. Aluminium-associated toxicity has been implicated in impairment of the central nervous system and neurodegenerative diseases such as Alzheimer's.[3.5-3.8] Owing to its significant impact on the biosphere and human health, development of sensors for rapid and sensitive detection of Al^{3+} has stimulated great scientific interest amongst chemists at large.

Fluorescence-based systems are considered to be pertinent in the context of sensing of biological and environmentally relevant metal ions as they can afford rapid, convenient and sensitive detection of target analytes. [3.9-3.14] In the domain of aluminium sensing, fluorescence TURN-ON chemosensors have been described, wherein the mechanism of sensing has been largely attributed to internal charge transfer (ICT), chelation-enhanced fluorescence (CHEF), photo-induced electron transfer (PET) or fluorescent resonance energy transfer (FRET). [3.15-3.22] In recent years, fluorescent probes that display aggregation-induced emission (AIE) have come to limelight. These probes display a weak emission in dilute solution, which is subsequently enhanced manifold as a consequence of aggregation of the fluorophore species driven by probe-target interaction in solution or solid state and thus AIE active probes are perceived to be attractive candidates for robust and quantitative sensing of various target analytes. [3.23-3.27] It is also conceivable that the emission of an AIE-based system is likely to be responsive to an additional competing species that can modulate the probe-target interaction, thereby enabling the probe to render dual sensing.

On the other hand, Copper is an important essential trace element found in the human body and it plays important roles in various physiological processes.[3.28-3.32] It has been found that Copper deficiency can increase the risk of coronary heart disease whereas excessive copper intake may lead to several neurodegenerative diseases including Alzheimer's, Parkinson's, Menkes, Wilson's, and prion diseases.[3.33-3.37] Copper-containing enzymes play various significant roles in different catalytic processes.[3.38] Hence, due to its physiological significance and associated biomedical implications, developing an efficient copper sensor capable of displaying sharp visible colorimetric response is always an indispensable task.

Based on this rationale, in this chapter we describe an AIE- active Schiff base probe **L_1** (**Scheme 3.1**), which displays a selective fluorescence TURN-ON response toward Al^{3+} and interestingly the subsequent interaction of **L_1**-Al^{3+} ensemble with DNA could be captured through a systematic fluorescence TURN-OFF response of the highly emissive ensemble. Additionally, the probe can also sense Cu^{2+} through a conspicuous selective colorimetric response.

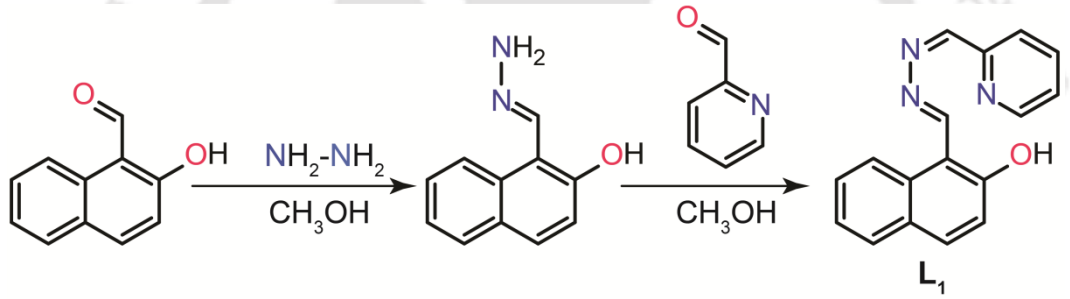

Scheme 3.1: Synthesis of the probe **L_1**

3.2. UV-Vis spectroscopic studies of L_1 in presence of metal ions

UV−Vis spectra of **L_1** revealed two absorption maxima at 334 nm (π−π*) and 384 nm (n−π*) in CH_3OH/aqueous HEPES buffer (5 mM, pH 7.3; 9:1, v/v). The selectivity of **L_1** was checked with chloride or nitrate salts of various metal ions which included Na^+, K^+, Ca^{2+}, Mg^{2+}, Cr^{3+}, Hg^{2+}, Cu^{2+}, Pb^{2+}, Zn^{2+}, Fe^{3+}, Al^{3+}, Co^{2+}, Ni^{2+}, Cd^{2+} and Ag^+. Amongst all the tested metal ions, the presence of Cu^{2+} resulted in an observable change in the UV-visible spectra with emergence of a new peak at 502 nm (**Figure 3.1A**), which also enabled naked eye detection of Cu^{2+} with intense red color of the solution (**Figure 3.1B**). Furthermore, gradual addition of Cu^{2+} resulted in the generation of distinct isosbestic points at 310 nm and 430 nm, respectively (**Figure 3.1C**). Job's plot (**Appendix, Figure A3.1**) and mass spectrum analysis (**Appendix, Figure A3.2**) suggested the formation of 1:1 complex with Cu^{2+} (m/z = 337.03, **L_1**+Cu-H^+). MS data also suggested ligand deprotonation upon complexation. It is significant to mention that the detection limit of **L_1** for Cu^{2+} ions was found to be 1.095 nM, (**Appendix, Figure A3.3**) which is much

lower than the U.S. EPA maximum allowable limit for Cu^{2+} ions (1.3 µM) in drinking water. The distinctive red shift of absorbance maxima in presence of Cu^{2+} (**Figure 3.1C**) could perhaps be attributed to deprotonation with enhancement of conjugation and planarity of $\mathbf{L_1}$ upon complexation, which is supported by theoretical calculation. Amongst the metals tested, Al^{3+} and Co^{2+} were also able to induce some colorimetric changes (**Figure 3.1A**) though those changes were insignificant compared to the spectral change induced by Cu^{2+}.

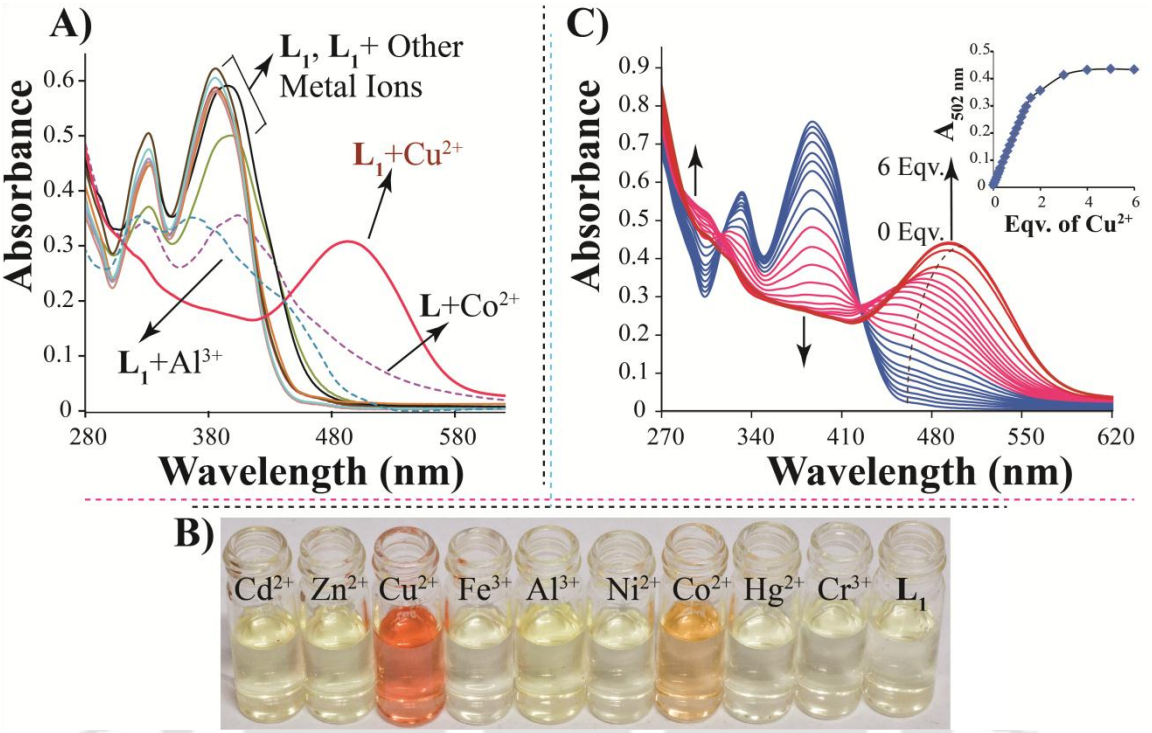

Figure 3.1: (A) UV-Visible spectra of $\mathbf{L_1}$ (10 µM) in presence of different metal ions in mixed solvent. (B) Visual color change of $\mathbf{L_1}$ in presence of different metal ions in daylight. (C) UV-Vis spectra of $\mathbf{L_1}$ (10 µM) in presence of varying concentration of Cu^{2+}. INSET: Changes in the absorbance at 502 nm with concentration of Cu^{2+}.

3.3. Aggregation induced emission (AIE) properties of L_1 in light of structural elucidation:

Interestingly it was observed that the weakly emissive $\mathbf{L_1}$ in pure methanol became highly emissive when a suspension was formed in methanol-water mixture (**Figure 3.2A**). This observation suggested that $\mathbf{L_1}$ is an AIE-active compound. It is significant to note that AIE was observable only when the water fraction in the medium reached the threshold of 80% and above (**Figure 3.2**). A photograph of the vials under UV-light containing solutions of $\mathbf{L_1}$ witnessed the formation of highly emissive (green) suspension of $\mathbf{L_1}$ in methanol water mixture with water fractions 80% and above (**Figure 3.2C**) which clearly reiterates the AIE active nature of $\mathbf{L_1}$. It may be mentioned here that the crystal structure of the compound also supports the propensity of the ligand to form aggregation via non-covalent interaction (**Figure 3.3**). The block shaped

yellow crystal of **L_1** obtained from DCM solvent by slow evaporation was found to be highly fluorescent in nature in the solid state itself.

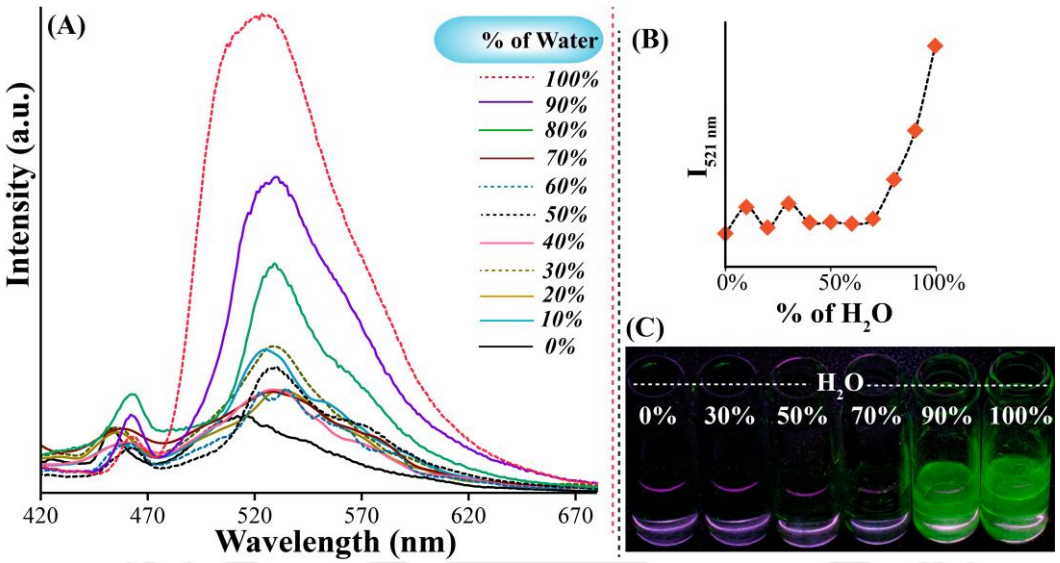

Figure 3.2: (A) Fluorescence emission spectra of **L_1** (10 μM) in different ratios of H_2O/MeOH at λ_{ex} = 400 nm. (B) Change in the intensity with different water fractions (C) Visual change observed with increase in percentage of water (0–100%) to a 10 μM solution of **L_1** as seen under UV light.

The crystal packing of **L_1** suggested that each molecule of **L_1** is subjected to seven intermolecular short interactions (two C–H···π, two C–H···O and three π···π). It may be mentioned here that each of the existed intermolecular C–H···O interactions has the distance 2.599Å whereas each of the intermolecular C–H···π interactions has the distance 2.657 Å (**Figure 3.3A**); which underlines the strong nature of these short interactions. On the other hand all the weak π···π interactions have the distances in the range of 3.356–3.393 Å. Strong intermolecular interactions like C–H···π & C–H···O; could be instrumental in reducing the non-radiative deactivation of excitons by locking the molecular motion in the crystal lattice.[3.39-3.40] In other words presence of the strong C–H···π & C–H···O intermolecular interactions in **L_1** helped to enhance the molecular rigidity and initiated its turn-on emission significantly due to the restriction of intramolecular rotation.

Hence, **L_1** is a classic AIE active compound which can display its aggregation induced emission properties both in solution and solid state. However, as AIE of **L_1** was observable only when the water fraction in the medium reached the threshold of 80% and above; all the fluorescence spectral study of the probe in presence of metal ions was carried out in a 9:1 methanol-aqueous HEPES buffer medium wherein the probe itself does not show AIE behavior.

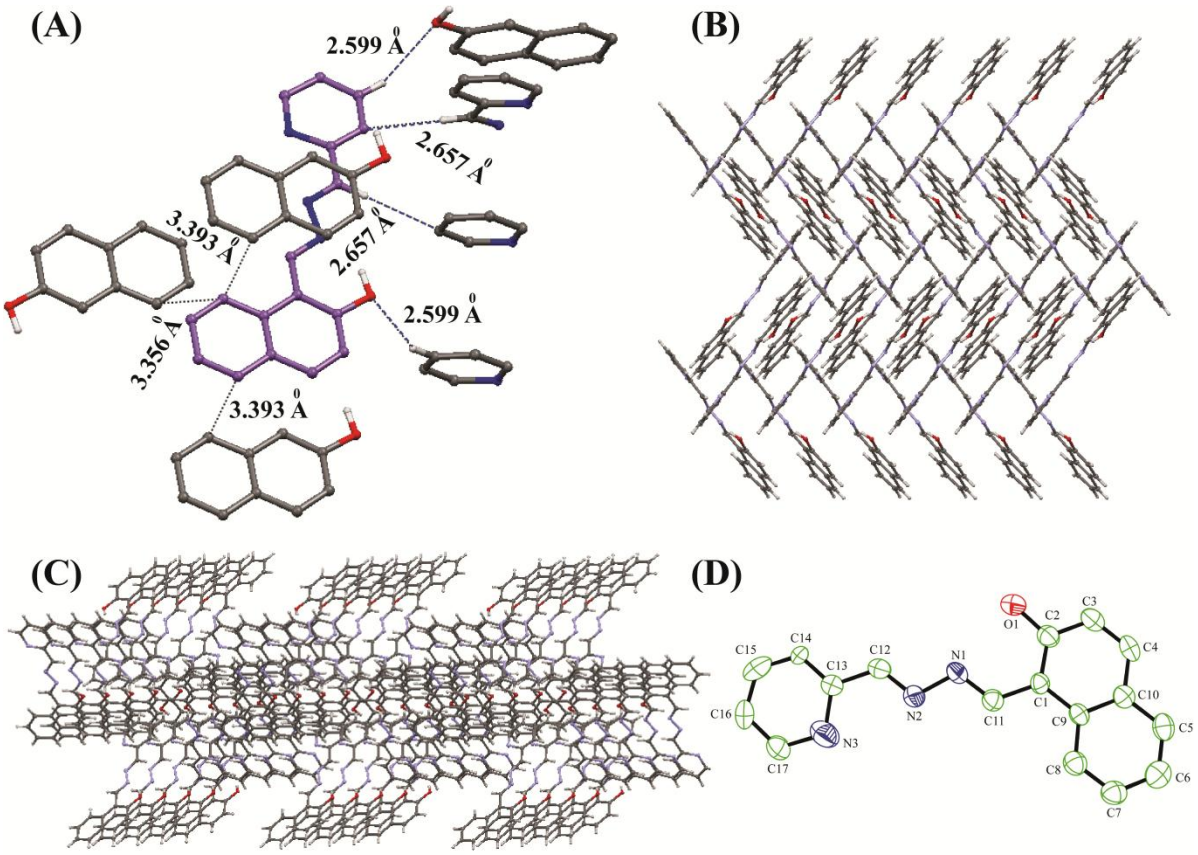

Figure 3.3: Intermolecular interactions (A); molecular packing along 'a' axis (B) & along 'b' axis (C); and ORTEP molecular structure (D); in single crystals of $\mathbf{L_1}$.

3.4. Fluorescence spectroscopic studies of L_1 in presence of metal ions

Fluorescence spectra of $\mathbf{L_1}$ revealed a weak emission band at 506 nm on excitation at 400 nm in CH_3OH/aqueous HEPES buffer (5 mM, pH 7.3; 9:1, v/v). The binding selectivity of $\mathbf{L_1}$ was checked with aforementioned metal ions. Interestingly amongst all tested metal ions only Al^{3+} rendered a remarkable TURN-ON fluorescence response with a 31 nm red shifted new peak emerging at 537 nm along with a manifold increase in fluorescence intensity (**Figure 3.4A**). Furthermore, naked eye detection of this selective TURN-ON response of $\mathbf{L_1}$ toward Al^{3+} was also feasible under UV light, which rendered a bright yellowish green fluorescence (**Figure 3.4B**). It is worth mentioning that addition of all other metal ions to $\mathbf{L_1}$ either showed negligible change in the emission behavior of the probe or resulted in the quenching of fluorescence. Particularly, the addition of excess of Cu^{2+} and Co^{2+} to $\mathbf{L_1}$ led to the immediate quenching of the fluorescence of $\mathbf{L_1}$ to make it absolutely non-fluorescent. Hence, $\mathbf{L_1}$ can sense Al^{3+} by a highly selective TURN-ON fluorescence response in mixed aqueous buffer medium. Interestingly no other metal ions interfered with the TURN-ON fluorescence response of $\mathbf{L_1}$ in presence of Al^{3+}

(**Appendix, Figure A3.4**), which expands the scope of the sensor for interference free specific detection of Al^{3+}.

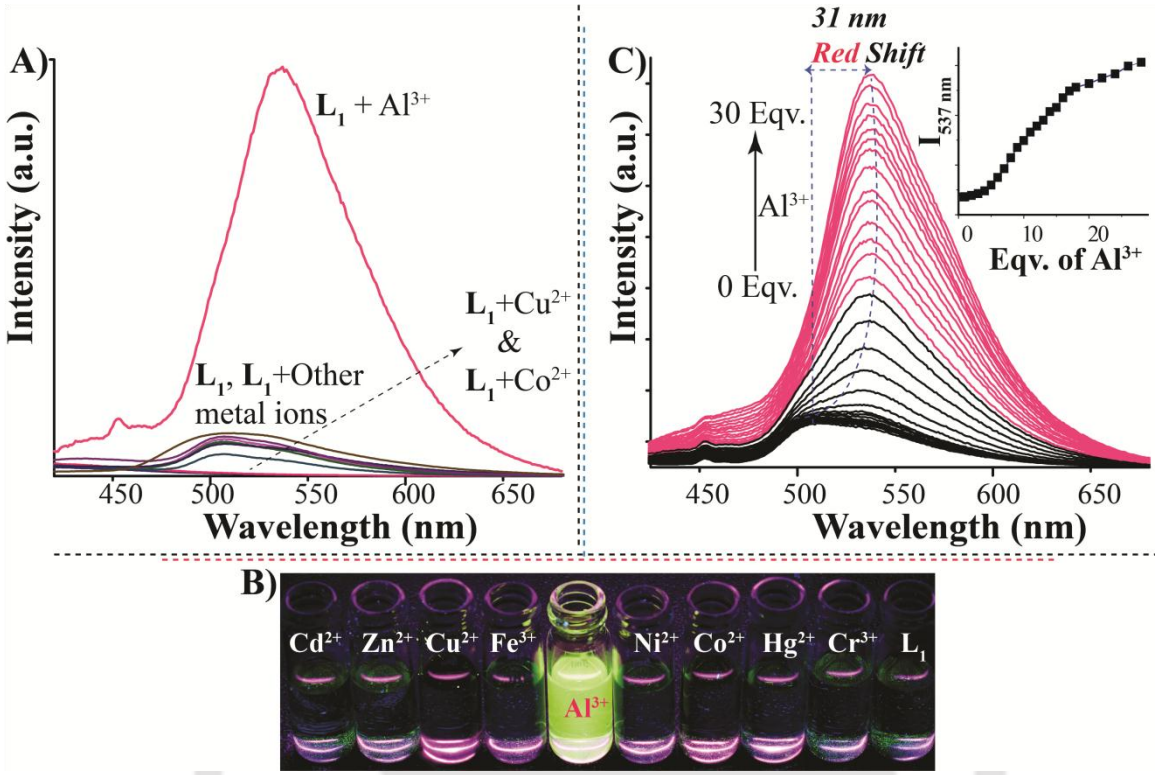

Figure 3.4: (A) Fluorescence spectra of $\mathbf{L_1}$ in presence of 10 equivalents of various metal ions. (B) Visual changes in fluorescence of $\mathbf{L_1}$ in presence of different metal ions under UV-light. (C) Fluorescence spectra of $\mathbf{L_1}$ (10 μM) with varying concentration of Al^{3+}. λ_{ex} = 400 nm. INSET: Emission intensity change at 537 nm with concentration of Al^{3+}.

To get a quantitative appraisal of the interaction between $\mathbf{L_1}$ and Al^{3+}, a titration experiment was pursued. Incremental addition of Al^{3+} ions resulted in a systematic increase in the emission intensity of $\mathbf{L_1}$ with a gradual red shift in emission maxima (**Figure 3.4C**). Based on this titration experiment, detection limit for Al^{3+} was calculated. Detection limit for Al^{3+} was found to be ~2.8 μM (**Appendix, Figure A3.5**), which is well below the permissible level of Al^{3+} in drinking water according to the USEPA.

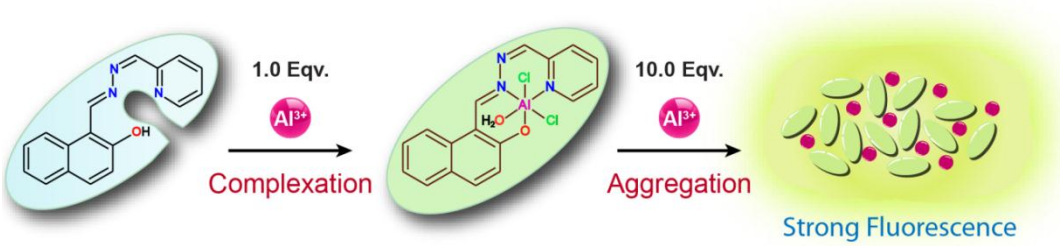

Scheme 3.2: Plausible mechanism of complexation and Al^{3+} induced aggregation.

3.5. Realization of the sensing mechanism:

Mass spectrum analysis (**Appendix, Figure A3.6**) confirmed the formation of 1:1 $\mathbf{L_1}$-Al^{3+} complex with the generation of molecular ion peak at m/z=391.2 ($[Al+ \mathbf{L_1}+H_2O+2Cl]^+$). Presumably, metal chelation is involved in the selective turn on fluorescence. However, fluorescence titration experiment failed to indicate the 1:1 complex formation as the fluorescence intensity increased linearly up to addition of 30 equivalents of Al^{3+} (**Figure 3.4C**).

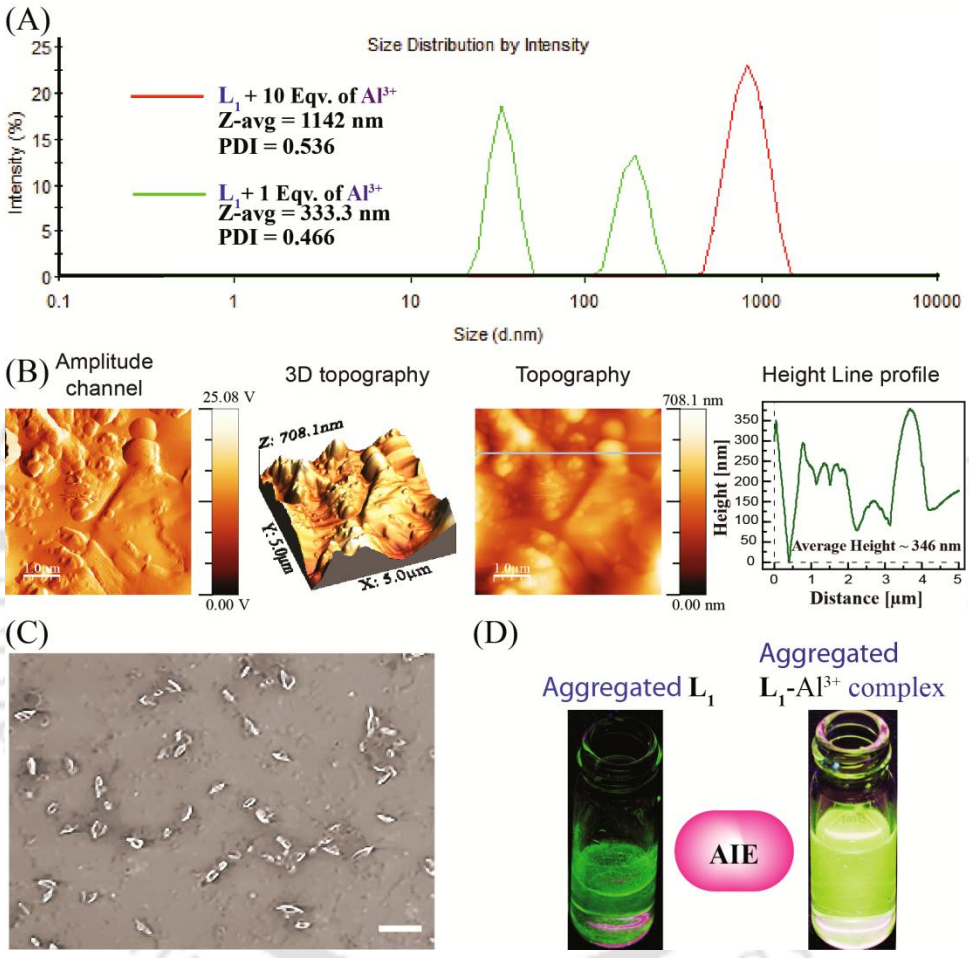

Figure 3.5: (A) DLS-based particle size analysis upon addition of 1.0 equivalent of Al^{3+} (green) and 10 equivalent of Al^{3+} (red) to $\mathbf{L_1}$ in mixed aqueous media. (B) AFM image and (C) FESEM image of the aggregates obtained after addition of Al^{3+} (10 equivalent) to $\mathbf{L_1}$ (D) Fluorescence outcome upon aggregation of $\mathbf{L_1}$ and $\mathbf{L_1}$-Al^{3+} complex respectively.

Thus it may be assumed that along with formation of complex, Al^{3+} also helped to form aggregates in the solution when added in excess, which in turn triggered the AIE activity of $\mathbf{L_1}$ (**Scheme 3.2**). Initial complexation resulted in the enhanced fluorescence intensity along with red shift in maxima as the chelation inhibited the free rotation and increased the delocalization of the ligand. However, further addition of Al^{3+} from 2.0 to 30 equivalents initiated the

aggregation of already formed complex, a phenomenon which manifested as a dramatic enhancement in fluorescence intensity due to AIE activation.

Dynamic light scattering (DLS) studies of **L_1** in a mixed aqueous media suggested that the average particle size increased from 333 nm to 1140 nm on changing the Al^{3+} concentration from 1.0 equivalent to 10 equivalents, which also supports the observed Al^{3+}-triggered AIE activity of the compound (**Figure 3.5A**). Atomic force microscope (AFM) and field emission scanning electron microscope (FESEM) analysis provided additional evidences for the formation of aggregates of **L_1**-Al complex (**Figure 3.5B-C**). It also might be noticed that there was conspicuous red shift in fluorescence for the aggregates of **L_1**-Al^{3+} complex compared to free **L_1** aggregates (**Figure 3.5D**).

Addition of appropriate amount of EDTA solution restored the native fluorescence of **L_1** when added to the highly fluorescent Al^{3+}-treated **L_1**, which substantiated the role of Al^{3+} in triggering aggregation and that aggregation was initiated after complex formation (**Appendix, Figure A3.7**). Detailed theoretical calculations also supported this premise. Density functional calculation(s) of **L_1**, **L_1**-Al^{3+} complex and **L_1**-Cu^{2+} complex were carried out to ascertain the effect of chelation on spectroscopic signatures. The substantial decrease in the HOMO to LUMO energy gap on chelation of **L_1** with Al^{3+} clearly testified the theoretical basis of the observed red shift in emission maxima of **L_1** when treated with Al^{3+} (**Appendix, Figure A3.8**). A similar decrease in HOMO to LUMO energy gap in the case of Cu^{2+} complex of **L_1** compared to **L_1** alone (**Appendix, Figure A3.9**) also explains the prominent red shift in UV-visible maxima (**Figure 3.1A**). All the optimized structures and their energy levels, which are directly influencing the spectral outcome, are indicated in the supporting information (**Appendix, Figure A3.10 and A3.11**).

3.6. Effect of pH on the Al^{3+} sensing by L_1

At lower pH (<3.0), **L_1** was unable to sense Al^{3+} ions may be due to the protonation of the pyridine moiety present in the receptor. However, fluorescence spectra of **L_1** and **L_1**-Al^{3+} system taken at various pH revealed that **L_1** can sense Al^{3+} in a wide range of pH (from pH 4.0 to pH 9.0) (**Appendix, Figure A3.12**). It may be mentioned here that the fluorescence intensity of **L_1** itself remained stable over a wide range of pH (from pH 4.0 to pH 11) which enhances the analytical prospect of the probe.

3.7. Biological studies of L_1 in presence of Al^{3+}

The selective sensing property of **L_1** towards Al^{3+} was encouraging and it indicated that the ligand could perhaps be exploited as a fluorescence-based probe for intracellular sensing of Al^{3+}. However, to pursue this objective it was paramount to initially verify the cytotoxic effect of **L_1** and its Al^{3+} complex on cells. To this end, an MTT assay revealed that the ligand **L_1**, Al^{3+} as well as the **L_1**-Al^{3+} complex did not influence the viability of cultured HeLa cells even at the highest tested concentration of 96 µM (**Figure 3.6A**). Given the non-toxic nature of **L_1** and **L_1**-Al^{3+} complex, intracellular detection of Al^{3+} was pursued. Fluorescence microscopic analysis indicated that HeLa cells treated with ligand **L_1** alone did not exhibit any intracellular fluorescence emission (**Figure 3.6B**). Furthermore, retention of the distinctive morphology of HeLa cells treated with the ligand was observed in the bright field image (**Figure 3.6B**), which validated the non-toxic nature of the ligand established earlier in MTT assay (**Figure 3.6A**).

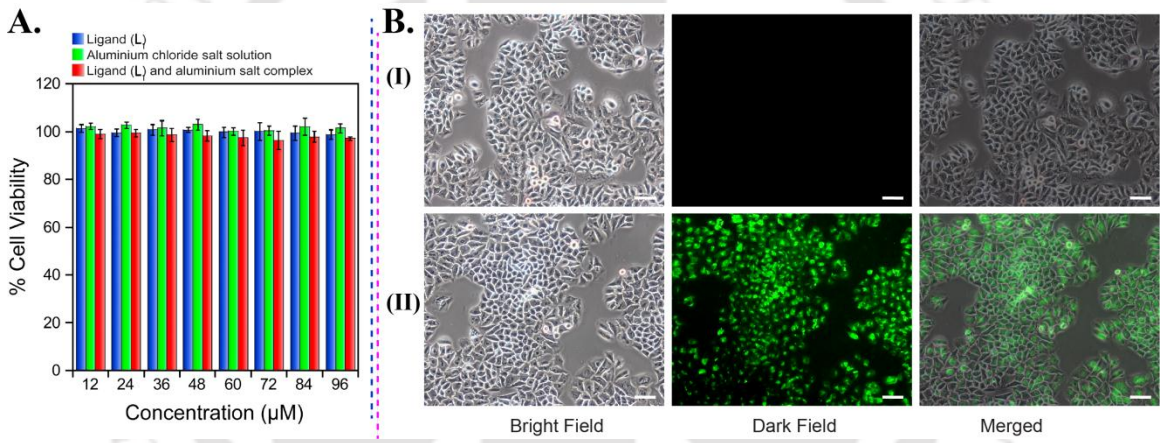

Figure 3.6: (A) MTT-based assay to ascertain the cytotoxic effect of **L_1**, aluminium chloride salt and **L_1**-Al^{3+} complex on HeLa cells. (B) Fluorescence microscope images of HeLa cells (under blue light) for (I) cells treated with 5.0 µM of **L_1**, (II) cells pre-treated with 5.0 µM of **L_1** followed by addition of 50 µM Al^{3+} solutions. Scale bar for the images is 100 µm.

Interestingly, when ligand-pretreated HeLa cells were incubated with hydrated Al^{+3} salt, a significant TURN-ON fluorescence emission was manifested (**Figure. 3.6B**). This suggested that the ligand **L_1** could translocate across the membrane and render selective sensing of Al^{3+} within HeLa cells. Given the neurotoxic implications of Al^{3+}, this finding is significant and it enhances the analytical merit of the ligand as a non-invasive probe for intracellular sensing of Al^{3+}.

3.8. Tracking of DNA

Studies on the interaction between Al^{3+} and DNA hold significant interest as reports suggest that the potential toxicity of Al^{3+} may be associated with its DNA binding property.[3.41-3.42] We envisaged that the $\mathbf{L_1}$-Al^{3+} ensemble is likely to interact with DNA, given the high affinity of Al^{3+} for phosphate groups and this event could be tracked through the change in the emissive response of the AIE active probe. Interestingly, incremental addition of calf-thymus DNA (ctDNA) to the highly fluorescent $\mathbf{L_1}$-Al^{3+} ensemble solution resulted in a dose-dependent fluorescence quenching (**Figure 3.7A**), which suggested disaggregation of $\mathbf{L_1}$-Al^{3+} ensemble. It is plausible that given the high affinity of Al^{3+} for phosphate groups present in ctDNA, interaction of $\mathbf{L_1}$-Al^{3+} ensemble with ctDNA and subsequent sequestration of Al^{3+} may ensue, analogous to the interaction of the metal chelator EDTA with $\mathbf{L_1}$-Al^{3+} ensemble (**Appendix, Figure A3.7**). This phenomenon perhaps manifests as disaggregation of the $\mathbf{L_1}$-Al^{3+} ensemble upon interaction with ctDNA and reduction in AIE activity of $\mathbf{L_1}$ (**Figure 3.7B**).

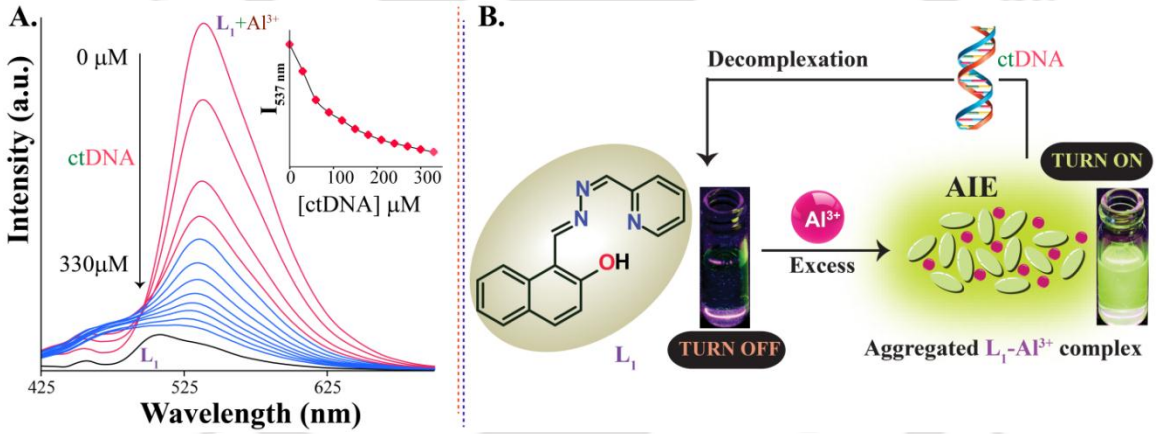

Figure 3.7. (A) Change in emission spectra of $\mathbf{L_1}$+ Al^{3+} ensemble with varying concentration of ctDNA, λ_{ex} = 400 nm. INSET: Changes in the emission intensity at 537 nm with incremental addition of ctDNA; (B) Plusible mechanism for tracking ctDNA.

3.9. Conclusion

In summary we developed a new AIE-active fluorophore that selectively exhibited a TURN-ON fluorescence response towards Al^{3+} in solution and rendered non-invasive detection of Al^{3+} in live HeLa cells. The assimilation of facile Al^{3+} sensing and subsequent tracking of DNA interaction in a single AIE-active system significantly enhances the scope of the developed chemosensor to probe the cellular and molecular basis of Al^{3+} toxicity in future investigations. Additionally the probe can detect Cu^{2+} through a selective colorimetric response among various tested metal ions in similar conditions. The conspicuous display of the turn-on fluorescence

response of $\mathbf{L_1}$ toward Al^{3+} (non-emissive to strong green fluorescence) and the colorimetric response of $\mathbf{L_1}$ toward Cu^{2+} (colourless to deep red) provided the scope for instant naked eye detection of these metal ions using $\mathbf{L_1}$.

References

3. 1 G.R. Rout, S.S. Roy, P. Das, *Agronomie*, 2001, **21**, 3.

3. 2 V.K. Gupta, A.K. Jain, G. Maheshwari, *Talanta* , 2007, **72**,1469.

3. 3 J. Barcelo´and C. Poschenrieder, *Environ. Exp. Bot.*, 2002, **48**, 75.

3. 4 Z. Krejpcio and R. W. P. Wojciak, *J. Environ. Stud*., 2000, **205**, 251.

3. 5 A. Salifoglou, *Coord. Chem. Rev.*, 2002, **228**, 297.

3. 6 M. E. Percy, T. P.A. Kruck, A. I. Pogue and W. J. Lukiw, *J. Inorg. Biochem*., 2011, **105**, 1505.

3. 7 G. D. Fasman, *Coord. Chem. Rev.*, 1996, **149**, 125

3. 8 D. Krewski, R. A. Yokel, E. Nieboer, D. Borchelt, J. Cohen, J. Harry,. S. Kacew, J, Lindsay, A. M. Mahfouz and V. Rondeau, *J. Toxicol. Environ. Health, Part B: Crit. Rev.*, 2007, **10:S1**, 1.

3. 9 G. Aragay, J. Pons and A. Merkoc, *Chem. Rev*. 2011, **111**, 3433.

3. 10 K. M. Dean, Y. Qin and A. E. Palmer, *Biochim. Biophys. Acta*, 2012, **1823**, 1406.

3. 11 S. Samanta, S. Goswami, A. Ramesh and G. Das, *Sens. Actuators B*., 2014, **194**, 120.

3. 12 B. K. Datta, S. Mukherjee, C. Kar, A. Ramesh and G. Das, *Anal. Chem*., 2013, **85**, 8369.

3. 13 C. Kar, M. D. Adhikari, A. Ramesh and G. Das, *Inorg. Chem.*, 2013, **52**, 743.

3. 14 B. K. Datta, D. Thiyagarajan, C. Kar, A. Ramesh and G. Das, *Org. Biomol. Chem.*, 2014, **12**, 4975.

3. 15 H. M. Park, B. N. Oh, J. H. Kim, W. Qiong, I. H. Hwang, K. Jung, C. Kim and J. Kim, *Tet. Lett*., 2011, **52**, 5581.

3. 16 D. Maity and T. Govindaraju, T., *Chem. Commun*. 2010, 4499.

3. 17 S. H. Kim, H. S. Choi, J. Kim, S. J. Lee, D. T. Quang and J. S. Kim, *Org. Lett*., 2010, **12**, 560.

3. 18 Y. Lu, S. Huang, Y. Liu, S. He, L. Zhao and X. Zeng, *Org. Lett*., 2011, **13**, 5274.

3. 19 M. Arduini, F. Felluga, F. Mancin, P. Rossi, P. Tecilla, U. Tonellato and N. Valentinuzzi, *Chem. Commun*. 2003, 1606.

3. 20 T. H. Ma, M. Dong, Y. M. Dong, Y. W. Wang and Y. Peng, *Chem. Eur. J.*, 2010, **16**, 10313.

3. 21 W. H. Ding, W. Cao, X. J. Zheng, D. C. Fang, W. T. Wong and L. P. Jin, *Inorg. Chem.* 2013, **52**, 7320.

3. 22 X. Sun, Y. W. Wang, and Y. Peng, *Org. Lett.*, 2012, **14**, 3420.

3. 23 J. Luo, Z. Xie, J. W. Y. Lam, L. Cheng, H. Chen, C. Qiu, H. S. Kwok, X. Zhan, Y. Liu, D. Zhu and B. Z. Tang, *Chem. Commun.*, 2001, 1740.

3. 24 Y. Hong, J. W. Y. Lam and B. Z. Tang, *Chem. Commun*., 2009, 4332.

3. 25 Y. Hong, J. W. Y. Lam and B. Z. Tang, *Chem. Soc. Rev.*, 2011, **40**, 5361.

3. 26 Y. Liu, Y.Tang, N. N. Barashkov, I. S. Irgibaeva, J. W. Y. Lam, R. Hu, D. Birimzhanova, Y. Yu and B. Z. Tang, *J. Am. Chem. Soc*., 2010, **132**, 13951.

3. 27 X. Chen, X. Y. Shen, E. Guan, Y. Liu, A. Qin, J. Z. Sun and B. Z. Tang, *Chem. Commun.*, 2013, **49**, 1503.

3. 28 M. C. Linder and M. Hazegh-Azam, *Am. J. Clin. Nutr.* 1996, **63**, 797S.

3. 29 R. Uauy, M. Olivares and M. Gonzalez, *Am. J. Clin. Nutr.*, 1998, **67**, 952S.

3. 30 D. Strausak, J. F. Mercer, H. H. Dieter, W. Stremmel and G. Multhaup, *Brain Res. Bull*., 2001, **55**, 175.

3. 31 L. Banci, I. Bertini, S. Ciofi-Baffoni, T. Kozyreva, K. Zovo and P. Paulmaa, *Nature*, 2010, **465**, 645.

3. 32 E. L. Que, D.W. Domaille and C.J. Chang, *Chem. Rev*., 2008,**108**, 1517.

3. 33 P. Grandini, F. Mancin, P. Tecilla, P. Scrimin and U. Tonellato, *Angew.Chem. Int. Ed*., 1999, **38**, 3061.

3. 34 D. J. Waggoner, T.B. Bartnikas and J.D. Gitlin, *Neurobiol. Dis*., 1999, **6**, 221.

3. 35 D. R. Brown and H. Kozlowski, *Dalton Trans*., 2004, 1907.

3. 36 K. J. Barnham and A.I. Bush, *Curr.Opin. Chem. Biol*., 2008, **12**, 222.

3. 37 R. R. Crichton, D.T. Dexter and R.J. Ward, *Coord. Chem. Rev*., 2008, 252, 1189.

3. 38 E. Gaggelli, H. Kozlowski, D. Valensin and G. Valensin, *Chem. Rev*., 2006, **106**, 1995.

3. 39 A. J. Qin, J. W. Y. Lam, F.Mahtab, C. K. W. Jim, L.Tang, J. Z. Sun, H. H. Y. Sung, I. D. Williams and B. Z. Tang, *Appl. Phys. Lett.*, 2009, **94**, 253308.

3. 40 M. Chen, L. Li, H. Nie, J. Tong, L. Yan, B. Xu, J. Z. Sun, W. Tian, Z. Zhao, A. Qin, B. Z. Tang, *Chem. Sci.*, 2015, DOI: 10.1039/c4sc03365e.

3. 41 J. Wu, F. Du, P. Zhang, I. A. Khan, J. Chen and Y. Liang, *J. Inorg. Biochem*., 2005, **99**, 1145.

3. 42 M. L. Hegde, S. Anitha, K. S. Latha, M. S. Mustak, R. Stein, R. Ravid and K. S. J. Rao, *J. Mol. Neurosci*., 2003, **22**, 19.

Appendix

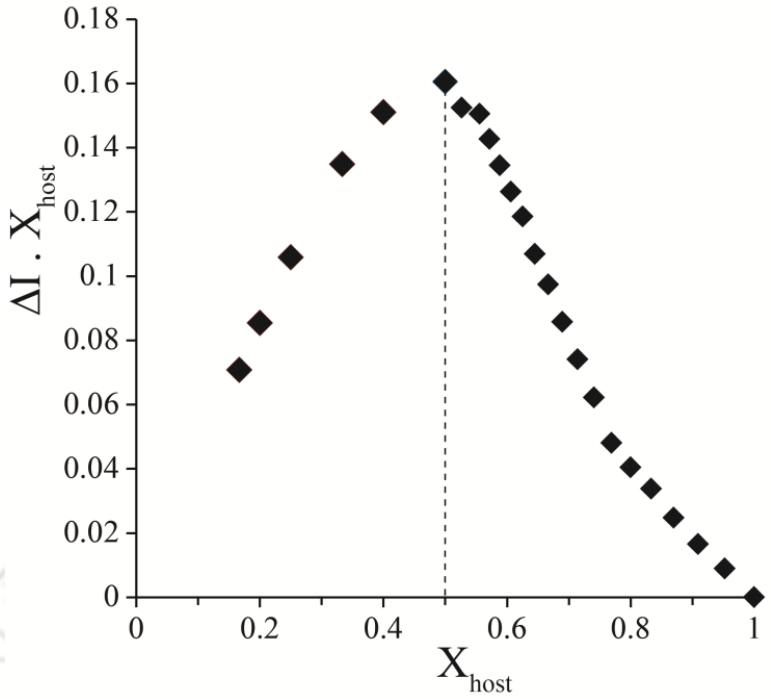

Figure A3.1: Job's plot for $\mathbf{L_1}$-Cu^{2+} complex formation using UV-visible titration experiment. Where X_{host} = the mole fraction of $\mathbf{L_1}$ and ΔI is the change ($I-I_0$) in the intensity of the emission spectra in presence of guest.

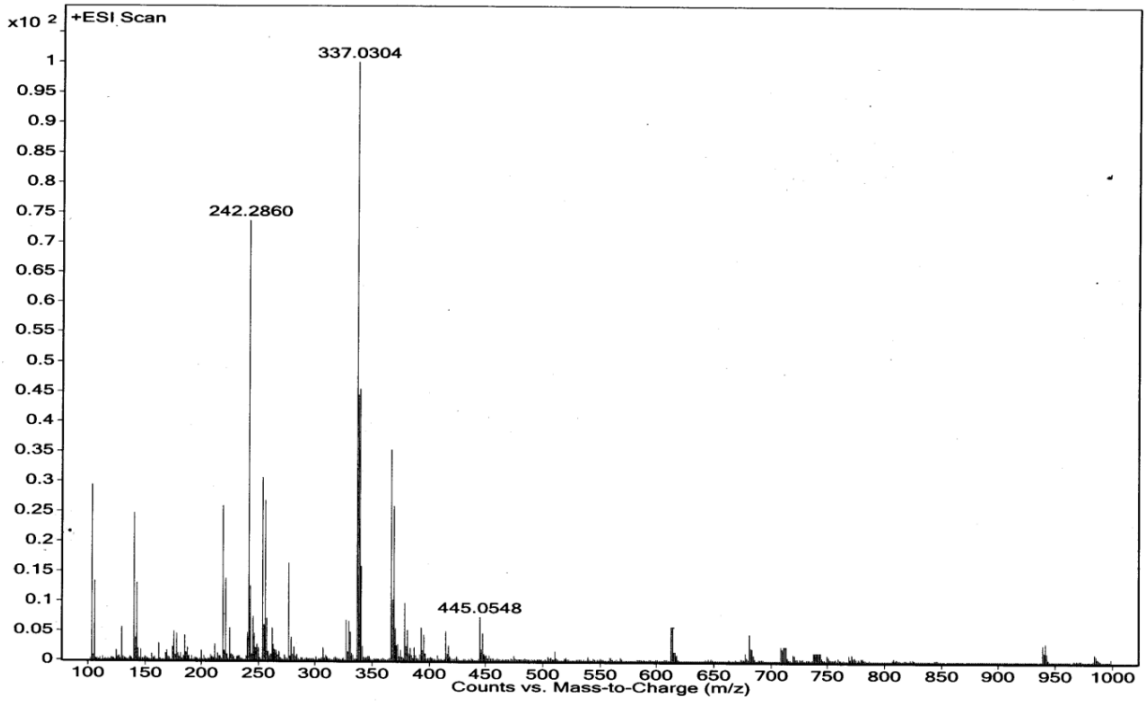

Figure A3.2: Mass spectrum of $\mathbf{L_1}$-Cu^{2+} complex.

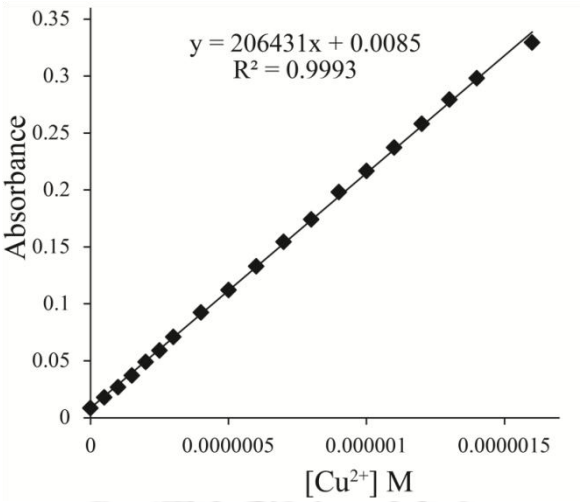

Figure A3.3: Absorbance versus concentration plot for calculating the detection limit (3σ/k, σ= 0.0000753) of Cu^{2+} by $\mathbf{L_1}$.

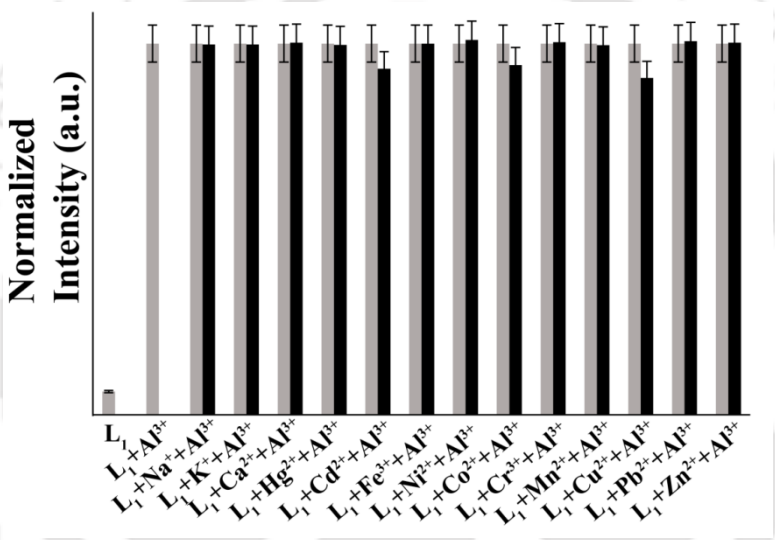

Figure A3.4: Effect of various metal ions on the fluorescence intensity of $\mathbf{L_1}$+Al^{3+}.

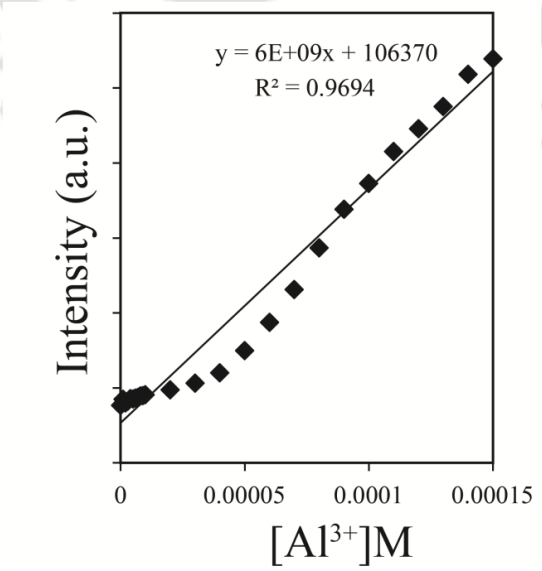

Figure A3.5: Determination of detection limit for Al^{3+} sensing by $\mathbf{L_1}$ from fluorescence titration experiment.

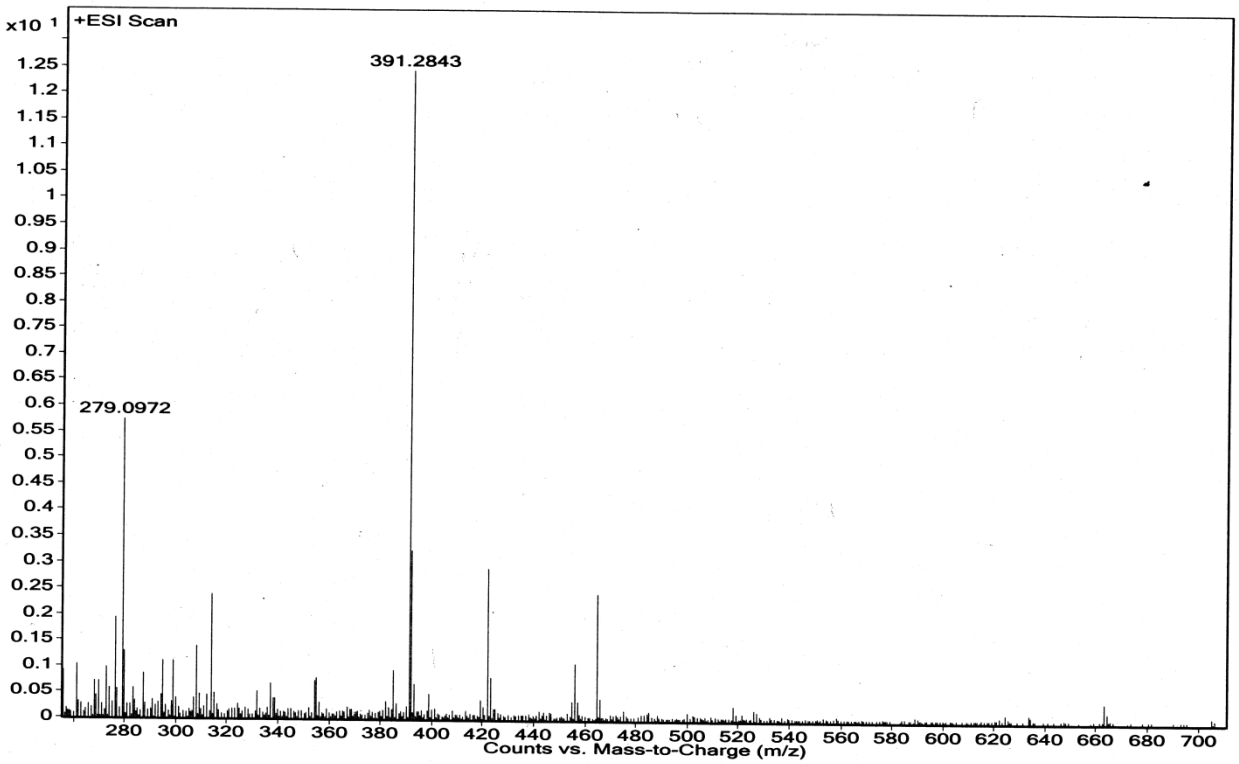

Figure A3.6: Mass spectrum of $\mathbf{L_1}$-Al^{3+} complex.

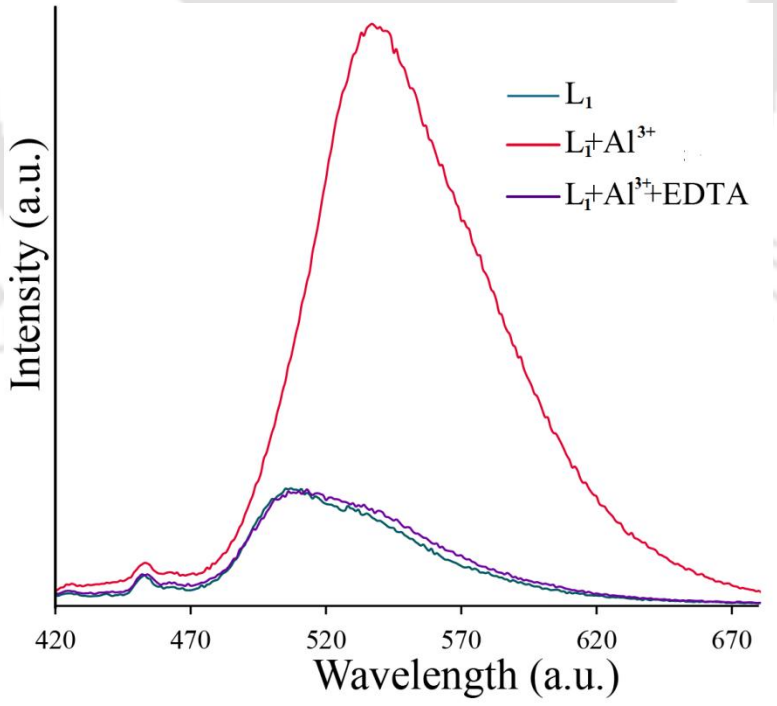

Figure A3.7: Fluorescence spectra of $\mathbf{L_1}$ (10 μM) in presence of 10 equivalents of Al^{3+} before and after treatment with excess EDTA. λ_{ex} = 400 nm.

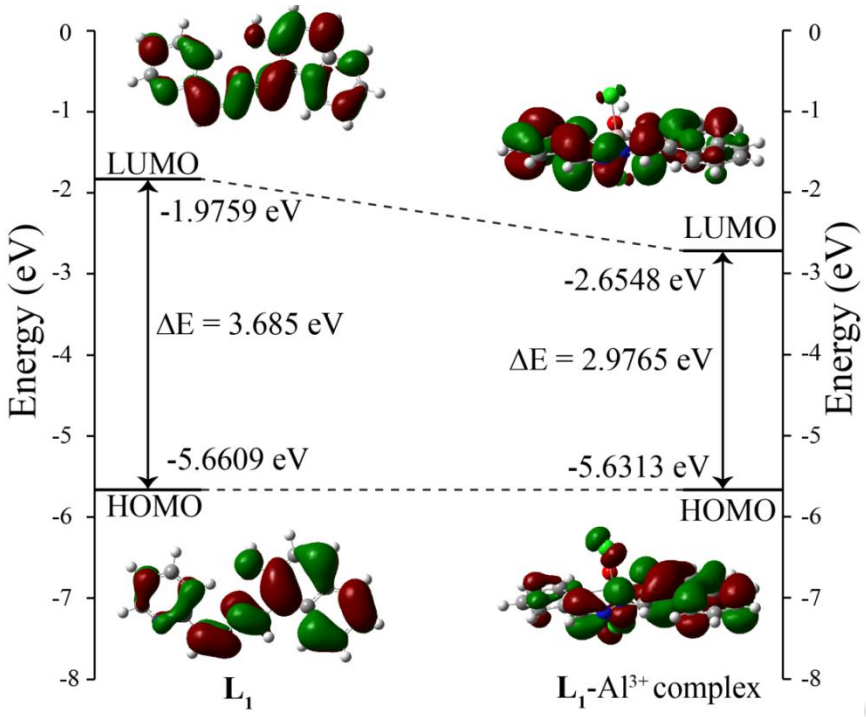

Figure A3.8: Frontier molecular orbital plots and energy level diagrams of $\mathbf{L_1}$ and $\mathbf{L_1}$-Al^{3+} complex. The calculations were performed using B3LYP/6-31 G (d,p) as implemented on Gaussian 03.

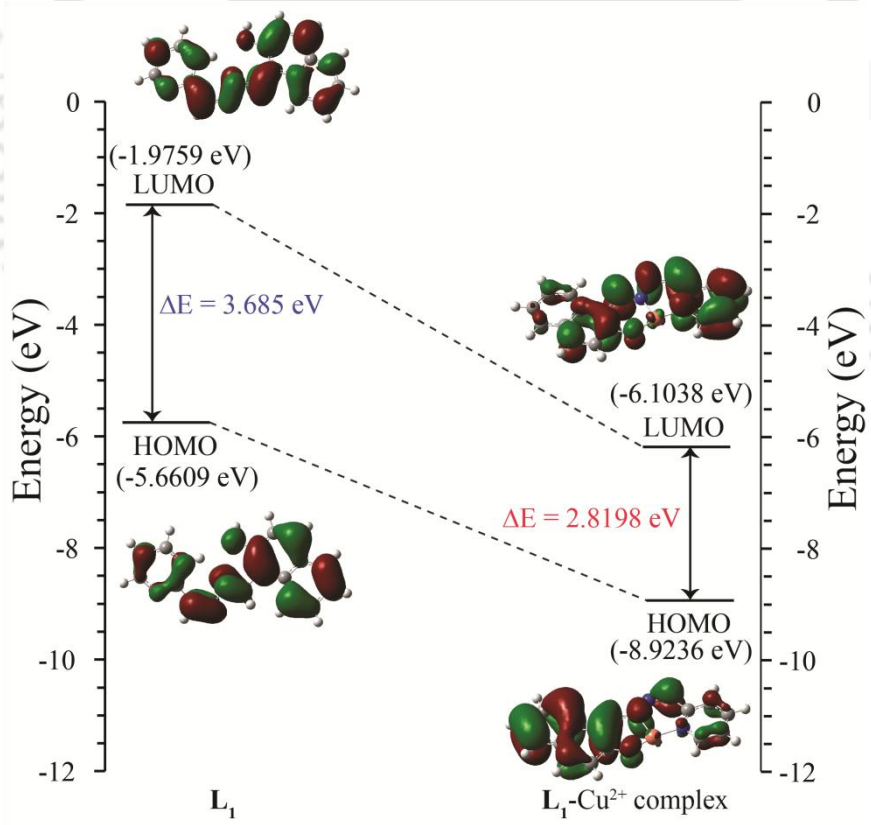

Figure A3.9: Frontier molecular orbital plots and energy level diagrams of $\mathbf{L_1}$ and $\mathbf{L_1}$-Cu^{2+} complex. The calculations were performed using B3LYP/6-31 G (d,p) as implemented on Gaussian 03.

Occupied Orbitals	Energy (eV)	Vacant Orbitals	Energy (eV)
HOMO-2 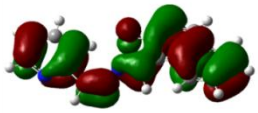	-6.5492	LUMO 	-1.9758
HOMO-1 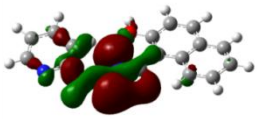	-5.8942	LUMO+1 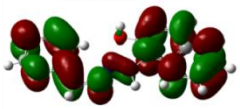	-1.0778
HOMO 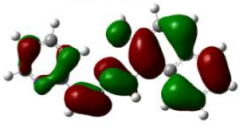	-5.6609	LUMO+2 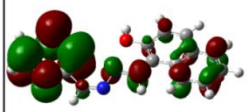	-0.4123

Figure A3.10: Important orbitals and the energies of $\mathbf{L_1}$. The calculations were performed using B3LYP/6-31 G (d,p) as implemented on Gaussian 03.

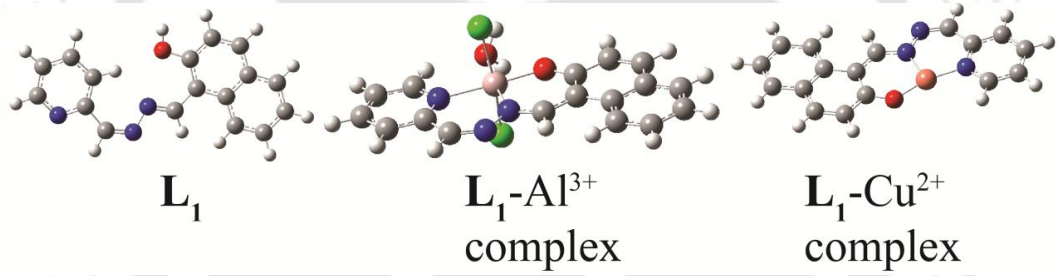

Figure A3.11: Optimized structures of $\mathbf{L_1}$, $\mathbf{L_1}$-Al^{3+} complex and $\mathbf{L_1}$-Cu^{2+} complex. The calculations were performed using B3LYP/6-31 G (d,p) as implemented on Gaussian 03.

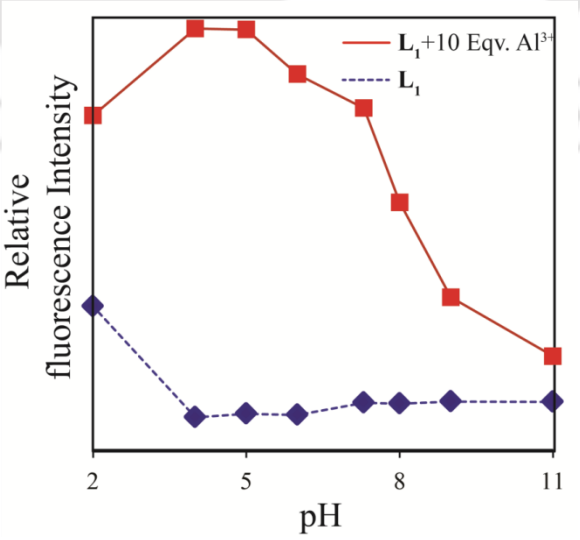

Figure A3.12: Dependence of the fluorescence intensity of $\mathbf{L_1}$ and $\mathbf{L_1}$-Al^{3+} on pH. Blue trace: $\mathbf{L_1}$ (10 μM) and red trace: $\mathbf{L_1}$ with excess (20.0 equivalents) of Al^{3+}.

Ref. A3.1. M. J. Frisch, G. W. Trucks, H. B. Schlegel, G. E. Scuseria, M. A. Robb, J. R. Cheeseman, J. A. Montgomery, Jr., T. Vreven, K. N. Kudin, J. C. Burant, J. M. Millam, S. S. Iyengar, J. Tomasi, V. Barone, B. Mennucci, M. Cossi, G. Scalmani, N. Rega, G. A. Petersson, H. Nakatsuji, M. Hada, M. Ehara, K. Toyota, R. Fukuda, J. Hasegawa, M. Ishida, T. Nakajima, Y. Honda, O. Kitao, H. Nakai, M. Klene, X. Li, J. E. Knox, H. P. Hratchian, J. B. Cross, V. Bakken, C. Adamo, J. Jaramillo, R. Gomperts, R. E. Stratmann, O. Yazyev, A. J. Austin, R. Cammi, C. Pomelli, J. W. Ochterski, P. Y. Ayala, K. Morokuma, G. A. Voth, P. Salvador, J. J. Dannenberg, V. G. Zakrzewski, S. Dapprich, A. D. Daniels, M. C. Strain, O. Farkas, D. K. Malick, A. D. Rabuck, K. Raghavachari, J. B. Foresman, J. V. Ortiz, Q. Cui, A. G. Baboul, S. Clifford, J. Cioslowski, B. B. Stefanov, G. Liu, A. Liashenko, P. Piskorz, I. Komaromi, R. L. Martin, D. J. Fox, T. Keith, M. A. Al-Laham, C. Y. Peng, A. Nanayakkara, M. Challacombe, P. M. W. Gill, B. Johnson, W. Chen, M. W. Wong, C. Gonzalez, and J. A. Pople, *Gaussian 03, Revision E.01,Gaussian, Inc., Wallingford CT*, 2004.

Chapter 4

A Solo Fluorogenic Probe for Real-time Sensing of SO_3^{2-} and SO_4^{2-}/ HSO_4^- in Aqueous Medium and Live Cells by Distinct Turn-On Emission Signals

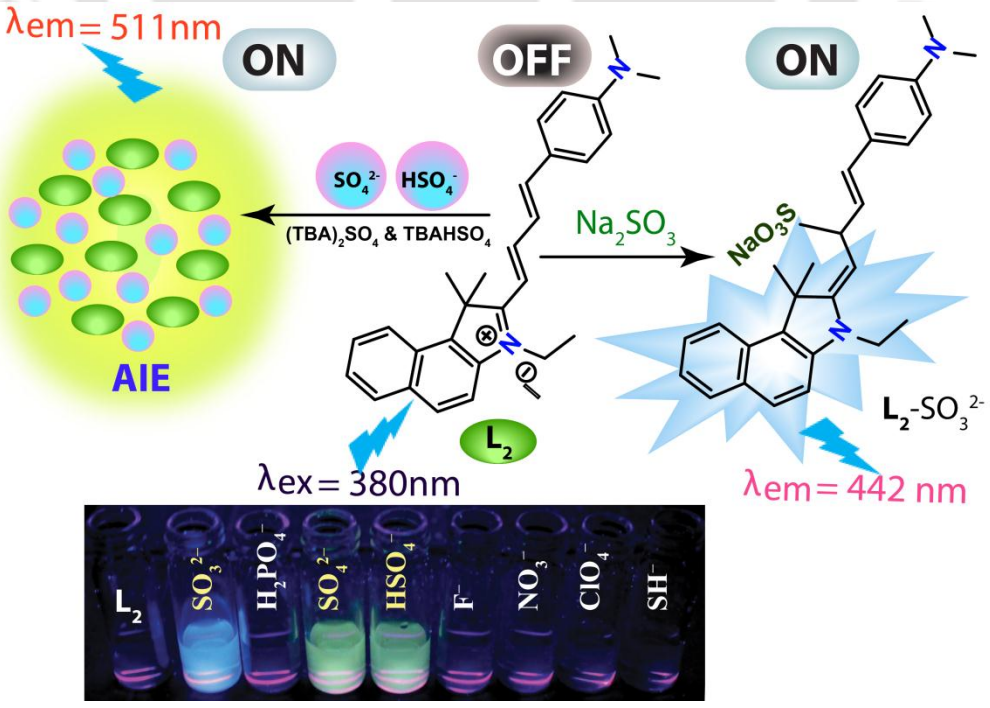

Chapter 4

4.1. Background and focus of the chapter

Sulfur dioxide (SO_2) is a major air pollutant, which is often liable to be exposed to the atmosphere due to the extensive combustion of fossil fuels across the world. Epidemiological studies suggest that prolonged SO_2 exposure may lead to lung cancer, cardiovascular diseases,[4.1] many neurological disorders including migraine headaches, stroke and brain cancer [4.2] besides causing some respiratory ailments.[4.3] The toxicity of SO_2 is mainly attributed to the two derivatives, sulfite (SO_3^{2-}) and bisulfite (HSO_3^-) (3:1 M/M, in neutral fluid)[4.4], wherein the sulfurous acid produced in the respiratory tract from inhaled hydrated SO_2 facilitates the generation of these two derivatives. Though sodium sulfite is commonly used to preserve food and beverages from oxidation, excess sulfite intake could lead to asthma and other allergic reactions in some individuals.[4.5] Further, toxicological studies revealed that SO_2 and/or its derivatives could change the characteristics of voltage-gated sodium channels as well as potassium channels in rat hippocampal neurons,[4.1a] affect thiol levels to hamper redox balance in cells,[4.6a] and thus potentially could produce a neuronal perturbation.[4.6b] At the same time it has been found that SO_2 might regulate vascular smooth muscle tone in synergy with NO.[4.7] Though SO_2 gas can be produced endogenously from sulfur-containing amino acids,[4.8] the exact role of SO_2 in the context of tumor cell physiology as well as in normal cells is yet to be resolved. Hence, developing an efficient probe for the detection of trace SO_2 (and its derivatives) in aqueous medium and biological samples (especially in live cells) has spurred great interest amongst the analytical chemists at large.

On the other hand, sulfate (SO_4^{2-}) being one of the dominant sulfur species in aquatic environment may pose threat of environmental pollution if its level is greatly elevated in atmosphere by acidic deposition owing to the vast use of coal, oil and other sulfur-containing fuel.[4.9] It has been established that hydrogen sulfate (HSO_4^-) may dissociate at high pH to generate toxic sulfate, which can cause irritation of the skin and eyes and may even lead to respiratory paralysis.[4.10] Development of sulfate/bisulfate selective probes has currently become an area of immense interest as these anions play various important roles in biological systems and disease[4.11] along with their acknowledged role in radioactive waste remediation.[4.12]

However, designing sulfate/bisulfate selective probe that can effectively bind the anion in water is extremely challenging as sulfate (SO_4^{2-}) has very high free energy of hydration.[4.13]

Fluorescence-based sensing probes are advantageous over other sensing systems for the detection of biological species as they can render rapid, non-invasive, temporal and sensitive detection of target analytes.[4.14, 4.15] Although a few fluorescent probes for the detection and visualization of sulfite in living cells have recently been reported based on nucleophilic reaction with aldehyde,[4.16] selective deprotection of levulinate,[4.17] Michael-type additions [4.18] and coordinative interactions,[4.19] most of these sensing systems suffer from drawbacks in terms of detection limit and response time (5 min to 10 h). Moreover, the levulinate-type probes are likely to generate high background signal in biological imaging owing to the presence of the labile ester linkage.[4.20] Even though, more recently *Liu et.al*[4.21a] and *Zhu et.al*[4.21b] reported two new sensors for reliable detection of SO_2 in cells, these probes too require 30% DMF and 40% glycerol, respectively, as co-solvents along with water. However, for fluorescence-based sensing of SO_2 derivatives in cells, the challenge is to develop a probe that would afford detection of target analyte in a completely aqueous medium, which is relevant to the biological milieu.

On the other hand, though there are few reported fluorescent probes for sulfate/bisulfate[4.22] sensing, most of them suffers from drawbacks like questionable selectivity, unsatisfactory detection limit and use of organic/mixed-organic solvents as medium.

In order to address these issues, in this chapter we describe a new and versatile probe (**L_2**) that can rapidly sense SO_2 derivative (SO_3^{2-}) as well as SO_4^{2-}/HSO_4^- through highly selective and differential Turn-On fluorescence responses in 100% aqueous medium and live cells.

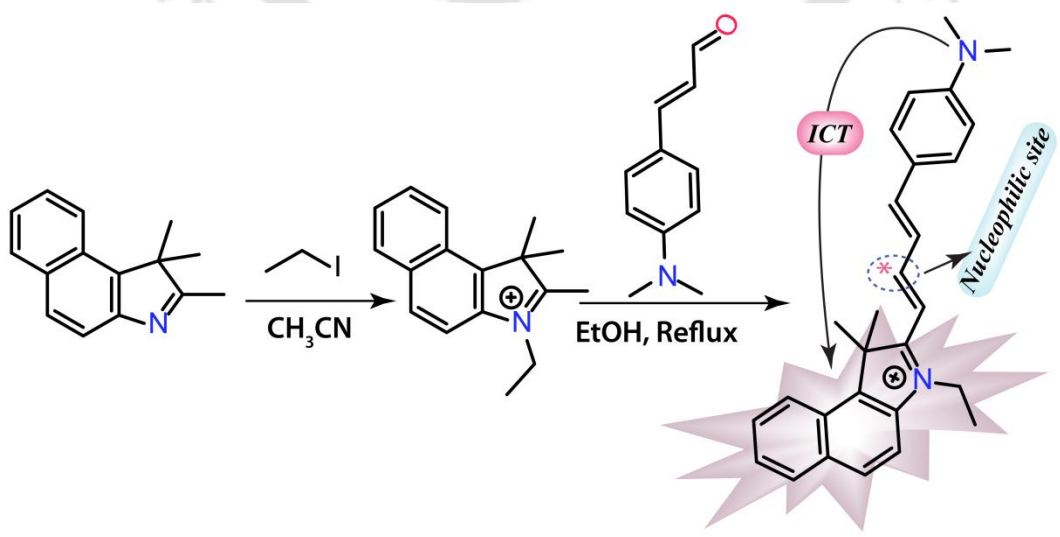

Scheme 4.1. Design and synthesis of the Probe **L_2**

5.2. Design and synthesis of probe L_2

It is well established that SO_2 derivatives (SO_3^{2-} and HSO_3^-) can readily react with α,β–unsaturated compounds very rapidly in aqueous solution.[4.23] Hence in the present study, the design of the probe was based on this fundamental notion of a nucleophilic addition reaction, which can subsequently be tracked by a rapid change in fluorescence. The probe (**L_2**) was synthesized by the simple condensation reaction of 4-(Dimethylamino)cinnamaldehyde with 3–ethyl–1,1,2–trimethyl–1*H*–benzo[*e*]indol–3–ium in dry ethanol **(Scheme 4.1)**. The detailed synthetic procedures as well as the characterization (^{1}H NMR, ^{13}C NMR and HRMS) of the product (**L_2**) have been presented in the Experimental section (**Figure A2.5-A2.7, chapter 2**). It can be mentioned here that 1*H*-Benzo[*e*]indolium was used not only as a fluorophore but also to improve the solubility of the fluorescent probe in aqueous medium. Optical properties of the probe were then ascertained in detail to explore its sensing ability.

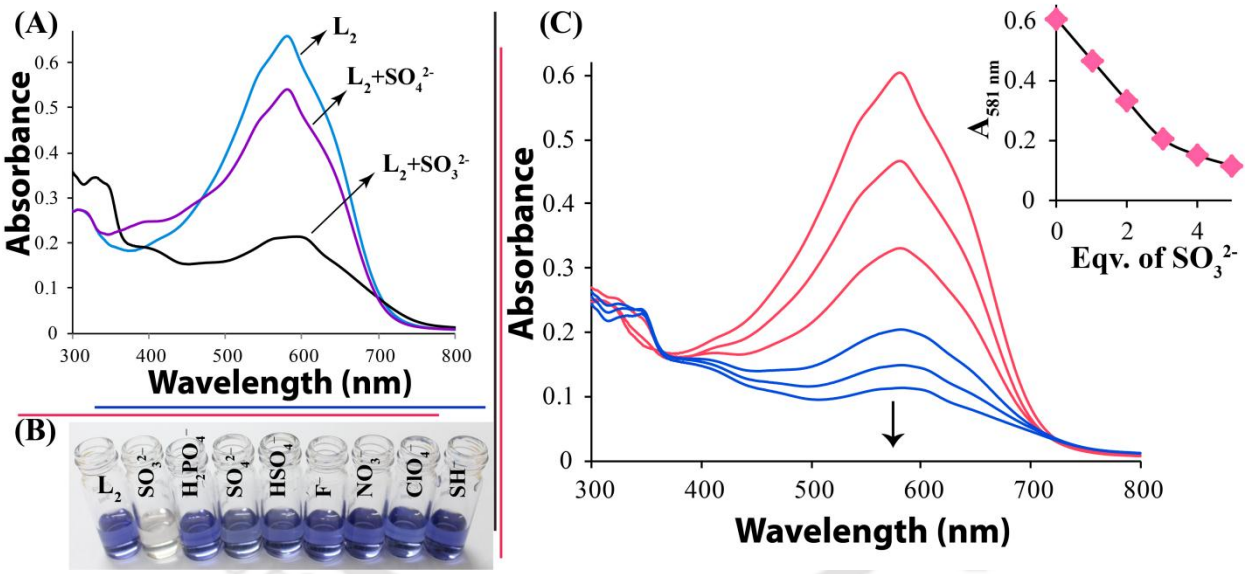

Figure 4.1: (A) UV-Visible spectra of **L_2** (10 μM) in aqueous medium in presence of excess of (20 equivalents) SO_3^{2-} and SO_4^{2-}. (B) Visual changes in color of the solution of **L_2** in presence of different anions under day light; (C) UV-Visible spectra of **L_2** (10 μM) in presence of varying concentration of SO_3^{2-}; INSET: Changes in the absorbance at 580 nm with addition of equivalents of SO_3^{2-}

4.3. UV-Visible spectroscopic study of L_2

UV-Vis spectra of the probe **L_2** taken in almost 100% aqueous (actual 99.998% aqueous medium containing 0.002% DMSO) medium revealed a well-defined strong absorbance maximum (ϵ=65904.5$M^{-1}cm^{-1}$) at 580 nm due to the π-π* charge transfer transition (**Figure 4.1A**). Interestingly, addition of 20 equivalents of SO_3^{2-} to **L_2** rendered a rapid colorimetric change as the absorbance peak (ϵ=21277.2$M^{-1}cm^{-1}$) at 580 nm reduced substantially with the

simultaneous emergence of a new absorbance maximum at 360 nm (**Figure 4.1A**) which was accompanied by clear visual change in the color of the experimental solution from violet to colorless; whereas interaction of other analytes ($H_2PO_4^-$, SO_4^{2-}(ϵ=54072.7$M^{-1}cm^{-1}$), HSO_4^-, F^-, NO_3^-, ClO_4^- and SH^-) with **L_2** failed to yield any significant colorimetric response (**Figure 4.1B**). A systematic and gradual reduction in the absorbance of **L_2** at 580 nm was witnessed with the incremental addition of SO_3^{2-} (**Figure 4.1C**). The selective colorimetric response of the probe **L_2** towards SO_3^{2-} clearly suggested the possibility that addition reaction of the target analyte (SO_3^{2-} in the present case) to **L_2** disrupted the extended conjugation in **L_2**, which in turn hindered the π-π* charge transfer transition. Hence it was prudent to pursue a detailed fluorescence study.

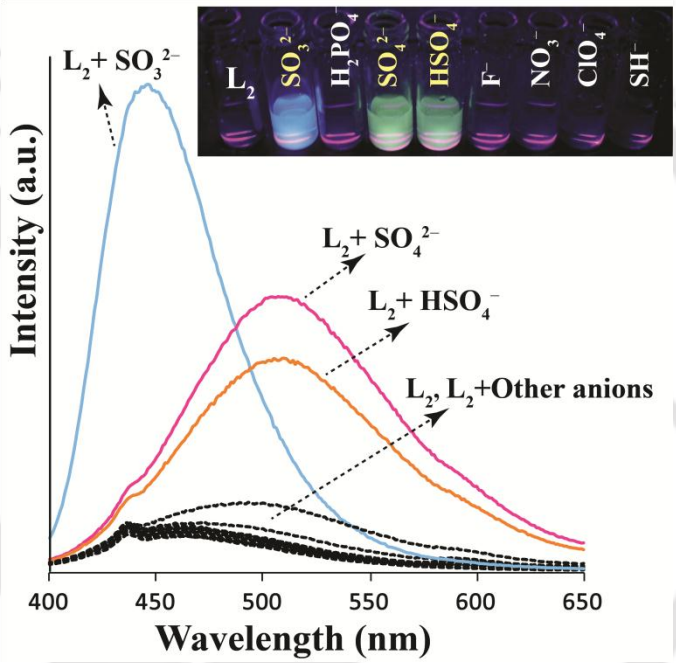

Figure 4.2: Fluorescence spectra of **L_2** (10 μM) in aqueous medium in presence of excess of (20 equivalents) various anions and nucleophilic reagents (Cys, Hcy). INSET: Visual change in fluorescence of **L_2** in presence of different anions under UV light.

4.4. Fluorescence spectroscopic study of L_2

On excitation at 380 nm, **L_2** exhibited a very weak emission band near 440 nm in ~100% aqueous medium **(Figure 4.2)**. To ascertain the selectivity of the probe, fluorescence spectra of **L_2** were recorded in presence of 20 equivalents of various ionic and neutral species including F^-, Cl^-, Br^-, I^-, NO_2^-, NO_3^-, CH_3COO^-, $H_2PO_4^-$, PPi, HCO_3^-, SO_4^{2-}, HSO_4^-, PF_6^-, ClO_4^-, SCN^-, $S_2O_3^{2-}$, $S_2O_8^{2-}$, $C_6H_7O_6^-$ (ascorbate), SO_3^{2-}, SH^-, Cys, Hcy and GSH. It was interesting to note that no other ionic or neutral species altered the emission behavior of the probe except SO_3^{2-} and SO_4^{2-}/HSO_4^-. Addition of SO_3^{2-} to **L_2** resulted in a high Turn-On fluorescence and a dramatic

enhancement (~12 fold) in the florescence intensity at 442 nm was observed (**Figure 4.2**). On the other hand, addition of SO_4^{2-}/HSO_4^- to **L_2** under similar conditions resulted in the emergence of a new red shifted emission maximum at 511 nm accompanied by ~10 fold enhancement in the fluorescence intensity of **L_2** (**Figure 4.2**). Eventually it was found that the fluorescence quantum yield of the probe **L_2** (φ=0.014) was very low which increased reasonably upon interacting with SO_3^{2-} (φ=0.098), and SO_4^{2-} (φ=0.091). These highly selective and distinct Turn-On fluorescence responses of **L_2** towards SO_3^{2-} and SO_4^{2-}/HSO_4^- were also noticeable by naked eye as the non-fluorescent solution of **L_2** emitted a strong bluish-green fluorescence upon interaction with SO_3^{2-} and greenish-yellow fluorescence upon interaction with SO_4^{2-}/HSO_4^- (**Figure 4.2 INSET**). However, it was interesting to note that **L_2** preferentially showed selectivity towards SO_3^{2-} or SO_4^{2-} based on whichever has the higher concentration in a SO_3^{2-} and SO_4^{2-} mixture (**Appendix, Figure A4.1**).

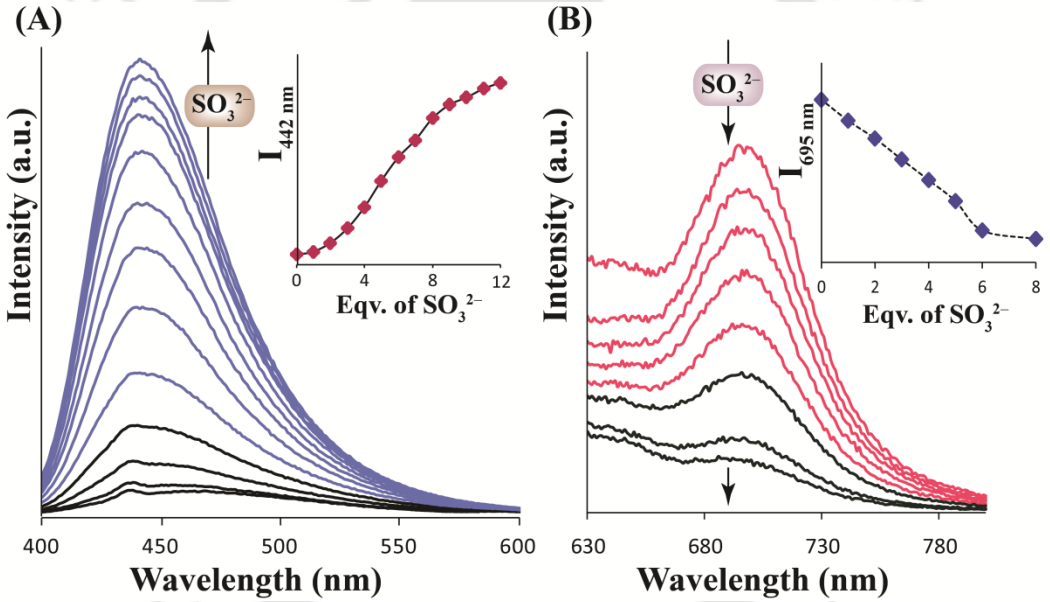

Figure 4.3: (A) Fluorescence spectra of **L_2** (10 μM) in presence of varying concentration of SO_3^{2-}; INSET: Changes in the emission intensity at 442 nm with addition of equivalents of SO_3^{2-}; λ_{ex} = 380 nm (B) Fluorescence spectra of **L_2** (10 μM) in presence of varying concentration of SO_3^{2-}; INSET: Changes in the emission intensity at 695 nm with addition of equivalents of SO_3^{2-}; λ_{ex} = 580 nm.

It is worth mentioning here that all the fluorescence spectra were recorded within 1 min of the addition of the analytes, which implied that the Turn-On fluorescence response of **L_2** towards SO_3^{2-} in solution was rapid. Subsequently, when the time-dependent change in the fluorescence of **L_2** with and without addition of SO_3^{2-} was investigated, a significant Turn-On response for **L_2**-SO_3^{2-} could be observed within 30 seconds, which again highlighted the scope for the real-time detection of SO_3^{2-} using the probe **L_2** (**Appendix, Figure A4.2**). It is also significant to

highlight that even the interaction of 200 equivalents of some inorganic sulfur compounds (SCN^-, $S_2O_3^{2-}$, $S_2O_8^{2-}$), nucleophilic reagents (Cys, Hcy and GSH) and reducing agent (sodium ascorbate) with **L_2** for more than 10 min could not induce any noticeable change in the emission behavior of **L_2**, which further reiterated the high selectivity of **L_2** towards SO_3^{2-} (**Appendix, Figure A4.3, A4.4**).

To obtain a quantitative insight of the relation between fluorescence spectral change of **L_2** and the equivalents of SO_3^{2-} interacted; a fluorescence titration experiment was carried out with varying concentration of SO_3^{2-}. An incremental addition of SO_3^{2-} to the solution of **L_2** in aqueous medium resulted in a systematic enhancement in its emission intensity at 442 nm upon excitation at 380 nm (**Figure 4.3A**).

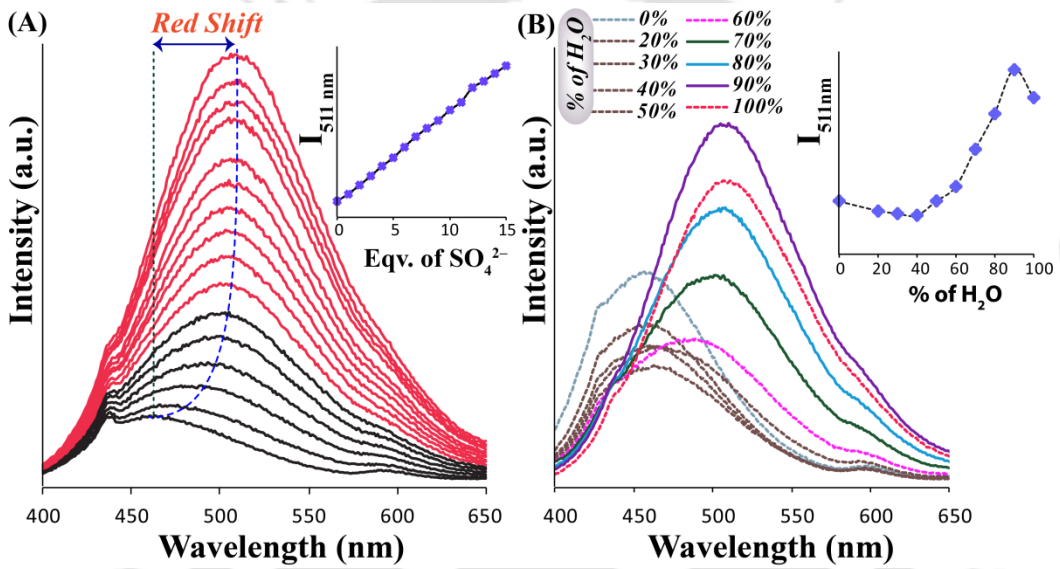

Figure 4.4: (A) Fluorescence spectra of **L_2** (10 μM) in presence of varying concentration of SO_4^{2-}; INSET: Changes in the emission intensity at 511 nm with addition of equivalents of SO_4^{2-}; λ_{ex} = 380 nm. (B) Emission spectra of **L_2**- SO_4^{2-} (1:20 equivalent) combine upon changing the water fraction of methanol-water mixed solvent; λ_{ex} = 380 nm. INSET: change in the fluorescence intensity with different water fractions.

Interestingly, when excited at 580 nm, the emission peak of **L_2** at 695 nm decreased gradually upon interaction with increasing concentration of SO_3^{2-} (**Figure 4.3B**). Hence the systematic reduction of the emission intensities at 695 nm provided an additional handle for tracking SO_3^{2-}. The ratio of the intensities at two different wavelengths (I_{442}/I_{695}) varied from 0.66 to 69.61 up to addition of 8 equivalent of SO_3^{2-}, which implied that measuring the signal ratios at two wavelengths would provide a wide dynamic range for ratio-metric sensing of SO_3^{2-} in aqueous solution. It can be mentioned here that the detection limit for SO_3^{2-}, determined from the fluorescence titration experiment (**Figure 4.3A**) was found to be 1.06×10^{-7} M or 8.50 ppb (**Appendix, Figure A4.5**) which is much lower compared to several reported probes.[16-21a]

Similar fluorescence titration experiment was also pursued with varying concentration of SO_4^{2-}. A gradual incremental addition of SO_4^{2-} to the solution of **L_2** in similar condition resulted in a systematic enhancement in its emission intensity along with gradual red shift in maxima and eventually a new red shifted emission maximum was established at 511 nm (**Figure 4.4A**). It can be mentioned here that the detection limit for SO_4^{2-} ascertained from this fluorescence titration experiment was found to be 5.31×10^{-7} M or 51.03 ppb (**Appendix, Figure A4.6**). It also may be noted that the probe **L_2** has lower detection limit for HSO_4^-/SO_4^{2-} compared to various other reported sensing systems.[22b,d,f]

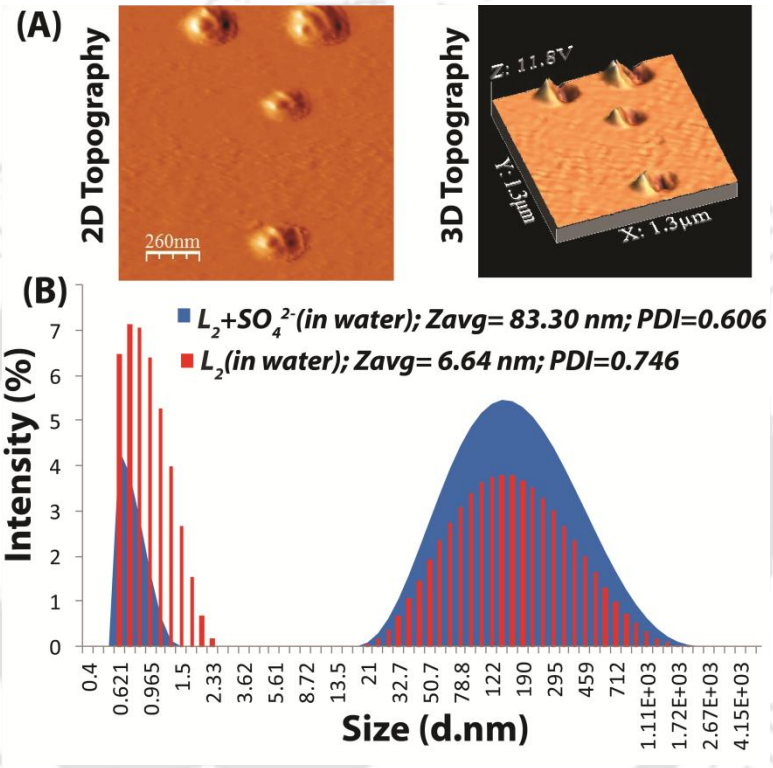

Figure 4.5: (A) AFM image (amplitude) of the aggregates obtained after addition of SO_4^{2-} (20 equivalent) to **L_2** (10 µM) in aqueous medium; (B) DLS-based particle size analysis: Change in particle size, with and without addition of SO_4^{2-} (20 equivalents) to **L_2** (10 µM) in aqueous medium.

4.5. Plausible mechanism of sensing

It is well established that α,β–unsaturated compounds are prone to nucleophilic attack by reactive anionic species in aqueous medium.[4.23] Meanwhile, the solvent (polarity) dependent change in emission and absorption spectra (**Appendix, Figure A4.7-4.8**) of **L_2** indicated towards the existing intramolecular charge transfer (ICT) process in the free **L_2**. Hence we conjectured that sensing of the anionic SO_3^{2-} by **L_2** was essentially based on the restriction in intramolecular charge transfer (ICT) due to the rupture of extended conjugation in **L_2,** which in turn, enabled a fluorescence Turn-On response.

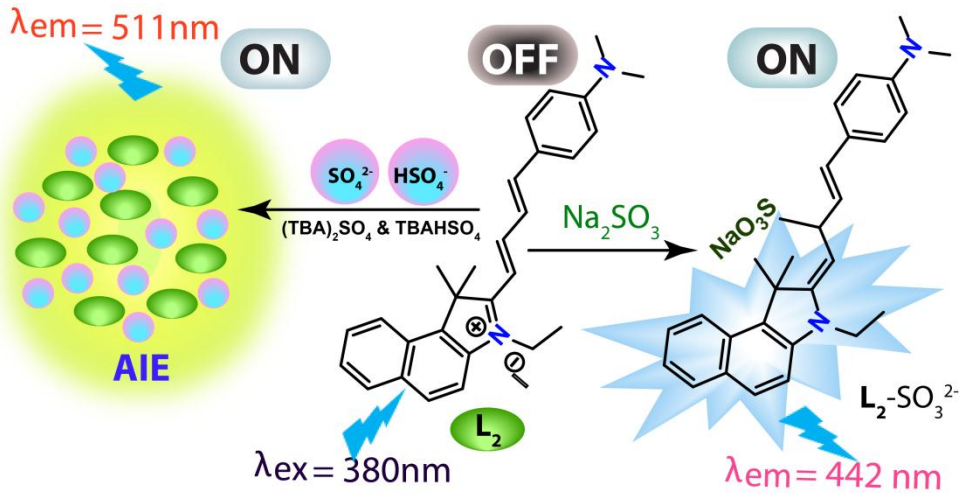

Scheme 4.2: Plausible sensing mechanism

The proposed sensing mechanism has been presented in **Scheme 4.2**. In order to validate the sensing mechanism, a mass spectrometry was conducted. Mass spectrum of $\mathbf{L_2}$ following interaction with sodium sulfite indicated a prominent peak at m/z = 498.29, (**Appendix, Figure A4.9**) which corresponds to the expected mass of the product $\mathbf{L_2}$-SO_3^{2-} (**Scheme 4.2**). The ^{1}H NMR spectra of $\mathbf{L_2}$ taken in presence of SO_3^{2-} too further validated the premise (**Appendix, Figure A4.10**).

On the other hand, sensing of SO_4^{2-}/HSO_4^- by the probe $\mathbf{L_2}$ is quite unprecedented. Certainly there are no binding sites for SO_4^{2-}/HSO_4^- in $\mathbf{L_2}$. Also the titration experiment along with mass spectral study (no expected mass peak, **Appendix, Figure A4.11**) negate the possibility of 1:1 or 1:2 chelation as the emission intensity increased linearly up to addition of 10-15 equivalents of SO_4^{2-} (**Figure 4.4A**). Hence we tried to explore the possibility of aggregation in explaining the sensing mechanism. The probe $\mathbf{L_2}$ itself did not exhibit any aggregation induced emission (AIE) property due to its moderate solubility in water. However, it was astonishing to note that though $\mathbf{L_2}$-SO_4^{2-} (1:20 equivalent) ensemble was weakly emissive in methanol it became highly emissive in a methanol–water mixture (**Figure 4.4B**) with higher water content (70% water content and above). Hence, unlike probe alone, $\mathbf{L_2}$-SO_4^{2-} (1:20 equivalent) ensemble displayed an aggregation induced emission (AIE) behaviour (**Scheme 4.2**). Thus it can be argued that the presence of SO_4^{2-}/HSO_4^- introduced the aggregation induced emission (AIE) behaviour to the system to enable the TURN-ON fluorescence response wherein plausibly the higher hydration energy of sulfate helped in facilitating the aggregation by lowering solubility of $\mathbf{L_2}$.[24] Evidence for the aggregation phenomenon was strengthened by obtaining atomic force microscope images of $\mathbf{L_2}$-SO_4^{2-} (1:20 equivalent) ensemble (**Figure 4.5A**). Dynamic light scattering (DLS) studies of $\mathbf{L_2}$ and $\mathbf{L_2}$-SO_4^{2-} (1:20 equivalent) ensemble in aqueous medium further revealed that the

average particle size increased from 6 nm to 83 nm upon interaction of **L_2** with 20 equivalent of SO_4^{2-} (**Figure 4.5B**), which strongly suggested the SO_4^{2-} mediated aggregation of **L_2**-SO_4^{2-} ensemble.

4.6. Sensing of SO_3^{2-} and SO_4^{2-} in cells

These solution studies were encouraging to explore the possibility of using **L_2** for intracellular detection of sulfite and sulfate by fluorescence-based imaging in live cells. However, to pursue this objective, it was essential to initially evaluate the cytotoxic potential of the probe **L_2** both in absence as well as in presence of sulfite and sulfate. A standard MTT assay, based on mitochondrial dehydrogenase activity of viable cells, demonstrated that the probe **L_2** did not exert any significant detrimental effect on the viability of HeLa cells (viability was greater than 80%), up to concentrations around 8.0 µM (**Appendix, Figure A4.12**). Similarly **L_2** (5.0 µM) treated with SO_3^{2-} or SO_4^{2-} (in 1:5 and 1:10 ratio) too showed about 80% viability of HeLa cells (**Appendix, Figure A4.13-A4.14**). To promote the reaction between **L_2** and SO_3^{2-}, HeLa cells pretreated with 5 µM **L_2** solution (for 1 h) was incubated with 25 µM of sodium sulfite (Na_2SO_3). Fluorescence microscope analysis revealed that though the probe **L_2** alone failed to exhibit any fluorescence in HeLa cells (**Figure 4.6, panel i**), when it interacted with sulfite salt it induced strong green fluorescence (**Figure 4.6, panel iv**), inside the cells. It was also observed that as a consequence of the formation of **L_2**-SO_3^{2-} adduct, the green fluorescence exhibited by HeLa cells were essentially perinuclear (**Figure 4.6, panel iv**). This observation was also corroborated by counterstaining HeLa cell nuclei with DAPI, wherein the green fluorescence exhibited by **L_2**-SO_3^{2-} adduct was distinctly localized in the cytoplasm (**Figure 4.6, panel iv-vi**). The formation of the **L_2**-SO_3^{2-} adduct and its cytoplasmic distribution in HeLa cells was also supported by the signal overlay in the green and blue channel of a cytofluorogram wherein the low Pearson's co-localization coefficient (0.59) indicated that **L_2**-SO_3^{2-} adduct could not penetrate nucleus (**Appendix, Figure A4.15A**). In case of sulfate sensing, fluorescence-based imaging studies indicated a strong green fluorescence emitted by HeLa cells (**Figure 4.6, panel vii**). However, counterstaining HeLa cells with DAPI stain suggested that in contrast to **L_2**-SO_3^{2-} adduct, the localization of **L_2**-SO_4^{2-} ensemble was essentially observed in the nucleus of the HeLa cells (**Figure 4.6, panel vii-ix**). The localization of **L_2**-SO_4^{2-} ensemble (1:5 equivalents) in the nucleus of HeLa cells was also corroborated by analyzing the cytofluorogram (**Appendix, Figure A4.15B**), wherein the Pearson's coefficient was 0.82.

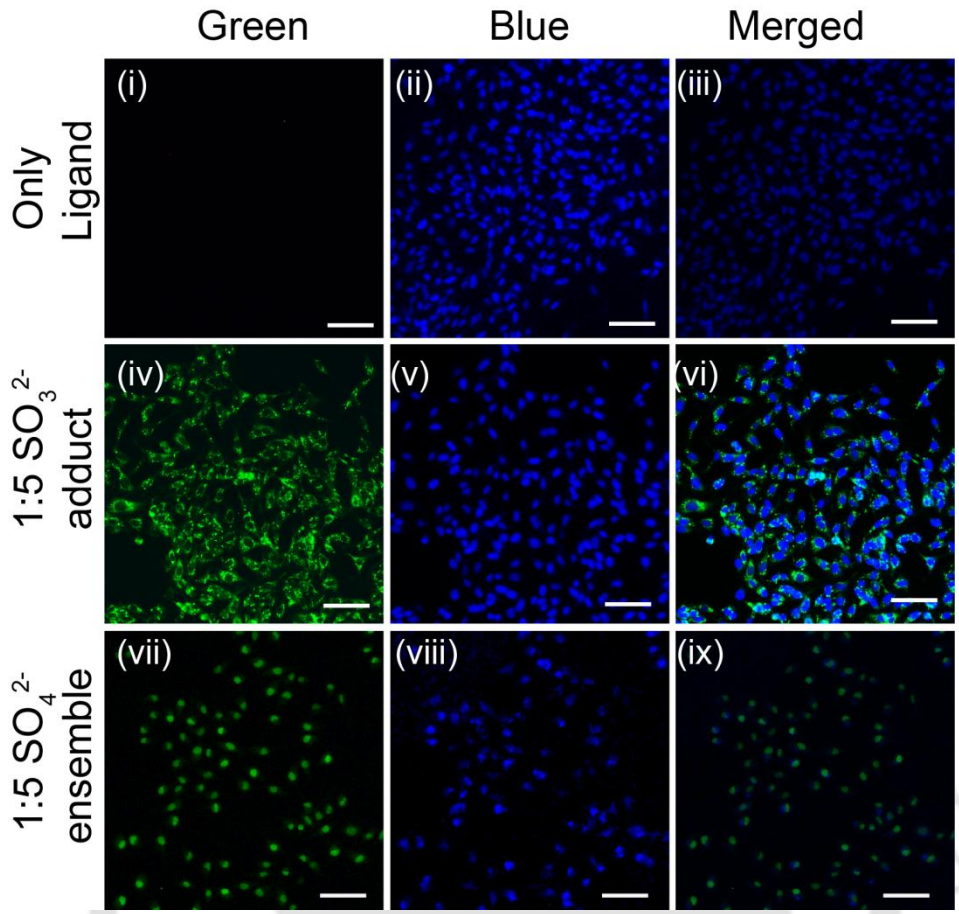

Figure 4.6: Fluorescence microscopic images of HeLa cells treated with 5.0μM $\mathbf{L_2}$ only (panel i-iii) as well as HeLa cells pre-treated with 5.0 μM $\mathbf{L_2}$ followed by addition of 25.0 μM sulfite (panel iv-vi) and sulfate (panel vii-ix) salt solution. The images were observed under green emission (panel i, iv and vii), blue emission for DAPI counterstaining (panel ii, v and viii) and merged channel (panel iii, vi and ix). Scale bar for the images is 50 μ.

4.7. Conclusion

In the present study, a versatile fluorescent probe was developed, which exhibited high selectivity and sensitivity towards SO_3^{2-} and SO_4^{2-}/HSO_4^- over competing analytes. The probe displayed beneficial attributes such as sensing in completely aqueous medium and an extremely fast response time towards the target analyte. Interestingly, the dual yet discerning sensing of SO_3^{2-} and SO_4^{2-}/HSO_4^- in solution by the designed probe was captured in mechanistic studies, which revealed a ratiometric fluorescence-based sensing of SO_3^{2-} based on restriction in intramolecular charge transfer (ICT), while SO_4^{2-} sensing could be attributed to an aggregation induced emission phenomena. Moreover, distinct conspicuous display of the fluorescence outputs too provided the scope for instant naked eye detection of $SO_3^{2-}$and SO_4^{2-}/ HSO_4^-. To the best of our knowledge this is the first report of a single probe enabling discriminatory sensing of SO_3^{2-} and SO_4^{2-} in aqueous solution. Importantly, the designed probe was biocompatible, cell permeable and rendered a fluorescence-based detection of SO_3^{2-} in the cytoplasm of live HeLa

cells as verified by co-localization based imaging studies. On the other hand, the probe could also facilitate intracellular detection of SO_4^{2-}, which appeared to be localized in the nucleus of HeLa cells. Based on the encouraging findings of the present study, it is envisaged that the judiciously designed probe holds considerable potential as an analytical tool to investigate the physiological implications of sulfate/sulfite derivatives in cell.

References

4.1. (a) G. Li and N. Sang, *Ecotoxicol. Environ. Saf*., 2009, **72**, 236; (b) J. Li, R. Li and Z. Meng, *Eur. J. Pharmacol*., 2010, **645**, 143.

4.2. N. Sang, Y. Yun, H. Li, L. Hou, M. Han and G. K. Li, *Toxicol. Sci*., 2010, **114**, 226.

4.3. S. Iwasawa, Y. Kikuchi, Y. Nishiwaki, M. Nakano, T. Michikawa and T. Tsuboi, *J. Occup. Health*, 2009, **51**, 38.

4.4. (a) Z. Q. Meng, G. H. Qin, B. Zhang and J. L. Bai, *Mutagenesis*, 2004,**19**, 465; (b) X. Shi, *J. Inorg. Biochem*., 1994, **56**, 155.

4.5. (a) S. L. Taylor, N. A. Higley and R. K. Bush, *Adv. Food Res*., 1986, **30**, 1; (b) H. Vally, N. L. A. Misso and V. Madan, *Clin. Exp. Allergy*, 2009, **39**, 1643.

4.6. (a) L. Migliore and F. Coppede, *Mutat. Res*., 2009, **674**, 73; (c) N. Sang, Y. Yun, G. Yao, H. Li, L. Guo and G. Li, *Toxicol. Sci*., 2011, **124**, 400.

4.7. (a) J. Li and Z. Meng, *Nitric Oxide*, 2009, **20**, 166; (b) J. Li, R. Li and Z. Meng, *Eur. J. Pharmacol*., 2010, **645**, 143.

4.8. M. H. Stipanuk, J. E. Dominy Jr, J. Lee and R. M. Coloso, *J. Nutr*., 2006, **136**, 1652S.

4.9. (a) J. W. Moore, Inorganic Contaminants of Surface Water: Research and Monitoring Priorities, *Springer-Verlag*, NY, 1992, pp. 266–272; (b) J. O. Nriagu and J.D. Hem, Chemistry of pollutant sulfur in natural waters, in: J.O. Nriagu (Ed.), Sulfur in the Environment. Part II. Ecological impacts, *Wiley*, NY, USA, 1978, pp. 211–270.

4.10. (a) H. J. Kim, S. Bhuniya, R. K. r. Mahajan, R. Puri, H. Liu, K. C. Ko, J. Y. Lee and J. S. Kim, *Chem. Commun*., 2009, 7128; (b) P.I. Jalava, R.O. Salonen, A.S. Pennanen, M.S. Happo, P. Penttinen, A.I. Halinen, M. Sillanpaa, R. Hillamo and M.-R. Hirvonen, *Toxicology and Applied Pharmacology*, 2008, **229**, 146.

4.11. J. W. Pflugrath and F. A. Quiocho, *Nature*, 1985, **314**, 257.

4.12. B. A. Moyer, L. H. Delmau, C. J. Fowler, A. Ruas, D. A. Bostick, J. L. Sessler, E. Katayev, G. D. Pantos, J. M. Llinares, Md. A. Hossain, S. O. Kang and K. Bowman-James, *Advances in Inorganic Chemistry: Template Effects and Molecular Organisation*, Vol. **59**; Van Eldik, R., Bowman-James, K., Eds.; Academia Press: London, 2007; Vol. **59**, pp 175-204.

4.13. (a) R. Custelcean and B. A. Moyer, *Eur. J. Inorg. Chem*., 2007, 1321; (b) Y. Marcus, *J. Chem. Soc. Faraday Trans*. 1991, **87**, 2995.

4.14. (a) G. Aragay, J. Pons and A. Merkoc, Chem. Rev. 2011, **111**, 3433; (b) X. Zhang, J. Yin and J. Yoon, *Chem. Rev*., 2014, **114**, 4918; (c) H. S. Jung, X. Chen, J. S. Kim and J. Yoon, *Chem. Soc.*

Rev., 2013, **42**, 6019; (d) S Samanta, S. Goswami, A. Ramesh and G. Das, *J. Photochem. Photobiol. A*, 2015, **310**, 45; (e) S. Samanta, T. Ray, F. Haque and G. Das, *J. Lumin*., 2016, **171**, 13.

4.15. (a) S. Samanta, S. Goswami, Md. N. Hoque, A. Ramesh and G. Das, *Chem. Commun.*, 2014, **50**, 11833; (b) S. Samanta, S. Goswami, A. Ramesh and G. Das, *Sens. Actuators B.*, 2014, **194**, 120; (c) S. Samanta, C. Kar and G. Das, *Anal. Chem.*, 2015, **87**, 9002 (d) S. Samanta, U. Manna, T. Ray and G. Das, *Dalton Trans*., 2015, **44**, 18902.

4.16. X. Cheng, H. Jia, J. Feng, J. Qin and Z. Li, *Sens. Actuators, B*, 2013, **184**, 274.

4.17. (a) X. Gu, C. Liu, Y.-C. Zhu and Y. Z. Zhu, *J. Agric. Food Chem*., 2011, **59**, 11935; (b) X. Ma, C. Liu, Q. Shan, W. Guo, D. Wei and Y. Du, *Sens. Actuators, B*, 2013, **188**, 1196.

4.18. (a) H. Tian, J. Qian, Q. Sun, H. Bai and W. Zhang, *Anal. Chim. Acta*, 2013, **788**, 165; (b) M.-Y. Wu, T. He, K. Li, M.-B. Wu, Z. Huang and X.-Q. Yu, *Analyst*, 2013, **138**, 3018; (c) Y. Sun, S. Fan, S. Zhang, L. Duan and R. Li, *Sens. Actuators, B*, 2014, **193**, 173; (d) Y. Q. Sun, J. Liu, J. Zhang, T. Yang and W. Guo, *Chem. Commun.*, 2013, **49**, 2637.

4.19. (a) J. Xu, K. Liu, D. Di, S. Shao and Y. Guo, *Inorg. Chem. Commun*.,2007, **10**, 681; (b) Y. Sun, C. Zhong, R. Gong, H. Mu and E. Fu, *J. Org. Chem*., 2009, **74**, 7943.

4.20. (a) M. G. Choi, J. Hwang, S. Eor and S. K. Chang, *Org. Lett.*, 2010, **12**, 5624;(b) S. Chen, P. Hou, H. Wang and X. Song, *RSC Adv.*, 2012, **2**, 10869.

4.21. (a) Y. Liu, K. Li, M.-Yu. Wu, Y.-H. Liu, Y.-M. Xie and X.-Q. Yu, *Chem. Commun.*, 2015, **51**, 10236; (b) L. Zhu, J. Xu, Z. Sun, B. Fu, C. Qin, L. Zeng and X. Hu, *Chem. Commun.*, 2015, **51**, 1154.

4.22. (a) M. J. Langton and P. D. Beer, *Chem. Eur. J.*, 2012, **18**, 14406; (b) M. Alfonso, A. T.arraga and P. Molina, *Org. Lett.*, 2011, **13**, 6432; (c) W. Xue, L. Li, Q. Li and A. Wu, *Talanta*, 2012, **88**, 734; (d) H. J. Kim, S. Bhuniya, R. K. Mahajan, R. Puri, H. Liu, K. C. Ko, J. Y. Lee and J. S. Kim, *Chem. Commun*., 2009, 7128; (e) N. R. Song, J. H. Moon, J. Choi, E. J. Jun, Y. Kim, S. J. Kim, J. Y. Lee and J. Yoon, *Chem. Sci*., 2013, **4**, 1765; (f) W. Lu, J. Zhou, K. Liu, D. Chen, L. Jiang and Z. Shen, *J. Mater. Chem. B*, 2013, **1**, 5014.

4.23. M. Morton and H. Landfield, *J. Am. Chem. Soc*., 1952, **74**, 3523.

4.24. C. Gao, G. Gao, J. Lan and J. You, *Chem. Commun*., 2014, **50**, 5623.

Appendix

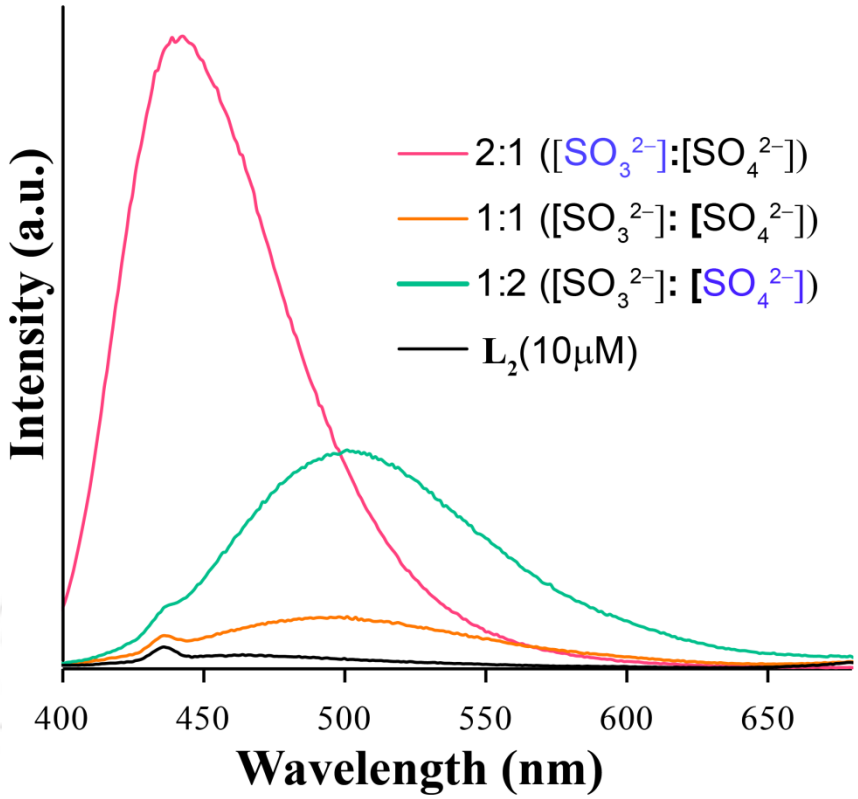

Figure A4.1: Fluorescence spectra of $\mathbf{L_2}$ (10 μM) in presence of (SO_3^{2-} + SO_4^{2-}) mixture with varying SO_3^{2-} & SO_4^{2-} concentrations; λ_{ex} = 380 nm.

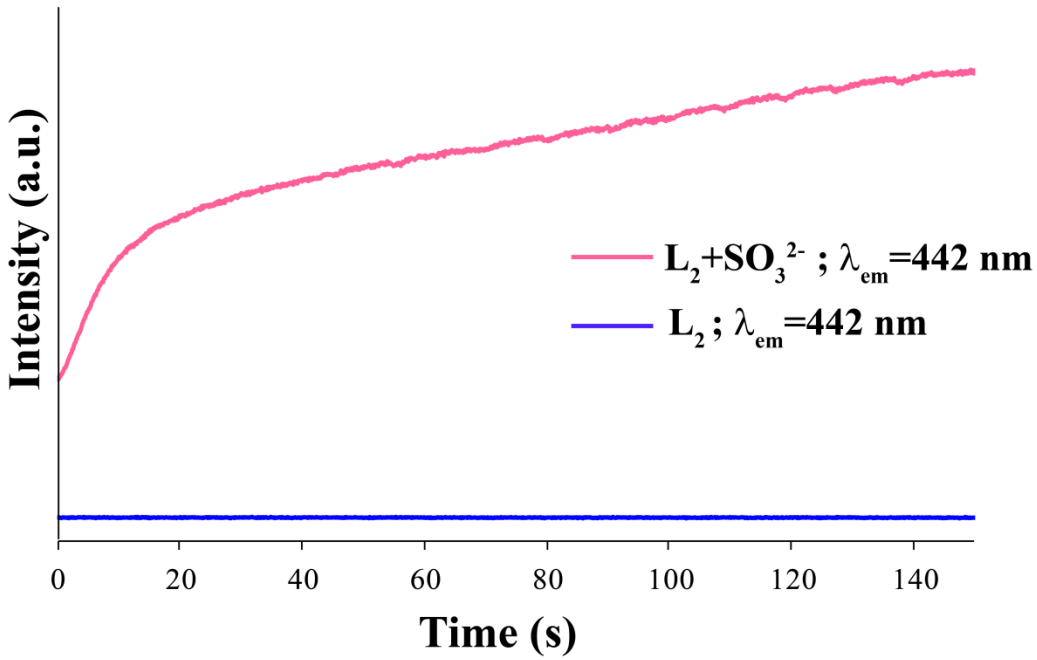

Figure A4.2: Changes in the emission intensity of $\mathbf{L_2}$ at 442 nm with time upon interaction with SO_3^{2-}; λ_{ex} = 380 nm.

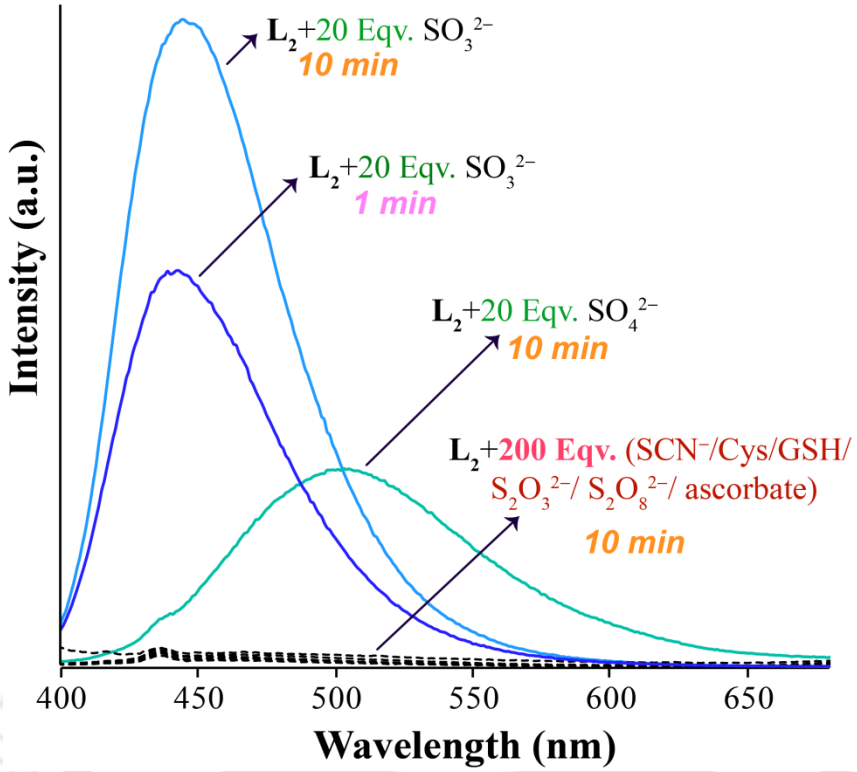

Figure A4.3: Fluorescence spectra of $\mathbf{L_2}$ (10μM) in presence of various analytes; λ_{ex} = 380 nm.

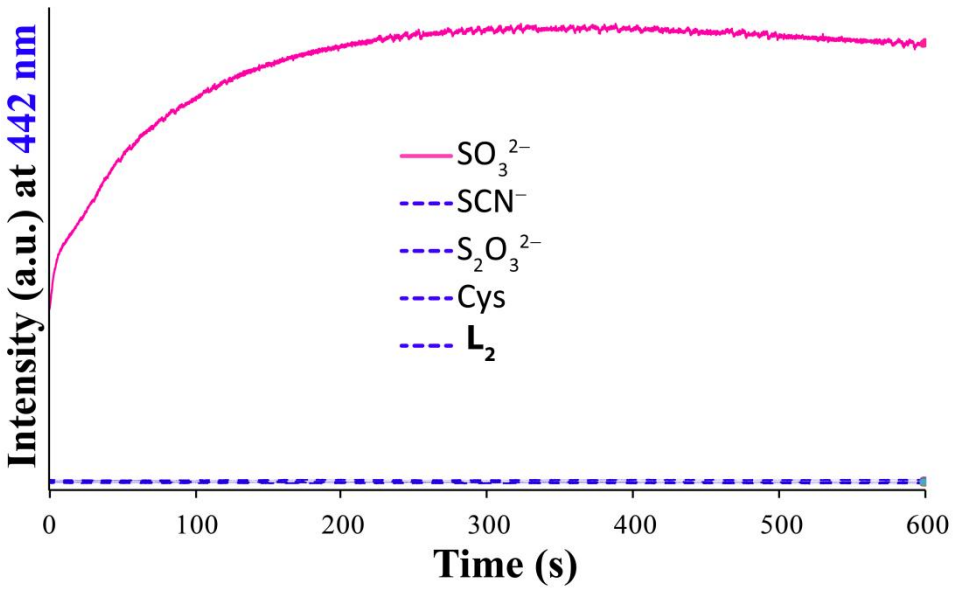

Figure A4.4: Changes in the emission intensity of $\mathbf{L_2}$ at 442 nm with prolonged time upon interaction with SO_3^{2-}, SCN^-, $S_2O_3^{2-}$ and Cys; λ_{ex} = 380 nm

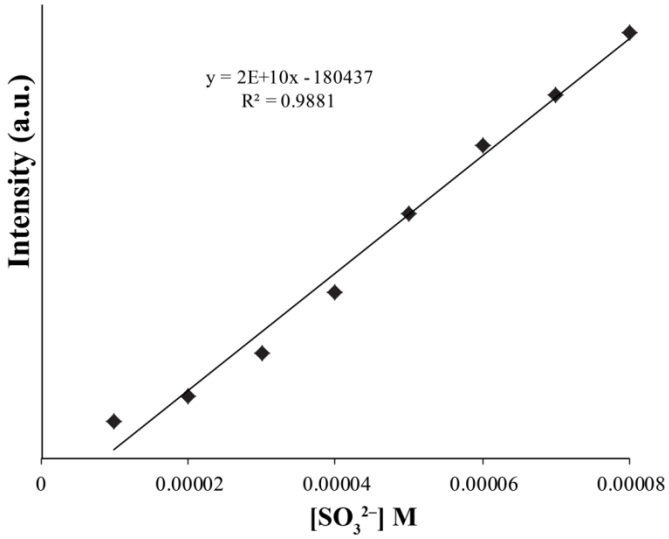

Figure A4.5: Fluorescence intensity vs. concentration of SO_3^{2-} plot for determination of detection limit

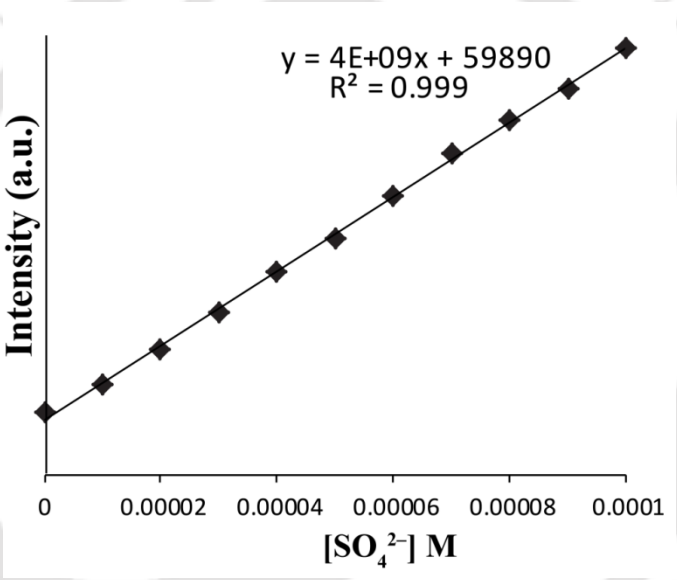

Figure A4.6: Fluorescence intensity vs. concentration of SO_4^{2-} plot for determination of detection limit.

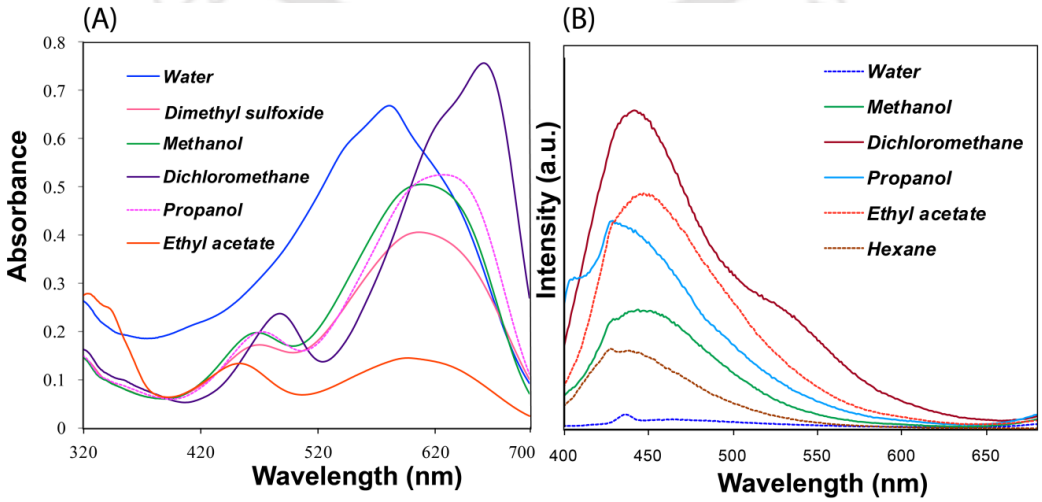

Figure A4.7: (A) UV-Visible spectra and (B) Fluorescence spectra (λ_{ex} = 380 nm) of **L_2** (10 μM) in different solvents.

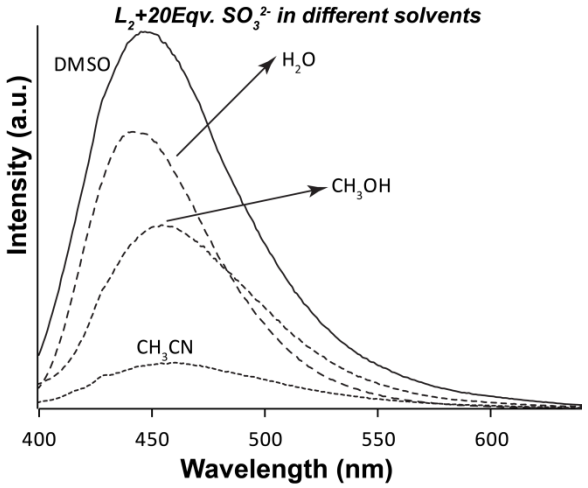

Figure A4.8: Fluorescence spectra of $\mathbf{L_2}$ (10 μM) in presence of 20 equivalents of SO_3^{2-} in different solvents; λ_{ex} = 380 nm.

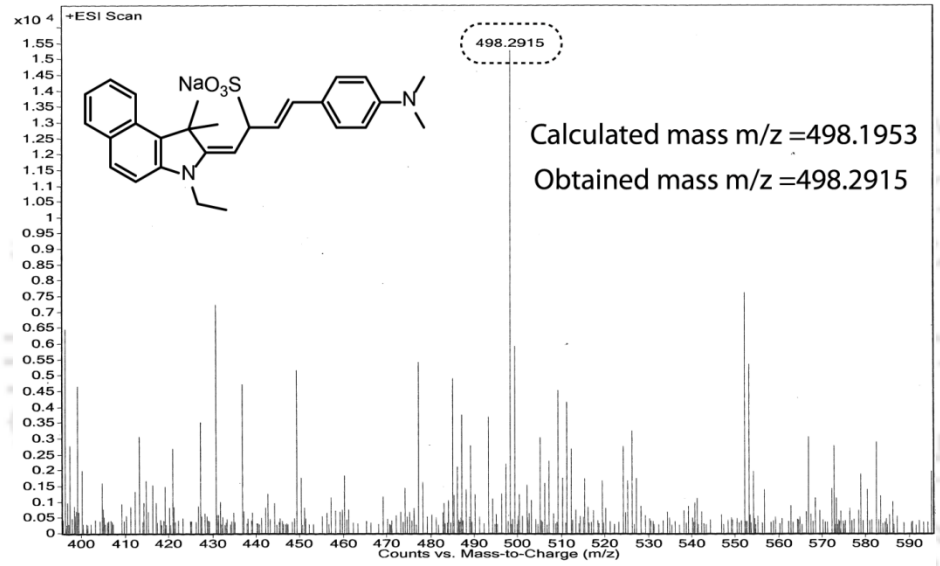

Figure A4.9: Mass spectrum of $\mathbf{L_2}$ in presence of Na_2SO_3.

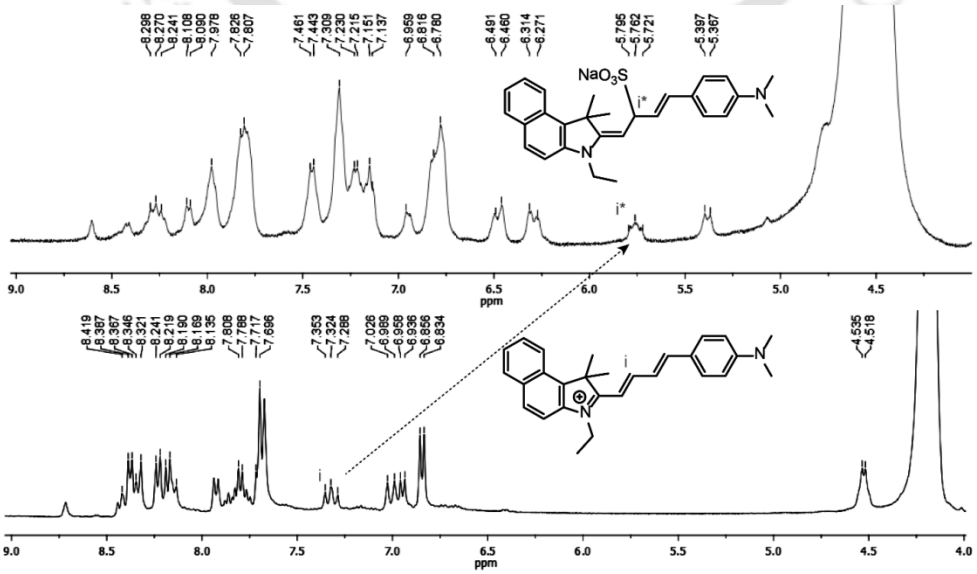

Figure A4.10: NMR spectra (400 MHz) of $\mathbf{L_2}$ and $\mathbf{L_2}$+ SO_3^{2-} in DMSO-d_6+D_2O (3:2; v/v) mixed solvent.

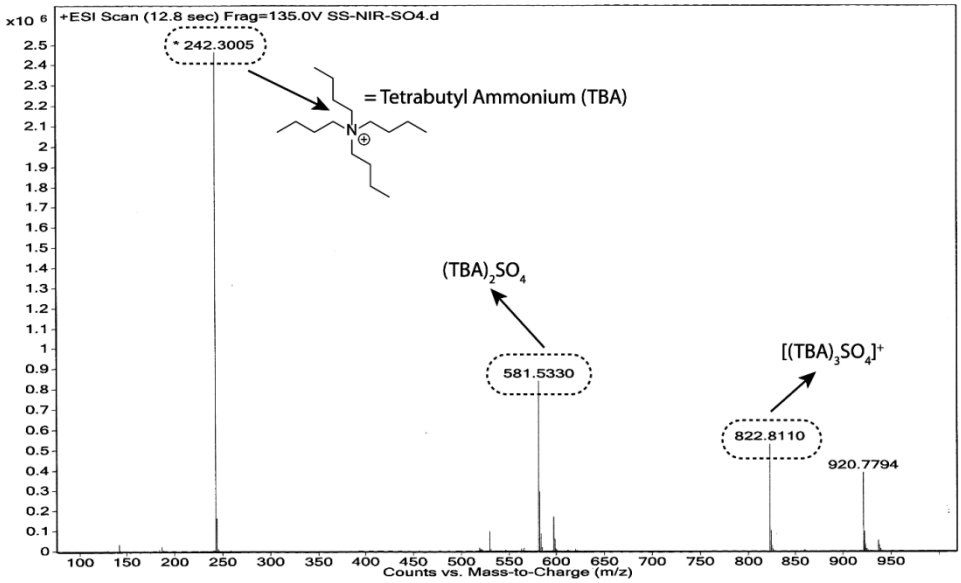

Figure A4.11: Mass spectrum of $\mathbf{L_2}$ in presence of tetrabutylammonium sulfate $(TBA)_2SO_4$

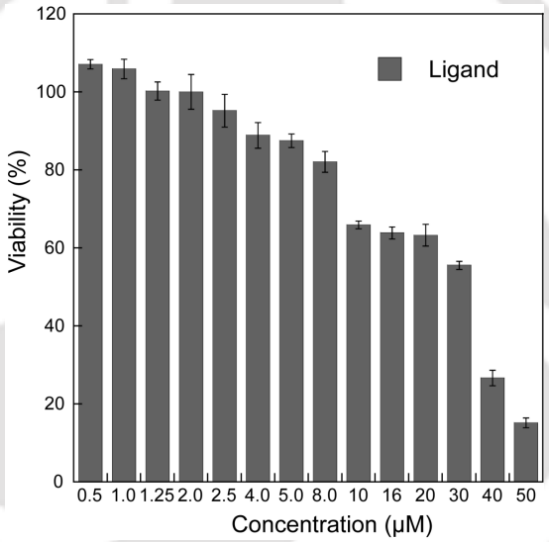

Figure A4.12: MTT assay to evaluate the cytotoxic effect of the probe $\mathbf{L_2}$ on HeLa cells

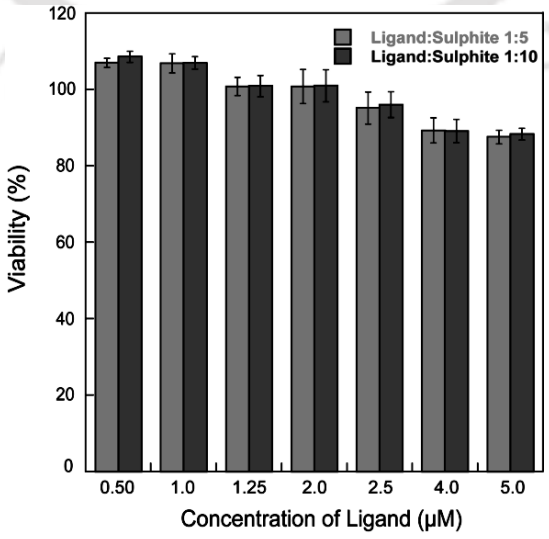

Figure A4.13: MTT assay to evaluate the cytotoxic effect of the probe $\mathbf{L_2}$-SO_3^{2-} ensemble on HeLa cells

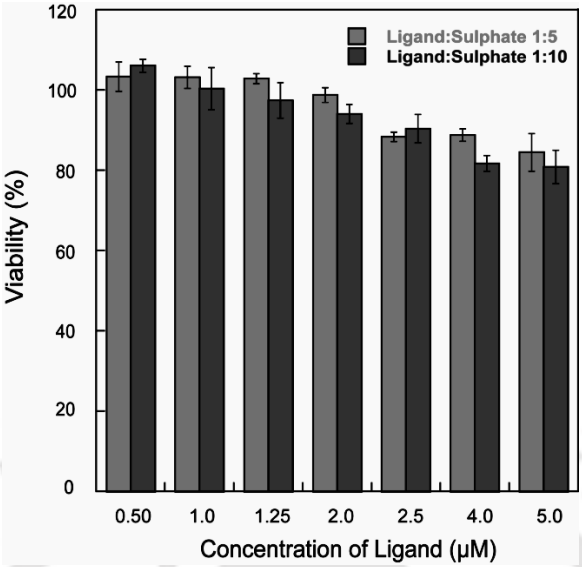

Figure A4.14: MTT assay to evaluate the cytotoxic effect of the probe $\mathbf{L_2}$-SO_4^{2-} ensemble on HeLa cells.

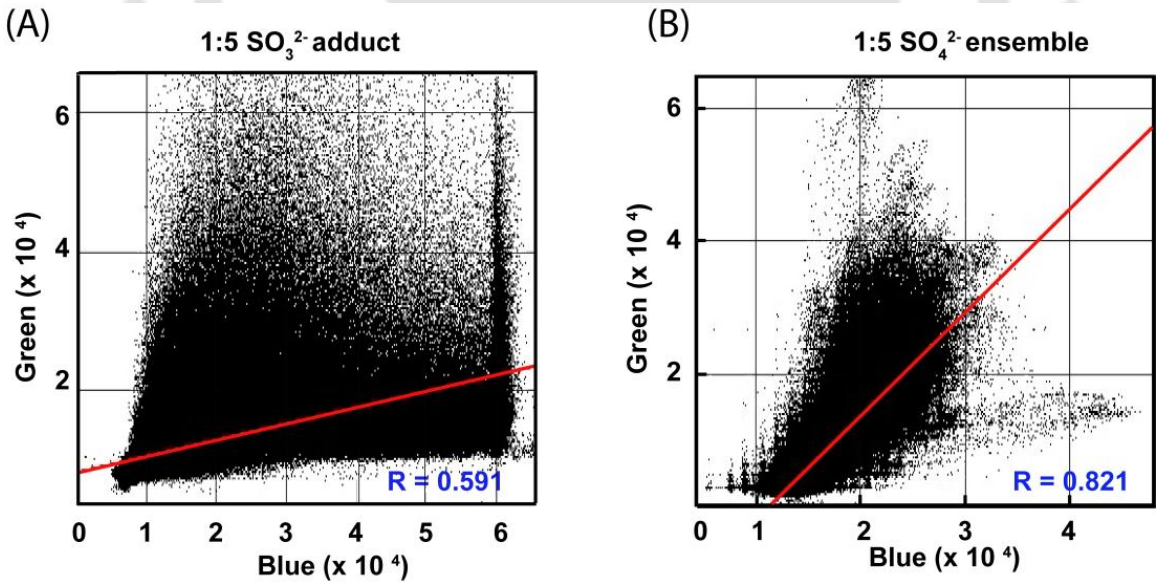

Figure A4.15: Co-localization coefficient (Pearson's coefficient) of (A) $\mathbf{L_2}$-SO_3^{2-} adduct (Pearson coefficient is 0.59) and (B) $\mathbf{L_2}$-SO_4^{2-} ensemble (Pearson coefficient is 0.82); based on green and blue channel emission.

Chapter 5

An Aggregation-Induced Emission (AIE) active probe for multiple targets: Fluorescent sensor for Zn^{2+} and Al^{3+} & colorimetric sensor for Cu^{2+} and F^-

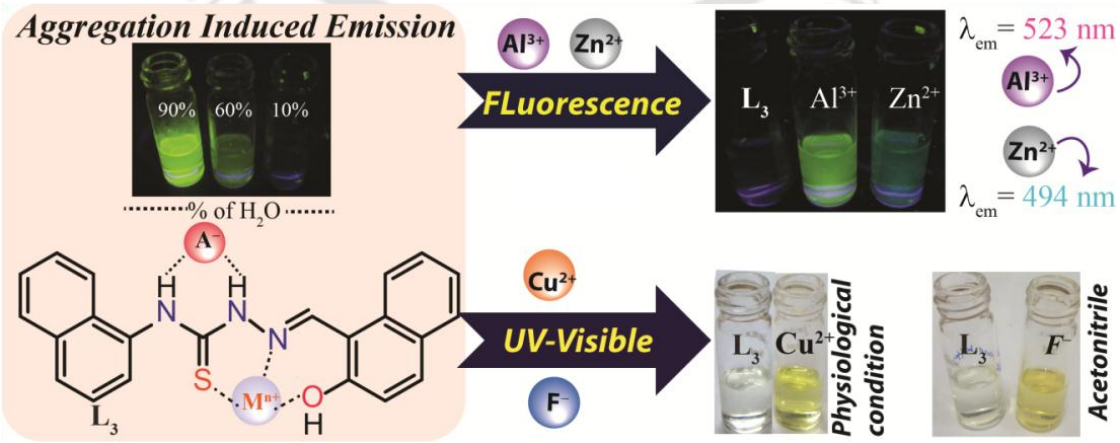

Chapter 5

5.1. Background and focus of the chapter

Zinc, an essential element in human body, is involved in several biological processes, for instance cellular metabolism, gene transcription, regulation of metalloenzymes, neurotransmission, and apoptosis.[5.1] Despite its several crucial roles in many Zn(II)-containing enzymes and DNA-binding proteins, imbalance of Zn^{2+} in body may cause several neurological diseases.[5.2] Particularly in children under the age of 5 years, deficiency of Zn(II) could eventually lead to immune dysfunction, diarrhoea, and even death in some cases.[5.3] Zinc, being a harmful pollutant for environment, also raises concern over its open exposure.[5.4] Thus designing an efficient Zn^{2+} sensor is indispensable. Difficulties in developing Zn^{2+} sensors[5.5a, b] in many cases suffer from a limited choice of spectroscopic instruments due to its inherent d^{10} shell, poor selectivity or sensitivity, and interference from other d^{10} metal ions like Cd^{2+} and Hg^{2+}.[5.5c, d] Hence, to develop highly selective and sensitive zinc sensors, workable in physiological condition would be of great interest.

Aluminium, the third most abundant metal in the earth's crust is widely known as a neurotoxic agent.[5.6] Aluminium toxicity could adversely affect the central nervous system of human to induce Alzheimer's disease, Parkinson's disease, and amyotrophic lateral sclerosis.[5.7] Meanwhile, the widespread use of Aluminium in medicines (antacids), bleached flour, paper industry, food additives, aluminum-based pharmaceuticals, storage/cooking utensils, makes it vulnerable to be exposed to the environment in its trivalent ion form Al^{3+} which often causes drinking water contamination.[5.8] Thus developing an efficient chemo-sensor for rapid and sensitive detection of Al^{3+} has earned great scientific interest amongst analytical chemists at large.

Fluorescence based sensing probes are advantageous over other sensing systems for the detection of biological and environmentally relevant metal ions as they can provide more rapid, convenient and sensitive detection of target analytes.[5.9] Fluorescent probes, displaying aggregation-induced emission (AIE) have grabbed tremendous attention in very recent time. Though these probes display weak emission in dilute solutions, their emission intensity enhances dramatically due to the aggregation facilitated by probe–target interaction in solution or in the solid state. Hence, AIE active probes, that could yield enhancement in fluorescence instead of

quenching on aggregation, have become very attractive candidates for robust and quantitative sensing of various biologically and environmentally important target analytes.[5.10]

On the other hand, copper, an essential trace element of human body and being present in the active sites of several enzymes, plays many indispensable role to sustain important physiological processes.[5.11] Copper deficiency increases the risk of coronary heart disease whereas overdose of copper could lead to detrimental effects by causing oxidative stress and disorders associated with neurodegenerative diseases including Alzheimer, Parkinson, Menkes, Wilson, and prion diseases.[5.12-5.13] Thus rapid visual sensing Cu^{2+} in physiological condition is much anticipated.

Fluoride is recognized as one of the biologically as well as environmentally important anions. Though at low concentration fluoride could help in treating osteoporosis and protecting dental health, it apparently becomes toxic at higher doses. Several types of diseases in humans, caused due to the intake of high concentration of the fluoride anion in drinking water are being tracked over the years. Fluoride toxicity also leads to fluorosis.[5.14] In this context, design and synthesis of simpler organic probe for visible detection of F^- is much expected. A thorough literature survey revealed that there are very few reported fluoride ion selective optical probe.[5.15] Vazquez *et. al.* developed an effective simple thiourea based optical probe where they demonstrated that the interaction of the thiourea hydrogen atoms with fluoride could enhance π delocalization and thereby shifted the π-π^* transition from the UV to the visible region to display yellow color.[5.15b] Similarly, Ambrosi *et. al.* has also demonstrated the selective off–on fluorescence response of a coumarin–urea derived probe towards fluoride ion.[5.15c] Visible detection of fluoride ion by a core-substituted naphthalene di-imide probe has also been reported recently.[5.15d] However, probes with urea/thiourea moiety are found to be more useful for selective sensing of fluoride ion in solution. Thus designing a thiosemicarbazone probe consist of thiourea group could potentially be envisioned as a fluoride sensor.

Moreover, designing a versatile molecule that produces different fluorescence or colorimetric responses for different analytes can simultaneously be used to detect more than one analytes. Thus development of a multi-analyte sensor provides the scope for analytical time, labour and cost reduction.[5.16] Recently, in this context, some thiosemicarbazone compounds have been used for selective sensing of various cations as well as anions.[5.17]

In this context, in the present chapter we have discussed about a single versatile aggregation induced emission (AIE) active multiple target probe $\mathbf{L_3}$ that not only can fluorometrically sense Zn^{2+} and Al^{3+} in physiological conditions but also can distinguish one from another through individual fluorescence responses. The probe also demonstrated a selective colorimetric

response towards Cu^{2+} in physiological condition. Alongside, the probe is also capable of displaying selective naked eye chromogenic detection of F^- in acetonitrile. The sensing behaviour of the probe was well supported with theoretical calculations.

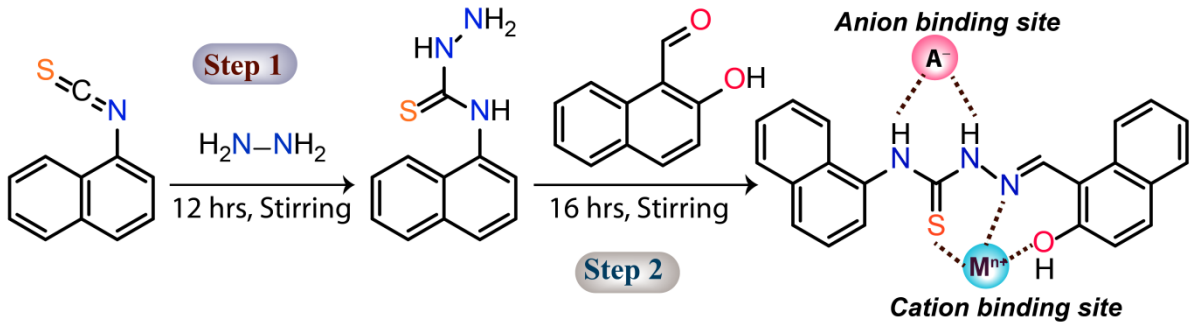

Scheme 5.1. Design and synthesis of the Probe $\mathbf{L_3}$

5.2. Rationale behind the design of probe L_3

In **chapter 3** and **chapter 4** we have discussed about fluorescent probes ($\mathbf{L_1}$& $\mathbf{L_2}$) capable of sensing cations (Cu^{2+} and Al^{3+}) and anions (SO_3^{2-} and SO_4^{2-}/HSO_4^-) respectively. So, we tried to explore the possibility of sensing cation and anion together by a single sensing system in the present study. However, it is very difficult to design an efficient sensing probe that can simultaneously sense cation and anion. Hence, the design principle for the probe to sense multi-analytes is based on the following fundamental features: (1) The probe should contain chromophore/fluorophore with an excitation/emission in the relatively higher wavelength to get rid of the interference from biological systems and (2) it should possess both the cation and anion binding sites within a single molecule. The probe $\mathbf{L_3}$ was synthesized with good yield and in pure form by multi-step reactions (**Scheme 5.1**). Extensive UV-visible and fluorescence spectroscopic studies were perused to harvest the selective optical responses of $\mathbf{L_3}$ towards various cations and anions.

5.3. Interaction of metal ions with L_3: UV−Vis spectroscopic studies

UV-Visible spectra of $\mathbf{L_3}$ revealed a broad absorbance maximum at 405 nm and a sharp absorbance maximum at 384 nm in CH_3OH/aqueous HEPES-buffer (5mM, pH~7.3; 9:1, v/v) medium, which might be attributed to the presence of naphthalene chromophore in the probe (**Figure 5.1A**).The selectivity of $\mathbf{L_3}$ was checked with chloride, nitrate or perchlorate salts of various metal ions which encompassed Na^+, K^+, Ca^{2+}, Mg^{2+}, Cr^{3+}, Hg^{2+}, Cu^{2+}, Pb^{2+}, Zn^{2+}, Fe^{3+}, Al^{3+}, Co^{2+}, Ni^{2+}, Cd^{2+} and Ag^+. Addition of Cu^{2+} to $\mathbf{L_3}$ yielded characteristic colorimetric change as a new absorbance maximum emerged at 456 nm, with the concurrent disappearance of the

original peaks at 405 nm and 384 nm (**Figure 5.1A**). Though, addition of Co^{2+}, Fe^{3+} and Zn^{2+} also brought slight spectral change to the UV-Visible spectra of $\mathbf{L_3}$, those changes were very insignificant compared to colorimetric change induced by Cu^{2+}. All other metal ions hardly influenced the spectral property of $\mathbf{L_3}$. Thus ligand $\mathbf{L_3}$ can sense Cu^{2+} through selective colorimetric response. Interestingly the spectral response of $\mathbf{L_3}$ toward Cu^{2+} was accompanied by a sharp visual color change of the experimental solution from almost colorless to yellow, which provided the scope for naked eye visible detection of Cu^{2+} (**Figure 5.1A, Inset**).

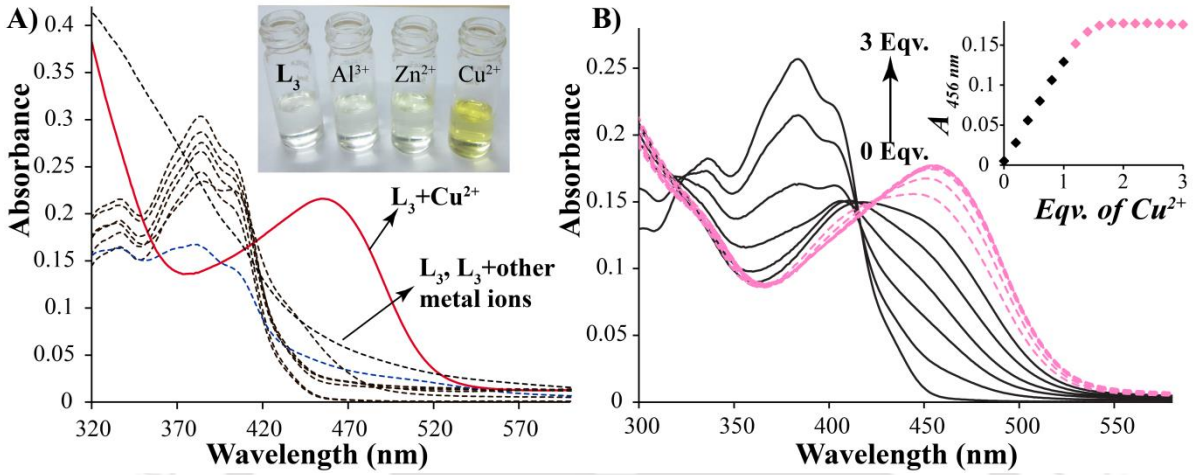

Figure 5.1: (A) UV-Visible spectra of $\mathbf{L_3}$ (20μM) in presence of 10 equivalents of various metal ions in CH_3OH/aqueous HEPES buffer (5mM, pH 7.3; 9:1, v/v) medium; Inset: Visual changes of the solution of $\mathbf{L_3}$ (20μM) in presence of Al^{3+}, Zn^{2+} and Cu^{2+} ions. (B) UV-Visible titration spectra of $\mathbf{L_3}$ (20μM) with incremental addition of Cu^{2+} ion in CH_3OH/aqueous HEPES buffer (5mM, pH 7.3; 9:1, v/v) medium, Inset: Change in absorbance at 456 nm with the equivalents of Cu^{2+} added into the solution.

To get a quantitative appraisal of the interaction between $\mathbf{L_3}$ and Cu^{2+} a titration experiment was carried out (**Figure 5.1B**). The gradual incremental addition of Cu^{2+} to $\mathbf{L_3}$ rendered a systematic growth of the absorbance maxima at 456 nm with a simultaneous downfall of the peaks at 384 nm and 405 nm. It is to be noted that a well-defined isosbestic point was generated at around 420 nm up to addition of 1 equivalent of Cu^{2+} (spectra with solid black traces in **Figure 5.1B**). With the addition of excess amount of Cu^{2+} results in a slight deviation from the isosbestic point (spectra with dotted pink lines in **Figure 5.1B**). Thus initially the selective colorimetric response of $\mathbf{L_3}$ towards Cu^{2+} might be attributed to the chelation between $\mathbf{L_3}$ and Cu^{2+} ion. Job's plot obtained from the titration experiment (**Appendix, Figure A5.1**) hinted towards an approximate 1:1.2 complex formation between $\mathbf{L_3}$ and Cu^{2+}. However, a conventional Job's plot experiment (detailed as mentioned in experimental section) has directly validated a 1:1 complex formation between $\mathbf{L_3}$ and Cu^{2+} (**Appendix, Figure A5.2**). Thus the appearance of the absorption band at 456 nm with Cu^{2+} plausibly attributed to the deprotonated naphthol to metal charge transfer

(LMCT) where the metal chelation facilitated the deprotonation of the naphthol moiety. The binding constant for the formation of **L_3**–Cu complex is calculated using the B–H (Benesi–Hildebrand) method, on the basis of change in absorbance at 456 nm, considering a 1:1 binding stoichiometry between **L_3** and Cu^{2+}. The binding constant was found to be 3.33×10^4 M^{-1} (**Appendix, Figure A5.3**). This high binding constant value also endorsed the strong binding affinity of **L_3** toward Cu^{2+} in solution. Hence the probe **L_3** is capable of detecting Cu^{2+} through a selective colorimetric response, even conspicuous by naked eye. The detection limit was calculated according to the IUPAC method [5.18] and it was found to be 4.64×10^{-6} M or, 0.29 ppm (**Appendix, Figure A5.4**) which is way below the US-EPA permissible limit of Cu^{2+} in drinking water.

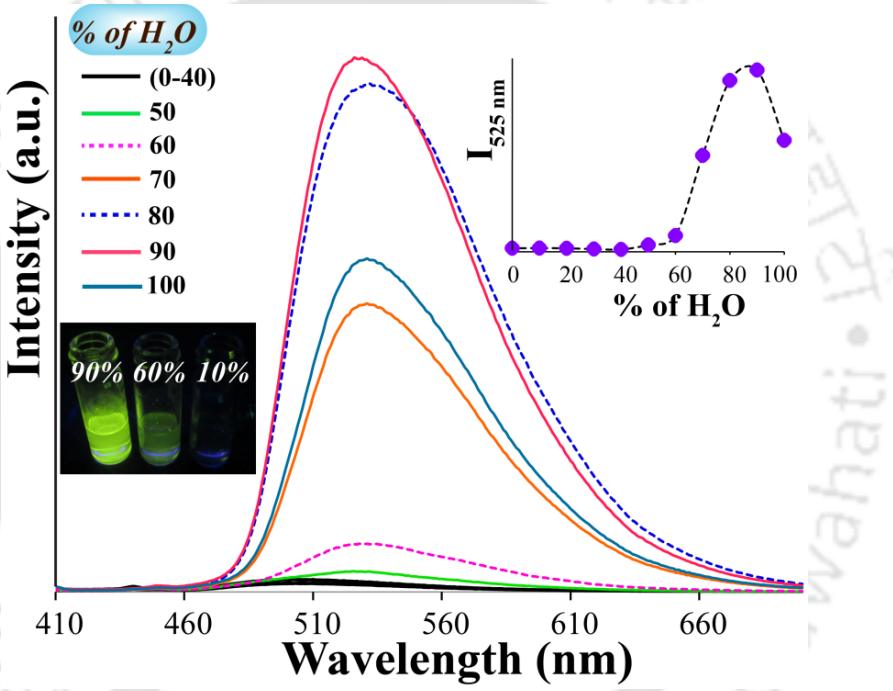

Figure 5.2: Emission spectra of **L_3** (10μM) upon changing the water fraction of methanol-water mixed solvent; λ_{ex} = 390 nm. Inset: Change in the emission intensity at 525 nm and visual changes in fluorescence (under UV light) with different water fractions.

5.4. Interaction of metal ions with L_3: Fluorescence spectroscopic studies

L_3 is very weakly emissive in pure methanol. Interestingly weakly emissive **L_3** in methanol became highly emissive in a methanol–water mixture with higher water content (**Figure 5.2**). Dynamic light scattering (DLS) studies of **L_3** in a mixed aqueous media suggested that the average particle size increased to 1545 nm from 612 nm with increasing water content of the medium from 10% to 90%. These results strongly recommended that **L_3** is an aggregation induced emission (AIE) active compound. As the water fraction above 50% only could lead to aggregation of **L_3** in medium itself (**Figure 5.2, inset**), all the fluorescence experiments in

presence of metal ions were performed in 9:1 methanol-aqueous HEPES buffer medium, where the ligand itself does not indulge in self-aggregation.

A weak emission band at 501 nm was observed when **L_3** was excited at 390 nm in mixed solvents. The binding selectivity of **L_3** was perused with chloride, nitrate or perchlorate salts of various metal ions, as mentioned earlier. It was interesting to note that amongst all tested metal ions only Al^{3+} and Zn^{2+} rendered significant TURN-ON fluorescence responses (**Figure 5.3**). Addition of Al^{3+} to **L_3** manifested a 22 nm red shifted new peak at 523 nm along with a ~4 fold increase in fluorescence intensity. On the other hand, interaction of Zn^{2+} with **L_3** witnessed emergence of a 7 nm blue shifted emission maximum at 494 nm also accompanied by ~3.8 fold enhancement in fluorescence intensity (**Figure 5.3**).

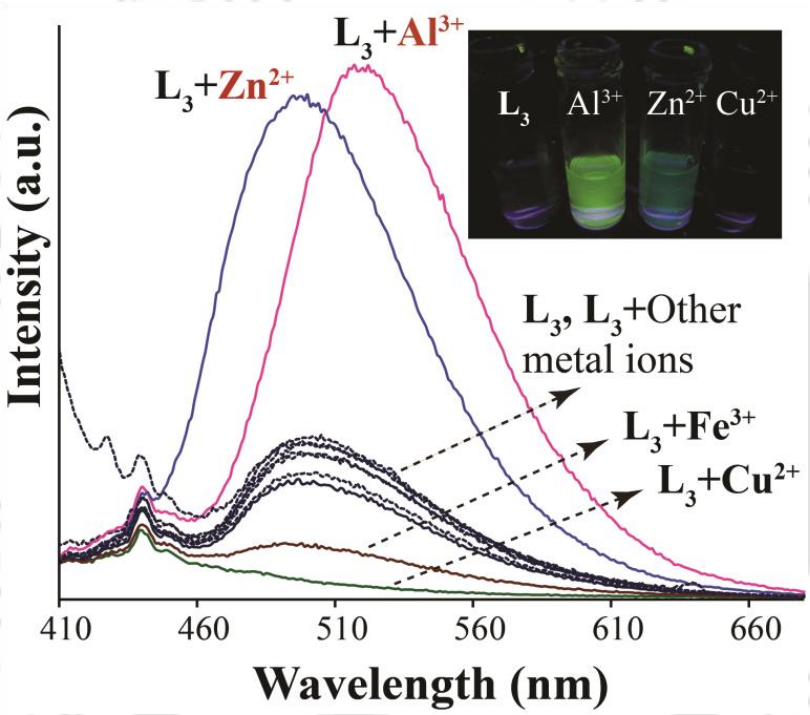

Figure 5.3: Fluorescence spectra of **L_3** (10μM) in CH_3OH/aqueous HEPES buffer (5mM, pH 7.3; 9:1, v/v) medium in presence of 20 equivalents of different metal ions. INSET: Visual changes observed for **L_3** in presence of Al^{3+}, Zn^{2+} and Cu^{2+} ions under UV light.

Moreover, naked eye detection of these selective individual TURN-ON responses of **L_3** toward Al^{3+} and Zn^{2+} was also feasible under UV light, which rendered a bright yellowish green fluorescence for Al^{3+} and a bluish-green fluorescence for Zn^{2+} (**Figure 5.3, inset)**. However, the TURN-ON fluorescence response of **L_3** either in the presence of Al^{3+} or Zn^{2+} ion was interfered moderately by Cu^{2+}, Co^{2+} and Fe^{3+} ions. Thus there is a scope for interference free sensing of Al^{3+} and Zn^{2+} in presence of all other metal ions except Cu^{2+}, Co^{2+} and Fe^{3+} in 9:1 methanol-aqueous HEPES buffer medium (**Appendix, Figure A5.5**). To get a quantitative appraisal of the relation between the change in fluorescence of **L_3** and the amount of metal ions interacted with

it, detailed fluorescence titration experiments were conducted with both Al^{3+} as well as Zn^{2+}. It was observed that the incremental addition of Al^{3+} or Zn^{2+} to **L_3** resulted in a systematic gradual enhancement of the fluorescence intensity (**Figure 5.4A & 5.4B**). However, contrary to the generation of the 22 nm red shifted emission maxima in case of titration experiment with Al^{3+}, fluorescence titration with Zn^{2+} witnessed formation of the 7 nm blue shifted emission maxima. Mass spectrum analysis confirmed the formation of a 1:1 **L_3**–Al^{3+} complex (**Appendix, Figure A5.6**) as well as a 1:1 **L_3**–Zn^{2+} complex (**Appendix, Figure A5.7**) with the generation of molecular ion peaks at m/z = 478.33 ($[Al + L_3 + H_2O + NO_3]^+$) and m/z = 490.85 ($[Zn + L_3 + 3H_2O]^+$) respectively.

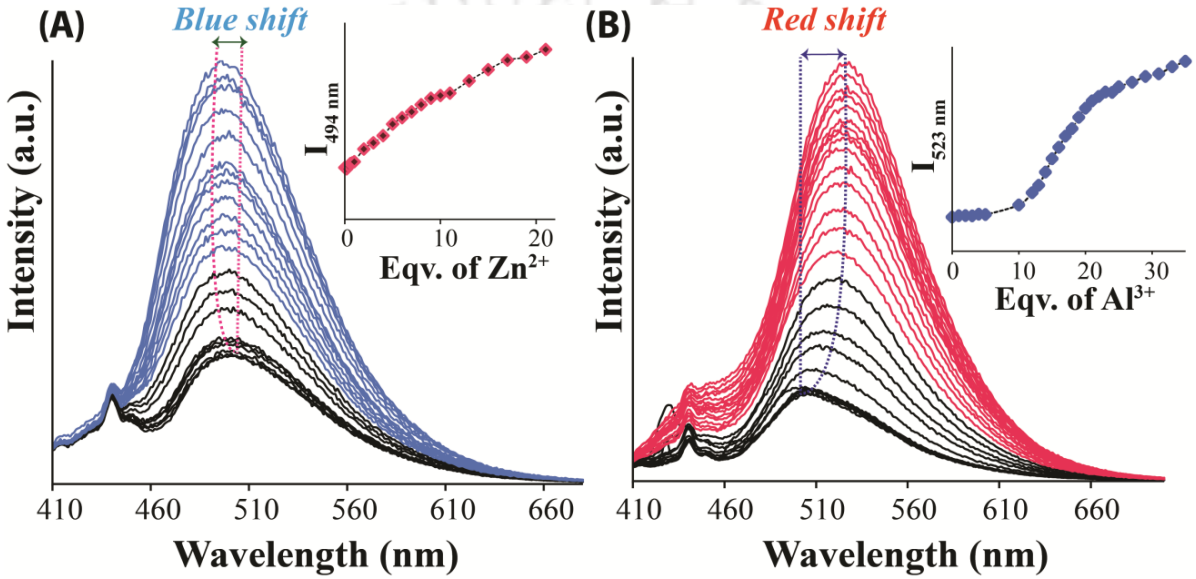

Figure 5.4: (A) Fluorescence titration spectra of **L_3** (10μM) with incremental addition of Zn^{2+} in CH_3OH/aqueous HEPES buffer (5 mM, pH 7.3; 9:1, v/v) medium. INSET: Changes in the emission intensity at 494 nm with different concentration of Zn^{2+} ion. (B) Fluorescence titration spectra of **L_3** (10μM) with incremental addition of Al^{3+} in CH_3OH/aqueous HEPES buffer (5 mM, pH 7.3; 9:1, v/v) medium. INSET: Changes in the emission intensity at 523 nm with different concentration of Al^{3+} ion. λ_{ex} = 390 nm.

^{1}H NMR experiments of the ligand **L_3** were also carried out in presence of Al^{3+} and Zn^{2+}. NMR experiments too supported the chelation phenomena, as the –OH peak of **L_3** at ~ 12.9 ppm broadened substantially after addition of the metal ions (Al^{3+} and Zn^{2+}), which actually imply that –OH was deprotonated during complexation with either of the metal ions (**Appendix, Figure A5.8, A5.9**). The detection limits for Al^{3+} and Zn^{2+} were calculated according to the IUPAC convention and those were found to be 6.86×10^{-7} M (**Appendix, Figure A5.10**) and 1.03×10^{-6} M for Al^{3+} and Zn^{2+} (**Appendix, Figure A5.11**) respectively, which are well below the USEPA permissible level of Al^{3+} and Zn^{2+} in drinking water.

Presumably, metal chelation was held responsible for the selective turn on fluorescence responses for Al^{3+} and Zn^{2+} as mass spectra indicated formation of a 1:1 **L_3**–Al^{3+} and **L_3**–Zn^{2+}

complex. However, fluorescence titration experiment for both Al^{3+} and Zn^{2+} downplayed the possibility of simple coordination between **L_3** with Al^{3+} or Zn^{2+} by showing steady enhancement of the emission intensity of **L_3** up to addition of 20-30 equivalents of concerned metal ions (**Figure 5.4A & 5.4B**). Thus there is a possibility that presence of excess Zn^{2+} or Al^{3+} facilitated the aggregation process in solution along with formation of complex in the initial stages, which subsequently triggered the AIE activity of **L_3** (**Scheme 5.2**).

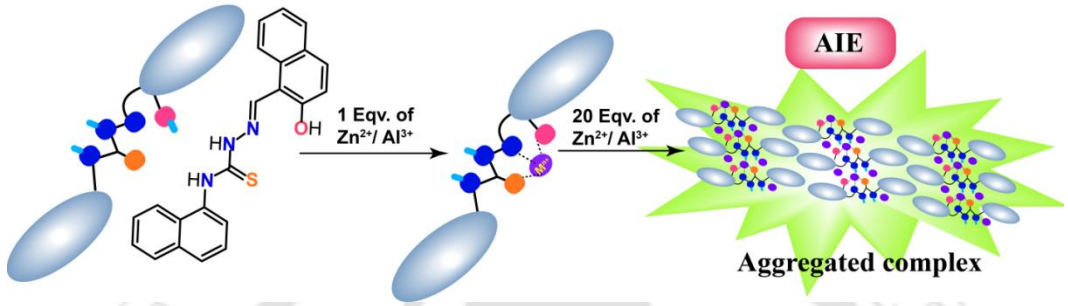

Scheme 5.2: Plausible sensing mechanism for metal ions

Initially the complexation between **L_3** and Al^{3+}/Zn^{2+} led to the red/blue shift respectively up to addition of 1 equivalent of the concerned metal ion; however further addition of metal ions both in case of Zn^{2+} and Al^{3+} actually assisted the aggregation of the already formed complexes to enable the AIE behavior of **L_3** and consequently revealed dramatic enhancement in the corresponding fluorescence intensities. Extensive dynamic light scattering (DLS) studies of **L_3** in a mixed aqueous media were performed to understand the aggregation behavior of **L_3** in presence of excess of Al^{3+} and Zn^{2+}.

DLS studies revealed that the average particle size of the probe **L_3** in mixed-aqueous (9:1 methanol-water; v/v) is 612 nm (**Figure 5.5**). Excitingly average particle size increased from 612 nm to 811 nm in similar condition in presence of 20 equivalents of Al^{3+}. The addition of 20 equivalents Zn^{2+} also resulted in substantial increase in the average particle size from 612 nm to 754 nm (**Figure 5.5**). These results also support the observed metal ion (Al^{3+} and Zn^{2+})-triggered AIE activity of the probe **L_3** (Figure 3A). It may be mentioned here that though a similar type of probe (only differ in use of phenol moiety in place of naphthol moiety), [5.17b] reported by Tong and co-workers showed ratio-metric fluorescent response toward Zn^{2+} in aqueous ethanol; our sensing system is much more effective and versatile compared to that as it not only can sense Al^{3+} and Zn^{2+} through selective differential TURN-ON fluorescence responses but also can sense Cu^{2+} and fluoride via sharp colorimetric responses. Alongside, simply changing the phenol moiety by naphthol moiety induces the interesting aggregation induced emission (AIE) activity of the probe to influence the sensing mechanism.

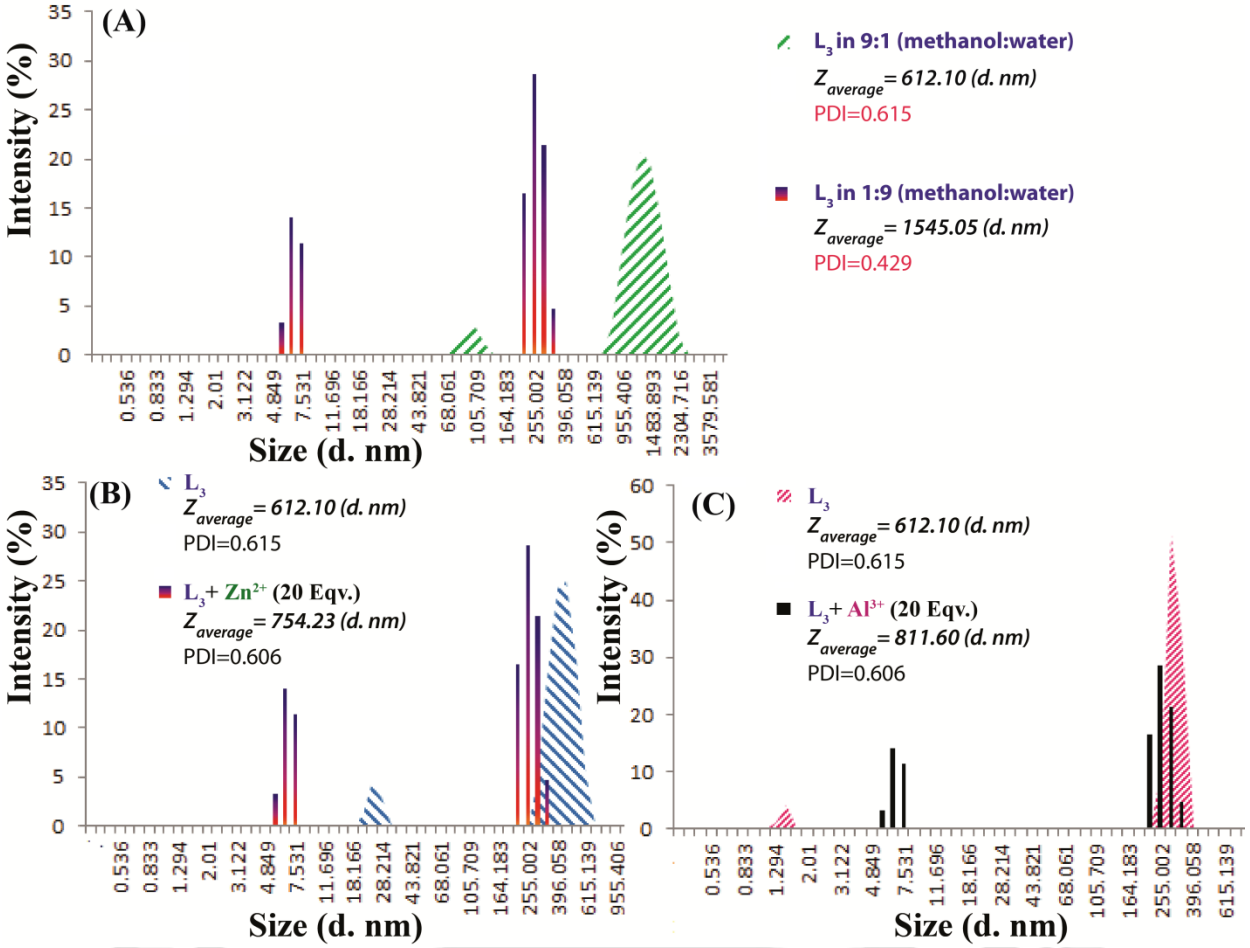

Figure 5.5: DLS-based particle size analysis of $\mathbf{L_3}$ (10μM) (A) upon changing the solvent from 9:1 methanol-water to 1:9 methanol-water, (B) upon addition of 20 equivalents of Zn^{2+} ion, (C) upon addition of 20 equivalents of Al^{3+} ion.

5.5. Interaction of anions with L_3: UV−Vis spectroscopic studies

The ligand $\mathbf{L_3}$ has potential anion binding sites too. Thus it was prudent to peruse the spectral outcome of $\mathbf{L_3}$ in presence of various anions (**Figure 5.6A**). Hence, binding selectivity of $\mathbf{L_3}$ was checked in presence of various anions such as, F^-, Br^-, Cl^-, I^-, SO_4^{2-}, HSO_4^-, PF_6^-, NO_3^-, HPO_4^-, $H_2PO_4^-$, OAc^-, ClO_4^- etc. It was astonishing to note that only the presence of excess (10 equivalents) tetra-butyl-ammonium salts of fluoride was able to induce significant colorimetric response in acetonitrile (**Figure 5.6A**) whereas all other anions hardly influenced the spectral nature of $\mathbf{L_3}$. Interaction of fluoride with $\mathbf{L_3}$, resulted in the emergence of a new absorbance maximum at 480 nm, with subsequent disappearance of the original peak at 378 nm. Moreover, this spectral change was also accompanied by some visual change in color from colorless to orange (**Figure 5.6A, Inset**) which offers the scope for the naked eye detection of Fluoride in organic medium.

Titration experiment was performed to get a quantitative insight of the interaction between **L_3** and F^-. The titration experiment revealed the systematic increase in the absorbance at 480 nm with concurrent fall of the absorbance at 378 nm with the gradual incremental addition of fluoride to **L_3** (**Figure 5.6B**). It may be mentioned here that addition of strong base (tetra-butyl ammonium hydroxide) to **L_3** also generated a new absorbance peak at around 462 nm which is in contrast to the absorbance peak generated at around 480 nm by fluoride in similar condition (**Appendix, Figure A5.12**). Also the nature of spectral response of the two curves is quite different from each other. Meanwhile, mass spectral analysis advocated for the 1:1 complex formation between **L** and fluoride ion by showing molecular ion peak at m/z = 494.88 ([**L_3** + F^- + $2CH_3CN$ + Na^+]) (**Appendix, Figure A5.13**). Thus presumably this selective colorimetric response towards fluoride ion is mainly attributed to the specific coordination of the basic fluoride anion with **L_3** through strong hydrogen bonding. NMR titration experiment revealed that addition of fluoride ion up to one equivalent, actually favored coordination process through strong hydrogen bonding, as the –NH proton peaks became weakened and broadened (**Appendix, Figure A5.14**) during this titration. Further addition of fluoride up to 2.0 equivalents, led to the deprotonation, and thus furnished a peak at ~15.5 ppm, corresponds to HF_2^- (**Appendix, Figure A5.14**). Hence, the fluoride sensing may be attributed to the combined effect of coordination and deprotonation of the probe.

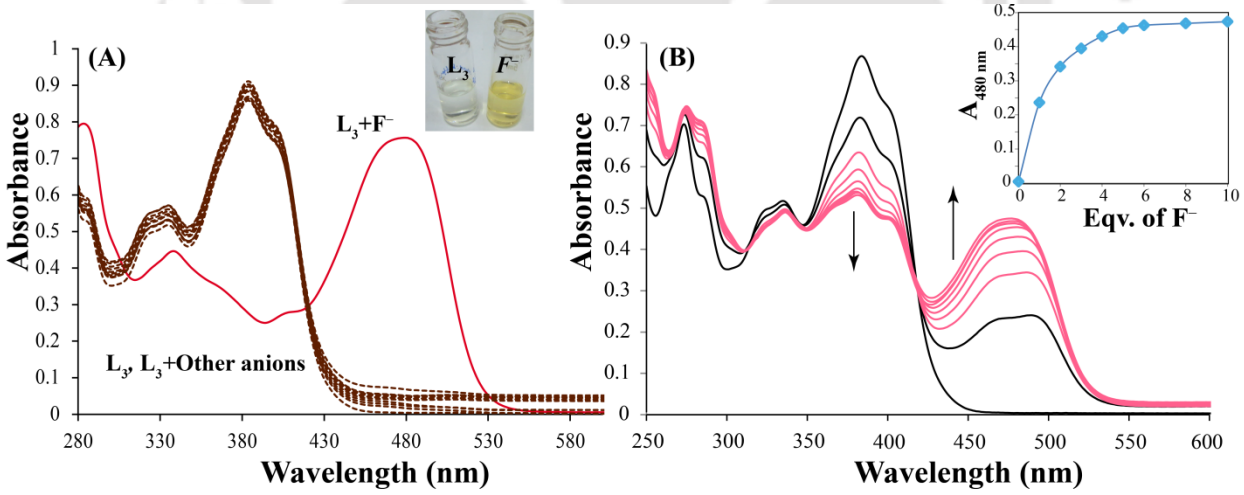

Figure 5.6: UV-visible spectra of **L_3** (20μM) in presence of 10 equivalents of different anions in acetonitrile. Inset: Visual changes observed for **L_3** in presence of fluoride ion under daylight. (B) UV-vis spectra of **L_3** (20μM) in presence of varying concentration of fluoride ion in acetonitrile. INSET: Changes in the absorbance at 480 nm with incremental addition of F^- ion.

5.6. Density Functional Theory (DFT) calculations

Extensive Density functional theory (DFT) calculations were perused to get the theoretical aspects of the observed selective emission responses of **L_3** towards Al^{3+} and Zn^{2+}. DFT optimizations of **L_3** and it's Zn^{2+} and Al^{3+} complexes were carried out with the B3LYP/6-31+G(d,p) method basis set using the Gaussian 03 program. The optimized structures, HOMO and LUMO of **L_3**, **L_3**–Zn^{2+} complex and **L_3**–Al^{3+} complex are presented in **Figure 5.7**. It was astonishing to note that there is an increase in the HOMO to LUMO energy gap in case of **L_3**–Zn^{2+} complex whereas HOMO to LUMO energy gap decreases in case of **L_3**–Al^{3+} complex compared to **L_3**. Hence, these changes in the energy gaps clearly backed strongly the observed blue shift in emission maxima in case of Zn^{2+} and red shift in emission maxima in case of Al^{3+}. Thus theoretically it is also likely that chelation followed by subsequent aggregation leads towards the selective turn-on fluorescence responses for both Al^{3+} and Zn^{2+}.

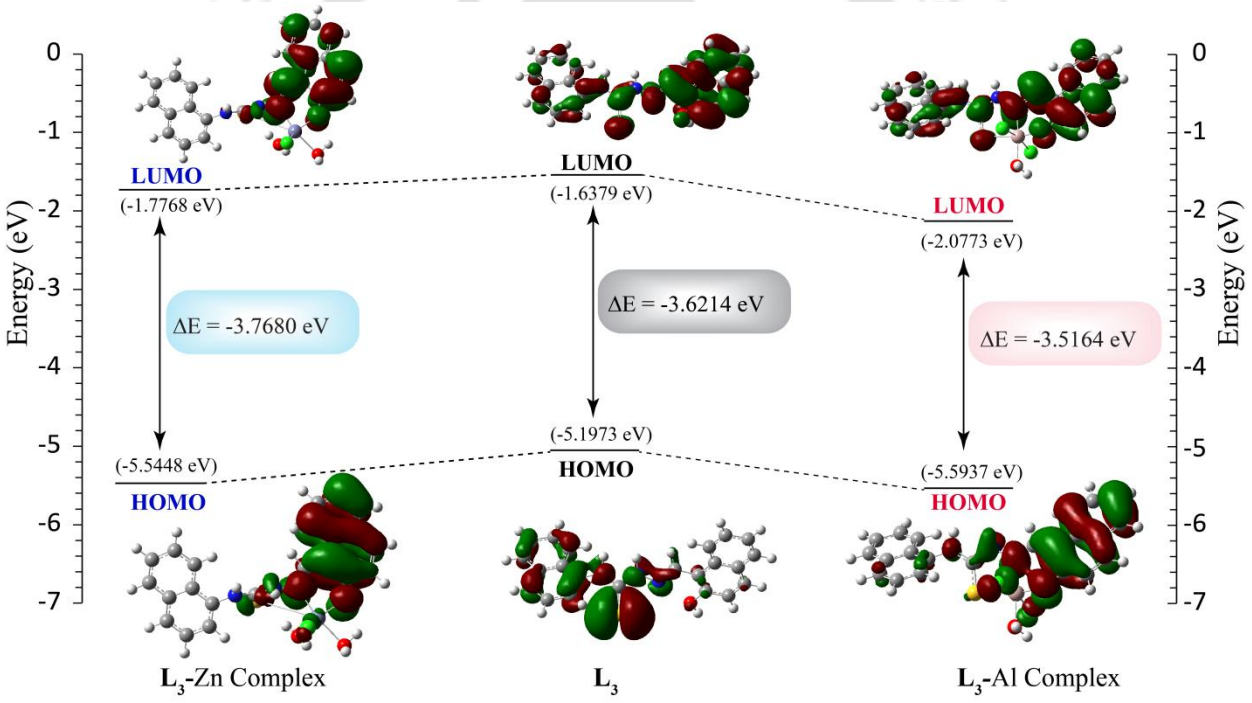

Figure 5.7: Frontier molecular orbital plots and energy level diagrams of **L_3**, **L_3**-Zn^{2+} complex and **L_3**-Al^{3+} complex. The calculations were performed using B3LYP/6-31 G (d,p) as implemented on Gaussian 03.

Density functional theory (DFT) calculations were also carried out for **L_3**-F^- and **L_3**-Cu^{2+} complexes. For the **L_3**-F^-, the lowering in the energy of HOMO to LUMO energy gap also validated the generation of observed red shifted absorbance maximum at 480 nm (**Appendix, Figure A5.15**). Similarly, in case of **L_3**-Cu^{2+} complex crunch in the HOMO to LUMO energy gap supported the emergence of the new red shifted absorbance maximum when Cu^{2+} was added to **L_3** (**Appendix, Figure A5.16**). The optimized structures of all the complexes are provided in the ESI (**Appendix**, **Figure A.5.17**).

5.7. Conclusion

In summary, here in we have synthesized a new fluorogenic probe, which is capable of displaying interesting aggregation induced emission (AIE) active property. The probe can detect multiple targets at a time through differential colorimetric and fluorometric responses. It can selectively sense Cu^{2+} through sharp colorimetric output through 1:1 chelation. Alongside, **L** can sense Zn^{2+} and Al^{3+} in mixed buffer medium through individual selective turn-on fluorescence responses which might be attributed to the chelation mediated triggering of the AIE behaviour of the probe. Nevertheless, as probe contains anion binding sites also, it is capable of detecting fluoride through a selective chromogenic response in acetonitrile.

References

5.1. (a) E. L. Que, D. W. Domaille and C. J. Chang, *Chem. Rev.*, 2008, **108**, 1517; (b) C. J. Frederickson, J. Y. Koh and A. I. Bush, *Nat. Rev. Neurosci*., 2005, **6**, 449; (c) A. G. Scrimgeoura, C. H. Stahl, J. P. McClung, L. J. Marchitelli and A. J. Young, *J. Nutr. Biol.* 2007, **18**, 813; (d) J. M. Berg and Y. Shi, *Science*, 1996, **271**, 1081.

5.2. (a) Z. Xu, J. Yoon and D. R. Spring, *Chem. Soc. Rev*., 2010, **39**, 1996; (b) P. Jiang and Z. Guo, *Coord. Chem. Rev*., 2004, **248**, 205; (c) E. J. Song, H. Kim, I. H. Hwang, K. B. Kim, A. R. Kim, I. Noh and C. Kim, *Sens. Actuators B*, 2014, **195**, 36.

5.3. M. Hambidge, *J. Nutr.*, 2000, 130, 1344.

5.4. A Voegelin, S Poster., A. C. Scheinost, M. A Marcus and R. Kretzsch-mar, *Environ. Sci. Technol.*, 2005, **39**, 6616.

5.5. (a) D. Y. Zhang, M. Azrad, W. Demark-Wahnefried, C. J. Frederickson, S. J. Lippard, and R. J. Radford, *ACS Chem. Biol*., 2015, **10**, 385; (b) A. Loas, R. J. Radford, and S. J. Lippard, *Inorg. Chem.*, 2014, **53**, 6491; (c) L. Xue, C. Liu and H. Jiang, *Org. Lett.*, 2009, **11**, 1655. (d) L. Xue, C. Liu and H. Jiang, *Org. Lett.*, 2009, **11**, 3454.

5.6. (a) R. A. Yokel, *Fundam. Appl. Toxicol*., 1987, **9**, 795; (b) G. Muller, V. Bernuzzi and D. Desor, *Teratology*, 1990, **42**, 253; (c) J. M. Donald and M. S. Golub, *Neurotoxicol. Teratol.*, 1989, **11**, 341.

5.7. (a) A. Salifoglou, *Coord. Chem. Rev.*, 2002, **228**, 297. (b) M. E. Percy, T. P. A. Kruck, A. I. Pogue and W. J. Lukiw, *J. Inorg. Biochem*., 2011, **105**, 1505; (c) G. D. Fasman, *Coord. Chem. Rev.*, 1996, **149**, 125. (d) D. Krewski, R. A. Yokel, E. Nieboer, D. Borchelt, J. Cohen, J. Harry S. Kacew, J. Lindsay, A. M. Mahfouz and V. Rondeau, *J. Toxicol. Environ. Health, Part B*, 2007, **10(S1)**, 1.

5.8. (a) P. Jiang, L. Chen, J. Lin, Q. Liu, J. Ding, X. Gao and Z. Guo, *Chem. Commun.*, 2002, 1424; (b) S. Goswami, S. Paul and A. Manna, *RSC Adv.*, 2013, **3**, 10639; (c) A. Sahana, A. Benerjee, S. Lohar, A. Banik, S. K. Mukhopadhyay, D. A. Safin, M. G. Babashkina, M. Bolte, Y. Garcia and D. Das, *Dalton Trans.*, 2013, 13311; (d) D. Karak, S. Lohar, A. Sahana, S. Guha, A. Banerjee and D. Das, *Anal. Methods*, 2012, **4**, 1906; (e) G. D. Fasman, *Chem. Rev*., 1996, **149**, 125; (f) P. Nayak, *Environ. Res*., 2002, **89**, 101.

5.9. (a) J. Wang, W. Lin and W. Li, *Chem. Eur. J*. 2012, **18**, 13629; (b) J. Y. Zhang, B. L. Xing, J. Z. Song, F Zhang, C. Y. Nie, L. Jiao, L. B. Liu, F. T. Lv and S. Wang, *Anal. Chem*. 2014, **86**, 346; (c) L. H. Feng, C. L. Zhu, H. X. Yuan, L. B. Liu, F. T. Lv and S. Wang, *Chem. Soc. Rev*. 2013, **42**, 6620; (d) L. Yuan, W. Lin, K. Zheng and S. Zhu, *Acc. Chem. Res*., 2013, **46**, 1462.

5.10. (a) J. Luo, Z. Xie, J. W. Y. Lam, L. Cheng, H. Chen, C. Qiu, H. S. Kwok, X. Zhan, Y. Liu, D. Zhu and B. Z. Tang, *Chem. Commun*., 2001, 1740; (b) Y. Hong, J. W. Y. Lam and B. Z. Tang, *Chem. Commun*., 2009, 4332; (c) Y. Hong, J. W. Y. Lam and B. Z. Tang, *Chem. Soc. Rev*., 2011, **40**, 5361.

5.11. (a) M. C. Linder and M. Hazegh-Azam, *Am. J. Clin. Nutr*., 1996, **63**, 797S; (b) R. Uauy, M. Olivares and M. Gonzalez, *Am. J. Clin. Nutr*., 1998, **67**, 952S; (c) G. E. Cartwright and M. M. Wintrobe, *Am. J. Clin. Nutr*., 1964, **14**, 224; (d) D. G. Barceloux, *J. Toxicol., Clin. Toxicol*., 1999, **37**, 217; (e) D. Strausak, J. F Mercer, H. H. Dieter, W. Stremmel, and G. Multhaup, *Brain Res. Bull*., 2001, **55**, 175.

5.12. (a) C. Vulpe, B. Levinson, S. Whitney, S. Packman and J. Gitschier, *Nat. Genet*., 1993, **3**, 7; (b) D. J. Waggoner, T. B. Bartnikas and J. D. Gitlin, *Neurobiol., Dis*. 1999, **6**, 221; (c) J. S. Valentine and P. J. Hart, *Proc. Natl. Acad. Sci. U.S.A*., 2003, **100**, 3617; (d) D. R. Brown and H. Kozlowski, *Dalton Trans*., 2004, 1907; (e) K. J. Barnham, C. L. Masters and A. I. Bush, *Nat. Rev. Drug Discov*., 2004, **3**, 205; (f) B. E. Kim, T. Nevitt and D. J. Thiele, *Nat. Chem. Biol*., 2008, **4**, 176.

5.13. (a) G. J. Brewer, *Curr. Opin. Chem. Biol*., 2003, **7**, 207; (b) G. L. Millhauser, *Acc. Chem. Res*., 2004, **37**, 79; (c) S. P. Leach, M. D. Salman and D. Hamar, *Anim. Health Res. Rev*., 2006, **7**, 97; (d) K. J. Barnham and A. I. Bush, *Curr. Opin. Chem. Biol*., 2008, **12**, 222; (e) R. R. Crichton, D. T. Dexter and R. J. Ward, *Coord. Chem. Rev*., 2008, **252**, 1189.

5.14. (a) T. Jentsch, *Curr. Opin. Neurobiol*., 1996, **6**, 303; (b) A. Wiseman, Handbook of Experimental pharmacology **XX/2, Part 2**; Springer-Verlag: Berlin, 1970, 48; (c) J. A. Weatherall, Pharmacology of Fluorides. In Handbook of Experimental pharmacology **XX/2, Part 2**; Springer-Verlag: Berlin, 1969, 141; (d) R. H. Dreisbuch, Handbook of Poisoning; Lange Medical Publishers: Los Altos, CA, 1980.

5.15. (a) P. A. Gale, N. Busschaert, C. J. E. Haynes, L. E. Karagiannidis and I. L. Kirby, *Chem. Soc. Rev*., 2014, **43**, 205; (b) M. Vazquez, L. Fabbrizzi, A. Taglietti, R. M. Pedrido, A. M. Gonzalez-Noya and M. R. Bermejo, *Angew. Chem. Int. Ed.* 2004, **43**, 1962; (c) G. Ambrosi, M. Formica, V. Fusi, L. Giorgi, E. Macedi, G. Piersanti, M. Retini, M. A. Varrese and G. Zappia, *Tetrahedron*, 2012, **68**, 3768; (d) D. Buckland, S. V. Bhosale and S. J. Langford, *Tetrahedron Lett*., 2011, **52**, 1990.

5.16. (a) L. Wang, H. Li and D. Cao, *Sens. Actuators B*., 2013, **181**, 749; (b) M. Wang, J. Wang, W. Xue and A. Wu, *Dyes Pigm*., 2013, **97**, 475; (c) P. N. Basa and A. G. Sykes, *J. Org. Chem*., 2012, **77**, 8428; (d) H. J. Jung, N. Singh, D. Y. Lee and D. O. Jang, *Tetrahedron Lett*., 2010, **51**, 3962; (e) A. Liu, L. Yang, Z. Zhang, Z. Zhang and D. Xu, *Dyes Pigm*., 2013, **99**, 472; (f) C. Kar, S Samanta, S. Goswami, A. Ramesh and G. Das, *Dalton Trans*., 2015, **44**, 4123;(g) S Samanta, S. Goswami, A. Ramesh and G. Das, *J. Photochem. Photobiol. A*, 2015, **310**, 45.

5.17. (a) M. J. C. Marenco, C. Fowley, B. W. Hyland, G. R.C. Hamilton, D. G.-Riano and J. F. Callan, *Tetrahedron Lett.*,2012, **53**, 670; (b) Z. Li, Y. Xiang and A. Tong, *Anal. Chim. Acta*, 2008, **619**, 75; (c) H. Su, W. Huang, Z. Yang, H. Lin and H. Lin, *J. Incl. Phenom. Macrocycl. Chem.* 2012, **72**, 221; (d) W. Radchatawedchakoon, W. Sangsuwan, S. Kruanetr and U. Sakee, *Spectrochim. Acta. A*, 2014,**121,** 306.

5.18. J. Lncze´dy, T. Lengyel, and A. M. Ure, (Eds.), IUPAC Compendium of Analytical Nomenclature, Definitive Rules, 1997, web edition, IUPAC, 2002.

Appendix

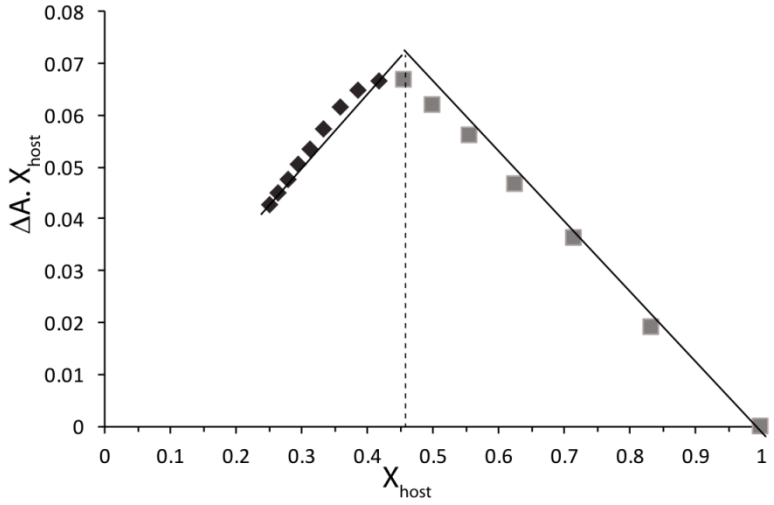

Figure A5.1: Job's plot for Cu^{2+} from the titration spectra.

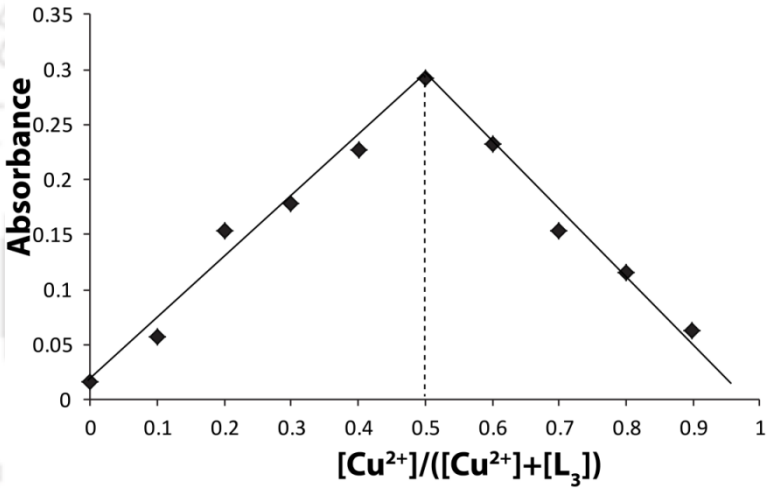

Figure A5.2: Job's plot for Cu^{2+} indicating 1:1 chelation from conventional Job's plot experiment

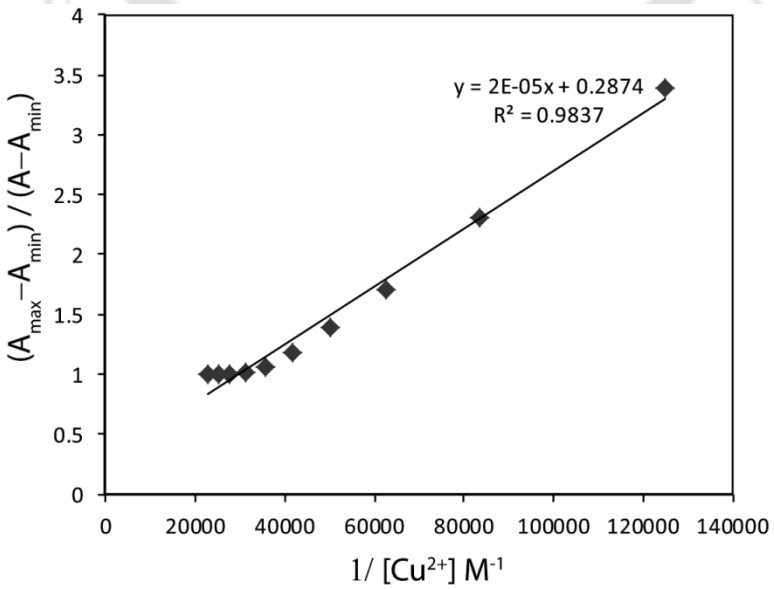

Figure A5.3: B-H plot for determination of Binding constant for Cu^{2+}.

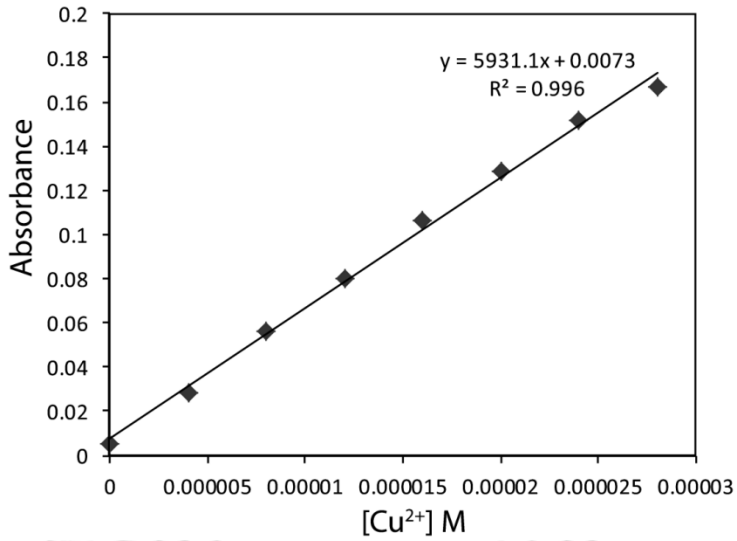

Figure A5.4: Absorbance vs. concentration of Cu^{2+} plot for determination of detection limit

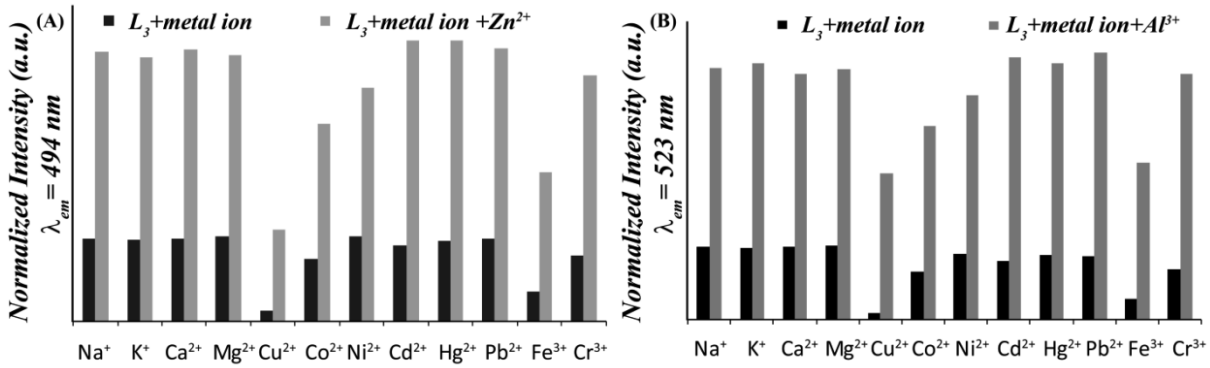

Figure A5.5: (A) Interference of other metal ions in Zn^{2+} sensing. In the solution of $\mathbf{L_3}$ (10μM) various metal ions (100μM) were added followed by addition of Zn^{2+} (100μM) in 9:1 methanol/HEPES buffer (5mM, pH 7.3; 9:1, v/v) medium. (B) Interference of other metal ions in Al^{3+} sensing. In the solution of $\mathbf{L_3}$ (10μM) various metal ions (100μM) were added followed by addition of Al^{3+} (100μM) in 9:1 methanol/HEPES buffer (5mM, pH 7.3; 9:1, v/v) medium.

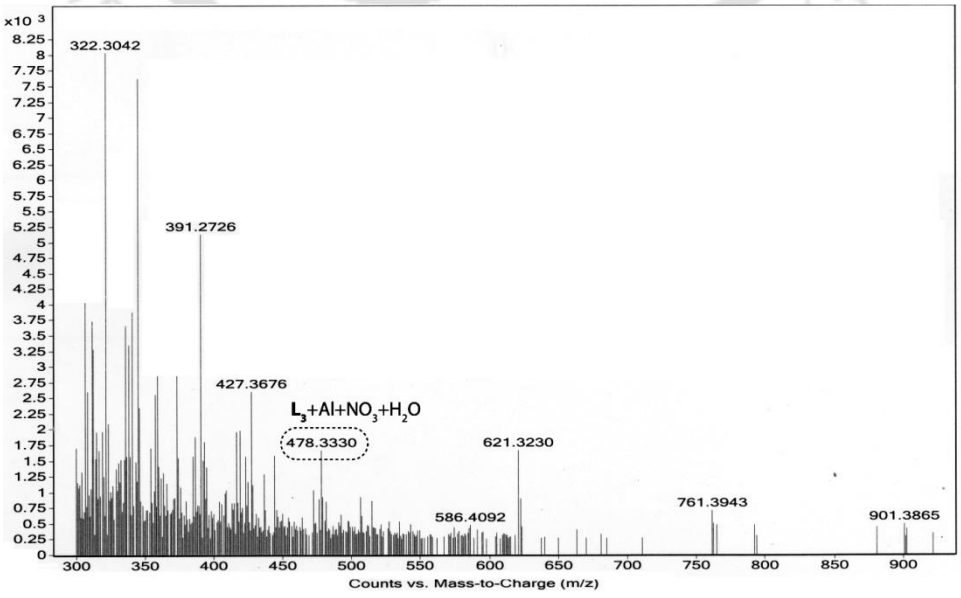

Figure A5.6: Mass spectrum of $\mathbf{L_3}$ in presence of Al^{3+}.

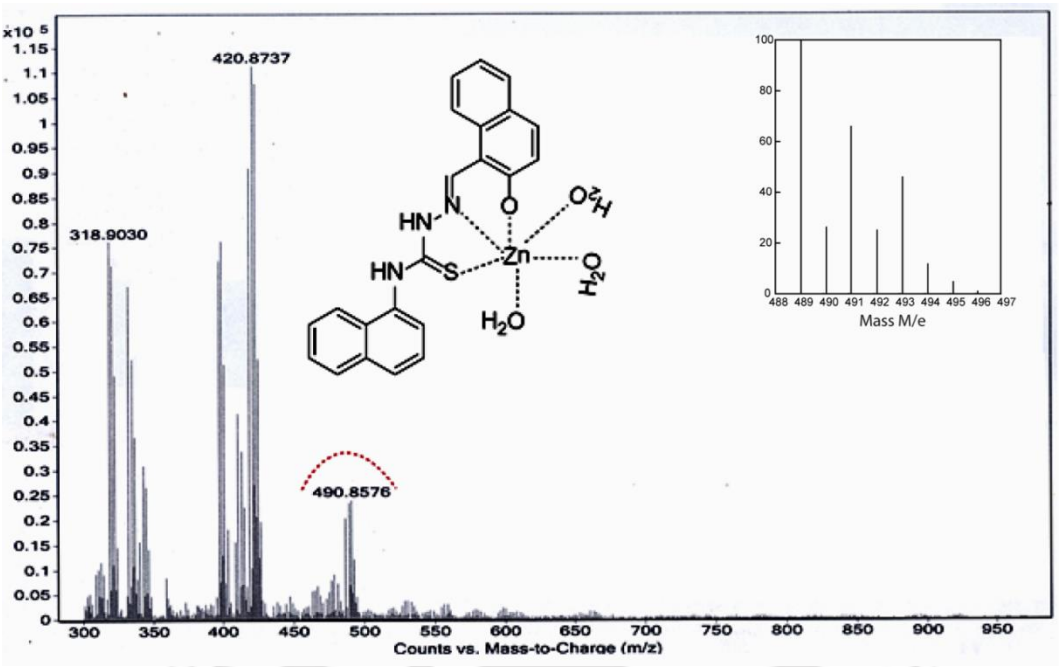

Figure A5.7: Mass spectrum of $\mathbf{L_3}$ in presence of Zn^{2+}; as expected the isotope pattern of Zn-complex is matched well with the observed mass spectra with peaks separated by m/z 2.

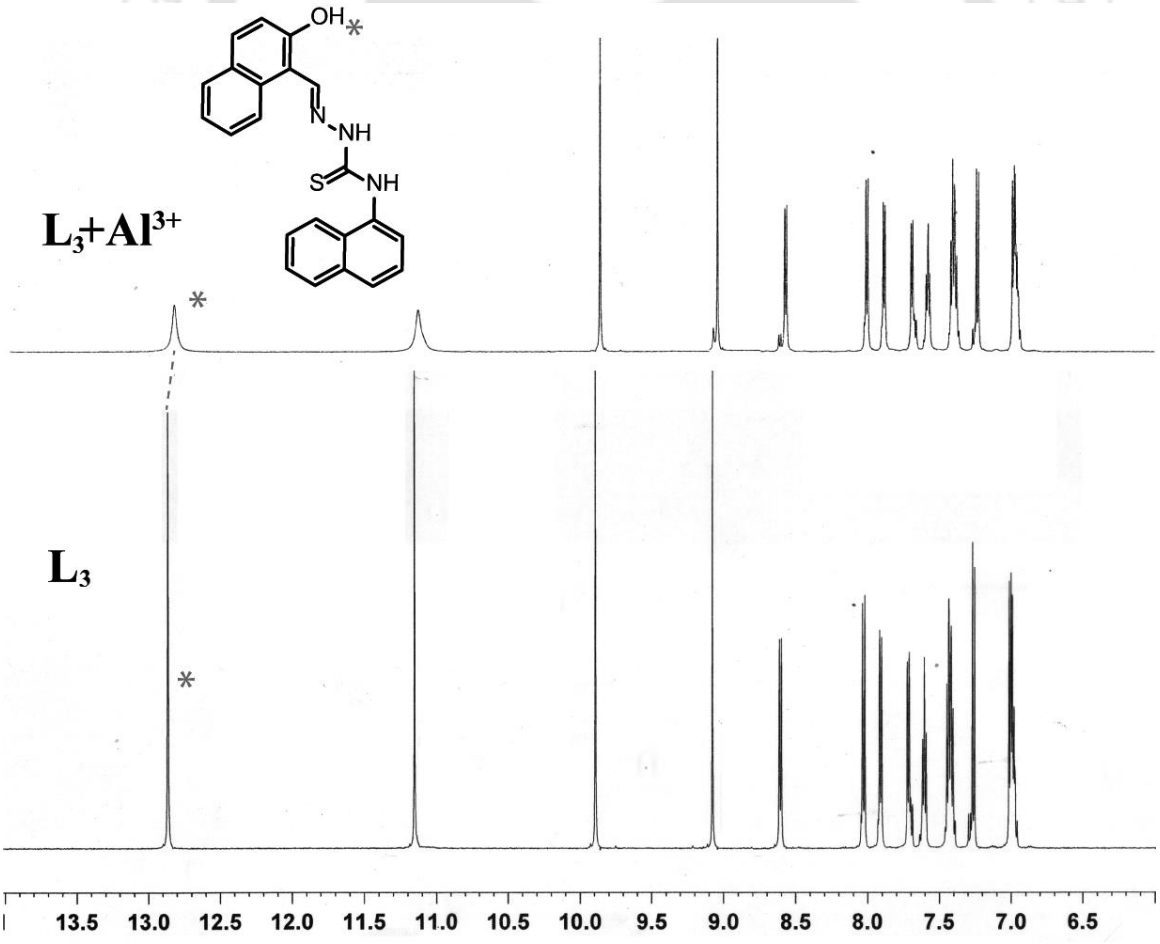

Figure A5.8: ^{1}H NMR spectrum of $\mathbf{L_3}$ in presence of Al^{3+} in DMSO-d_6.

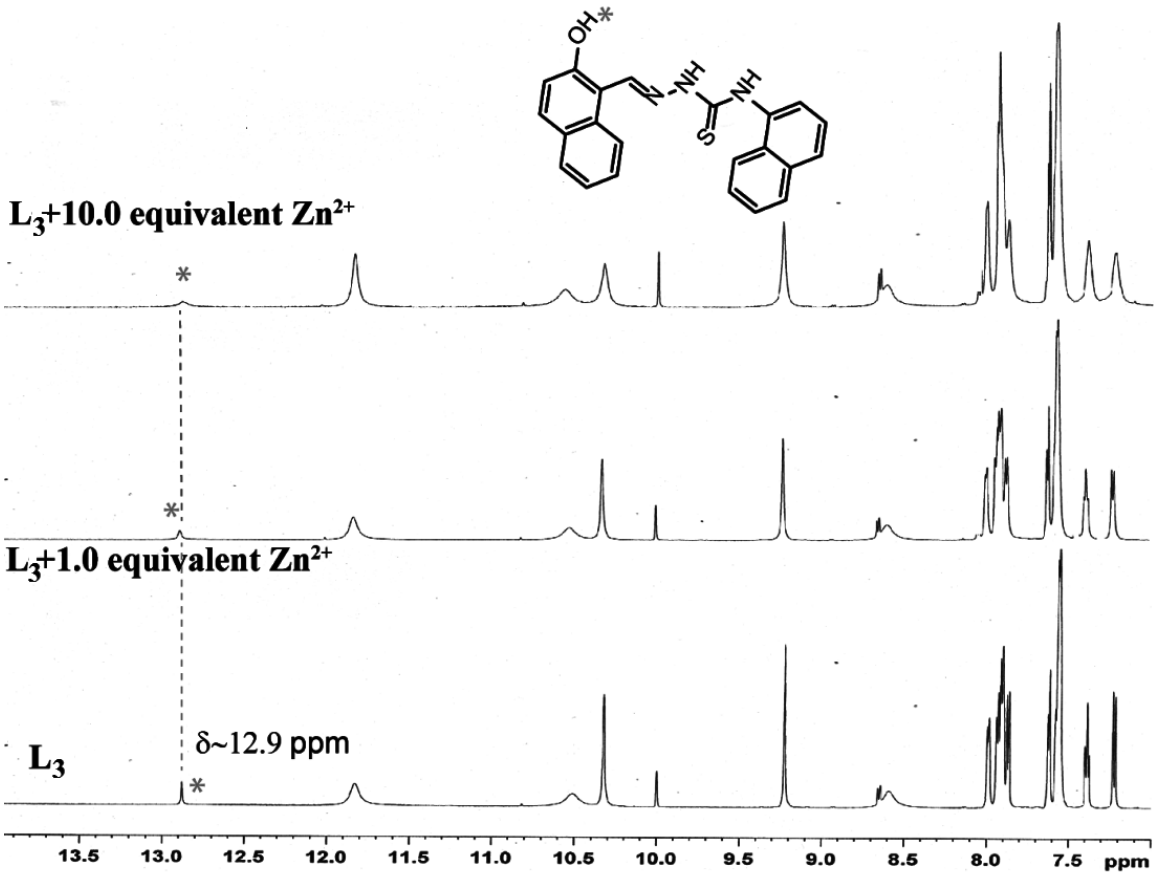

Figure A5.9: ^{1}H NMR spectrum of $\mathbf{L_3}$ in presence of Zn^{2+} in DMSO-d_6.

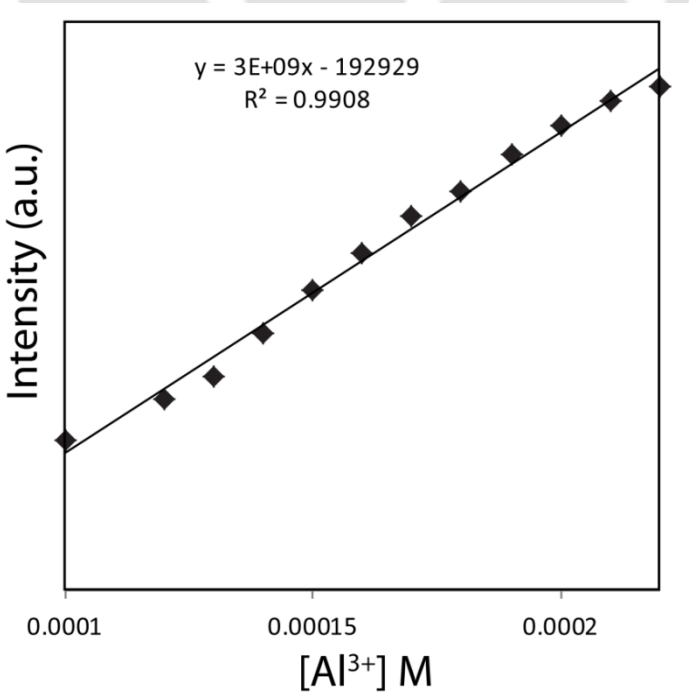

Figure A5.10: Fluorescence intensity vs. concentration of Al^{3+} plot for determination of detection limit

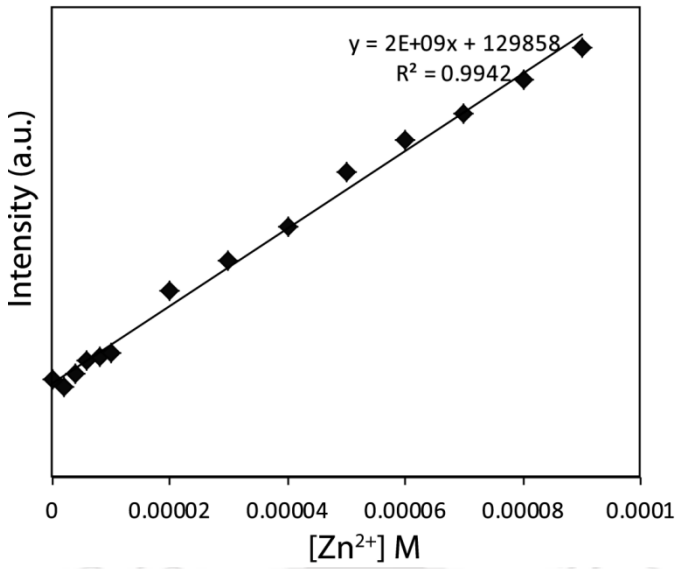

Figure A5.11: Fluorescence intensity vs. concentration of Zn^{2+} plot for determination of detection limit

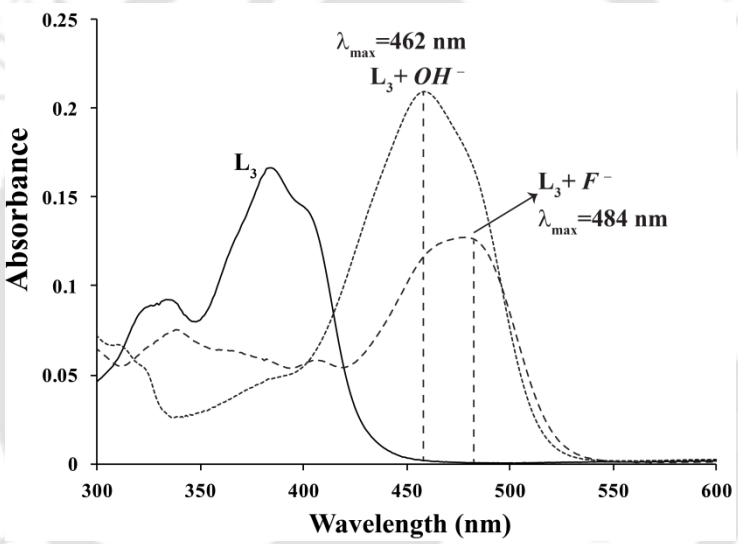

Figure A5.12: UV-Vis spectra of $\mathbf{L_3}$ (5μM) in presence of 10 equivalents of tetra-butyl ammonium hydroxide and tetra-butyl ammonium fluoride in acetonitrile

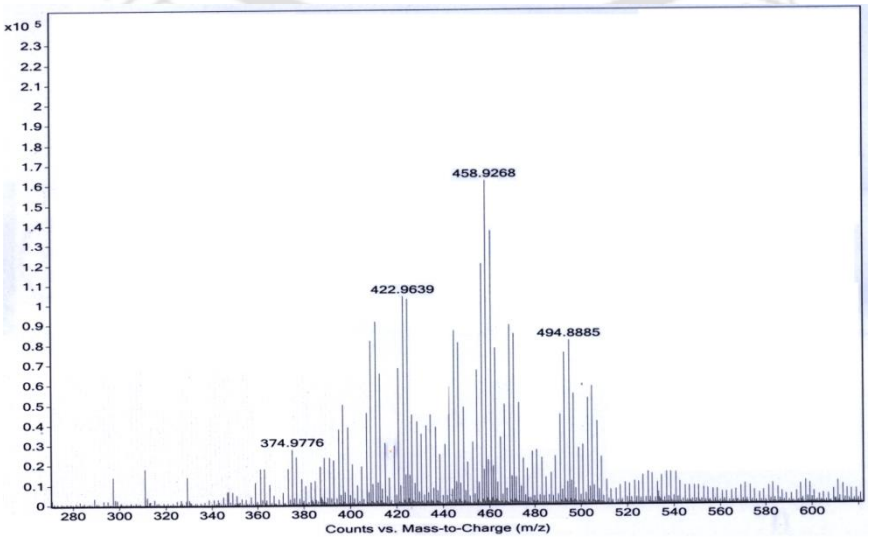

Figure A5.13. Mass spectrum of $\mathbf{L_3}$ in presence of Fluoride

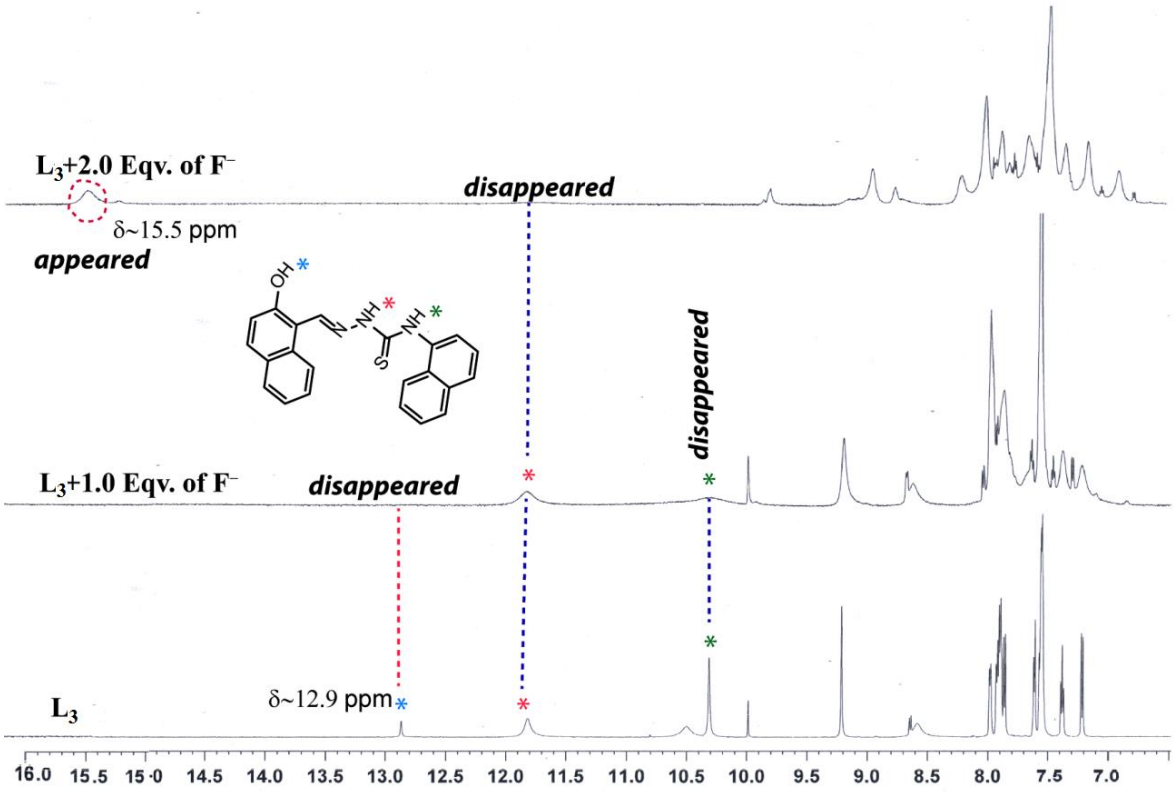

Figure A5.14: ^{1}H NMR spectrum of $\mathbf{L_3}$ in presence of tetra-butyl ammonium fluoride in DMSO-d_6

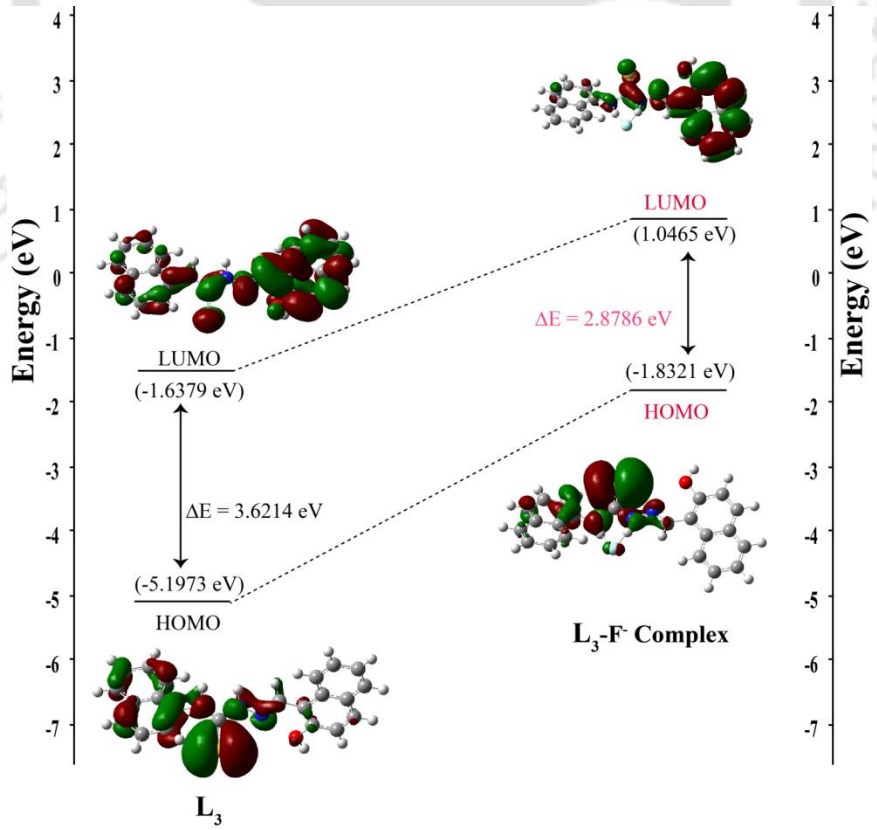

Figure A5.15: Frontier molecular orbital plots and energy level diagrams of $\mathbf{L_3}$ and $\mathbf{L_3}$-F⁻ complex. The calculations were performed using B3LYP/6-31 G (d,p) as implemented on Gaussian 03.

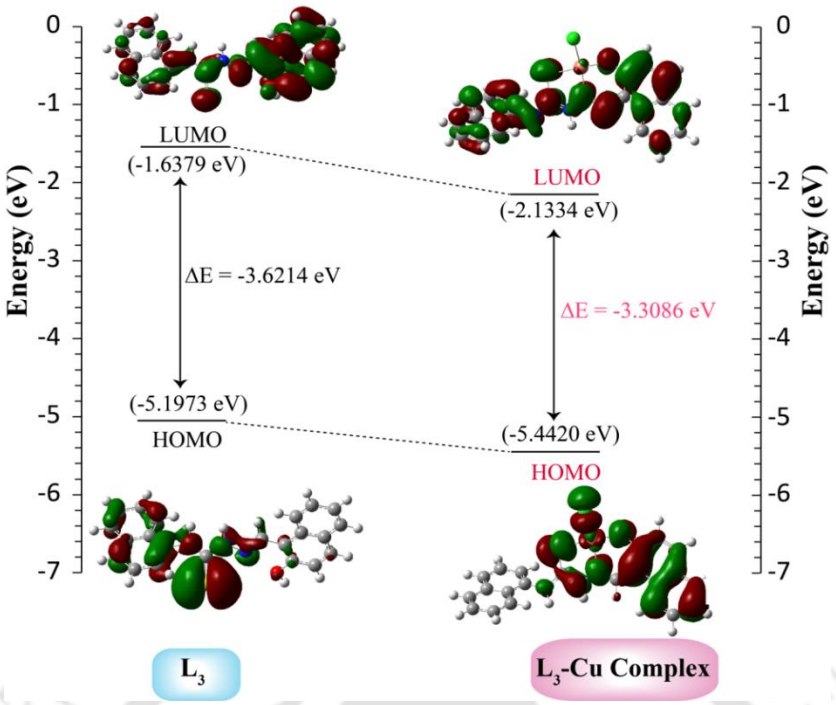

Figure A5.16: Frontier molecular orbital plots and energy level diagrams of $\mathbf{L_3}$ and $\mathbf{L_3}$-Cu^{2+} complex. The calculations were performed using B3LYP/6-31 G (d,p) as implemented on Gaussian 03.

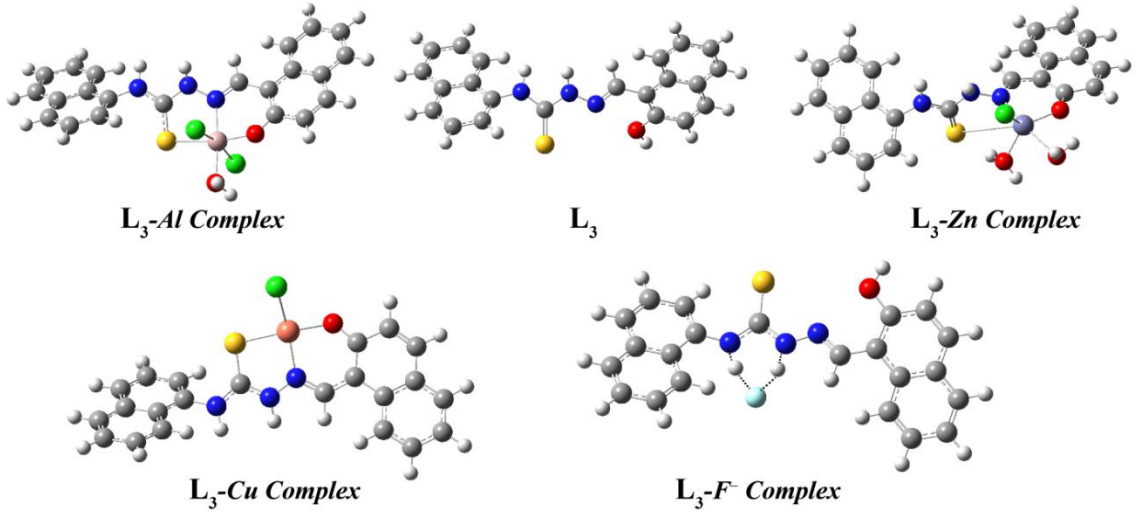

Figure A5.17: Optimized structures of $\mathbf{L_3}$ and its complexes. The calculations were performed using B3LYP/6-31 G (d,p) as implemented on Gaussian 03.

Ref.A5.1. M. J. Frisch, G. W. Trucks, H. B. Schlegel, G. E. Scuseria, M. A. Robb, J. R. Cheeseman, J. A. Montgomery, Jr., T. Vreven, K. N. Kudin, J. C. Burant, J. M. Millam, S. S. Iyengar, J. Tomasi, V. Barone, B. Mennucci, M. Cossi, G. Scalmani, N. Rega, G. A. Petersson, H. Nakatsuji, M. Hada, M. Ehara, K. Toyota, R. Fukuda, J. Hasegawa, M. Ishida, T. Nakajima, Y. Honda, O. Kitao, H. Nakai, M. Klene, X. Li, J. E. Knox, H. P. Hratchian, J. B. Cross, V. Bakken, C. Adamo, J. Jaramillo, R. Gomperts, R. E. Stratmann, O. Yazyev, A. J. Austin, R. Cammi, C. Pomelli, J. W. Ochterski, P. Y. Ayala, K. Morokuma, G. A. Voth, P. Salvador, J. J. Dannenberg, V. G. Zakrzewski, S. Dapprich, A. D. Daniels, M. C. Strain, O. Farkas, D. K. Malick, A. D. Rabuck, K. Raghavachari, J. B. Foresman, J. V. Ortiz, Q. Cui, A. G. Baboul, S. Clifford, J. Cioslowski, B. B. Stefanov, G. Liu, A. Liashenko, P. Piskorz, I. Komaromi, R. L. Martin, D. J. Fox, T. Keith, M. A. Al-Laham, C. Y. Peng, A. Nanayakkara, M. Challacombe, P. M. W. Gill, B. Johnson, W. Chen, M. W. Wong, C. Gonzalez, and J. A. Pople, *Gaussian 03, Revision E.01,Gaussian, Inc., Wallingford CT*, 2004.

Chapter 6

Colorimetric and Fluorometric Discrimination of Geometrical Isomers (Maleic Acid vs Fumaric Acid) With Real-Time Detection of Maleic Acid in Solution and Food Additives

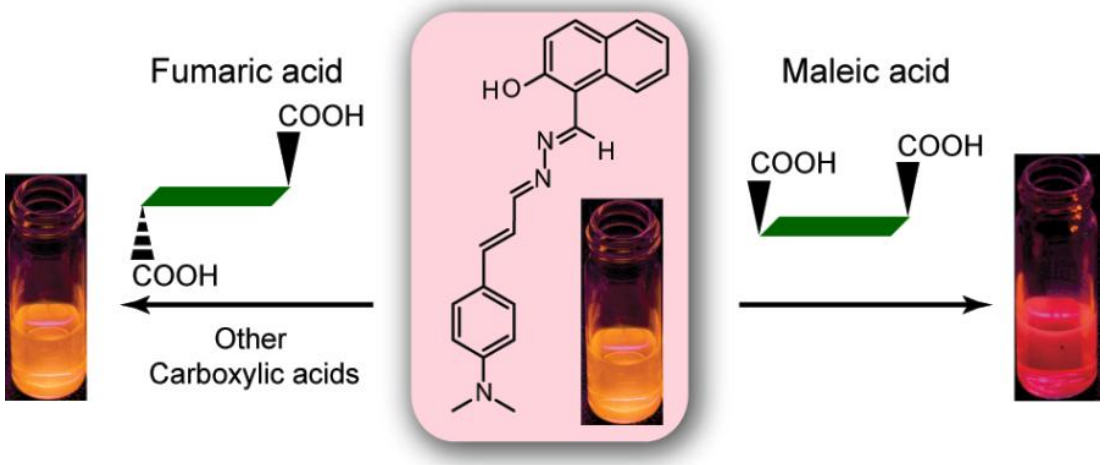

Chapter 6

6.1. Background and focus of the chapter

Molecular recognition of di-carboxylic acids has grabbed the limelight due to their presence as key structural moieties in many bioactive molecules along with their involvement in the biosynthesis of some important intermediates.[6.1] Moreover, they have some important roles in various metabolic processes.[6.2-6.3] Among these several carboxylic acids, Fumaric (Fum) and maleic (Mal) acids are the two important geometrical isomers having vast biological impacts, *viz.* they are extensively used in medicine, food and polymer industries. [6.2-6.3] Recently, some advancement in using fumaric acid derivatives for the treatment of multiple sclerosis and patients with psoriasis are reported.[6.4-6.7] Maleic acid, plays important role as an inhibitor of the Krebs cycle whereas fumarate is generated in the Krebs cycle. Excessive consumption of maleic acid found to be detrimental to kidney and can cause several kidney diseases.[6.8-6.10] The widespread use of these two isomeric acids as ingredients in food as well as beverages raises a great concern over their adverse influences on human health upon prolonged exposure. Thus it is very important to develop an efficient chemosensor for their recognition and quantitative estimation in aqueous medium.

Compared to the large number of chromogenic receptors for the sensing of metal ions,[6.11-6.13] very few chromogenic receptors for anions and small molecules have been developed that are based on recognition approaches.[6.13-6.16] In fact, a thorough literature survey revealed that there are very few colorimetric or fluorogenic sensors which dealt with the use of synthetically constructed receptors in carboxylic acids sensing purpose.[6.17-6.18]

Supramolecular concepts[6.19-6.20] in designing new optical chemosensors has become a very common trend in recent-past based on changes in fluorescence[6.21-6.23] and in absorbance[6.24-6.26] as the output signals. In most of the cases the fluorescent probes are abiotic supramolecular systems that produce certain fluorogenic changes upon binding to the analytes by non-covalent interactions, such as hydrogen bonding, electrostatic attractions and coordination phenomena.[6.27-6.28] But in most of the cases these receptors encountered several limitations in terms of poor specificity towards the analytes.[6.29-6.38]

Differentiation of isomers is, in general, a difficult task because of their rather similar chemical and physical properties. A chemodosimetric reagent was reported by Manez and co-workers

which could discriminate between maleate and fumarate ions.[6.39] But this probe had also some limitations as the selectivity of the system was poor and the probe rendered similar optical response in presence of phthalate if tested instead of maleate.

In this context, as an advancement of this field, herein we report a chromogenic system which not only can discriminate geometrical isomers (Maleic acid vs. Fumaric acid) but also can sense Maleic acid rapidly among various carboxylic acids through sharp colorimetric as well as fluorogenic responses in both physiological condition and food additives.

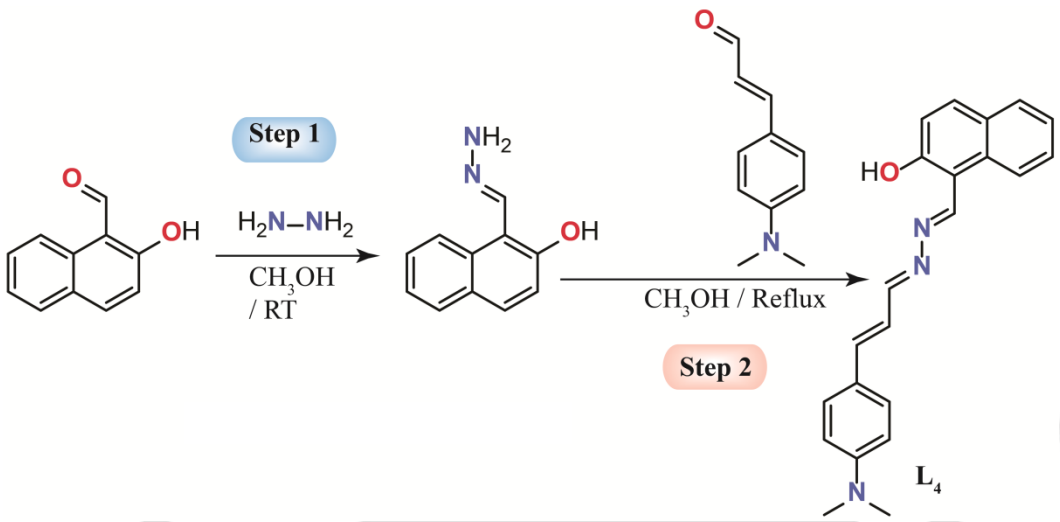

Scheme 6.1: Synthesis of probe $\mathbf{L_4}$

6.2. Rationale behind the design of probe $\mathbf{L_4}$

A new hetero bis-imine fluorogenic probe $\mathbf{L_4}$ was synthesized (**Scheme 6.1**) with good yield and in pure form. The probe was purposely designed to have a push-pull chromophoric platform along with protonation as well as H-bonding site for effective molecular recognition. It is to be noted that unlike the previously discussed probes $\mathbf{L_1}$, $\mathbf{L_2}$ and $\mathbf{L_3}$; the current probe $\mathbf{L_4}$ does not contain any cation binding site or any anion binding site or any nucleophilic reaction site. Hence, we conjectured that contrary to the previously discussed probes $\mathbf{L_1}$, $\mathbf{L_2}$ and $\mathbf{L_3}$; this molecular design is a way forward to sense some neutral guests. The UV-Visible and fluorescence spectral properties of $\mathbf{L_4}$ were studied in detail to investigate the sensing behavior of $\mathbf{L_4}$ towards various organic acids.

6.3. UV-Visible spectral study

UV-Visible spectra of $\mathbf{L_4}$ in 9:1 ethanol-HEPES buffer (5mM, pH~7.4) solvent revealed a sharp absorbance maximum at 430 nm due to π–π^* transition. Binding selectivity of $\mathbf{L_4}$ towards different carboxylic acids was investigated by studying UV-Visible spectra of $\mathbf{L_4}$ in presence of

various mono and di-carboxylic acids *viz.* Acetic acid, Tartaric acid, Benzoic acid, Malonic acid, Succinic acid, Cinamic acid, Citric acid, Stearic acid, Glutamic acid, Phthalic acid, Teraphthalic acid, Isophthalic acid, Gallic acid, Succinic acid, Fumaric acid and Maleic acid. It was astonishing to note that in presence of excess (200 equivalents) of these carboxylic acids, **L_4** rendered no significant change in its colorimetric behavior except for maleic acid (**Figure 6.1A**). Addition of excess of Maleic acid to **L_4** in mixed solvent resulted in the generation of a new red shifted absorbance maximum at 552 nm with the subsequent decrease in the absorbance of its prior original maxima at 430 nm (**Figure 6.1B**). This UV-Visible spectral outcome was accompanied by a distinct visual change in the color of the experimental solution from pale yellow (only **L_4**) to dark red (**L_4**+Maleic acid) (**Figure 6.1C**). This visual display of the color change is encouraging for the naked eye detection of maleic acid using **L_4** through a colorimetric response.

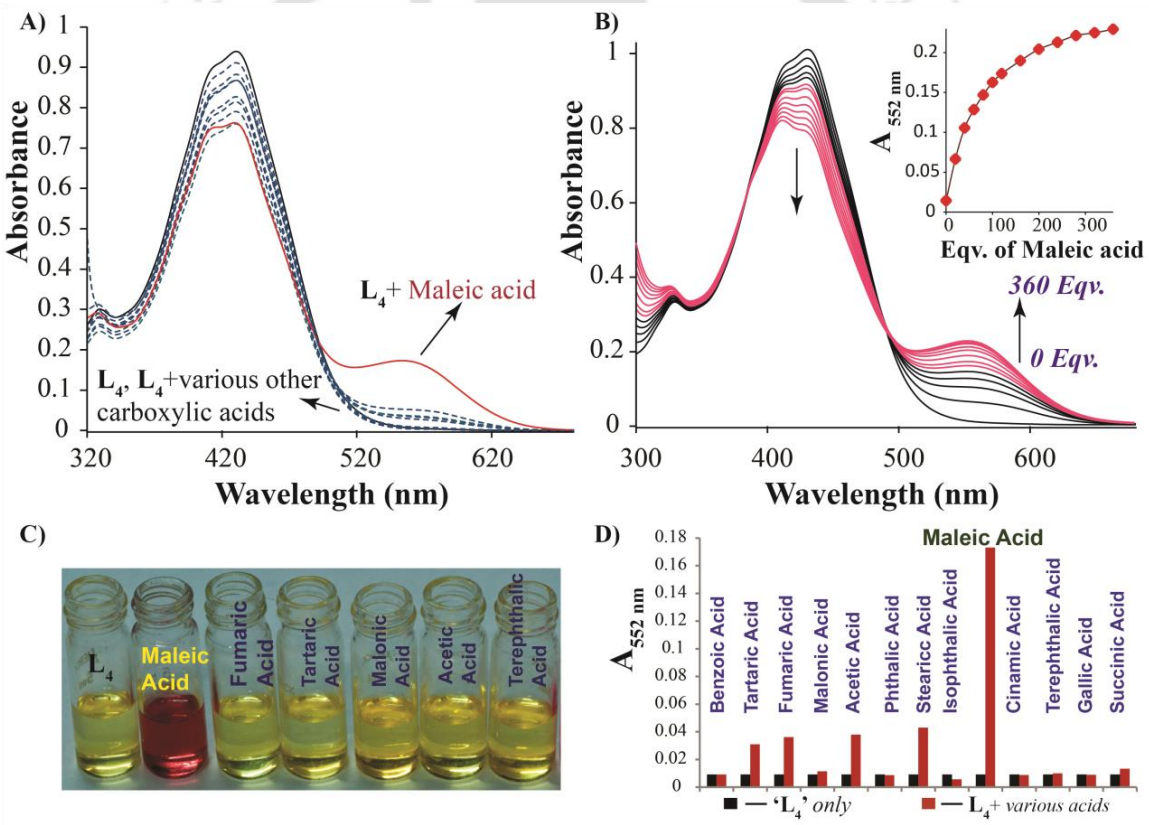

Figure 6.1: A) UV-Visible spectra of **L_4** (20 µM) in presence of various carboxylic acids 4×10^{-3} M in 9:1 ethanol-HEPES buffer (5mM, pH~7.4). B) UV-vis spectra of **L_4** (20 µM) in presence of varying concentration of Maleic acid. INSET: Changes in the absorbance at 552 nm with addition of equivalents of maleic acid C) Visual color change of **L_4** in presence of different carboxylic acids in daylight. D) Comparison of the absorbance at 552nm of **L_4** on interaction with various carboxylic acids.

To understand the sensing of maleic acid by **L_4**, it is important to draw a quantitative appraisal of the relation between the spectral change and the equivalents of maleic acid interacted with **L_4**.

Thus we carried out an UV-Visible titration experiment, where we found that incremental addition of Maleic acid to the solution of **L_4** resulted in a systematic growth of the new red shifted absorbance maxima at 552 nm, with a regular decline of the original absorbance maxima of **L_4** at 430 nm (**Figure 6.1B**). It is to be noted from the titration spectra that a clear isosbestic point arose at 495 nm. Interestingly no such optical changes were furnished by its isomer, fumaric acid in similar condition. Hence, the probe **L_4** not only can sense maleic acid among various other carboxylic acids but also can distinguish it from its geometrical isomer fumaric acid through a stupendous colorimetric response which is even conspicuous by naked eye.

A bar graph has been plotted to show the exact changes in absorbance of **L_4** at 552 nm when treated with different carboxylic acids (**Figure 6.1D**) and this bar graph also clearly support the distinguished colorimetric feature in case of maleic acid.

Preliminarily, we presumed that coordination of maleic acid with **L_4** through strong hydrogen bonding facilitated by *cis*-positioning of two acid groups of maleic acid over other tested carboxylic acids led to the chromogenic spectral response alike earlier reported many carboxylic acid sensors. But, it was astounding to observe that addition of excess strong mineral acid like hydrochloric acid to **L_4** also generated a new absorbance maximum at 552 nm similar to that of maleic acid (**Appendix, Figure A6.1**). Although unlike the case of maleic acid, actual absorbance peak of **L_4** at 430 nm was almost obliterated here. Hence there is a possibility that a new protonated species has formed, which led to the colorimetric response at 552 nm. To better explore the selectivity and sensitivity of **L_4** toward maleic acid we have perused a detailed fluorescence study, followed by mass spectral analysis, ^{1}H NMR experiment and theoretical study for unraveling the exact sensing mechanism.

6.4. Fluorescence spectral study

On excitation at 450 nm **L_4** renders a sharp emission maximum around 590 nm at the same experimental condition and emits a strong orange-yellow fluorescence (**Figure 6.2**). Interestingly addition of maleic acid only yielded significant change in the fluorescence spectra, whereas it geometric isomer fumaric acid has hardly any effect on emission of **L_4** in similar experimental condition. Addition of maleic acid induced a slight decrease in the fluorescent intensity of **L_4** with about ~15 nm red shift in the emission maximum to render a new emission maximum at 606 nm while interaction of fumaric acid with **L_4** remain quiet to the spectral change (**Figure 6.2**). It can be mentioned here that similar fluorescence experiment was carried out in pure ethanol in presence of maleic and fumaric acid, which renders similar optical response (**Appendix, Figure A6.2**). These observations ensured that distinction of these two geometrical isomers is independent of buffer capacity and medium. However it may also be

noted that addition of strong mineral acid HCl to the receptor **L_4** in ethanol medium resulted in substantially quenching (70%) of the fluorescence of **L_4** to make it very less fluorescent unlike the case of Maleic acid (**Appendix, Figure A6.2**).

UV-Visible spectral study suggested that addition of maleic acid to **L_4** might lead to the formation of a new species as a new absorbance maximum emerged at 552 nm (**Figure 6.1**). Therefore, it was prudent to study the emission behavior of **L_4** in presence of maleic acid with an excitation wavelength of 550 nm.

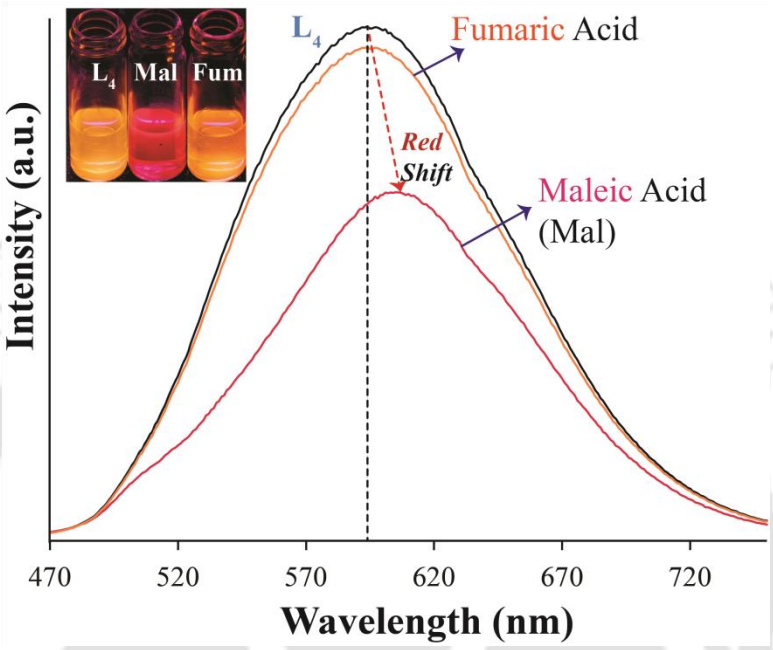

Figure 6.2: Fluorescence spectra of **L_4** (20μM) in presence of 200 equivalents of Maleic acid and Fumaric acid in 9:1 ethanol-HEPES buffer (5mM, pH~7.4). λ_{ex} = 450 nm. INSET: Visual changes observed for **L_4** in absence and in presence of Maleic acid and Fumaric acid under UV light.

However, **L_4** showed a very weak fluorescence when excited at 550 nm (**Figure 6.3**). Selectivity of sensing was confirmed by studying fluorescence spectra of **L_4** (λ_{ex}=550 nm) in presence of various mono and di-carboxylic acids as mentioned earlier. The change in the emission spectral properties was at par with the results of absorbance spectra.

Among all tested carboxylic acids, only maleic acid revealed a certain enhancement in the fluorescence intensity of **L_4** with a well-defined emission maximum at 606 nm (**Figure 6.3A**). Moreover, a selective conspicuous display of the pink-red fluorescence response of the probe upon interaction with maleic acid compared to the orange-yellow fluorescence display of **L_4** upon interaction with all other carboxylic acids provided the scope for naked eye detection (**Figure 6.3C**). A bar graph plot of the comparative normalized emission intensity of **L_4** at 606 nm, on interaction with various carboxylic acids also clearly indicates the exceptional selective turn-on florogenic response of **L_4** towards Maleic acid (**Figure 6.3D**). Thus, not only **L_4** could

discriminate maleic acid from its isomer fumaric acid, but also selectively sensed it among various carboxylic acids through unique fluorescence as well as colorimetric responses. It may be highlighted here that selectivity of our probe **L_4** is superior compared to the probe reported by Manez and co-workers[39] as probe **L_4** does not respond to phthalic acid at all in our sensing system.

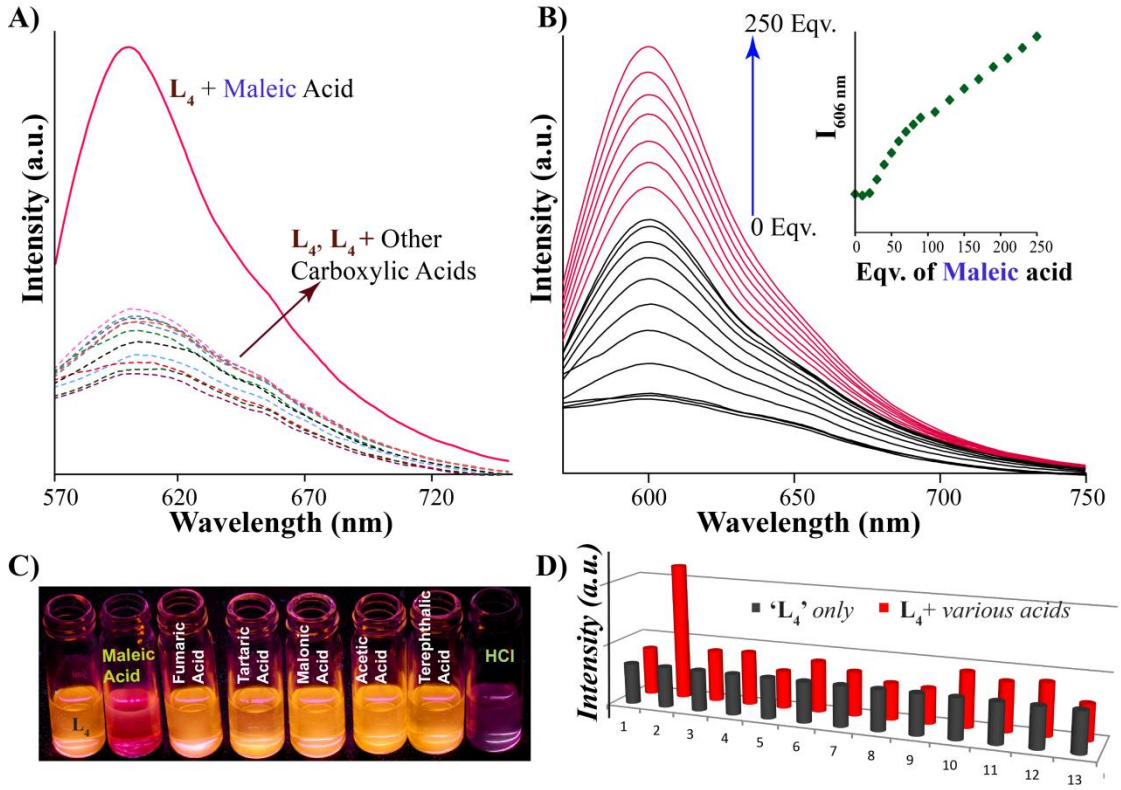

Figure 6.3: A) Fluorescence spectra of **L_4** (20 μM) in presence of various carboxylic acids 4×10^{-3} M in 9:1 ethanol-HEPES buffer (5mM, pH~7.4); λ_{ex} = 550 nm. B) Fluorescence spectra of **L_4** (20 μM) in presence of varying concentration of Maleic acid; λ_{ex} = 550 nm. INSET: Changes in the emission intensity at 606 nm with addition of equivalents of maleic acid. C) Visual color change of **L_4** in presence of different carboxylic acids and HCl under UV light. D) Comparison of the normalized emission intensity of **L_4** at 606 nm on interaction with various carboxylic acids (1= Fumaric acid, 2= Maleic acid, 3= Tartaric acid, 4= Citric acid, 5 = Cinamic acid, 6= Malonic, 7= Acetic acid, 8= Benzoic acid, 9= Gallic acid, 10= Stearic acid, 11= Terephthallic acid, 12= Phthalic acid and 13= Succinic acid).

To get a quantitative appraisal of the spectral change a titration experiment was carried out with varying concentration of maleic acid. A systematic incremental addition of maleic acid to the solution of **L_4** in in 9:1 ethanol-HEPES buffer (5mM, pH~7.4) medium resulted in a sequential enhancement in its emission intensity at 606 nm when excited at 550 nm (**Figure 6.3B**). Interestingly the linear enhancement of the emission intensity of **L_4** up to addition of 360 equivalents of maleic acid downplayed the possibility of simple coordination between **L_4** and maleic acid. Instead both the UV-visible and fluorescence titration spectra indicated towards the

possibility of a new species formation via protonation, which led to the unique spectral outcome. It may be mentioned here that the detection limit for the maleic acid was determined from this fluorescence titration experiment, and it was found to be 2.1×10^{-5} M or 2.4 ppm (**Appendix, Figure A6.3**).

6.5. Plausible sensing mechanism

There is a possibility that, the proton acceptor site $-NMe_2$ group present in **L_4** could easily be protonated to generate a new species in solution. A close look of the acidity constant value revealed that among all of the tested carboxylic acids maleic acid had the lowest pK_{a1} value (pK_{a1}=1.9 **Table A6.1, Appendix**) compared to its isomer fumaric acid (pK_{a1}=3.03) which in turn facilitated easy proton generation in solution in the case of maleic acid. Thus maleic acid only could generate selective optical response through protonation.

As discussed earlier, HCl could also generate a new absorbance maximum at 552 nm similar to maleic acid; however, it resulted in the formation of pink-red solution in contrast to the generation of dark brown-red solution in presence of maleic acid. Also the noticeable new feature was that, though in case of HCl the newly generated maximum was more prominent with much higher absorbance, the previous actual absorbance peak of **L_4** at 430 nm became almost nonexistent (**Appendix, Figure A6.1**) unlike the case of Maleic acid. The emission spectral studies in presence of HCl also incited some major distinct spectral features with respect to maleic acid (**Appendix Figure A6.2**). These results substantiate that though the actual sensing mechanism was someway inclined by the protonation of the probe, but this is not the sole criterion for sensing mechanism. It maybe envisaged that some other factor, along with protonation is simultaneously governing the Maleic acid sensing. Protonation with subsequent complexation of the analyte(s) to the probe may be accountable for the whole sensing mechanism. It may also be noted that, oxalic acid, which has even lower pK_{a1} (1.25) value than maleic acid pK_{a1} (1.9) only could induce 65% less emission intensity (**Appendix, Figure A6.4**) with respect to the enhancement in emission intensity initiated by maleic acid in ethanol. This observation again reiterated the preposition that complexation too has a role along with protonation to endorse the maleic acid sensing.

Thus to uncover the precise mechanism behind this spectral change we pursued extensive ^{1}H NMR and mass spectral experiments. ^{1}H NMR study of **L_4** revealed that the presence of maleic acid led to the protonation of **L_4** ($-NMe_2$ group) by signaling the appearance of a new peak at ~6.38 ppm (**Appendix, Figure A6.5**. At the same time the almost disappearance of the phenolic –OH peak at ~13.4 ppm or ~13.0 ppm may suggest the strong complexation of maleic acid with

successive de-protonation of the phenolic –OH. In addition, the mass spectra of the receptor **L_4** taken in presence of maleic acid witnessed the emergence of a new base peak at m/z=627. 6553. The peak corresponds to [**L_4** + 2Malate+ $3H_2O$+ H^+], which clearly validates the protonation of **L_4** as well as coordination of maleic acid with **L_4** (**Appendix, Figure A6.6**). The whole sensing phenomenon has been summarized and presented with a schematic representation in **Scheme 6.2**.

In contrary, addition of HCl to **L_4** yielded a NMR spectra indicating breaking of Schiff base linkage in the probe (**Appendix, Figure A6.7**). Moreover the mass spectra of **L_4** taken in presence of HCl witnessed the appearance of mass peaks at 157.0385, 225.1048 and 347.2257. All these together pointed towards the disintegration of hetero-Schiff base **L_4** and generation of a homo bis-imine (**Appendix, Figure A6.8**). Probably the generation of the 4-(3-hydrazonoprop-1-en-1-yl)-N,N-dimehtylbenzenaminium led to the UV-Vis spectral outcome when strong inorganic acid has been added to **L_4**.

Further a control experiment was carried out by studying the UV-Visible spectra of **L_4** in presence of maleic acid and HCl respectively followed by addition of excess NaOH to both the solutions (**Appendix, Figure A6.9**).

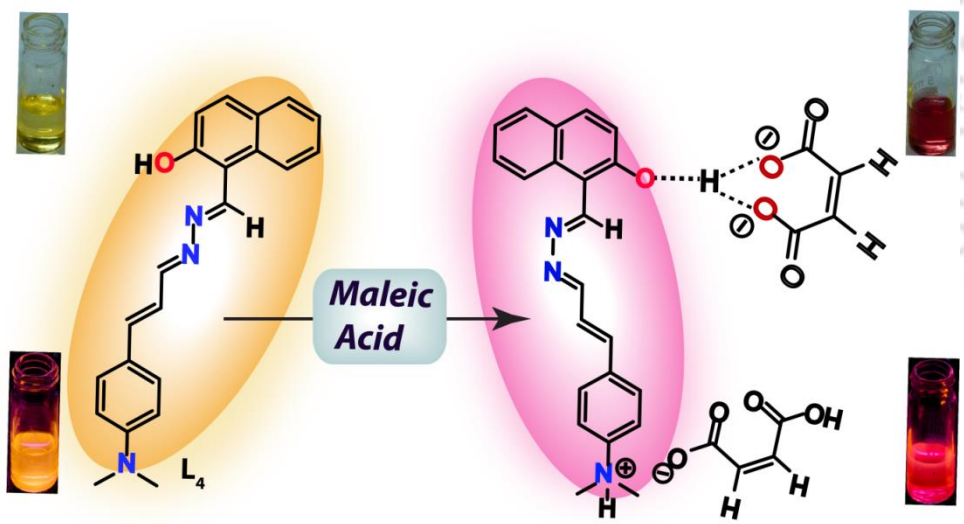

Scheme 6.2: Plausible sensing mechanism

The result showed that subsequent addition of NaOH could retrieve the actual spectra of **L** in case of Maleic acid (**Appendix, Figure A6.9**). However, it failed to salvage the absorbance peak of **L_4** at 430 nm in case of HCl. In the later case, formation of two distinct new absorbance peaks at 370 nm and 450 nm (**Appendix, Figure A6.9**) is actually insinuating towards the breaking of imine bond of **L_4** and generation of two different new specie in solution in accordance with the earlier predicted mass spectra (**Appendix, Figure A6.8**).

6.6. Density functional theory (DFT) study

An extensive Density functional theory (DFT) and Time dependent Density functional theory (TDDFT) calculations were pursued to understand the theoretical aspect of this sensing mechanism. To ascertain the effect of protonation on spectroscopic signatures of **L_4**, DFT optimizations of **L_4** and protonated- **L_4** were carried out with the B3LYP/6-31+G(d,p) method basis set using the Gaussian 03 program. The optimized geometry and the highest occupied molecular orbital (HOMO) and the lowest unoccupied molecular orbital (LUMO) of **L_4** and protonated **L_4** (**LH^+**) are presented in **Figure 6.4**. The substantial decrease in the HOMO to LUMO energy gap on protonation of **L_4** undoubtedly validated the theoretical basis of the observed red shift (**Figure 6.2**) in emission maxima as well as generation of new red shifted absorption maxima (**Figure 6.1**) of **L_4** when treated with maleic acid (**Figure 6.4**).

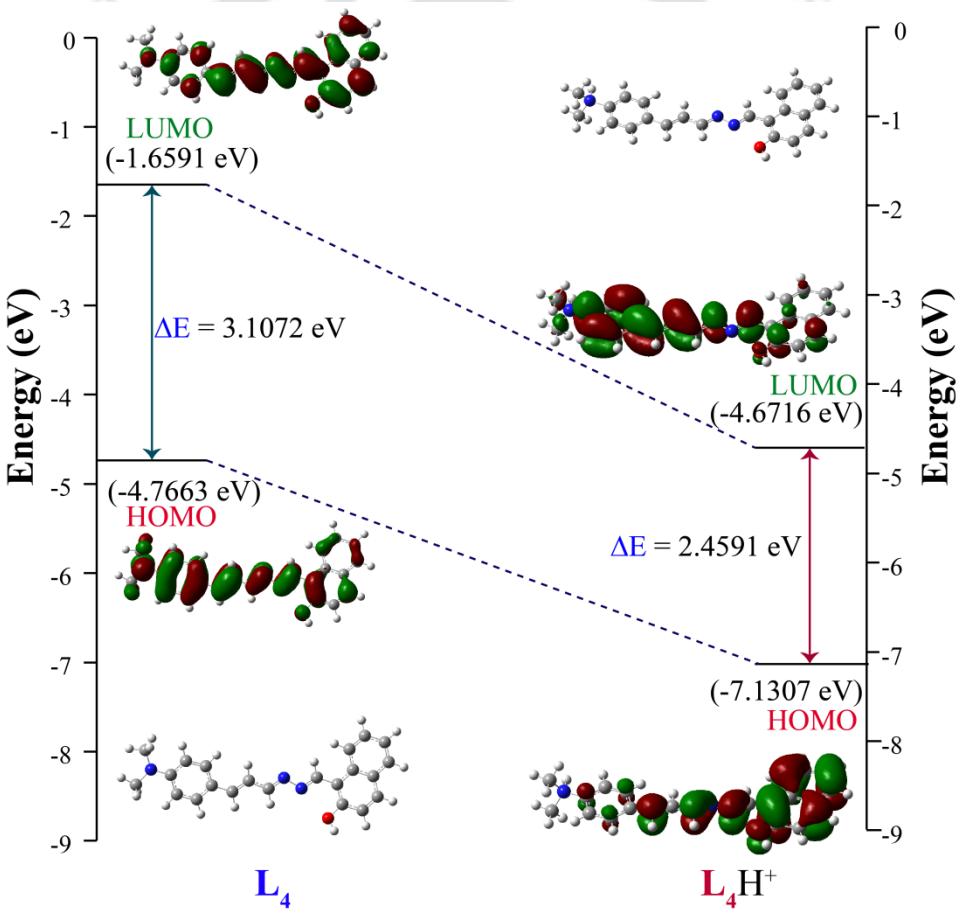

Figure 6.4: Frontier molecular orbital plots, optimized structures and energy level diagrams of **L_4** and **L_4H^+**. The calculations were performed using B3LYP/6-31 G (d,p) as implemented on Gaussian 03.

UV-Vis spectra of **L_4** and **L_4H^+** were calculated using the TDDFT method (No specific solvent model was used) with the same B3LYP/6-31+G(d,p) basis set. The results of the calculation indicated that in the case of **L_4**, the transition from HOMO to LUMO, HOMO-2 to LUMO and

HOMO-1 to LUMO / HOMO to LUMO+1 contributed mainly to the excitation at 427 nm, 412 nm and 360 nm respectively. Similarly, for mono-protonated **L_4** (**LH^+**), absorption peaks in the long wavelength region at 544 nm, 520 nm, 420 nm and 403 nm were mainly generated due to the transition from HOMO to LUMO, HOMO-1 to LUMO, HOMO-2 to LUMO and HOMO to LUMO + 1 respectively. Selected orbitals and their corresponding energies for **L_4** and **L_4H^+** which are likely to be critical in the optical spectral outcome are provided in supporting information (**Table A6.2 and Table A6.3; Appendix**).

The calculated absorption peaks of **L_4** and **L_4H^+** found to be matched impressively with the experimentally observed peaks. Likewise the experimental UV visible spectrum of **L_4** having an absorbance maximum at 430 nm, theoretically calculated spectrum of **L_4** showed excitation at 427 nm, which is in remarkably well agreement. Alongside calculated UV-visible spectra for **L_4** witnessed emergence of a new excitation peak at 544 nm that agreed well with the newly generated absorbance maximum of **L_4** at 550 nm on interaction with Maleic acid (**Appendix, Figure A6.10**). Not only that the theoretical and experimental spectral natures of **L_4** / **L_4H^+** are very similar which have been demonstrated in **Figure A6.10**, (**Appendix**). Thus undoubtedly lower pK_{a1} of Maleic acid assisted the mono-protonation of **L_4** along with coordination which governed to the observed unprecedented sensing outcome of Maleic acid by **L_4** (**Appendix, Figure A6.11-A6.12**).

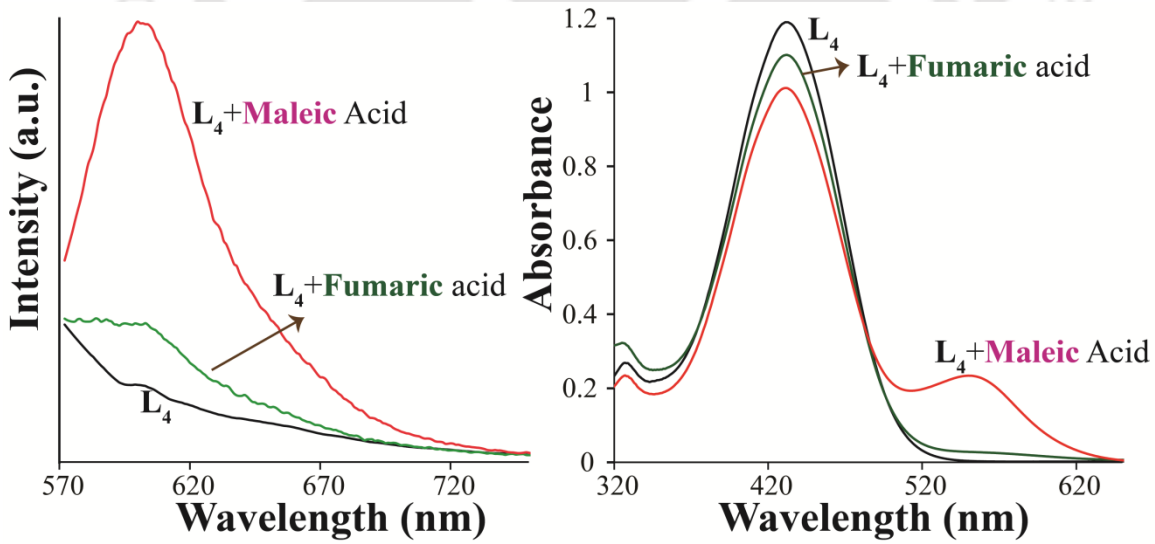

Figure 6.5: Determination of Maleic acid (spiked) in starch-rich food A) from Fluorescence spectroscopy B) from UV-Visible spectroscopy.

6.7. Determining Maleic acid in food additives

Use of Maleic acid as food additives in starch rich foods like tapioca starch, tapioca balls, rice noodles, and hotpot ingredients are not desierable.[6.40-6.42] It was envisaged that the use of probe

L_4 to detect Maleic acid quantitatively in a starch rich food sample would be an encouraging real application. Thus we prepared a sample by simple liquid extraction of the starch rich food which is described in detail in experimental section. The extract of the food in methanol was divided in three parts and in each part maleic acid, fumaric acids and nil (as control) was added respectively in appropriate amount. Rising above our expectation **L_4** revealed the same spectral outcome as earlier and hence was able to detect maleic acid both calorimetrically as well as fluorometrically with the same detection limit. Thus we have developed a probe which could well be used to detect maleic acid in starch rich food samples optically (both fluorescence and UV-visible spectroscopy) even conspicuous through naked eye.

6.8. Conclusion

In summery here in we have synthesized a new Schiff base probe **L_4** with two hetero-imine bonds, which is capable of discriminating Maleic acid from its geometrical isomer Fumaric acid through colorimetric as well as fluorescence responses. Not only that, it can also sense the maleic acid among various mono, di and tri-carboxylic acids in mixed aqueous ethanol-buffer solution. The unique colorimetric as well as fluorescence responses of **L_4** towards Maleic acid is also conspicuous through naked eye. Theoretical DFT and TDDFT calculation well supported the premise that protonation of **L_4** is actually governing the sensing process along with complexation. The sensing process was also replicated in starch rich food to detect added Maleic acid.

References

6.1. J. M. Berg, T J. L.ymoczko and L. Stryer, Biochemistry, 5th ed.; W. H. Freeman: New York, 2002; pp 465−484.

6.2. I.M. Perez-Dıaz and R. F. McFeeters, *J. Food Sci.*, 2010, **75**, M204.

6.3. S. Rouse and D. J. van Sinderen, *J. Food Prot.*, 2008, **71**, 1724.

6.4. D. M. Khiabani, A. Blank, T. Skripuletz, E. Miller, A. Kotsiari, V. Gudi and M. Stangel, *PLoS One*, 2010, **5**, e11769.

6.5. B. D. Trapp, K. A. Nave, *Annu. Rev. Neurosci.*, 2008, **31**, 247.

6.6. J. Wernerman and F. Hammarkvist, *Lancet*, 1990, **335**, 701.

6.7. R. H. Grubbs and W. Tumas, *Science*, 1989, **243**, 907.

6.8. J. Stepinski, D. Pawlowska and S. Angielski, *Acta Biochim. Pol.*, 1984, **31**, 229.

6.9. A. Gougoux, G. Lemieux and N. Lavoie, *Am. J. Physiol.*, 1976, **231**, 1010.

6.10. S. EiamOng, M. Spohn, N. A. Kurtzman and S. Sabatini, *Kidney Int.*, 1995, **48**, 1542.

6.11. H. N. Kim, W. X. Ren, J. S. Kim and J. Yoon, *Chem. Soc. Rev.*, 2012, **41**, 3210.

6.12. R. D. Hancock, *Chem. Soc. Rev.*, 2013, **42**, 1500.

6.13. Y. Ding, Y. Tang, W. Zhu and Y. Xie, *Chem. Soc. Rev.*, 2015, **44**, 1101.

6.14. V. S. Lin, W. Chen, M. Xian and C. J. Chang, *Chem. Soc. Rev*., 2015, Advance Article. DOI: 10.1039/C4CS00298A.

6.15. T. Wang, E. F. Jr. Douglass, K. J. Fitzgerald and D. A. Spiegel, *J. Am. Chem. Soc.*, 2013, **135**, 12429.

6.16. L. He, W. Lin, Q. Xu and H. Wei, *Chem. Commun.*, 2015, **51**, 1510.

6.17. U. G. Reddy, R. Lo, S. Roy, T. Banerjee, B. Ganguly and A. Das, *Chem. Commun.*, 2013, **49**, 9818.

6.18. Y. P. Tseng, G. M. Tu, C. H. Lin, C. T. Chang, C. Y. Lin and Y. P. Yen, *Org. Biomol. Chem.*, 2007, **5**, 3592.

6.19. 'Chemosensors for Ion and Molecular Recognition': J. P. Desvergne, A.W. Czarnik, NATO ASI Ser. Ser. C 1997, 492.

6.20. A. Bianchi, K. Bowman-James, E. GarcÌa-EspaÊa, Supramolecular Chemistry of Anions, Wiley-VCH, New-York, 1997.

6.21. A. P. de Silva, H. Q. N. Gunaratne, T. Gunnlaugsson, A. J. M. Huxley, C. P. McCoy, J. T. Rademacher and T. E. Rice, *Chem. Rev.*, 1997, **97**, 1515.

6.22. C. Bargossi, M. C. Fiorini, M. Montalti, L. Prodi and N. Zaccheroni, *Coord. Chem. Rev*., 2000, **208**, 17.

6.23. A. B. Descalzo, D. Jimenez, M. D. Marcos, R. Martinez-Manez, J. Soto, J. El Haskouri, C. Guillem, D. Beltrµn, P. AmorÛs and M. V. Borrachero, *Adv. Mater.*, 2002, **14**, 966.

6.24. H. G. Lohr and F. Vogtle, *Acc. Chem. Res*., 1985, **18**, 65.

6.25. M. Inouye, *Color. Non-Text. Appl.*, 2000, 238.

6.26. S. L. Wiskur, H. Ait-Haddou, J. J. Lavigne and E. V. Anslyn, *Acc. Chem. Res.*, 2001, **34**, 963.

6.27. P. D. Beer and P. A. Gale, *Angew. Chem., Int. Ed*., 2001, **40**, 486.

6.28. B. Valeur and I. Leray, *Coord. Chem. Rev.*, 2000, **205**, 3.

6.29. J. Raker and T. E. Glass, *J. Org. Chem.*, 2002, **67**, 6113.

6.30. A. Metzger and E. V. Anslyn, *Angew. Chem.*, 1998, **37**, 649.

6.31. J. J. Lavigne and E. V. Anslyn, *Angew. Chem. Int. Ed.*, 1999, **38**, 3666- 3669.

6.32. D. A. Jose, I. Mon, H. F. Perez, E. C. E. Adan, J. B. Buchholz and A. V. Ferran, *Org. Lett.*, 2011, **13**, 3632.

6.33. M. Takeuchi, T. Imada and S. Shinkai, *Angew. Chem.*, 1998, **37**, 2096.

6.34. T. Ikeda, O. Hirata, M. Takeuchi and S. Shinkai, *J. Am. Chem. Soc.*, 2006, **128**, 16008.

6.35. Y. Wu, H. Guo, X. Zhang, T. D. James and J. Zhao, *Chem.–Eur. J.*, 2011, **17**, 7632.

6.36. M. Hu and G. Feng, *Chem. Commun.*, 2012, **48**, 6951.

6.37. L. Tang, J. Park, H.-J. Kim, Y. Kim, S. J. Kim, J. Chin and K. M. Kim, *J. Am. Chem. Soc*., 2008, **130**, 12606.

6.38. (a) F. Li, S. Carvalho, R. Delgado, M. G. B. Drew and V. Fe´lix, *Dalton Trans.*, 2010, **39**, 9579; (b) K. Ghosh, T. Sen, A. Patra, J. S. Mancini, J. M. Cook and C. A. Parish, *J. Phys. Chem. B*., 2011, **115**, 8597; (c) S. Samanta, B. Nath and J. B. Baruah, *Inorg. Chem. Commun*., 2012, **22**, 98.

6.39. F. Sancenun, R. Martinez-Manez, M. A. Miranda, M.-J. Segui and J. Soto, *Angew. Chem.*, 2003, **115**, 671.

6.40. http://www.fda.gov.tw/EN/newsContent.aspx?ID=9918&chk=454d1df8-1f26-43a3-9a85-5540dc07caae

6.41. http://www.ava.gov.sg/NR/rdonlyres/9253E7B2-E57D-4992-982C1304E73748D6/26074/Pressrelease_Recallofstarchba sedproductsfromTaiwan.pdf

6.42. http://www.fda.gov.ph/advisories/food/76474-fda-advisoryon-maleic-acid

Appendix

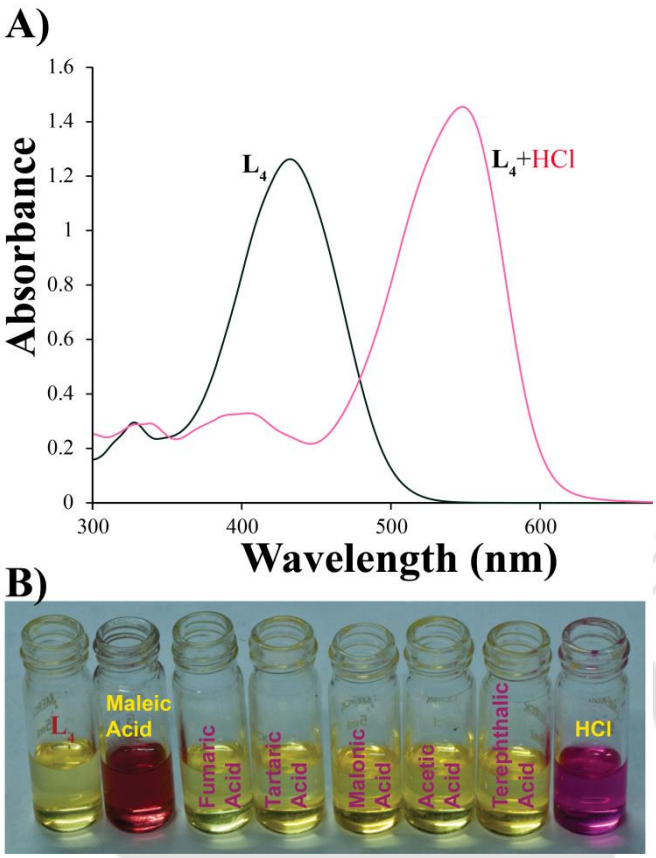

Figure A6.1. (A) UV-Vis spectra of L_4 (20 µM) in presence of 200 equivalents of HCl. (B) Visual pictures of L_4 solution in presence of excess of different acids under day light.

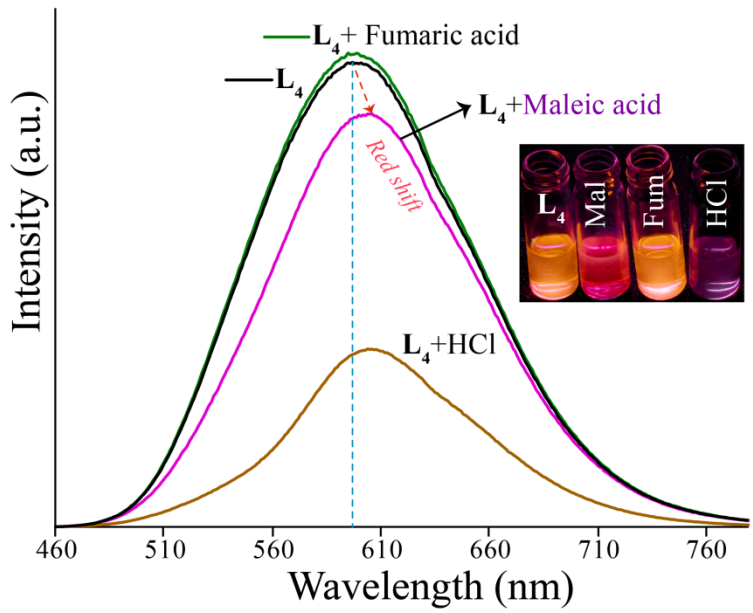

Figure A6.2. Fluorescence spectra of L_4 (20µM) in ethanol in presence of 200 equivalents of Maleic acid, Fumaric acid and HCl. λ_{ex} = 450 nm. INSET: Visual changes observed for L_4 in absence and in presence of Maleic acid, Fumaric acid and HCl under UV light.

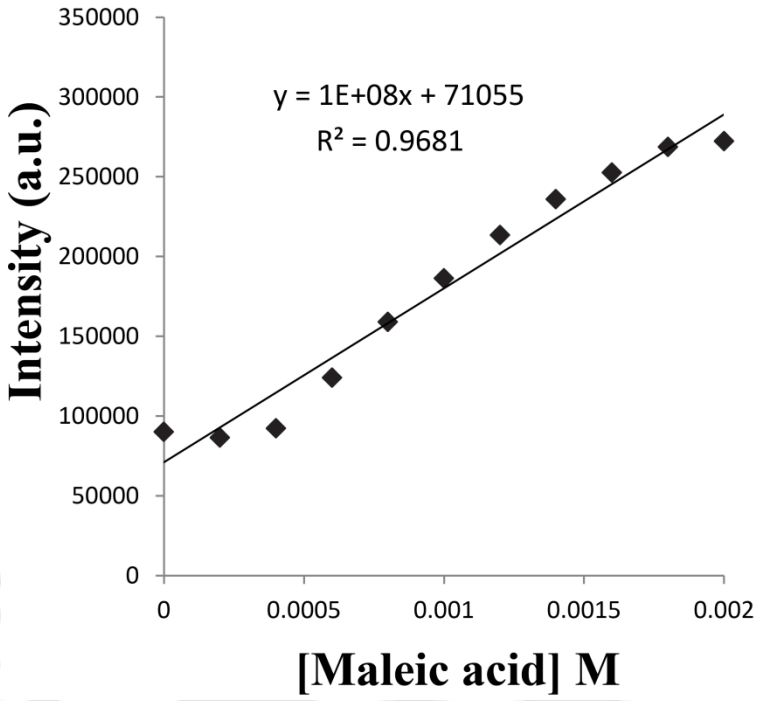

Figure A6.3: Fluorescence intensity vs. concentration of Maleic acid plot for determination of detection limit.

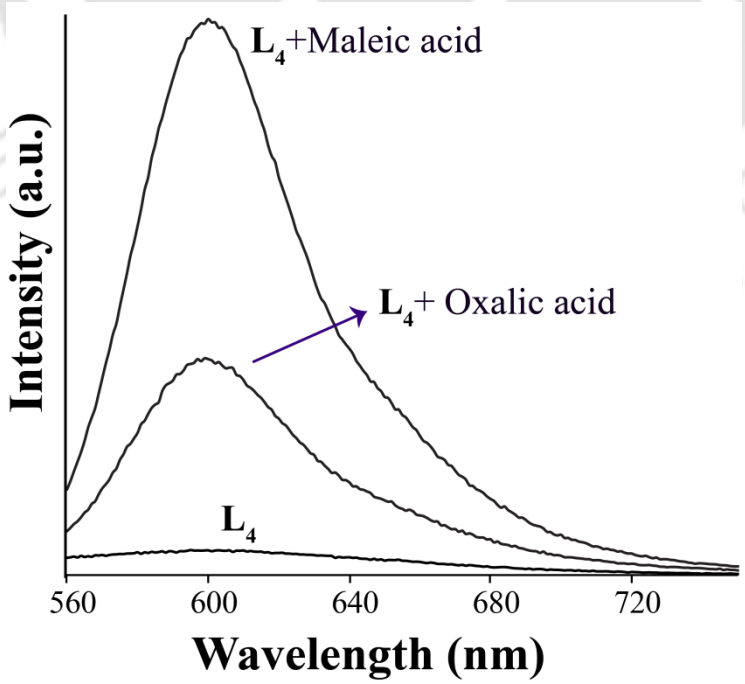

Figure A6.4: Fluorescence spectra of $\mathbf{L_4}$ (20μM) in ethanol in presence of 200 equivalents of Maleic acid and Oxalic acid. λ_{ex} = 550 nm.

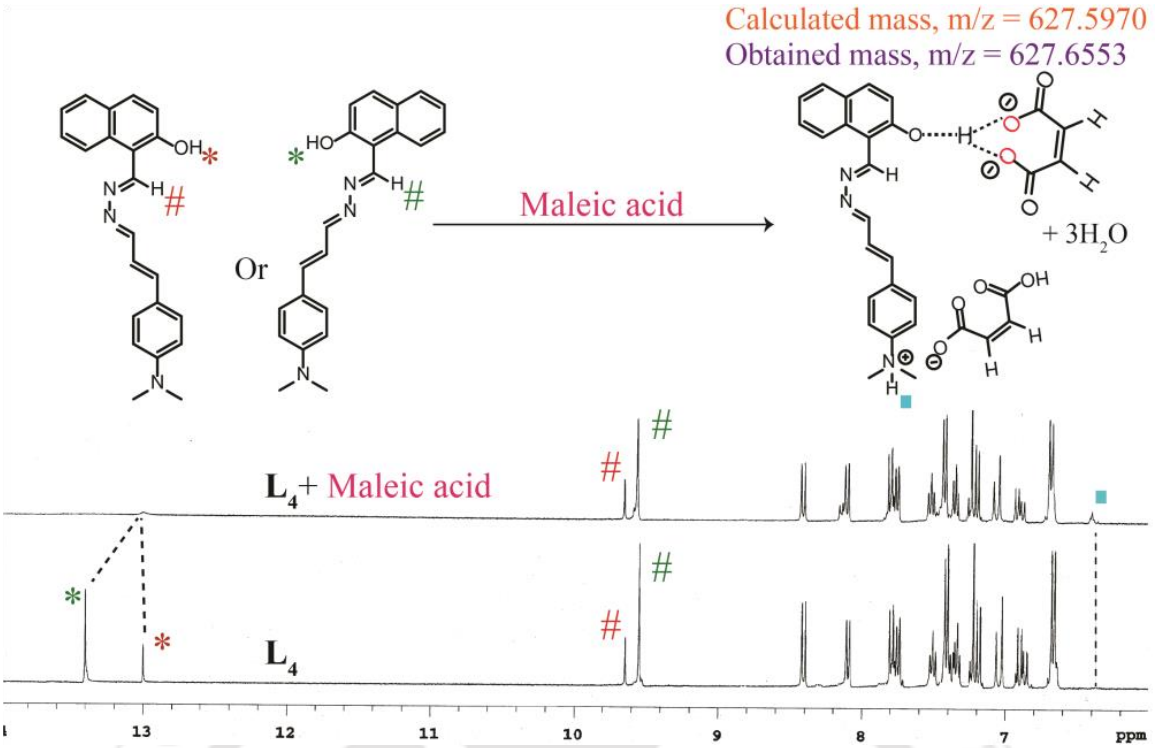

Figure A6.5: ^{1}H NMR spectrum of **L_4** in presence of Maleic acid in $CDCl_3$.

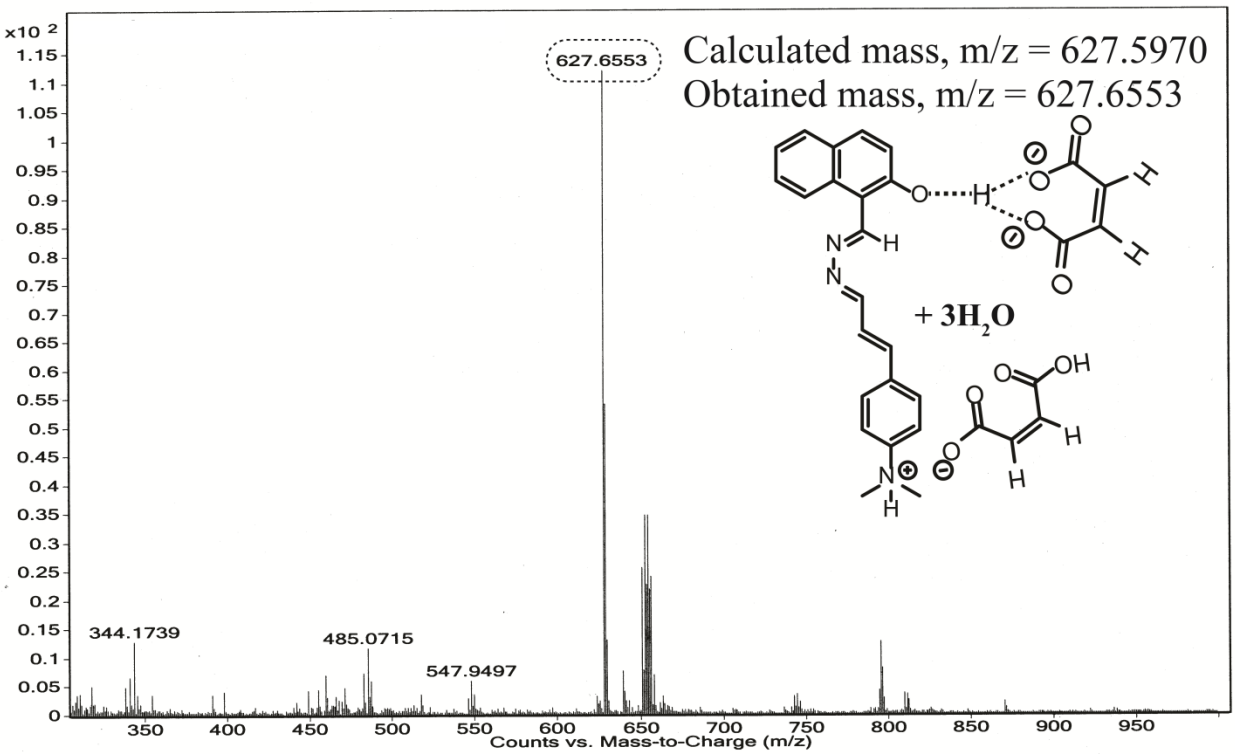

Figure A6.6: Mass spectrum of **L_4** in presence of Maleic acid.

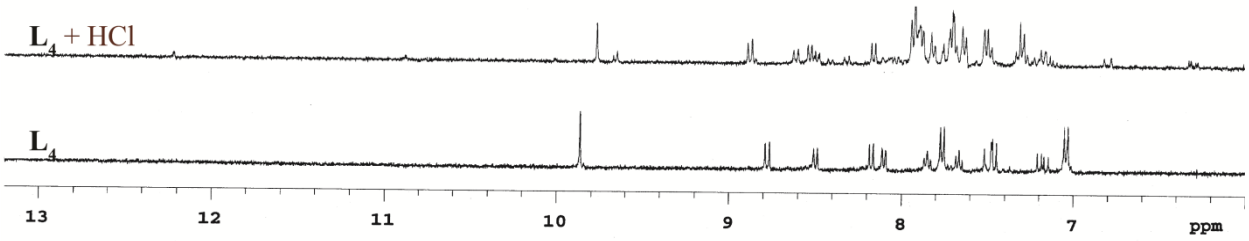

Figure A6.7: ^{1}H NMR spectrum of **L_4** in presence of **HCl** in CD_3OD.

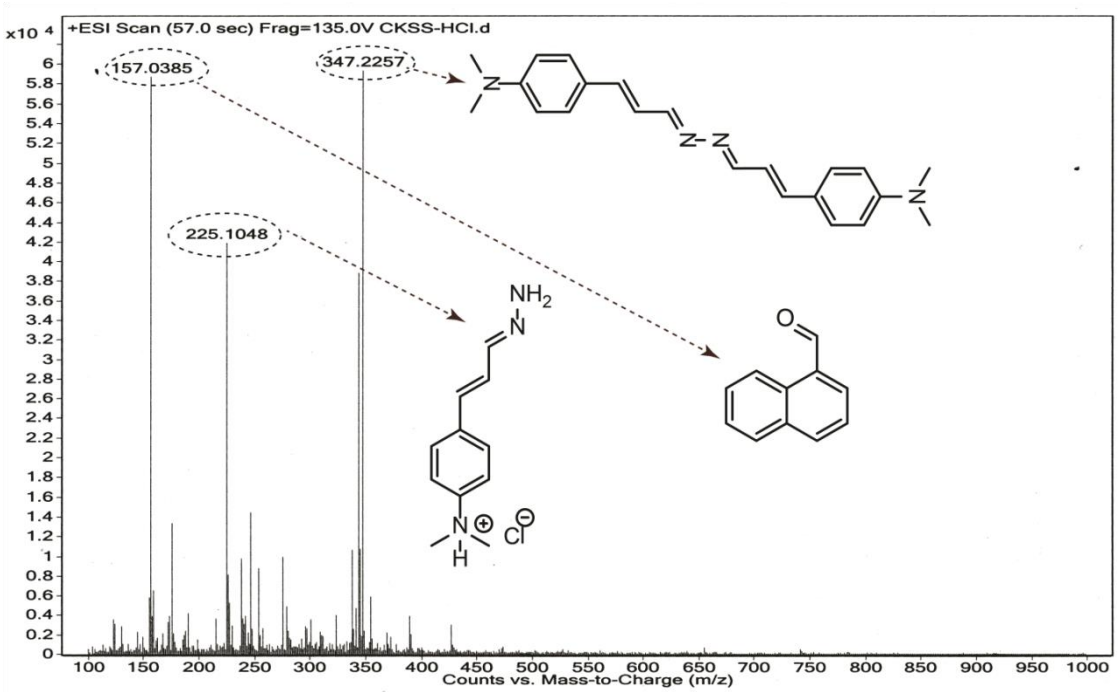

Figure A6.8: Mass spectrum of **L_4** in presence of HCl.

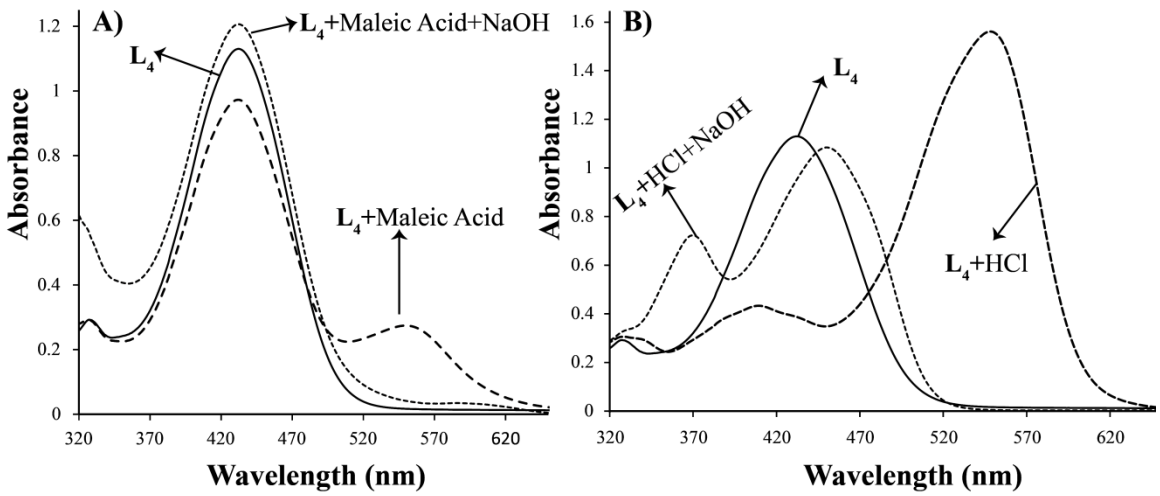

Figure A6.9: UV-Vis spectra of **L_4** (20μM) in presence of excess of A) Maleic acid; B) HCl; followed by addition of excess NaOH in ethanol.

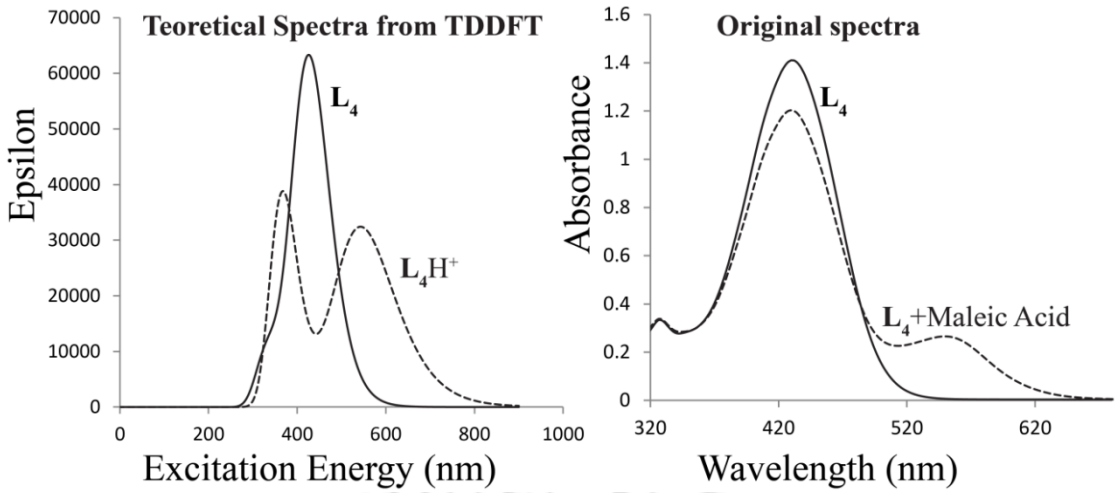

Figure A6.10: Comparison between theoretical UV-Visible spectra and experimentally obtained UV-visible spectra. TDDFT calculations were done using B3LYP/6-31 G (d,p) as implemented on Gaussian 03..

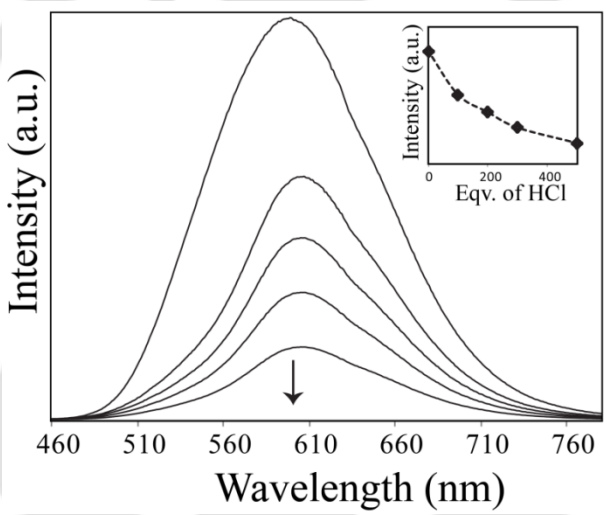

Figure A6.11: Fluorescence spectra of **L4** (20μM) in ethanol with increasing concentration of HCl. λ_{ex} = 450 nm.

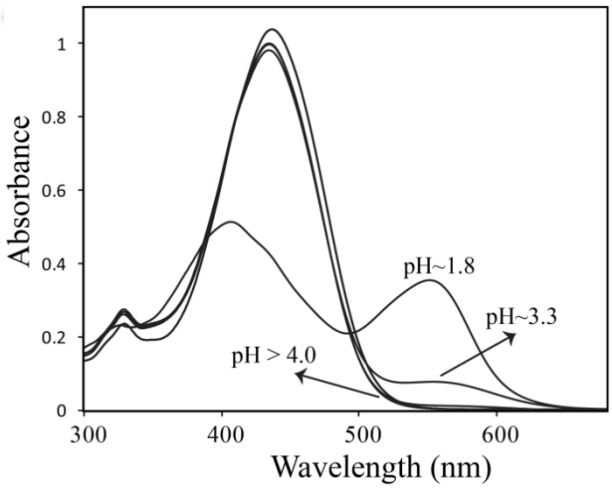

Figure A6.12: UV-Visible spectra of **L4** (20μM) in different pH values.

Table A6.1: pK_a values of various carboxylic acids.

Carboxylic Acids	pK_{a1}	pK_{a2}	pK_{a3}
Maleic Acid	1.9	6.07	–
Fumaric Acid	3.03	4.44	–
Tartaric Acid	2.89	4.4	–
Citric Acid	3.13	4.76	6.39
Cinamic Acid	4.44	–	–
Malonic Acid	2.83	5.69	–
Acetic Acid	4.76	–	–
Benzoic Acid	4.202	–	–
Gallic Acid	4.5	–	–
Terephthalic Acid	3.51	4.82	–
Isophthalic Acid	3.46	4.46	–
Malic Acid	3.4	5.2	–
Phthalic acid	2.89	5.51	–
Succinic acid	4.2	5.6	–
Oxalic acid	1.25	4.14	–

Table A6.1: Important orbitals and the energies of $\mathbf{L_4}$. The calculations were performed using B3LYP/6-31 G (d,p) as implemented on Gaussian 03.

Occupied Orbitals	Energy (eV)	Vacant Orbitals	Energy (eV)
HOMO -2 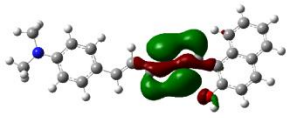	-5.6694	LUMO 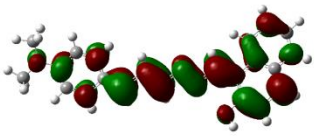	-1.6591
HOMO -1 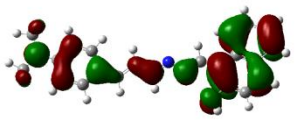	-5.4787	LUMO+1 	-0.8531
HOMO 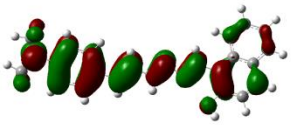	-4.7663	LUMO+2 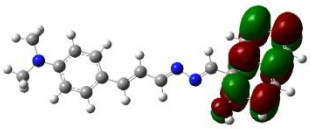	-0.0152

Table A6.1: Important orbitals and the energies of $\mathbf{L_4H^+}$. The calculations were performed using B3LYP/6-31 G (d,p) as implemented on Gaussian 03.

Occupied Orbitals	Energy (eV)	Vacant Orbitals	Energy (eV)
HOMO -2 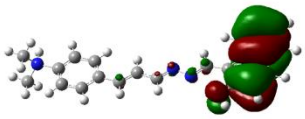	-7.9830	LUMO 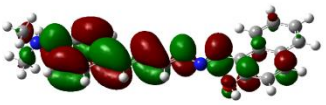	-4.6716
HOMO -1 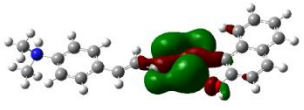	-7.9179	LUMO+1 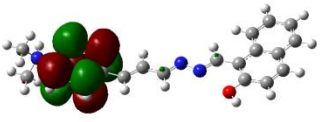	-3.7020
HOMO 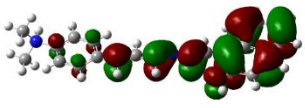	-7.1307	LUMO+2 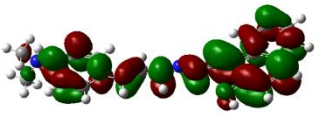	-3.2678

***Ref. A6.1*:** Frisch, M. J.; Trucks, G. W.; Schlegel, H. B.; Scuseria, G. E.; Robb, M. A.; Cheeseman, J. R.; Montgomery, J. A.; Vreven, Jr., T.; Kudin, K. N.; Burant, J. C.; Millam, J. M.; Iyengar, S. S.; Tomasi, J.; Barone, V.; Mennucci, B.; Cossi, M.; Scalmani, G.; Rega, N.; Petersson, G. A.; Nakatsuji, H.; Hada, M.; Ehara, M.; Toyota, K.; Fukuda, R.; Hasegawa, J.; Ishida, M.; Nakajima, T.; Honda, Y.; Kitao, O.; Nakai, H.; Klene, M.; Li, X.; Knox, J. E.; Hratchian, H. P.; Cross, J. B.; Bakken, V.; Adamo, C.; Jaramillo, J.; Gomperts, R.; Stratmann, R. E.; Yazyev, O.; Austin, A. J.; Cammi, R.; Pomelli, C.; Ochterski, J. W.; Ayala, P. Y.; Morokuma, K.; Voth, G. A.; Salvador, P.; Dannenberg, J. J.; Zakrzewski, V. G.; Dapprich, S.; Daniels, A. D.; Strain, M. C.; Farkas, O.; Malick, D. K.; Rabuck, A. D.; Raghavachari, K.; Foresman, J. B.; Ortiz, J. V.; Cui, Q.; Baboul, A. G.; Clifford, S.; Cioslowski, J.; Stefanov, B. B.; Liu, G.; Liashenko, A.; Piskorz, P.; Komaromi, I.; Martin, R. L.; Fox, D. J.; Keith, T. M.; Al-Laham, A.; Peng, C. Y.; Nanayakkara, A.; Challacombe, M.; Gill, P. M. W.; Johnson, B.; Chen, W.; Wong, M. W.; Gonzalez, C.; Pople, J. A., *Gaussian 03, Revision E.01,Gaussian, Inc., Wallingford CT*, **2004**.

Conclusion and Future Perspective

In conclusion, the overall thesis not only elucidates some important results in the field of developing advanced chemosensors for some biologically and environmentally relevant analytes but also addresses some critical issues related to discrimination of geometrical isomers. To get rid of aggregation caused quenching effect (ACQ) which often compromises the sensitivity of the probe; we have developed a new class of aggregation induced emission (AIE) active probes (Schiff base) and discussed the role of AIE in sensing outcome. As mentioned in the introduction, our primary aim was to introduce sensing systems that can rapidly sense target analytes by some form of optical responses which is conspicuous by naked eye; so that even an uneducated person could identify the sensing outcomes. Hence, all of the reported probes in this thesis were purposely designed to have the inherent feature of naked eye sensing ability. In general, the research works described in the thesis provide a clear insight of the design principle involved in developing simple organic optical chemosensor molecules which can detect various ionic as well as neutral species in aqueous (fully or partially) solution and/or inside living cells.

Newly developed AIE-active probe $\mathbf{L_1}$ exhibited a selective TURN-ON fluorescence response towards Al^{3+} in solution and rendered non-invasive detection of Al^{3+} in live HeLa cells. Achieving subsequent tracking of DNA interaction in a single AIE-active system by a dose dependant quenching of the highly emissive $\mathbf{L_1}$-Al^{3+} ensemble could potentially throw some light on the cellular and molecular basis of Al^{3+} toxicity in future. $\mathbf{L_1}$ can also selectively detect Cu^{2+} through sharp colorimetric response. So, basically $\mathbf{L}_1$ is a metal ion responsive colorimetric and fluorescent probe which additionally can track DNA. On the other hand, a versatile fluorescent probe ($\mathbf{L_2}$) has demonstrated highly sensitive dual yet discerning sensing of SO_3^{2-} and SO_4^{2-}/HSO_4^- over competing analytes with beneficial attributes such as sensing in completely aqueous medium and an extremely fast response time. Moreover, $\mathbf{L_2}$ holds considerable potential as an analytical tool to investigate the physiological implications of sulfate/sulfite derivatives in cell by demonstrating differential intracellular sensing of SO_3^{2-} and SO_4^{2-}. Another AIE active probe $\mathbf{L_3}$ can sense multiple targets at a time. It can sense cations Al^{3+} and Zn^{2+} through individual Turn-On fluorescence responses and Cu^{2+} through colorimetric changes. Interestingly, $\mathbf{L_3}$ can also selectively sense anion fluoride by specific colorimetric response. Lastly, sensing probe $\mathbf{L_4}$ can discriminate geometrical Isomers (Maleic Acid vs Fumaric Acid) by colorimetric as well as fluorescent changes. Alongside $\mathbf{L_4}$ can also detect Maleic Acid over various other carboxylic acids in Solution and Food Additives.

Hence, we have designed, synthesized and investigated some unique sensing platforms (**L_1-L_4**) which encompassed both simple and complex structures of the sensing probes. It should be noted that besides the conventional strategies we have included some added features in designing the sensing probes to upgrade their efficiency. For example AIE phenomenon has been coupled with chelation in probe **L_1** and **L_3** to achieve desired optical responses. In case of **L_2** also besides the nucleophilic reaction, aggregation played an important role in nurturing optical signals. However, in **L_4** combination of protonation as well as chelation has facilitated the sensing outcome.

Applications of chemosensors in analytical chemistry, supramolecular science, biochemistry, physical chemistry, medicinal chemistry, toxicology, forensic sciences and even modern nanosciences have reached an advance stage. However, to develop a smart, ready to use chemosensor, it is necessary to embed some important features like water solubility, turn-on or ratiometric response, non-cytotoxic nature, localization in particular compartment of cells, application in real samples, naked eye detection, rapid response, lowering cost and labour etc in molecular design. Although we tried to incorporate all these features conveniently in the respective results in this thesis which are extremely useful from the perspective of progressive chemo-sensing, there are still other challenges in supramolecular chemistry to deal with.

It should also be highlighted that to maintain a chronology we moved from developing all cation sensor (**chapter 3**) to all anion sensor (**chapter 4**) to cation and anion sensing together (**chapter 5**) to neutral molecule sensor at last (**chapter 6**). Essentially we believe that this chronological progress in designing optical probes would be instrumental in understanding comprehensive advancement in the particular field to the analytical chemists community.

Soham Samanta

Academic Summary

2012 - Present	PhD student at Indian Institute of Technology Guwahati, India.
Thesis title:	"**A Progressive Endeavor to Develop Efficient Organic Chromogenic and Fluorogenic Sensing Probes for Ionic and Neutral Guests**"
2008-2010:	Masters in Chemistry, Indian Institute of Technology Guwahati, India. CPI: 8.65 out of 10.0
2004-2007:	Graduation (Chemistry honours), Dinabandhu Andrews College, University of Calcutta, West Bengal, India. 67.0%.
2001-2003:	12th (Science), WBCHSE, 84.4%.
2001	10th , WBBSE, 83.25%.

Honours and awards

- Qualified Joint Admission Test for M.Sc. (JAM 2010) Examination
- Qualified CSIR-UGC National Eligibility Test (NET 2012 June) Examination (for lectureship)
- Qualified Graduate Aptitude Test in Engineering (GATE 2016) Examination

Research Interests

- Design and synthesis of fluorescent probes
- Fluorescence sensing of biologically important ions and molecules
- Applications of new sensor technologies in biotechnology and environmental analysis

Expertise:

- Spectroscopic techniques (UV, Fluorescence, FT-IR), Optical and fluorescence microscopy, NMR spectroscopy, mass spectrometry, single crystal x-ray diffraction, FESEM, AFM, DLS, Gaussian 09, Gauss view.

Publications

1. **Soham Samanta**, Sudeep Goswami, Md. Najbul Hoque, Aiyagari Ramesh and Gopal Das, An aggregation-induced emission (AIE) active probe renders Al(III) sensing and tracking of subsequent interaction with DNA, ***Chem. Commun.***, 2014, **50**, 11833.

2. **Soham Samanta,** Poulomi Dey, Aiyagari Ramesh and Gopal Das, A solo fluorogenic probe for the real-time sensing of SO_3^{2-} and SO_4^{2-}/HSO_4^- in aqueous medium and live cells by distinct turn-on emission signals, ***Chem. Commun.***, 2016, **52**, 10381.
3. **Soham Samanta**, Utsab Manna, Turjya Ray and Gopal Das, An aggregation-induced emission (AIE) active probe for multiple targets: a fluorescent sensor for Zn^{2+} and Al^{3+} & a colorimetric sensor for Cu^{2+} and F^-, ***Dalton Trans.***, 2015, **44**, 18902.
4. **Soham Samanta**, Chirantan Kar and Gopal Das, Colorimetric and fluorometric discrimination of geometrical isomers (Maleic acid vs Fumaric acid) with real-time detection of Maleic acid in solution and food additives, ***Anal. Chem.***, 2015, **87**, 9002.
5. **Soham Samanta,** Sudeep Goswami, Aiyagari Ramesh and Gopal Das, A new fluorogenic probe for solution and intra-cellular sensing of trivalent cations in model human cells, ***Sens. Actuators B.***, 2014,**194**, 120.
6. **Soham Samanta,** Barun Kumar Datta, Madhurima Boral, Abhijit Nandan and Gopal Das, A multi-responsive turn-on flurogenic probe to sense Zn^{2+}, Cd^{2+} and Pb^{2+}: left-right-center emission signal swing, ***Analyst***, 2016,**141**, 4388.
7. **Soham Samanta,** Turjya Ray, Fajle Haque and Gopal Das, A turn-on Rhodamine B-indole based fluorogenic probe for selective sensing of trivalent ions, ***J. Lumin.***, 2016, **171**, 13.
8. **Soham Samanta,** Sudeep Goswami, Aiyagari Ramesh and Gopal Das, A new chemodosimetric probe for the selective detection of trivalent cations in aqueous medium and live cells, ***J. Photoch. Photobio. A***, 2015, **310**, 45.
9. **Soham Samanta,** Utsab Manna and Gopal Das, White light emission from simple AIE-ESIPT-Excimer tripled single molecular system, ***New J. Chem.***, 2017, **41**, 1064.
10. Chirantan Kar, **Soham Samanta,** Sandipan Mukherjee, Barun Kumar Datta, Aiyagari Ramesh and Gopal Das, A simple and efficient fluorophoric probe for dual sensing of Fe^{3+} and F^-: application to bioimaging in native cellular iron pools and live cells, ***New J. Chem.***, 2014, **38,** 2660.
11. Chirantan Kar, **Soham Samanta,** Sudeep Goswami, Aiyagari Ramesh and Gopal Das, A single probe to sense Al(III) colorimetrically and Cd(II) by turn-on fluorescence in physiological conditions and live cells, corroborated by X-ray crystallographic and theoretical studies, ***Dalton Trans.***, 2015, **44,** 4123.
12. Barun Kumar Datta, Durairaj Thiyagarajan, **Soham Samanta,** Aiyagari Ramesh and Gopal Das, A novel chemosensor with visible light excitability for sensing Zn^{2+} in physiological medium and in HeLa cells, ***Org. Biomol. Chem.***, 2014, **12**, 4975.
13. Abhijit Gogoi, **Soham Samanta** and Gopal Das, A benzothiazole containing CHEF based fluorescence turn-ON sensor for Zn^{2+} and Cd^{2+} and subsequent sensing of $H_2PO_4^-$ and $P_4O_7^{4-}$ in physiological pH, ***Sens. Actuators B.***, 2014**, 202**, 788.
14. Sudeep Goswami, Durairaj Thiyagarajan, **Soham Samanta**, Gopal Das and Aiyagari Ramesh, A zinc complex of a neutral pyridine-based amphiphile: a highly efficient and potentially therapeutic bactericidal material, ***J. Mater. Chem. B***, 2015, **3**, 7068.

Conference Attended

- "**FICS**" 2014 and 2016, IIT Guwahati, Assam, India (Poster presented).